THE UNIVERSITY
of EDINBURGH

Functional analysis of heterochromatin protein 1-driven localisation and activity of the chromosomal passenger complex

Jan Gustav Ruppert

Thesis submitted for the degree of Doctor of Philosophy
The University of Edinburgh

October 2018

Declaration

I declare that this thesis was composed by myself, that the work contained herein is my own except where explicitly stated otherwise in the text, and that this work has not been submitted for any other degree or processional qualification.

Parts of this work have been published in the EMBO Journal (Ruppert *et al.*, 2018), DOI: 0.15252/embj.201797677

Jan Gustav Ruppert
Edinburgh
16th of October 2018

Acknowledgments

I would like to thank the following people:

My supervisor, Bill Earnshaw, for his guidance, support, and all the opportunities throughout the years, as well as granting me freedom to pursue my own ideas. It was a great time working with you!

My second supervisor, Patrick Heun, for our enthusiastic discussions and his thoughtful suggestions.

Jeyaprakash Arulanandam and Martin Waterfall for their collaboration and support.

Shinya Ohta for sharing the HP1 knockout cell lines. I hope we will meet soon.

The former members of the Earnshaw lab that I met and all current members for sharing their expertise and for all the fun discussions and times we had together.

The European Union for funding my Ph.D. and for supporting the scientific exchange in Europe with their excellent Marie Curie ITNs. Furthermore, I would like to thank everyone involved in the brilliant *PloidyNet* network for making my Ph.D. an unforgettable experience.

Olaf Hardt for making my great secondment at Miltenyi Biotec possible and particularly Patricia, Dave, and Gritt for their fantastic support during my stay.

Hiroshi Kimura for inviting me to Japan and teaching me in his laboratory, it was an outstanding experience. All lab members, in particular Sato-San and Handa-San, for the warm welcome and interesting discussions. Domo arigato!

A big thank you to all my old and new friends in the institute, in Edinburgh, in Germany and all over the world, from the US to Japan. I hope we keep in touch, I cannot wait to hear about the next step of your life's journey.

Last but not least, I want to thank my family: Vielen lieben Dank für eure bedingungslose Unterstützung und dass ihr mich immer mit offenen Armen empfangt.

Lay Summary

Cells in our body must divide to allow growth or the renewal of tissues. In the process of cell division, it is essential that the two copies of the genetic material inside every cell are equally divided into the two new emerging cells. Our genetic information is stored as DNA, which can be described as a blueprint explaining how components of the cells are made. Therefore, it can have dramatic consequences when the DNA is not distributed correctly between dividing cells. The consequences can be, for example, problems in development or contribution to cancer formation. Because the length of our DNA is about 2 meters per cell, it is necessary that DNA is packed into chromosomes which form typical X-like structures. Each half of the X-shaped chromosome contains the same genetic material, forming two sister chromatids. In the process of cell division, all chromosomes align in the middle of the cell and in a subsequent step each sister chromatid is pulled to opposite sites within the cell by dynamic rod-like structures called microtubules. The complex process of how microtubules attach to chromosomes is precisely controlled by the Chromosome Passenger Complex (CPC). The CPC localises at the centromere of a chromosome, a region which is usually at the constriction site of chromosomes and also where microtubules attach.

It was recently shown that the binding of a protein called Heterochromatin Protein 1 (HP1) is essential for correct function of the CPC. Interestingly, cells that were taken from cancer tissue show a reduced amount of HP1 bound to the CPC and less HP1 at centromeres. This could be a reason why cancer cells have a higher rate of wrongly dividing chromosomes. Therefore, I tested whether increasing the amount of HP1 at centromeres could reduce the rate of improperly segregated chromosomes in cancer cells. I used a synthetic biology approach, which means creating a protein that does not exist like this in our cells, but helps to analyse and understand how processes normally work. The artificial protein consists of HP1 fused to a protein that is localised at centromeres, which results in recruitment of HP1 to the centromere

region. However, it appears that simply placing HP1 to the centromere in this way does not have a positive effect on chromosome segregation.

Nevertheless, the artificial protein helped me to reveal a strong interaction between HP1 and the CPC even at stages of the cell cycle prior to the process of chromosome segregation. My results indicate that an interaction with HP1 is the first step that concentrates the CPC at its site of action and helps us to understand how this important complex is activated. Interestingly, HP1-driven CPC clustering is a new mode of CPC localisation, in addition to two earlier discovered ways of CPC localisation at centromeres. This novel way of HP1-driven CPC localisation could help to identify new targets for cancer therapy because previous studies reported an altered HP1-CPC interaction in cancer cells compared to normal cells. Therefore, it might be possible to identify therapeutic targets that are specific in cancer cells and thus potentially allow a more precise therapy with fewer side effects.

Abstract

The ultimate goal of mitosis is the equal distribution of chromosomes between the two daughter cells. One of the key players that ensures faithful chromosome segregation is the chromosomal passenger complex (CPC). CPC localisation to mitotic centromeres is complex, involving interactions with Shugoshin and binding to phosphorylated histone H3T3. It was recently reported that Heterochromatin Protein 1 (HP1) has a positive impact on CPC function during mitosis. The interaction between HP1 and the CPC appears to be perturbed in cancer-derived cell lines, resulting in decreased HP1 levels at mitotic centromeres and may be a potential cause for increased chromosome mis-segregation rates.

In this study, I tethered HP1α to centromeres via the DNA-binding domain CENP-B. However, instead of improving the rate of chromosome mis-segregation, HP1α tethering resulted in activity of the spindle assembly checkpoint and destabilisation of kinetochore-microtubule attachments, most likely caused by the robust recruitment of the CPC. Tethered HP1α even traps the CPC at centromeres during mitotic exit, resulting in a catalytically active CPC throughout interphase. However, it was not clear whether endogenous HP1 contributes to CPC localisation and function prior to mitosis. Here I also describe a substantial interaction between endogenous HP1 and the CPC during the G_2 stage of the cell cycle. The two isoforms HP1α and HP1γ contribute to the clustering of the CPC into active foci in G_2 cells, a process that is independent of CDK1 kinase activity. Furthermore, the H3S10ph focus formation in the G_2 phase appears to be independent of H3T3ph and H2AT120ph, the two histone marks that determine the CPC localisation in early mitosis.

Together, my results indicate that HP1 contributes to CPC concentration and activation at pericentromeric heterochromatin in G_2. This novel mode of CPC localisation occurs before the Aurora B-driven methyl/phos switch releases HP1 from chromatin, which possibly enables the H3T3ph and H2AT120ph driven localisation of the CPC during mitosis.

Table of Contents

List of Figures

List of Tables

Abbreviations

APC/C	anaphase promoting complex/cyclosome
as	analogue sensitive
BIR	baculovirus IAP repeat
bp	base pair
BSA	bovine serum albumin
C-Mad2	closed mitotic arrest deficient 2
C. elegans	*Caenorhabditis elegans*
CB	CENP-B DNA-binding domain
CCAN	constitutive centromere associated network
CD	chromo domain
CDKs	Cyclin-dependent kinases
CENP	centromere protein
CPC	chromosomal passenger complex
CSD	chromo shadow domain
DBD	DNA-binding domain
ddH_2O	double-distilled water
DMSO	dimethyl sulfoxide
DNA	deoxyribonucleic acid
dNTP	deoxynucleotide triphosphate
E. coli	*Escherichia coli*
ECL	enhanced chemiluminescence
EY / EYFP	enhanced yellow fluorescent protein
FBS	foetal bovine serum
GAPDH	glyceraldehyde 3-phosphate dehydrogenase
HDAC	histone deacetylase
HP1	heterochromatin protein 1
IAP	inhibitor of apoptosis protein
INCENP	inner centromere protein
kDa	kilodalton
KLHL9 / 13	kelch like family member 9 / 13
KMN	Knl-1-Mis12-Ndc80
KO	knockout
MCAK	mitotic centromere-associated kinesin
min	minute
Mklp2	mitotic kinesin-like protein 2
ml	millilitre
mm	millimetre

mM	millimolar
mut	mutant
NEB	nuclear envelope breakdown
ng	nanogram
nM	nanomolar
O-Mad2	open mitotic arrest deficient 2
PBS	phosphate buffered saline
PCR	polymerase chain reaction
PFA	paraformaldehyde
Plk1	polo-like kinase 1
PP1	protein phosphatase 1
PP2A	protein phosphatase 2A
PRCs	polycomb repressive complexes
PTMs	post-translational modifications
RNA	ribonucleic acid
RZZ	Rod/Zw10/Zwilch complex
S. cerevisiae	*Saccharomyces cerevisiae*
SAC	spindle assembly checkpoint
SAH	single alpha helix
$t_{1/2}$	halftime of recovery
w/v	weight/volume
µg	microgram
µl	microlitre
µM	micromolar
µm	micrometre

1 Introduction

1.1 The cell division cycle

Cell division is the process of how cells multiply to fulfil growth and tissue turnover in multicellular organisms. Most molecular mechanisms of cell division are conserved and many processes described in this introduction were initially discovered in single-celled eukaryotes. Before a cell can divide, crucial steps of cell growth and genome replication are necessary. This is done in the so-called interphase of the cell cycle, which typically can be subdivided into three distinct parts. DNA synthesis takes place in S-Phase (S) and is flanked by gap phase 1 (G_1) and gap phase 2 (G_2), in which cell growth and further preparation for the cell division occur (Fig. 1). The step of genome segregation happens in mitosis (M) and takes only a small fraction (~ 1 h) of the whole cell cycle duration, which is typically 20 to 24 h in cultured human cells. The step of cytokinesis completes cell division in which two individual daughter cells form. Cells that do not divide, exit the cell cycle and stay in the so-called G_0 phase.

Cyclin-dependent kinases (CDKs) drive the progression of the cell cycle. Their activity is regulated by cyclins, which are essential subunits for the kinase function (Evans *et al.*, 1983; Booher *et al.*, 1989). The CDK/cyclin system is regulated through timely specific ubiquitin-dependent proteolysis of cyclins, as the CDK kinases are expressed throughout the cell cycle (Glotzer *et al.*, 1991). A further regulatory system is well described for the CDK1 kinase. The nuclear Wee1 kinase and the cytoplasmic Myt1 kinase inactives CDK1 through phosphorylation of residues threonine 14 and tyrosine 15 (Parker and Piwnica-Worms, 1992; Mueller *et al.*, 1995b). This control is subject to a double negative feedback mechanism: Once CDK1 becomes active, it phosphorylates and inactivates Wee1 (Mueller *et al.*, 1995a; Harvey *et al.*, 2005; Kim and Ferrell, 2007). Additionally, CDK1 activity simulates CDC25 which dephosphorylates inhibitory phosphorylations on CDK1 (Gautier *et al.*, 1991; Kumagai and Dunphy, 1991, 1992; Hoffmann *et al.*, 1993).

Various combinations of CDK and cyclin complexes exist that are active at different stages of the cell cycle and responsible for cell cycle progression: CDK4/6 and cyclin D are associated with the G_1 phase and together with CDK2 and cyclin E mediate the transition to S phase. CDK2 and cyclin A drive the progression from S-phase onward, but the kinase required for the G_2/M transition is CDK1 in conjunction with cyclin B and A (Sherr, 1993; van den Heuvel and Harlow, 1993). However, more recent studies suggest reconsidering this "classical model" of specific CDK/cyclin functions, based on work with knockout mice, which proposes overlapping functions of various CDKs other than CDK1 (Hochegger *et al.*, 2008).

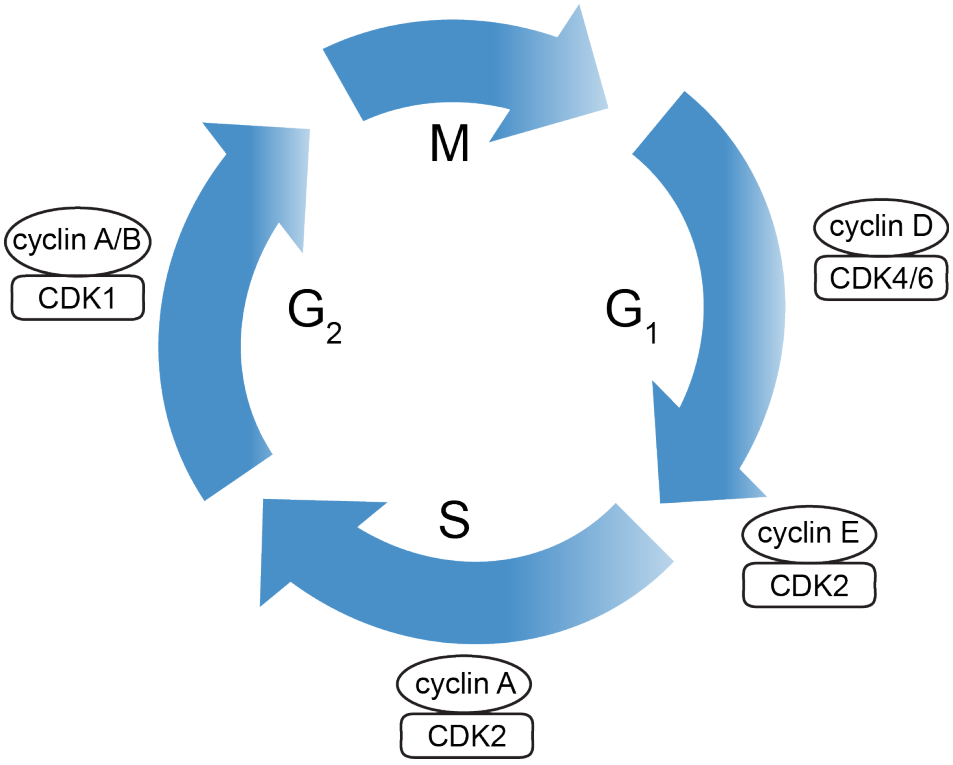

Figure 1: Scheme of the eukaryotic cell division cycle.
This simplified scheme shows the different stages of the cell cycle in eukaryotes and the combination of various cyclins and cyclin-dependent kinases (CDKs) that regulate the cell cycle progression.

The packaging of DNA is essential, as a total length of about two meters of DNA needs to be incorporated into the nucleus of human cells, which is only a few micrometres wide. The core unit of DNA packaging is the nucleosome, consisting of two copies of each histone protein H2A, H2B, H3, and H4, forming an octamer with 146 bp of DNA wrapped around it (Luger *et al.*, 1997). Importantly, histone N-terminal tails are subject to post-translational modifications (PTMs) that have an influence on nucleosome organisation and function. These consequences of histone PTMs are the basis of much of the field of epigenetics.

Nucleosomes are organised together with DNA, RNA and a large number of further structural and functional proteins in chromatin. Various higher order assembly and packing mechanism lead to the compact structure of mitotic chromosomes, allowing to segregate the genetic material in a highly organised manner during mitosis.

1.2 Stages of mitosis

Mitosis describes the cellular process by which the genome segregates into two daughter cells. I will describe this process as it occurs in metazoan cells that undergo an open mitosis (e.g. where the nucleus disassembles during mitosis). The nucleus exhibits drastic morphological changes, which involves the formation of mitotic chromosomes that eventually separate into the two emerging cells. This elaborate procedure can be subdivided into the five stages of prophase, prometaphase, metaphase, anaphase, and telophase, followed by cytokinesis in which two separate daughter cells are formed (Fig. 2). Based on microscopy observations, the different stages of mitosis were already described in the 19th century (Flemming, 1882) and are still nowadays defined as following:

In prophase, centrosomes, from which spindle microtubules emanate during mitosis, separate and move to opposite sides of the nucleus. Besides centrosomes, MT can also originate from chromosomes, particularly from kinetochores, or directly from pre-existing microtubules (Meunier and Vernos, 2012). At the same time

chromosomes start to condense and their typical structure becomes visible within the intact nuclear envelope.

Prometaphase begins with the breakdown of the nuclear envelope apparently initiated by the phosphorylation of lamins (Peter *et al.*, 1990). Additionally, phosphorylation induced dissociation of the nuclear pore complexes and microtubule mediated tearing contribute to the disassembly of the nuclear membrane (Beaudouin *et al.*, 2002; Laurell *et al.*, 2011). The nuclear envelope breakdown allows the mitotic spindle to access the chromosomes. With the help of the mitotic spindle, the initially randomly arranged chromosomes start to align at the spindle equator.

Metaphase describes the crucial stage of mitosis in which chromosome congression is completed and the so-called metaphase plate is formed. However, the spindle assembly checkpoint inhibits the onset of the next mitotic stage until all chromosomes successfully attach to the microtubules of the mitotic spindle and thereby bi-orientate. This checkpoint ensures that chromosome segregation does not occur prematurely and thus prevents chromosome mis-segregation (see section 1.5.1 for further detail).

With the onset of anaphase, the sister chromatids fully separate through cleavage of the remaining cohesin complexes that hold sister chromatids together. Forces generated by the mitotic spindle pull the separated chromatids towards the opposing spindle poles.

During telophase, the chromatids are pulled further apart and a cleavage furrow at the spindle midzone starts to form. The microtubules of the midzone continue to ingress and eventually form the compact midbody. At the same time, chromatids begin to decondense and the nuclear envelope starts to form again.

The process of cell division is completed with the step of cytokinesis. The microtubule bridge is separated through abscission and two individual daughter cells are formed.

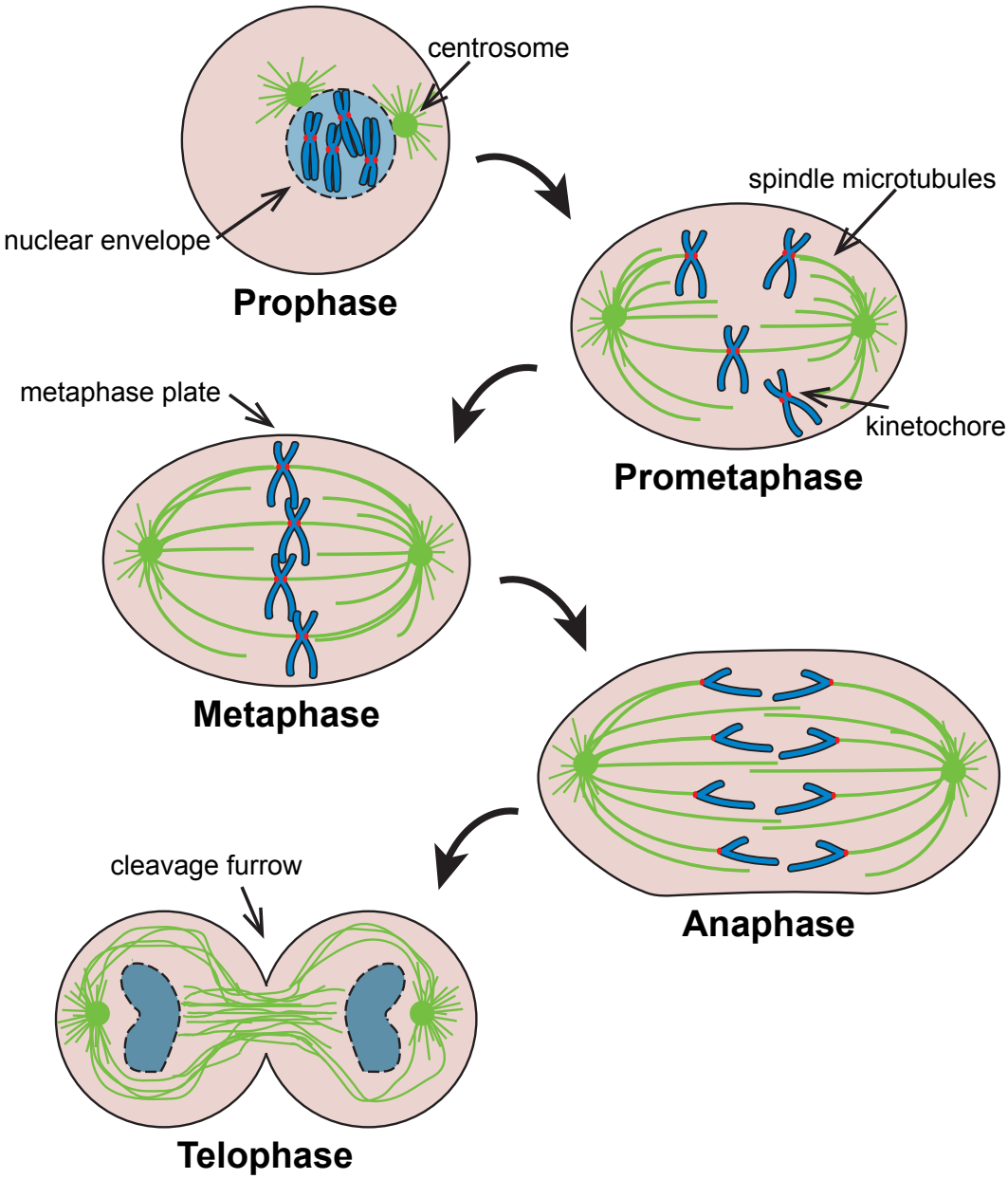

Figure 2: Stages of mitosis.
Chromosomes are shown in blue, the microtubules and centrosomes are depicted in green, and red dots represent kinetochores. Adapted and modified from (Ruchaud *et al.*, 2007).

1.3 The centromere

During mitosis, chromatin is condensed and assembled into characteristically shaped chromosomes. These consist of two sister chromatids, which contain a typical primary constriction at which sister chromatids are not resolved. This chromatin structure is called the centromere and is usually where kinetochores are established to facilitate the complex process of chromosome segregation (Hinshaw and Harrison, 2018). Secondary constrictions are typically formed at the nucleolus organizer regions and contain genes coding for ribosomal RNA, but are not linked to kinetochore formation (Henderson *et al.*, 1972; Goodpasture and Bloom, 1975).

Besides serving as the chromatin region for kinetochore assembly, centromeres also contribute to chromosome segregation through maintaining cohesion between the sister chromatids until anaphase onset. The cohesin protein complex is protected specifically at centromeres through shugoshin and by resisting their separation, it enables the orientation of the two sister kinetochores to opposite spindle poles (Haarhuis *et al.*, 2014).

The centromeric DNA of humans and other primates consists of α-satellite DNA with highly repetitive sequences. These arrays contain a typical 171 bp consensus sequence and arrange in higher-order repeat pattern (Fukagawa and Earnshaw, 2014). A further distinguishing feature of centromeres is the flanking pericentromeric heterochromatin. It contains divergent α-satellite monomers with no higher-order repeat organisation and is enriched in histone H3 trimethylated on lysine 9 (H3K9me3) (Nakayama *et al.*, 2001; Schueler *et al.*, 2001). The exact function of pericentromeric heterochromatin remains elusive, however, it might act as a barrier between the kinetochore and flanking euchromatin regions and thus prevent centromere migration (Fukagawa and Earnshaw, 2014), as it was previously shown that the exact centromere position can “drift” a certain distance along chromatin in vertebrate cells after many cell divisions (Hori *et al.*, 2017). The contribution of pericentromeric heterochromatin to centromere cohesion was studied particularly in yeast, where it plays an important role especially in meiosis, but its contribution to

mitotic sister chromosome cohesion in higher eukaryotes is controversial (Koch *et al.*, 2008; Gartenberg, 2009; Serrano *et al.*, 2009; Kang *et al.*, 2011; Hahn *et al.*, 2013).

Importantly, the formation of centromeres in humans does not seem to be based on a specific DNA sequence, which became first apparent through the observation of dicentric chromosomes that show α-satellite repeats at which no kinetochores form (Earnshaw and Migeon, 1985). Further proof came from clinical samples where so-called neocentromeres form on regions on chromosome arms that lack α-satellite repeats (du Sart *et al.*, 1997; Marshall *et al.*, 2008). This suggests that human centromeres are not defined by the DNA sequence but rather by epigenetic mechanisms (Earnshaw *et al.*, 1989).

1.3.1 Centromere proteins

A hallmark of centromeres is the enrichment of CENP-A, which was first identified together with two other human centromere proteins (CENPs) using antibodies from serum of patients with CREST syndrome (Earnshaw and Rothfield, 1985). These antibodies recognise the three centromere proteins, named CENP-A, CENP-B, and CENP-C, which form together with other factors the foundation of the kinetochore.

1.3.1.1 CENP-A

CENP-A is a variant of histone H3 and a distinct feature of eukaryotic centromeres across the evolutionary spectrum. It replaces the canonical histone H3 in ~ 4 % of nucleosomes at centromeres resulting in ~ 400 molecules of CENP-A per typical human centromere (Bodor *et al.*, 2014). Although this appears only as a low ratio, it is a ∼50-fold enrichment compared to the overall genome. The C-terminal domain of human CENP-A shares a great sequence identity with the histone fold domain of histone H3, whereas the N-terminus forms a unique domain, which could explain its specific functions at centromeres (Sullivan *et al.*, 1994). Despite its feature of centromere specification, CENP-A itself is not sufficient to establish centromere formation if generally overexpressed in human cells (Van Hooser *et al.*, 2001). Even

though ectopic CENP-A is able to recruit certain kinetochore proteins, it lacks the ability to induce neocentromere formation, suggesting that further components or events are necessary to achieve full kinetochore assembly. However, in *Drosophila* overexpression of the CENP-A homologue CID leads to stable CID accumulation close to heterochromatic regions and ectopic kinetochore formation (Olszak *et al.*, 2011). Furthermore, a tethering approach using a CID-LacI fusion protein and lac operator arrays showed that clustered CID is sufficient for functional kinetochore assembly at these ectopic sites (Mendiburo *et al.*, 2011). In line with this, LacI tethering of HJURP, which is a crucial deposition factor for CENP-A, also leads to kinetochore assembly at lac operator arrays in human cells, suggesting that a local clustering of CENP-A nucleosomes is crucial for centromere formation (Barnhart *et al.*, 2011).

Surprisingly, a recent study focusing on the kinetochore components in kinetoplastid revealed no homology to conventional kinetochore proteins and indicates that for example in *Trypanosoma brucei* kinetochores are assembled in the absence of CENP-A (Akiyoshi and Gull, 2014).

1.3.1.2 CENP-B

CENP-B is a centromere protein localised from the inner kinetochore down through the central domain of the centromere (Cooke *et al.*, 1990). It is the only characterised human centromere protein that binds DNA in a sequence-dependent way. The recognised sequence is a 17 bp motif within the α-satellite repeats of human centromeres, known as the CENP-B box (Masumoto *et al.*, 1989). CENP-B recognises this motive via its N-terminal DNA binding domain (Pluta *et al.*, 1992).A further feature of this 80 kDa protein is a C-terminal dimerisation domain, suggesting that it can capture two distant CENP-B boxes simultaneously (Tawaramoto *et al.*, 2003).

The precise centromeric role and significance of CENP-B long remained uncertain. Cell lines containing chromosomes with neocentromeres suggest a dispensable role for CENP-B in centromere function. Experiments using patient-derived cell lines demonstrated that CENP-B continues binding to the α-satellite

region of inactive centromeres (Earnshaw *et al.*, 1989). However, in contrast to CENP-A which is present exclusively at the neocentromere, CENP-B does not locate at the newly formed neocentromere due to the absence of CENP-B boxes (Amor *et al.*, 2004; Bassett *et al.*, 2010). Furthermore, CENP-B knockout mice are viable and able to assemble functional kinetochores (Hudson *et al.*, 1998; Kapoor *et al.*, 1998; Perez-Castro *et al.*, 1998) and CENP-B is not present at the centromeric alpha-satellite repeats of the human Y chromosome (Earnshaw *et al.*, 1991).

However, a more recent study focusing on the functional role of CENP-B at human centromeres revealed that CENP-B enhances the fidelity of human centromere function through CENP-C stabilisation and kinetochore nucleation (Fachinetti *et al.*, 2015). Additionally, this study demonstrated that the Y and neocentromere chromosomes, both lacking centromeric CENP-B, show a higher mis-segregation frequency compared to chromosomes that have CENP-B at centromeres (Fachinetti *et al.*, 2015).

The work of Fachinetti and colleagues, together with previous studies, suggested that CENP-A, CENP-B, and CENP-C interact to establish centromeric chromatin and form the foundation for kinetochore nucleation (Ando *et al.*, 2002; Amor *et al.*, 2004; Fachinetti *et al.*, 2015; Musacchio and Desai, 2017). CENP-C plays a crucial role in this process as it links centromeric nucleosomes to subcomplexes of the outer kinetochore, which I will introduce in the following section.

1.4 The kinetochore

In this section, I give an overview of how mitotic chromosomes are linked to spindle microtubules. This is achieved through the multi-protein complex named the kinetochore that assembles at active centromeres. Studies have discovered more than 100 different kinetochore components, most of which are organized into subcomplexes (Cheeseman, 2014; Musacchio and Desai, 2017).

1.4.1 Kinetochore structure

As discussed in the previous section, the first discovered human centromere proteins CENP-A, CENP-B, and CENP-C form a portion of the inner kinetochore that interacts directly with centromeric chromatin. They are part of a group of proteins that interact with centromeres throughout the cell cycle, termed the constitutive centromere associated network (CCAN) (Cheeseman and Desai, 2008). The CCAN serves as the platform linking the centromere chromatin with the protein complexes of the outer kinetochore. The main platform necessary for microtubule end-on binding is the outer kinetochore KMN network, named after the scaffolding protein Knl1, the Mis12 complex, and the Ndc80 complex. In contrast to the constitutively localised proteins of the CCAN, the outer kinetochore complexes assemble on the CCAN platform at different stages of the cell cycle. The Mis12 complex and Knl1 localise to the centromere in S phase and the Ndc80 complex is recruited to kinetochores in late G_2 (Gascoigne and Cheeseman, 2013). CENP-C is a link between the centromere nucleosomes and the outer kinetochore Mis12 complex (Screpanti *et al.*, 2011). The Mis12 complex then promotes outer-kinetochore assembly through its interaction with Knl1 and the Ndc80 complex, with the latter being the key microtubule-binding component of the kinetochore (Cheeseman *et al.*, 2006; DeLuca *et al.*, 2006).

1.4.1.1 Mis12 complex

The human Mis12 complex consists of the four subunits Mis12, Dsn1, Nsl1 and Pmf1. Crystal structures of the complex revealed that it is an extended rod of ~ 20 nm length and the subunits form two distinct subcomplexes, Mis12 with Pmf1 and Dsn1 with Nsl1 (Petrovic *et al.*, 2016). Cross-linking experiments showed that the C-terminal end of Nsl1 makes individually contacts with Knl1 and the Ndc80 complex, highlighting the “hub” function of the Mis12 complex for KMN complex assembly (Petrovic *et al.*, 2010). The Aurora B kinase phosphorylates the Dsn1 subunit at serine residues 100 and 109 (Yang *et al.*, 2008; Welburn *et al.*, 2010). Interestingly, it was reported that this phosphorylation strengthens the interaction between the Mis12

complex and CENP-C (Kim and Yu, 2015). However, the stronger interaction upon phosphorylation is not achieved by creating a binding site but probably rather through removing an inhibitory mechanism by which unphosphorylated Dsn1 hinders the interaction of CENP-C with the Mis12 complex (Kim and Yu, 2015; Petrovic *et al.*, 2016).

1.4.1.2 Knl1

Knl1 is a large outer kinetochore protein that serves as a signalling platform within the KMN network. It is critical for processes such as chromosome congression and spindle assembly checkpoint (SAC) signalling (Caldas and DeLuca, 2014). The structure of Knl1 appears to be mostly intrinsically disordered, but a structured domain at its C-terminal end is responsible for the interaction with the Mis12 complex (Petrovic *et al.*, 2010).

A role of Knl1 in chromosome congression became apparent in Knl1 depletion experiments, resulting in partial chromosome alignment defects (Cheeseman *et al.*, 2008). However, the exact molecular mechanism remains elusive and different hypotheses exist, explaining how Knl1 depletion could perturb kinetochore-microtubule attachments (Caldas and DeLuca, 2014).

The molecular role of Knl1 in the mitotic checkpoint is understood in more detail. Knl1 serves as the binding scaffold for proteins involved in SAC signalling. Phosphorylation of the Knl1 MELT motifs creates a binding site for the Bub complex (the role of Bubs will be discussed in section 1.5.1). The MELT motifs are well conserved between Knl1 homologues, however, the number of MELT motifs is highly variable among different species (Vleugel *et al.*, 2012).

1.4.1.3 Ndc80 complex

The Ndc80 complex is the key component of the KMN network for microtubule attachments. It is composed of the four subunits Hec1 (also called Ndc80), Nuf2, Spc24, and Spc25, which form an extended rod-like structure with globular domains at each end (Ciferri *et al.*, 2008). The Hec1 and Nuf2 subunits form the microtubule

binding site through their N-terminal regions and the Spc24 and Spc25 subunits compose the kinetochore binding module via their C-terminal end. The microtubule binding region of Nuf2 and Hec1 consists of a calponin homology (CH) domain and an unstructured N-terminal tail, both positively charged (Wei *et al.*, 2007; Ciferri *et al.*, 2008). Besides this information revealed by crystal structures, functional studies also demonstrate an important contribution of the highly basic N-terminal Hec1 tail for the Ndc80 interaction with microtubules (Cheeseman *et al.*, 2006; DeLuca *et al.*, 2006). However, N-terminal Hec1 tail deletion mutants in model organisms like *S. cerevisiae* and in *C. elegans* do not result in the severe phenotypes expected from disrupted kinetochore-microtubule attachments, indicating that the precise molecular role of the N-terminal Hec1 tail requires further investigation (Musacchio and Desai, 2017).

Overall, the KMN network is a crucial part of the outer kinetochore, providing the platform for microtubule binding and allowing through its multicomplex structure monitoring and modulation of microtubule attachments.

1.4.2 Chromosome congression and kinetochore-microtubule attachments

Starting with an initially random distribution of chromosomes upon nuclear envelope breakdown, chromosome congression is necessary to align chromosomes at the spindle equator to eventually enable correct chromosome segregation. Different mechanisms are responsible for chromosome congression, depending on the initial positioning of the chromosomes relative to the spindle. “Direct congression” is achieved by direct attachment of microtubules to kinetochores in an end-on fashion, whereas “peripheral congression” applies mostly only to chromosomes close to the spindle poles and depends on lateral microtubule attachments to bring these chromosomes to the spindle equator (Maiato *et al.*, 2017). The lateral transport along microtubules depends on the kinetochore motor protein CENP-E and is directed by post-translational modifications of tubulin (Barisic *et al.*, 2015). In the so-called lateral to end-on conversion, the lateral attachments

are turned into stable plus-end microtubule attachments, a process depending on the microtubule depolymerising kinesin MCAK (Shrestha and Draviam, 2013).

Stable and correct end-on kinetochore-microtubule attachments result in chromosome bi-orientation and are a prerequisite for faithful chromosome segregation. Bi-orientation requires the amphitelic configuration of microtubule attachments with one kinetochore attached to microtubules emerging from only one spindle pole and microtubules attached to the sister kinetochore arising from the opposite pole. However, the process of microtubule attachments occurs in a stochastic manner, resulting in the existence of transient erroneous microtubule attachments that do not result in chromosome bi-orientation (Tanaka, 2010).

Possible erroneous configurations are syntelic attachments, when both sister kinetochores attach to microtubules from the same spindle pole and merotelic attachments with one kinetochore attached to microtubules emerging from both poles at the same time (Fig. 3). These attachment geometries would not allow faithful chromosome segregation. Therefore, mechanisms are necessary that resolve incorrect attachments and halt mitotic progression. Additionally, in situations with monotelic attachments, i.e. only one of the sister kinetochores is attached to microtubules, or when chromosomes completely lack microtubule attachments, the onset of anaphase and thus sister chromatid segregation has to be delayed (Tanaka, 2010). This is ensured through the spindle assembly checkpoint, which prevents mitotic exit and will be discussed in detail in the next section.

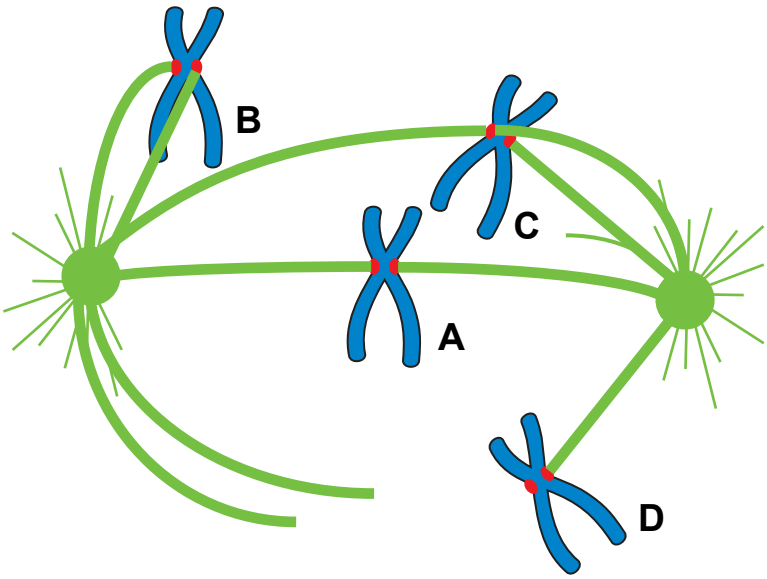

Figure 3: Different modes of microtubule-kinetochore attachments.
Chromosomes are shown in blue, microtubules and spindle poles in green and kinetochores in red. **(A)** represents the amphitelic mode in which chromosomes bi-orientate. **(B)** represents syntelic attachments where both sister kinetochores attach to microtubules from the same spindle pole. **(C)** represents merotelic attachments where one kinetochore is attached to microtubules that emerge from both poles at the same time. **(D)** represents monotelic attachments where only one of the sister kinetochores is attached to microtubules (after (Krenn and Musacchio, 2015)).

1.5 Control mechanism of chromosome segregation

During mitosis, the sister chromatids are held together through the protein complex cohesin. Once chromosomes are aligned and form the metaphase plate, the kleisin subunit of cohesin is cleaved by the protease Separase, allowing the sister chromatids to segregate and form two new daughter cells (Ciosk *et al.*, 1998; Cheeseman, 2014). However, to prevent chromosome mis-segregation, it is crucial that this process is initiated only after chromosomes are bi- orientated. The spindle assembly checkpoint (SAC) is a feedback system that monitors the attachment status of kinetochores and prevents mitotic progression until all kinetochores have microtubule attachments. However, the merotelic configuration does not induce a SAC-dependent arrest and is therefore a major risk for chromosome segregation errors (Gregan *et al.*, 2011).

1.5.1 Spindle Assembly Checkpoint (SAC)

The SAC detects whether kinetochores lack proper microtubule attachments and remains active even if only a single kinetochore is unattached (Rieder *et al.*, 1994). Until today it is unclear how exactly the SAC monitors whether unattached kinetochores are present, but the molecular mechanism of how the SAC components mediate the downstream signalling of the “anaphase halt signal” is well understood.

Besides being the anchor point for microtubules, the KMN complex serves also as a platform for the assembly of SAC components, such as Mad1, Mad2, Bub1, Bub3, and BubR1. The KMN subunit Knl1 is phosphorylated by the Mps1 kinase at its MELT motifs, creating a binding site for the Bub complex, consisting of Bub1, Bub3, and BubR1 (Taylor *et al.*, 1998; Yamagishi *et al.*, 2012). The C-terminal end of Mad1 binds Bub1 and facilitates Mad2 recruitment to unattached kinetochores (Kim *et al.*, 2012).

The SAC key player Mad2 (mitotic arrest deficient 2) exists in a “closed” (C-Mad2) or “open” (O-Mad2) structural configuration, with the latter being the inactive state (Mapelli and Musacchio, 2007). In the kinetochore-localised Mad1-Mad2

complex, Mad2 exists in the closed, thus active configuration (De Antoni *et al.*, 2005). C-Mad2 is able to induce a conformational change in O-Mad2, turning it into the active state. Activated C-Mad2 then diffuses away from kinetochores and forms together with BubR1 and Bub3 the mitotic checkpoint complex (MCC). The MCC inhibits Cdc20, which is a critical co-factor of the anaphase promoting complex (APC/C). The E3 ubiquitin ligase APC/C targets proteins for proteasomal degradation to allow anaphase onset (Chang and Barford, 2014). The targets include cyclin B, whose degradation results in a reduction of CDK1 activity and hence initiates mitotic exit (Glotzer *et al.*, 1991). Another of the APC/C key targets is Securin, an inhibitory factor of the protease Separase (Zou *et al.*, 1999). Once active, Separase cleaves the cohesin molecules holding the two sister chromatids together. Therefore, a crucial task of the MCC is to keep the APC/C inactive by sequestering Cdc20 and thereby inhibiting anaphase initiation. Additionally, recent work suggests that the MCC is able to bind to a second Cdc20, which is part of an active APC/C-Cdc20 complex (Izawa and Pines, 2015). This interaction occurs via BubR1 and appears to be essential for SAC functionality.

The SAC is "satisfied" once correct microtubule attachments are established at every kinetochore and needs to be inactivated to allow mitotic progression. The inactivation of the SAC signalling is supported by various mechanisms, including the inhibition of Mad2 by $p31^{comet}$, which competes with O-Mad2 for the binding to C-Mad2 (Xia *et al.*, 2004; Mapelli *et al.*, 2006). Additionally, the removal of SAC proteins from kinetochores by the cytoskeletal motor protein dynein, which is recruited partly by the Rod/Zw10/Zwilch (RZZ) complex contributes to SAC inactivation (Starr *et al.*, 1998; Howell *et al.*, 2001). Furthermore, phosphatase activity contributes to SAC silencing: The protein phosphatase 1 (PP1) is recruited to the RVSF motif of Knl1 and might dephosphorylate its MELT motifs, disrupting the Knl1 binding site of the Bub complex (Liu *et al.*, 2010; London *et al.*, 2012). Additionally, PP1 also dephosphorylates the C-terminus of zwint-1, a Zw10 binding protein, and is necessary for the dynein-driven removal of SAC proteins from kinetochores (Kasuboski *et al.*, 2011).

1.5.2 Error correction

The SAC serves as a roadblock to prevent mitotic progression when kinetochores lack proper microtubule attachments. As described in section 1.4.2, microtubule attachments to kinetochores occur in a stochastic manner. Therefore, it is not sufficient to simply delay mitotic progression through the SAC. In addition, a second control mechanism is necessary that resolves erroneous microtubule attachments. This mechanism is termed “error correction” and is, in contrast to the SAC, a local process destabilising microtubule attachments that are attached in an incorrect configuration, such as merotelic or syntelic attachments (Krenn and Musacchio, 2015). The mechanism of error correction is assumed to depend on the ability of the Chromosomal Passenger Complex (CPC) to respond to a lack of tension at centromeres and kinetochores, which can be a consequence of improperly attached microtubules (Tanaka *et al.*, 2002; Lampson *et al.*, 2004; Liu *et al.*, 2009).

The destabilisation of the kinetochore-microtubule attachments results in a disruption of end-on attachments (Kalantzaki *et al.*, 2015). Therefore, it is suggested that the error correction mechanism might also contribute to the maintenance of SAC signal activity until all chromosomes have correct kinetochore-microtubule attachments (Pinsky *et al.*, 2006). A weakening of the microtubule binding affinity is achieved through phosphorylation of kinetochore components and is a key function of the CPC, mediated through its kinase Aurora B (Tanaka *et al.*, 2002; Lampson *et al.*, 2004; Cheeseman *et al.*, 2006; DeLuca *et al.*, 2006; Tanaka, 2010). Due to the significance of the CPC for this project, I will introduce the CPC and its mode of action in error correction in greater detail in the following section.

1.6 Chromosomal Passenger Complex (CPC)

The CPC is a key regulator that controls various processes in mitosis and shows a highly mobile but distinct localisation at different stages of mitosis. First, the CPC is localised at chromosome arms and the centromere region. With the progression into prometaphase, the CPC starts to accumulate at centromeres where it controls chromosome behaviour in metaphase. Upon anaphase onset, the CPC localisation shifts from centromeres to the spindle midzone and eventually midbody region at which it functions in cytokinesis (Ruchaud *et al.*, 2007).

1.6.1 The CPC subunits

The CPC consists of two functional domains: the kinase module and the localisation module, which are connected through the scaffold component INCENP (Cooke *et al.*, 1987) (Fig. 4). The localisation module is composed of borealin, survivin and the N-terminus of INCENP. They are linked with each other via a three-helix bundle and determine the mitotic localisation of the CPC (Jeyaprakash *et al.*, 2007). The Aurora B kinase and the C-terminus of INCENP called the IN-box are the kinase module, which delivers the catalytic activity of the CPC (Adams *et al.*, 2000; Honda *et al.*, 2003). The interaction between Aurora B and INCENP plays a crucial role in CPC activation and will be discussed in the section 1.6.1.1 “Aurora B”.

The exact stoichiometry of the CPC subunits remains elusive. However, purified borealin and survivin interact in a 1:1 ratio and together with the N-terminal INCENP peptide (1-58) a 1:1:1 complex is formed (Bourhis *et al.*, 2007; Jeyaprakash *et al.*, 2007). Furthermore, structural experiments suggest that Aurora B and the INCENP C-terminus form a 1:1 complex (Sessa *et al.*, 2005).

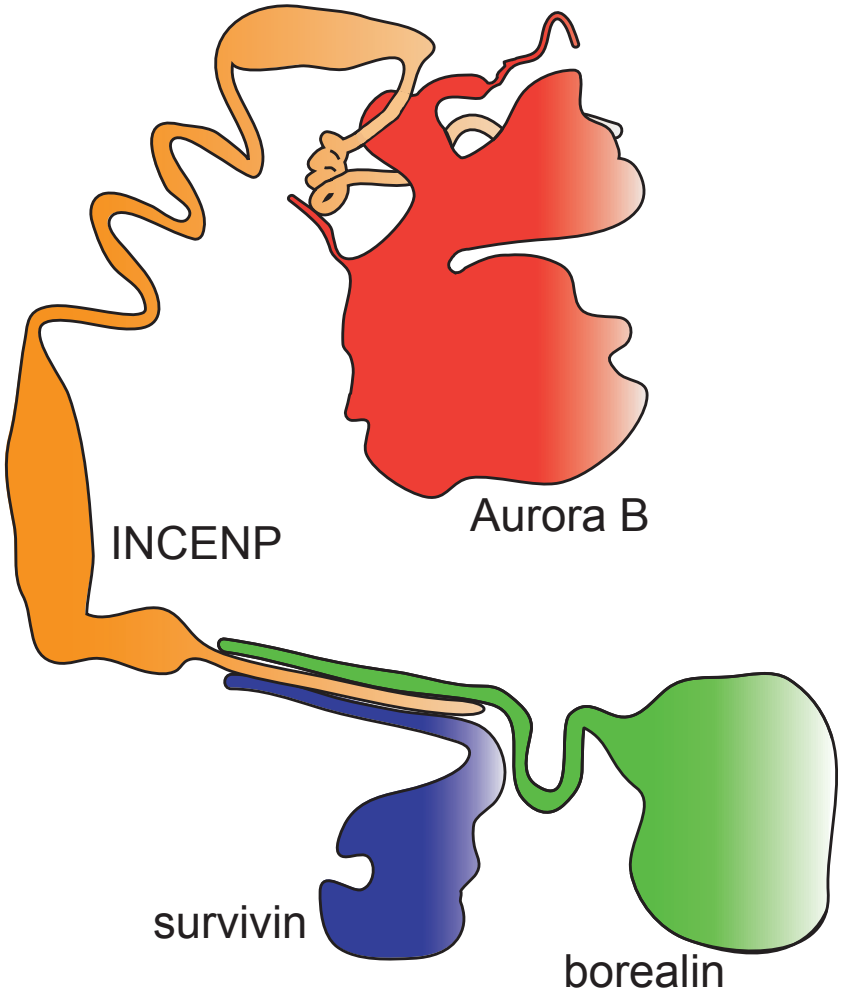

Figure 4: Subunits of the chromosomal passenger complex.

Survivin, borealin and the N-terminus of INCENP interact via a three-helix-bundle and form the localisation module. Aurora B and the C-terminus of INCENP form the kinase module. Adapted from (Carmena *et al.*, 2012).

1.6.1.1 Aurora B

Aurora B is a serine/threonine protein kinase and responsible for the kinase activity of the CPC. Two further members of the Aurora kinase family exist, named Aurora A and Aurora C. Aurora A localises at centrosomes and plays a role in their maturation (Hannak *et al.*, 2001). Aurora C is mainly involved in male meiosis and mutations result in infertility, but it is considered that Aurora C is not needed for somatic mitosis (Dieterich *et al.*, 2007; Kimmins *et al.*, 2007), though it may become abundant in cancer (Kimura *et al.*, 1999).

Activation of Aurora B is a multistep process involving the phosphorylation of the INCENP IN-box and Aurora B kinase itself. After binding to INCENP, Aurora B phosphorylates a threonine-serine-serine (TSS) motif at the INCENP C-terminus (Bishop and Schumacher, 2002; Honda *et al.*, 2003; Sessa *et al.*, 2005). Additionally, auto-phosphorylation of the Aurora B T-loop at threonine 232 further contributes to the activation of the Aurora B kinase (Yasui *et al.*, 2004). Both of these phosphorylations most likely occur in trans, which serves as a feasible explanation why the CPC is activated through local enrichment: Previous studies demonstrated that Aurora B activation occurs through increased local concentration and induced clustering using anti-INCENP antibodies or INCENP tethering (Kelly *et al.*, 2007; Wang *et al.*, 2011a). Additionally, microtubules are able to activate the CPC, presumably through the same mechanism of local enrichment (Tseng *et al.*, 2010).

Phosphatases regulate Aurora B kinase activity in complex feedback networks, counteracting phosphorylation of Aurora B substrates at centromeres and kinetochores, which is reviewed in detail by (Trivedi and Stukenberg, 2016). The two main phosphatases involved in these processes are PP1 and PP2A. Different pools of PP1 regulate CPC localisation and dephosphorylate CPC substrates. Interestingly, the recruitment of those PP1 pools is counteracted by Aurora B activity: Aurora B catalysed phosphorylation of Knl1 disrupts PP1 recruitment to kinetochores and phosphorylation of Repo-man perturbs the chromatin binding of the Repo-man-PP1 complex (Liu *et al.*, 2010; Qian *et al.*, 2013). In general, Aurora B phosphorylation at or adjacent to RVSF motifs opposes the recruitment of PP1 to various proteins during

mitosis (Kim *et al.*, 2010; Nasa *et al.*, 2018). Besides dephosphorylation of Aurora B substrates, PP2A also removes the activating phosphorylation in the Aurora B T-loop region at threonine 232, resulting in reduced CPC activity (Nijenhuis *et al.*, 2014; Meppelink *et al.*, 2015). Aurora B is ultimately thought to be regulated through its proteasomal degradation mediated by Cdh1 during mitotic exit. (Nguyen *et al.*, 2005; Stewart and Fang, 2005).

1.6.1.2 INCENP

INCENP was identified in a screen for new chromosome scaffold components and was the first CPC subunit to be discovered (Cooke *et al.*, 1987). The protein was named due to is localisation in the first part of mitosis (inner centromere protein) and surprised researchers with its unheard-of shift from centromeres to the spindle midzone upon anaphase onset and its midbody localisation in telophase cells. This dramatic change in mitotic localisation is a hallmark of the CPC and will be discussed further in section 1.6.2 “Localisation of the CPC”.

Acting as the main scaffold component, INCENP links the two functional domains of the CPC: The C-terminal end of INCENP contains the IN-box domain, which is responsible for binding and activating the Aurora B kinase. The INCENP N-terminus interacts with borealin and survivin, forming a three-helix bundle which acts as the CPC localisation module (Vader *et al.*, 2006; Jeyaprakash *et al.*, 2007).

INCENP interacts through a PxVxL/I motif with the chromo shadow domain of heterochromatin protein 1 (HP1) (Ainsztein *et al.*, 1998; Nozawa *et al.*, 2010; Kang *et al.*, 2011). This interaction is dispensable for correct mitotic localisation of INCENP but necessary to localise INCENP to heterochromatin in interphase cells, demonstrated in experiments using INCENP mutants missing the PxVxL/I motif region (Kang *et al.*, 2011).

The INCENP region that links the targeting and kinase module is of low-complexity and unlikely to form a tertiary structure. However, the central region of INCENP was shown to be a single alpha helix (SAH) rather than the previously

assumed coiled-coil domain (Samejima *et al.*, 2015). The SAH can stretch under force and might allow the kinase domain of the CPC to act on outer kinetochore substrates despite the targeting of the CPC localisation module to the inner centromere. This "dog leash" model is reviewed in detail by Krenn and Musacchio and can provide an explanation for the variable Aurora B phosphorylation gradient upon increased intra-kinetochore tension (Krenn and Musacchio, 2015).

1.6.1.3 Borealin

Borealin is also known as Dasra, because it was discovered simultaneously in two independent studies (Gassmann *et al.*, 2004; Sampath *et al.*, 2004). As described above, the N-terminal end of borealin forms together with survivin and INCENP the triple-helix bundle of the targeting module. CDK1 phosphorylates borealin, which is necessary for its interaction with shugoshin (Tsukahara *et al.*, 2010). The targeting of the CPC to mitotic centromeres is in part achieved through the binding of shugoshin to phosphorylated histone H2A. The exact centromere recruitment of the CPC will be discussed in subsection "Localisation of the CPC" of this chapter.

Besides the well-characterised interaction of the CPC member INCENP with HP1, a recent study suggests a direct interaction also of the borealin C-terminus with HP1 (Liu *et al.*, 2014). A mass spectrometry screen identified borealin as one of the proteins binding to the chromo shadow domain of HP1 (Nozawa *et al.*, 2010). However, borealin does not contain a typical PxVxL/I motif, but rather is supposed to interact with HP1 through a conserved LTVPV sequence (Liu *et al.*, 2014).

1.6.1.4 Survivin

Survivin was first identified as an anti-apoptotic protein, mainly expressed during development and in transformed cell lines (Ambrosini *et al.*, 1997). It contains a N-terminal baculovirus IAP repeat (BIR) domain, which is found in members of the "inhibitor of apoptosis protein" (IAP) family. However, the anti-apoptotic role of survivin is controversial. For instance, its BIR domain binds phosphorylated histone H3 with a higher affinity than peptides involved in apoptosis (Du *et al.*, 2012).

Furthermore, survivin is part of the CPC localisation module and its C-terminal helical domain forms together with INCENP and borealin a triple helical bundle as described earlier. Interestingly, most of the survivin protein is in complex with borealin in synchronised mitotic HeLa cells (Gassmann *et al.*, 2004). The contribution of survivin in recognising mitotic phosphorylation marks and positioning the CPC in mitosis is discussed in section 1.6.2.1 in greater detail.

1.6.2 Localisation of the CPC

By identifying the first CPC subunit INCENP, Cooke and colleagues first described the typical localisation of the CPC at chromosome arms and centromeres in early mitosis with the continued accumulation at centromeres until metaphase, followed by the shift to the spindle midzone upon anaphase onset (Cooke *et al.*, 1987). Since then a great number of studies focused on dissecting the molecular mechanisms involved in the localisation of the CPC throughout mitosis (Ruchaud *et al.*, 2007; Hindriksen *et al.*, 2017). A breakthrough was the discovery that the centromere localisation of the CPC in mitosis is defined by the two histone phosphorylation marks H3T3ph and H2AT120ph. Due to the relevance for this work, I will discuss these two histone marks in detail and focus mainly on the mechanism of centromere localisation of the CPC in this section.

1.6.2.1 Histone H3 threonine 3 phosphorylation

Haspin kinase phosphorylates histone H3 at threonine 3 (H3T3ph) during mitosis (Dai *et al.*, 2005). Survivin binds this mark via its BIR domain and locates the CPC to centromeres (Kelly *et al.*, 2010; Wang *et al.*, 2010). Depletion of Haspin kinase or mutation of the survivin BIR domain result in dispersed CPC localisation along chromosome arms instead of centromeric concentration in mitosis (Wang *et al.*, 2010).

Although no one has yet visualized the endogenous protein by indirect immunofluorescence, Haspin binds the cohesin protein complex, which links sister chromatids and holds them together until the onset of anaphase. Haspin binding to

cohesin is indirect via the cohesin modulator Pds5 (Zhou *et al.*, 2017). Cohesin is removed from chromosome arms in the prophase pathway, which is believed to concentrate Haspin at centromeres. An experiment supporting this model reported an increased amount of CPC localised to chromosome arms upon Wapl depletion (Haarhuis *et al.*, 2013). Similar to the stable localisation of cohesin between the sister chromatids at the centromere region, the H3T3ph mark is also specifically detected at the inner centromere in chromosome spreads (Wang *et al.*, 2010).

The enrichment of the H3T3 mark at centromeres is also regulated by Aurora B itself through various mechanisms. Wang and colleagues showed that Aurora B activates Haspin through direct phosphorylation (Wang *et al.*, 2011b). This possibly results in a positive feedback loop, concentrating H3T3ph and thereby Aurora B itself at centromeres. Opposing this, the H3T3ph mark is removed by the Repo-man-PP1 complex. However, Aurora B counteracts the Repo-man-PP1 function by phosphorylating Repo-man residue serine 893 (Qian *et al.*, 2013). The chromatin binding of Repo-man is perturbed when serine 893 is phosphorylated, and therefore, H3T3ph might be protected at sites where Aurora B is active. Additionally, CDK1 and Plk1 catalysed phosphorylation of Haspin also contributes to fully activate the kinase and to promote CPC localisation to centromeres (Ghenoiu *et al.*, 2013; Zhou *et al.*, 2014).

1.6.2.2 Histone H2A threonine 120 phosphorylation

A second mark that concentrates the CPC at centromeres is histone H2A phosphorylated at threonine 120 (H2AT120ph) (Yamagishi *et al.*, 2010). This residue is phosphorylated by the Bub1 kinase, which is recruited to kinetochores upon phosphorylation of Knl1 by the Mps1 kinase (Kawashima *et al.*, 2010; London *et al.*, 2012). In contrast to H3T3ph, the H2AT120ph mark is not directly recognised by a CPC subunit. Instead, shugoshin recognises H2AT120ph and then binds the borealin subunit of the CPC. According to the “tag along model”, shugoshin binds H2AT120ph and recruits the CPC to the kinetochore-proximal centromere (Hindriksen *et al.*, 2017). In a subsequent step, the CPC transfers to the inner centromere region when

shugoshin shifts to cohesin binding at the inner centromere. However, it is controversial whether shugoshin can bind cohesin and the CPC simultaneously or whether the binding is mutually exclusive, and therefore, two different pools of shugoshin may exist at centromeres, with one binding the CPC and the other binding cohesin (Trivedi and Stukenberg, 2016).

Similar to the H3T3ph mark, Aurora B has also a positive feedback loop in the H2AT120ph recruitment pathway. Aurora B activity indirectly protects the Mps1 phosphorylation mark on Knl1 by perturbing PP1 phosphatase activity (Liu *et al.*, 2010). This ensures that Bub1 binds Knl1, H2AT120 is phosphorylated, and the CPC is recruited.

1.6.2.3 CPC localisation upon anaphase onset

The CPC begins to shift from centromeres to the central spindle and the cell cortex at the region of the contractile ring with the onset of anaphase (Earnshaw and Cooke, 1991). This is facilitated by the removal of CPC targeting marks from chromatin and also through the transfer of the CPC from chromatin to the central spindle.

With the onset of anaphase and the concomitant decrease in CDK1 kinase activity, binding of the PP1 phosphatase to Repo-man is no longer inhibited (Qian *et al.*, 2015). This results in an active Repo-man-PP1 complex that removes the histone mark H3T3ph from chromatin (Qian *et al.*, 2011). Targeting the CPC to the spindle midzone requires the kinesin protein Mklp2 (mitotic kinesin-like protein 2). Upon removal of the CDK1-catalysed phosphorylation on INCENP, Mklp2 associates with INCENP and translocates with the CPC to the microtubules of the spindle midzone (Hümmer and Mayer, 2009). Furthermore, the E3 ligase Cul3 and the substrate-specific adaptors KLHL9 and KLHL13 promote the transfer of the CPC from chromatin to the central spindle and the cell cortex with the onset of anaphase (Sumara *et al.*, 2007). Interestingly, the CPC transfer to the spindle midzone requires higher Aurora B activity than needed for other CPC functions such as chromosome alignment (Xu *et al.*, 2009).

1.6.2.4 CPC localisation in interphase

The interphase localisation of the CPC is not nearly as well studied as its localisation in mitosis. Aurora B is expressed from S-phase onwards and the protein levels peak in mitosis (Stewart and Fang, 2005). Various studies reported that Aurora B localises at pericentromeric regions in G_2 cells, with Monier and colleagues highlighting that Aurora B accumulates especially at large pericentromeric regions, such as of chromosome 1 (Zeitlin *et al.*, 2001; Monier *et al.*, 2007; Hayashi-Takanaka *et al.*, 2009). Additionally, the CPC subunit survivin also clusters at pericentromeres in G_2 cells (Beardmore *et al.*, 2004). A more detailed study focusing on the interphase localisation of INCENP revealed that the clustering of INCENP in G_2 cells depends on its interaction with HP1. This was demonstrated by the use of INCENP mutants either lacking the PxVxL/I motif or containing alanine substitutions in this motif, both resulting in a disruption of the interaction with HP1. As a consequence, both INCENP mutants failed to localise to the centromere region in interphase and instead were enriched in nucleoli (Kang *et al.*, 2011).

1.6.3 Mitotic function of the CPC

The CPC acts in various processes during mitosis: These include chromosome condensation, sister chromatid cohesion, kinetochore assembly (Haase *et al.*, 2017), the release of erroneous chromosome-microtubule attachments, SAC regulation, and cytokinesis. The molecular function of the CPC in these processes is reviewed extensively by (Carmena *et al.*, 2012; van der Waal *et al.*, 2012; Trivedi and Stukenberg, 2016). Furthermore, Trivedi and Stukenberg highlight that a complex signalling network of phosphatases regulates the centromeric function of the CPC by counteracting Aurora B activity. These phosphatases are particularly PP1 and PP2A, which dephosphorylate Aurora B substrates, but also have an effect on CPC function by affecting CPC activity and localisation. Due to the relevance to this project, I will focus on the CPC function at centromeres in terms of regulation of chromosome attachments to the mitotic spindle and SAC activity.

1.6.3.1 Correction of erroneous kinetochore-microtubule attachments

The purpose of mitosis is the equal distribution of chromosomes between the two daughter cells. Sister-chromatid bi-orientation ensures error-free segregation as spindle microtubules from opposite poles bind to the kinetochores of each sister chromatid (see section 1.4.2 for further details). In cases where erroneous microtubule attachments occur, the CPC is able to weaken those interactions by phosphorylating kinetochore components and thereby lowering their affinity for microtubules (Lampson *et al.*, 2004).

One of the most extensively studied Aurora B substrates is the outer kinetochore protein Hec1, which is part of the Ndc80 complex and contributes to microtubule binding. (Cheeseman *et al.*, 2006; DeLuca *et al.*, 2006; Wei *et al.*, 2007; Miller *et al.*, 2008). The phosphorylation of several Hec1 N-terminal serine and threonine residues by Aurora B results in a decreased microtubule affinity (Cheeseman *et al.*, 2006; DeLuca *et al.*, 2006; Alushin *et al.*, 2010). Non-phosphorylatable mutants of Hec1 exhibit defects in chromosome congression and hyper-stretched centromeres due to overly stabilised microtubule attachments (DeLuca *et al.*, 2006, 2011). In line with this, mutations that mimic constitutive phosphorylation perturb kinetochore-microtubule attachments (Guimaraes *et al.*, 2008). The phosphorylation of the Hec1 N-terminus is strongest in early mitosis when bi-orientation is not yet established, and therefore, the tension at kinetochores is low (DeLuca *et al.*, 2011).

Besides Hec1, Aurora B also phosphorylates other KMN network components, including the Dsn1 subunit of the Mis12 complex and the microtubule binding domain of Knl1 (Yang *et al.*, 2008; Welburn *et al.*, 2010). An additional Aurora B substrate is the Ska complex, which contributes to the stabilisation of microtubule attachments. Upon Aurora B catalysed phosphorylation of the Ska complex, its interaction with the KMN network is perturbed and the formation of stable microtubule attachments is affected (Chan *et al.*, 2012).

1.6.3.2 Role of the CPC in SAC activity

The above described ability of Aurora B to weaken kinetochore-microtubule interactions suggests that the CPC contributes to SAC activity through this error correction pathway. Unattached kinetochores trigger continuous activity of the SAC, as described in detail in section 1.5. Moreover, the CPC contributes also directly to SAC activity by facilitating the recruitment of SAC key component Mps1 (Saurin *et al.*, 2011). However, Aurora B activity does not create a binding site for Mps1. Instead, Mps1 deletion mutants rather suggest that Aurora B phosphorylation causes a conformational change of Mps1 itself, necessary for its kinetochore binding (Nijenhuis *et al.*, 2013). Once Mps1 is recruited to kinetochores, it phosphorylates the kinetochore protein Knl1. The phosphorylation of the Knl1 MELT motifs recruits further downstream SAC components, which facilitate the active SAC signalling (Yamagishi *et al.*, 2012).

Overall, the correction of erroneous kinetochore-microtubule attachments by the CPC and its direct role in SAC activity allows chromosomes to bi-orientate, and therefore, ensures faithful chromosome segregation.

1.7 Histone H3 serine 10 phosphorylation

In addition to the chromatin marks H3T3ph and H2AT120ph that define CPC localisation in mitosis introduced above, a further important mitotic chromatin mark is histone H3 phosphorylated at serine 10 (H3S10ph). The CPC produces the H3S10ph mark and this is one of the most widely studied products of Aurora B kinase activity (Hsu *et al.*, 2000; Adams *et al.*, 2001; Hauf *et al.*, 2003).

Aurora B catalysed phosphorylation of H3S10ph typically emerges at pericentromeres in the G_2 phase of the cell cycle (Hendzel *et al.*, 1997; Crosio *et al.*, 2002; Monier *et al.*, 2007; Hayashi-Takanaka *et al.*, 2009). With progression toward the G_2/M transition the H3S10ph mark spreads through the nucleus, resulting in a prominent mark all over chromatin in prophase (Hendzel *et al.*, 1997; Crosio *et al.*, 2002) The H3S10ph signal is maintained in mitosis but starts to decrease with the shift of the CPC from chromatin to the spindle midzone in anaphase. Besides the relocation of the responsible kinase from chromatin, phosphatases also contribute to the active removal of H3S10ph. PP1 was identified as the phosphatase removing H3S10ph and thus counteracting the activity of Aurora B homologues in *S. cerevisiae* and *C. elegans.* (Hsu *et al.*, 2000). Later on, it was shown that PP1γ removes H3S10ph in vertebrate cells and a contribution of the PP1γ targeting subunit Repo-man was demonstrated in Repo-man depletion experiments (Qian *et al.*, 2011; Vagnarelli *et al.*, 2011).

Besides the strong H3S10ph signal produced by Aurora B in mitotic cells, H3S10ph can be also found under certain circumstances in interphase cells as a product of other kinases. Upstream environmental influences such as ultraviolet radiation, cytokines, and heat shocks activate these kinases and are typically linked to gene expression (Baek, 2011; Watson and Higgins, 2016). The response to these stimuli is mediated through the ERK and p38MAP kinase pathways with MSK1/2 as the effector kinases that phosphorylate histone H3S10, thereby contributing to the induction of certain immediate-early genes (Thomson *et al.*, 1999; Soloaga *et al.*, 2003). Tissue necrosis factor α (TNFα) also stimulates IKKα catalysed phosphorylation of H3S10, which promotes NF-κB-regulated gene expression (Anest

et al., 2003; Yamamoto *et al.*, 2003). Furthermore, the serine/threonine kinase PIM1 phosphorylates H3S10 at MYC binding sites upon growth factor stimulation and is important for MYC dependent transcriptional activation (Zippo *et al.*, 2007).

The exact function of the Aurora B-catalysed H3S10ph foci in G_2 cells is unclear. However, the emergence of H3S10ph differs between cell types and the later that H3S10ph foci emerge in interphase, i.e. closer to the G_2/M transition, the more likely chromosome segregation errors are to occur during mitosis (Hayashi-Takanaka *et al.*, 2009). Moreover, the role of the prominent H3S10ph chromatin labelling in mitotic cells is controversial. H3S10ph is often linked to chromosome condensation, as already early studies described a correlation between histone H3 phosphorylation and chromosome condensation, suggesting a histone H3 phosphorylation mediated chromosome condensation model (Gurley *et al.*, 1974, 1978). It is without a doubt that chromosome condensation is accompanied by a strong histone H3 phosphorylation in mitosis. However, various studies did not find a role of H3S10ph in chromosome condensation. *In vitro* experiments imply that phosphorylation of histone H3S10 is not important for chromosome condensation (De La Barre *et al.*, 2001). Additionally, *in vivo* studies preventing H3S10 phosphorylation by perturbing Aurora B activity either through depletion of INCENP or the use of specific Aurora B inhibitors suggest that a lack of H3S10ph has no dramatic effect on mitotic chromosome condensation (Adams *et al.*, 2001; Ditchfield *et al.*, 2003; Hauf *et al.*, 2003; Xu *et al.*, 2009). Two studies focusing on genetic alteration of the histone H3 sequence provide the strongest evidence for an actual role of H3S10ph in chromosome condensation. Wei and colleagues studied chromosome condensation in the model organism *Tetrahymena*, using a mutant histone H3 gene that codes for an alanine residue at position 10 instead of serine (S10A). This caused improper chromosome segregation and defects in chromosome condensation, particularly evident during meiotic chromosome condensation (Wei *et al.*, 1999). Another study that suggested a contribution of H3S10ph to chromosome condensation used a similar approach of mutating serine 10 to alanine in histone H3 genes of *S. cerevisiae*,

and subsequently analysing anaphase hypercondensation of an artificially generated extra-long chromosome arm (Neurohr *et al.*, 2011).

An alternative proposed function for H3S10ph is as a molecular switch. Adjacent to the serine 10 residue on histone H3 is a lysine residue localised at position 9 that is usually di- or tri-methylated (H3K9me2/3) in heterochromatin regions. Various proteins, which are typically linked to heterochromatin, recognise the H3K9me2/3 mark, with HP1 being the most widely studied example (Yun *et al.*, 2011). Phosphorylation of the adjacent H3S10 appears to disrupt the binding site provided by methylated H3K9. Specific antibodies that recognise simultaneously the presence of the dual-mark H3K9me2/3 + H3S10ph revealed the role of H3S10ph in HP1 release from chromatin, emphasising that the H3K9me2/3 mark is still present upon HP1 release (Fischle *et al.*, 2005; Hirota *et al.*, 2005). The concept of the methyl/phos switch applies not only to H3K9/H3S10, but several other methylated lysine residues on histone tails exist in the direct vicinity of phosphorylatable residues, such as H3K27/H3S28 and H3T3/H3K4, and presumably also undergo methyl/phos switch regulation (Watson and Higgins, 2016).

1.8 Chromatin states and heterochromatin protein 1

1.8.1 Euchromatin and heterochromatin

The genetic material in the nucleus can be classified into the two general categories: euchromatin and heterochromatin. This classification was originally described by Emil Heitz based on cytological observations of darker heterochromatin staining, and therefore, indicating greater compaction, whereas brighter regions represent euchromatin. (Heitz, 1929; Jost *et al.*, 2012). The distinction of euchromatin and heterochromatin still applies today, but the states are defined molecularly, mainly based on specific histone modifications.

Euchromatin is also termed "open-chromatin" and encompasses chromosome regions that are gene-rich and actively transcribed. Histone acetylations are typically found in euchromatin and are associated with chromatin accessibility (Hebbes *et al.*, 1988; Shogren-Knaak *et al.*, 2006). By contrast, heterochromatin describes the "closed-chromatin" state and covers mainly gene-poor regions that are transcriptionally repressed. An important feature of heterochromatin is a lack of histone acetylation, due to histone deacetylase (HDAC) activity, which was demonstrated by HDAC inhibition experiments (Neill and Turner, 1995; Taddei *et al.*, 2001; Toth *et al.*, 2004). In addition to the absence of histone acetylation, the presence of tri-methylation of histone H3K9 and H4K20 defines heterochromatic regions. These histone marks are typically present in highly repetitive genome regions, such as the satellite repeats of pericentromeric regions and the telomeres, or retrotransposons and endogenous retroviruses, which bear a risk of self-amplification. It is thought that transcriptional repression is important to keep genome integrity and is achieved through heterochromatin that makes these regions inaccessible to the transcription machinery. This so-called constitutive heterochromatin is present in all cell lineages and phases of the cell cycle (Becker *et al.*, 2016). In contrast, facultative heterochromatin is cell-type specific and depends on the histone mark tri-methylated H3K27 and the Polycomb repressive complexes (PRCs). The exact function of facultative heterochromatin and how it is established is

extensively reviewed in the literature, for example by (Simon and Kingston, 2009; Aloia *et al.*, 2013), but due to the focus of this work, I limit this introduction to constitutive heterochromatin.

Histone H3K9 methyltransferases of the Suv39 family, together with HDAC activity, are necessary to initiate and maintain constitutive heterochromatin (Wang *et al.*, 2016). HP1 binds methylated H3K9 and recruits further heterochromatin factors, such as DNA methyltransferases and the histone methyltransferase Suv4-20h that catalyses the methylation of histone H4K20 (Fuks *et al.*, 2003; Hahn *et al.*, 2013). Additionally, HP1 secures its own recruitment to heterochromatin by binding the methyltransferase Suv39h1, which creates the HP1 binding site methylated histone H3K9 in an amplification loop (Yamamoto and Sonoda, 2003). Overall, HP1 is an important chromatin mark reader that is able to recruit various proteins responsible for heterochromatin fidelity.

1.8.2 Heterochromatin protein 1

HP1 is a crucial component of heterochromatin and has three isoforms in mammals, called HP1α, HP1β, and HP1γ (Singh *et al.*, 1991; Saunders *et al.*, 1993). The three isoforms have similar sequences, but various studies describe differences in their localisations and functions. For example, HP1γ localises besides to heterochromatin also to euchromatic regions, which is associated with the phosphorylation of the HP1γ residue serine 83. (Minc *et al.*, 2000; Lomberk *et al.*, 2006). Furthermore, the localisation of HP1γ to heterochromatin foci appears to be lost upon HP1α and HP1β depletion (Dialynas *et al.*, 2007). On the contrary, HP1α and HP1γ seem to preferentially interact with Suv39h1 in heterochromatin foci compared to HP1β, suggesting similarities between HP1α and HP1γ in terms of binding partner interactions (Bosch-Presegué *et al.*, 2017). Additionally, HP1α and HP1γ appear to have redundant roles in protecting sister chromatid cohesion (Yi *et al.*, 2018).

To dissect the function of the individual HP1 isoforms in heterochromatin organisation and genome stability, a recent study used single knockout (KO) mouse

embryonic fibroblasts (Bosch-Presegué *et al.*, 2017). Bosch-Presegué and colleagues reported that a KO of HP1α leads to an increase of the histone marks H4K20me3 and H3K27me3 in pericentromeric heterochromatin compared to HP1β or HP1γ depletion. Furthermore, Suv4-20h2 interacts preferentially with HP1β and chromatin containing HP1β is enriched in the histone H4K20me3 mark, compared to HP1α or HP1γ containing chromatin.

The individual depletion of the HP1 isoforms results in different defects affecting genome stability. While HP1α KO leads to an increased frequency of syntelic and merotelic attachments, the KO of HP1β results in an increased number of cells with multipolar spindles. Interestingly, HP1γ depletion results in a mixture of the defects found in HP1α or HP1β KO cells and Bosch-Presegué et al. conclude that HP1γ shares redundant functions with the two other HP1 isoforms (Bosch-Presegué *et al.*, 2017).

Overall, small differences in the sequence and post translational modifications of the individual HP1 isoforms seem to have an influence on function and localisation. This led to the comparison of the HP1 isoforms to histone variants, which have a high degree of sequence similarity, but fulfil different functions (Canzio *et al.*, 2014).

Despite the described differences among the HP1 paralogues, work focusing on heterochromatin formation through nucleosome binding of HP1 did not describe a difference between the three HP1 isoforms (Machida *et al.*, 2018). This recent study, using cryo-electron microscopy, revealed the structure how HP1 binds H3K9me3 of two neighbouring nucleosomes. HP1 forms a symmetric dimer and bridges two nucleosomes without directly interacting with the linker DNA (Machida *et al.*, 2018). Earlier studies demonstrated that HP1 binds nucleosomes at histone H3K9me2/3 via an N-terminal chromo domain (CD) (Bannister *et al.*, 2001; Lachner *et al.*, 2001; Nakayama *et al.*, 2001). Additionally, methylated lysine 26 on linker histone H1.4 might serve as a further HP1 binding site on chromatin (Daujat *et al.*, 2005).

The C-terminal chromo shadow domain (CSD) is responsible for HP1 dimerisation and interaction with HP1 binding proteins that characteristically contain a PxVxL/I motif (Aasland and Stewart, 1995; Brasher *et al.*, 2000; Smothers and Henikoff, 2000; Nozawa *et al.*, 2010). Additionally, it was shown that murine HP1α, HP1β and, HP1γ can heterodimerise *in vitro and in vivo* (Nielsen *et al.*, 2001).

In a detailed study of HP1 binding partners, Nozawa and colleagues performed a proteomic analysis using various HP1α deletion mutants and amino acid residue substitutions that perturb specific HP1 functions (Nozawa *et al.*, 2010). The approach of HP1 immunoprecipitation and subsequent mass spectrometry revealed 82 HP1 binding partners in total, of which 85 % depended on CSD interaction. Importantly, the CPC members borealin, INCENP, and Aurora B were identified, further confirming an interaction of HP1 with the CPC (Nozawa *et al.*, 2010).

In interphase nuclei, HP1 typically localises to heterochromatin foci that are enriched in the H3K9me2/3 mark (Lachner *et al.*, 2001). Recent studies reported that HP1α contributes to heterochromatin formation through its phase separation properties, allowing liquid-like fusion of heterochromatin domains (Larson *et al.*, 2017; Strom *et al.*, 2017). Additionally, co-localisation of HP1α and HP1γ with promyelocytic leukemia (PML) nuclear bodies was described, however, the functional relevance remains unclear (Seeler *et al.*, 1998; Hayakawa *et al.*, 2003).

Upon mitotic entry, a clear displacement of HP1 from chromatin occurs. Two separate studies reported that phosphorylation of the adjacent serine 10 residue disrupts HP1 binding to H3K9me2/3 (Fischle *et al.*, 2005; Hirota *et al.*, 2005). *In vitro* experiments demonstrated a clear decrease in HP1 binding affinity for H3K9me2/3 if the H3S10ph mark is present (Fischle *et al.*, 2005). Furthermore, inhibition of Aurora B, resulting in a lack of H3S10ph, results in HP1 retention all over chromosomes in mitosis (Fischle *et al.*, 2005; Hirota *et al.*, 2005; Nozawa *et al.*, 2010). Interestingly, the potential HP1 binding site methylated histone H1.4K26 undergoes a similar methyl/phos switch regulation through phosphorylation of the adjacent serine 27 residue also by Aurora B (Daujat *et al.*, 2005; Hergeth *et al.*, 2011).

Despite the displacement of HP1 from chromatin by the methyl/phos switch, a small fraction of HP1 can be found at mitotic centromeres. In contrast to interphase chromatin binding, the inner centromere localisation of HP1 during mitosis depends on the CSD rather than the CD (Hayakawa *et al.*, 2003). This suggests that a binding partner recruits HP1 to mitotic centromeres. Indeed, Kang and colleagues demonstrated by use of an INCENP deletion mutant, lacking the PxVxL/I motif, that HP1 recruitment to mitotic centromeres depends on the interaction with INCENP (Kang *et al.*, 2011).

Importantly, recent work revealed that the HP1 binding to the CPC is necessary for full Aurora B activity in mitosis (Abe *et al.*, 2016). Abe and colleagues observed reduced levels of HP1 at mitotic centromeres in cancer-derived cells, compared to non-transformed cell lines, due to a reduced association of HP1 with INCENP in the cancer-derived cells. Furthermore, *in vitro* assays revealed that Aurora B catalyses substrate phosphorylation with a higher efficiency in the presence of HP1 than in its absence, which is mainly achieved through an increased reaction rate and only to a lesser extent by increased substrate affinity (Abe *et al.*, 2016). The decreased levels of HP1-bound CPC in cancer-derived cells result in impaired Aurora B activity, demonstrated by decreased levels of phosphorylated Dsn1 compared to non-transformed cells. Additionally, disrupting the HP1-INCENP interaction in non-transformed cells leads to a reduction of Aurora B activity and increased the frequency of chromosome segregation errors. However, the reverse experiment, namely to reduce the frequency of chromosome mis-segregation in cancer-derived cells by increasing the general HP1α level, was not successful. HP1α overexpression in cancer-derived cells that have reduced levels of HP1 at mitotic centromeres does not result in an overall increased amount of HP1 bound CPC and, importantly, does not rescue chromosome segregation errors (Abe *et al.*, 2016).

1.9 Aims of this work

In this project, I examined whether centromeric HP1 has a positive effect on the frequency of chromosome segregation errors. As described above, a simple overexpression of HP1α has no positive effect on chromosome mis-segregation rates in cells with a decreased level of centromeric HP1. Therefore, I chose an approach to actively tether HP1α to centromeres and used for this a simplified system in which HP1α localisation does not depend on chromatin marks, but is rather determined by the DNA-binding domain of CENP-B. Furthermore, based on recent work suggesting that HP1 is an essential CPC component (Abe *et al.*, 2016), I examined the interaction between HP1 and the CPC and focused on the role of HP1 in CPC clustering and activation in interphase.

2 Materials and Methods

2.1 Solutions, buffers and reagents

All listed buffers and solutions were prepared with double-distilled water and chemicals from Sigma-Aldrich unless otherwise stated.

Table 1 – General solutions and buffers

Name	Composition
2x Laemmli sample buffer	120 mM Tris-HCl pH 6.8, 4% SDS, 20% Glycerol; 1x reducing SB: 100 µl 2x SB, 90 µl ddH_2O, 10 µl 2-Mercaptoethanol
1x reducing sample buffer	100 µl 2x sample buffer, 10 µl 2-Mercaptoethanol, 90 µl ddH_2O
SDS Electrophoresis buffer	25 mM Tris, 192 mM glycine, 0.1% SDS; (pH 8.8)
Transfer Buffer	25 mM Tris, 192 mM glycine, 0.1% SDS, 20% methanol; (pH 8.8)
TAE	40 mM Tris-acetate, 1 mM EDTA; (pH 8.0)
PBS	137 mM NaCl, 2.7 mM KCl, 10 mM Na_2HPO_4, 2mM KH_2PO_4
PHEM	60mM PIPES, 25mM HEPES, 10mM EGTA, 2mM $MgCl_2$
Lower gel buffer	1.5 M Tris-HCl; (pH 8.8)
Upper gel buffer	0.5 M Tris-HCl; (pH 6.8)
LB	1% tryptone, 0.5% yeast extract, 10mM NaCl; (pH 7.4)
Lysis buffer	10mM Tris (pH 7.0), 100mM EDTA, 0.5% SDS
TE	10 mM Tris, 1mM EDTA; (pH 8.0)

Table 2 - Drugs

Drug	Diluent	Used Concentration	Source
ZM447439	DMSO	indicated	Tocris Bioscience
RO-3306	DMSO	9 µM	Tocris Bioscience
1NM-PP1	DMSO	10 µM	Linfeng Xie, James Paulson

2.2 Oligonucleotides

All oligonucleotides were purchased from Sigma-Aldrich and resuspended in double-distilled water.

Table 3 - Oligonucleotides used for cloning and sequencing

Description	Sequence (5' – 3')
Cloning	
HP1α_Fwd	CACCATGGGAAAGAAAACCAAGCGGACAGC
HP1α_Rev	GCTCTTTGCTGTTTCTTTCTCTTTGTTTTCC
HP1_Stop-codon_Fwd	GGTCGGCGCGCGCACCCTAGCTCTTTGCTG
HP1_Stop-codon_Rev	CAGCAAAGAGCTAGGGTGCGCGCGCCGACC
HP1_V22M_Fwd	AGAGGATGAGGAGGAGTATGTTATGGAGAAGGTGC
HP1_V22M_Rev	GCACCTTCTCCATAACATACTCCTCCTCATCCTCT
HP1_I165E_Fwd	GCTAATGTGAAATGTCCACAAATTGTGGAGGCATTTTATGAA GAGAGACTGACATGG
HP1_ I165E_Rev	CCATGTCAGTCTCTCTTCATAAAATGCCTCCACAATTTGTGGAC ATTTCACATTAGC
HP1_W174A_Fwd	TGATAGCATTTTATGAAGAGAGACTGACAGCGCATGCATATC CTGA
HP1_W174A_Rev	TCAGGATATGCATGCGCTGTCAGTCTCTCTTCATAAAATGCTA TCA
CDK1_Fwd	GCCGTGGGAGGATCCCCTGAGCCCAGGAGG
CDK1_Rev	GTGCGGCATTCTCAACTACCAAAAATAGGG
Sequencing	
T7 Promoter	TAATACGACTCACTATAGGG
tYIP_SEQ2	CTCTGGCTAACTAGAGAACCC
tYIP_SEQ4	CTGGAGTACAACTACAACAGCC

Table 4 - siRNA oligonucleotides

Description	Sequence	Reference
Mad2	ACCUUUACUCGAGUGCAGATTdTdT	(Nitta et al., 2004)
Control	CGUACGCGGAAUACUUCGAdTdT	(Elbashir et al., 2001)

2.3 Commercial kits

Table 5 - Commercial kits

Description (catalogue number)	Manufacturer
QIAfilter Plasmid Midi Kit (12243)	Qiagen
QIAprep Spin Miniprep Kit (27106)	Qiagen
QIAquick Gel Extraction Kit (28704)	Qiagen
QIAquick PCR Purification Kit (28104)	Qiagen
QuikChange II kit (200523)	Stratagene
Neon Transfection System 100 µL Kit (MPK10096)	Thermo Fisher Scientific
Zero Blunt TOPO PCR Cloning Kit (K280020)	Thermo Fisher Scientific
Quick Ligation Kit (M2200S)	New England Biolabs
BigDye Terminator v3.1 Cycle sequencing Kit (4337455)	Applied Biosystems

2.4 Molecular biology techniques

2.4.1 Restriction digestion of DNA plasmids and fragments

All plasmid DNA or DNA fragments synthesised by GeneArt (Thermo Fisher Scientific) were digested with appropriate endonuclease restriction enzymes from New England Biolabs. A typical 50 µl reaction contained the desired amount of DNA, 10 units of the relevant endonuclease per µg of DNA, and the recommended reaction buffer. The digestion was performed for two hours at the appropriate temperature. When required, the re-ligation of the digested plasmids was limited by removal of the 5' phosphate group using Calf Intestine Phosphatase (CIP) (New England Biolabs) after restriction digestion. One unit of CIP was used per µg of DNA and incubated for 30 min at 37 °C. Digested plasmids were recovered and purified by agarose gel electrophoresis, whereas digested GeneArt DNA fragments were purified using the QIAquick PCR Purification Kit (Qiagen).

2.4.2 Agarose gel electrophoresis and purification of DNA

A gel solution containing between 1% and 2% agarose (Sigma-Aldrich) was prepared with TAE buffer and 0.5 µg/ml ethidium bromide (Sigma-Aldrich). DNA samples in a final 1x dilution of 6x gel loading dye (New England Biolabs) were loaded on the gel and gel electrophoresis was performed in TAE buffer at a constant voltage of 100 V. DNA fragments were visualised under UV light and excised from the agarose gel. Purification of the desired DNA fragment was performed using the QIAquick gel extraction kit (Qiagen) according to the manufacturer's instructions.

2.4.3 DNA ligation

The ligation of DNA fragments was performed using the Quick Ligation kit (New England Biolabs). A reaction volume of 20 µl contained 10 µl 2x Quick Ligase reaction buffer and a molar ratio of 1:3 (vector to insert) was used. 1 µl of the Quick Ligase was added last and the reaction incubated at room temperature for 5 min. The entire reaction volume was used for transformation of competent *E. coli.*

2.4.4 Transformation

Chemically competent TOP10 *E. coli* cells were thawed on ice and 50 – 100 µl were mixed with the freshly ligated plasmid DNA. After 30 min incubation on ice, the cells were heat-shocked for 90 seconds at 42 °C and allowed to recover for 2 min on ice. Next, 500 µl LB medium was added to the cells, followed by an incubation at 37 °C for 1 hour. Cells were plated onto LB-agar plates containing 100 µg/ml ampicillin and plates were incubated at 37 °C over-night.

2.4.5 Recovery of plasmid DNA from *E. Coli*

LB medium supplemented with the appropriate antibiotic at concentrations described above were inoculated with a single colony from an LB-agar plate. Depending on the volume of the bacterial over-night culture, either the Qiagen mini-prep kit (small scale: ~ 2 ml bacterial culture) or the Qiagen midi-prep kit (large scale:

~ 50 ml bacterial culture) was used according to the manufacturer's instructions. If the plasmid DNA was used for transfection of mammalian cells, a step of 30 min incubation with endotoxin removal buffer (Qiagen) was included into the process of plasmid DNA isolation, as advised by the manufacturer.

2.4.6 Sequencing of plasmids

Plasmids were sequenced based on the Sanger dideoxynucleotide method. The BigDye Terminator v3.1 Cycle sequencing Kit (Applied Biosystems) was used and a 10 µl reaction contained: ~ 200 ng plasmid DNA prepared with a mini-prep kit, 4 µl BigDye mix, 2 µl of 5 µM primer.

After an initial denaturation for two minutes at 96 °C, a cycle with the following parameters was repeated 25x: 30 seconds denaturation at 96 °C, 15 seconds annealing at 50 °C and four minutes extension at 60 °C. The subsequent sequencing steps were performed at the Edinburgh Genomics Facility (University of Edinburgh, King's Buildings) and the resulting sequencing files were analysed using the Lasergene software or the Benchling online platform.

2.4.7 Genomic DNA extraction

Cells were harvested and lysed in 1 ml lysis buffer (see Table 1) per 5 x 10^6 cells. RNase A was added (20 µg/ml final concentration) and lysates were incubated for two hours at 37 °C. Proteinase K was added (100 µg/ml final concentration) and lysates were incubated over-night at 37 °C. The genomic DNA was isolated following a standard phenol/chloroform extraction procedure, precipitated with ethanol, and resuspended in TE buffer (see Table 1). Purity and concentration of the genomic DNA was determined using a NanoDrop 2000 spectrophotometer (Thermo Fisher Scientific).

2.4.8 PCR to amplify the CRISPR/Cas9 target site in the CDK1 gene

To characterise the CRISPR/Cas9 cut site, the sequence within the CDK1 gene was amplified using PCR. This was performed with Phusion High-Fidelity DNA Polymerase, suitable primer (see Table 3), and the genomic DNA as a reaction template. The PCR reactions were prepared in a total volume of 50 µl and contained 200 µM of each dNTP, 500 nM of forward and reverse primer, 250 ng genomic DNA and 0.5 µl of Phusion polymerase in 1x dilution of the provided reaction buffer. After an initial denaturation for 30 seconds at 98 °C, 30 cycles of following parameters were performed: 10 seconds denaturation at 98 °C and 60 seconds extension at 72 °C. A final extension was performed for 10 minutes at 72 °C. Yield and specificity of the PCR reaction was determined by agarose gel electrophoresis and the desired 500 bp fragment was excised from the agarose gel and purified. Next, the DNA fragment was cloned into the pCRII-Blunt-TOPO vector (Thermo Fisher Scientific) according to the manufacturer's instructions. This allowed the sequencing of the PCR fragment using a standard T7 promoter primer (see Table 3).

2.4.9 Generation of expression constructs

CENP-B^{DBD}-EYFP-HP1α

The initial vector expressing the CENP-B^{DBD}-EYFP-HP1α construct was cloned by Oscar Molina, Nuno M. C. Martins and Stephen Barrass. The sequence coding for the DNA-binding domain (DBD) of human CENP-B (aa 1–159) was codon-optimised for expression in human cell lines and synthesised by GeneArt (Thermo Fisher Scientific). The synthesised DNA was cloned into the NheI and AgeI restrictions sites of the pYIP-EYFP vector, containing attL and attR sites for Gateway cloning. The HP1α sequence was amplified from a HeLa cells cDNA library using the primers described in Table 3. The DNA fragment corresponding to HP1α was cloned into the pENTR vector and Gateway cloning was performed according to the manufacturer's instructions (Thermo Fisher Scientific), resulting in a construct expressing CENP-B^{DBD}-EYFP-HP1α

under a CMV promoter. This construct was lacking a stop codon after the HP1α sequence, allowing the fusion of additional proteins to the tethering construct. For the final vector, I introduced a stop codon after the codon coding for serine191 of HP1α by performing site-directed mutagenesis using the QuikChange II kit (Stratagene) (see Table 3 for the used oligonucleotides).

CENP-B^{DBD}-mut-EYFP-HP1α

To generate the vector expressing CENP-B^{DBD}-mut-EYFP-HP1α, the DNA fragment corresponding to the human CENP-B DNA-binding domain (1–159aa), but coding for the substitutions S40A, N120A, R125A, was synthesised by GeneArt (Thermo Fisher Scientific) and cloned into the NheI and AgeI restriction sites of the pYIP CENP-B^{DBD}-EYFP-HP1α vector, replacing the sequence of the wildtype CENP-B DNA-binding domain.

EYFP-HP1α

To generate the vector expressing EYFP-HP1α, the CENP-B^{DBD}-EYFP-HP1α vector was digested with ClaI and AgeI, which removed the CENP-B DNA-binding domain sequence between those restriction sites. The single stranded DNA ends were blunted by using 1 unit of T4 DNA polymerase (New England Biolabs) and 500 µM of each dNTP. The reaction was incubated for 10 minutes at 12 °C prior to heat inactivation for 10 minutes at 75 °C, followed by the above-described ligation protocol.

HP1 mutations in the CENP-B^{DBD}-EYFP-HP1α vector

The three HP1α mutants CENP-B^{DBD}-EYFP-HP1α^{V22M}, CENP-B^{DBD}-EYFP-HP1α^{I165E}, and CENP-B^{DBD}-EYFP-HP1α^{W174A} were generated using site-directed mutagenesis. The oligonucleotides described in Table 3 were used with the QuikChange II kit (Stratagene) to introduce the desired base changes.

2.5 Immunoblotting

Whole-cell lysates were prepared from HeLa cells that were transfected either with the indicated siRNAs or the indicated constructs 24 h before harvesting. Cells were lysed in reducing sample buffer (see Table 1), boiled at 95 °C for 5 min and sonicated for 20 min (settings: 30 s on, 30 s off, high intensity) using the Bioruptor sonication device (Diagenode). Proteins were resolved using sodium dodecyl sulphate polyacrylamide gel electrophoresis (SDS-PAGE). Polyacrylamide gels were prepared using a 30% acrylamide/bis-acrylamide solution (Ratio 37.5:1) (Severn Biotech) and the upper or lower gel solutions (see Table 1).

After proteins were transferred to a nitrocellulose membrane (GE Healthcare) in transfer buffer (see Table 1), the membrane was blocked with 5 % (w/v) milk in PBS with 0.05% Tween20 (VWR) (PBS-Tween) or with SuperBlock (PBS) blocking buffer (Thermo Fisher Scientific) for 1 hour and subsequently incubated with the appropriate primary antibodies (Table 6). The membrane was washed three times with PBS-Tween for 5 min and incubated with the appropriate secondary antibodies (Table 7) for 45 min. When determining the fluorescence intensities by using the imaging systems Odyssey or Odyssey CLx (LI-COR Biosciences), two PBS-Tween washes and a final PBS wash were performed before detection. When determining the HRP activity after incubation with ECL substrate (Thermo Fisher Scientific) by using the ChemiDoc MP imaging system (BioRad), three PBS-Tween washes were performed before detection.

Table 6 – Primary antibodies - Immunoblotting

Antibody	Dilution	Source	Lot no.
HP1α	1:750	Merck Millipore; 15.19s2 05-689	2908595
GAPDH	1:2,500	Abcam; ab9485	
α-tubulin	1:3,000	Sigma-Aldrich; B512	
Mad2	1:5,000	Bethyl; A300-301A	2
GFP	1:1,500	Thermo Fisher Scientific; A-11122	1828014
CDK1	1:200	Abcam; A17, ab18	GR133813-4

Table 7 – Secondary antibodies - Immunoblotting

Antibody	Dilution	Source
IRDye 680rd	1:10,000	LI-COR Biosciences
IRDye 800cw	1:10,000	LI-COR Biosciences
ECL horseradish peroxidase-linked	1:5,000	GE Healthcare

2.6 Cell culture

Cells were grown in Dulbecco's modified Eagle medium (DMEM; Thermo Fisher Scientific) supplemented with 10 % foetal bovine serum (FBS), penicillin (100 U/ml) and streptomycin (100 µg/ml) at 37 °C / 5% CO2 in a humidified atmosphere. Cells were washed with Dulbecco's phosphate buffered saline (DPBS; Thermo Fisher Scientific) and incubated with TrypLE (Thermo Fisher Scientific) at 37 °C for five minutes. Cells were diluted with media to an appropriate concentration and the procedure was repeated every other day.

2.7 Transient transfection

Transient transfection for fixed cell experiments was performed using jetPRIME according to the manufacturer's instructions (Polyplus Transfection). Cells were seeded in 12-well plates for indirect immunofluorescence experiments or in 6-well plates for immunoblotting experiments. 125 to 500 ng plasmid DNA and, where indicated, siRNA oligonucleotides (50 nM final concentration) were added to 100 µl of jetPRIME buffer. Additionally, 125 ng of UltraPure Salmon Sperm DNA (Thermo Fisher Scientific) or 40 nM of the 21mer oligonucleotide CGUACGCGGAAUACUU-CGAdTdT (Elbashir et al., 2001) was added to the transfection mixture, serving as a carrier to improve the transfection efficiency as previously reported (Pradhan and Gadgil, 2012). After vortexing, 2 µl of jetPRIME were added, followed by an additional vortexing step and 10 minutes incubation. The final mixture was added dropwise to the cells.

Transient transfection for live cell imaging experiments was performed with the Neon transfection system (Thermo Fisher Scientific). 2 – 4 x 10^5 cells were diluted in 100 µl buffer R of the Neon transfection kit and 1.5 – 4 µg of plasmid DNA was added. The electroporation parameter used are described in Table 8.

Table 8 – Neon transfection parameter

Cell Line	Pulse Voltage	Pulse Width	Pulse Number
HeLa	1,035 V	35 ms	2
U2OS	1,230 V	10 ms	4

2.8 Indirect immunofluorescence microscopy

Cells were grown on 16 mm polylysine-coated coverslips in 12 well plates. Cells were fixed for 10 min using pre-warmed 4% formaldehyde (Thermo Fisher Scientific) in PBS, permeabilised for 10 min with 0.5 % Triton X-100 (BioRad) in PBS and blocked

for 1 hour with 10 % donkey serum (Jackson ImmunoResearch) in PBS. Cells were incubated for 1 hour with primary antibodies diluted in PBS with 0.05 % Tween20 and 5 % donkey serum as indicated in Table 9. Cells were washed three times with PBS, prior to the incubation with suitable Alexa Fluor 488, 594, or 647 labelled secondary antibodies (Thermo Fisher Scientific). DNA was stained using Hoechst 33342, coverslips were mounted on glass slides using ProLong Diamond Antifade (Thermo Fisher Scientific) and cured for at least 24 h before imaging. For experiments in which pre-extraction was performed, cells were incubated for 1 min in pre-warmed PHEM buffer with 0.1% Triton X-100 prior to fixation. In experiments staining for Dsn1ph, the pre-extraction buffer contained 1x PhosSTOP (Roche).

Cold-stable microtubule assays were performed 24 h after transfection and cells were incubated in ice-cold Leibovitz's L-15 medium (Thermo Fisher Scientific) supplemented with 20 mM HEPES for 10 minutes on ice. Subsequently, cells were fixed in 4% formaldehyde in PBS containing 0.2% Triton X-100. Staining was performed as described above.

Imaging of fixed cells was performed using the widefield DeltaVision Spectris microscope (Applied Precision) with a 60× NA 1.4 PlanApo or a 100× NA 1.4 Plan Apochromat objective. Optical sections were acquired every 0.2 µm with a CoolSNAP HQ CCD camera (Photometrics). Deconvolution was performed using the softWoRx software (Applied Precision) and images were adjusted for display using OMERO.figures (Allan et al., 2012). Image stacks are shown as maximum intensity projection.

Table 9 – Primary antibodies - Immunofluorescence microscopy

Antibody	Dilution	Source	Lot no.
α-tubulin	1:500	Sigma-Aldrich; DM1A	074M4789V
Aurora B	1:600	Abcam; ab2254	GR171000-1
Aurora B	1:500	BD Transduction Laboratories; 611082	
CENP-C	1:500	Earnshaw lab.; R554; (Saitoh *et al.*, 1992)	
cyclin A2	1:100	Abcam; 6E6; ab16726	GR236737-14
cyclin B1	1:25	Santa Cruz Biotechnology; GNS1 sc-245	C2715
Dsn1ph	1:1,000	Iain Cheeseman; (Welburn *et al.*, 2010) phosphorylated Ser100/Ser109	
H2AT120ph	1:500	Active Motif; 61195	31511001
H3S10ph	1:400	Merck Millipore; 06-570;	L1003
H3S10ph	1:500	Hiroshi Kimura; 313	
H3T3ph	1:500	Hiroshi Kimura; 16B2	
Hec1	1:500	Abcam; 9G3; ab3613	GR260581-30
HP1α	1:200	Merck Millipore; MAB3584	2726144
MPM2	1:400	Abcam; ab14581	

2.9 Live cell imaging

For live cell imaging experiments determining the mitotic timing and frequency of abnormalities, cells were grown on imaging chambers CG with a glass bottom and DIC lid (Zell-Kontakt). The medium was exchanged to Leibovitz's L-15 medium (phenol red free) with 10 % FBS. Live cell imaging movies were captured with the Eclipse Ti wide-field microscope (Nikon) using a Plan Apo 60× NA 1.4 objective and in an environmental chamber at 37°C.

Optical sections were collected with a spacing of 2 µm using the ORCA-Flash 4.0 CMOS camera C11440-22CU (Hamamatsu), with 2 × 2 binning to enhance the signal intensity. Expression levels of the HP1α tethering constructs were determined by the EYFP intensity measured with Fiji (Schindelin et al., 2012). Maximum intensity

values of EYFP were measured in the frame in which NEB occurred by applying a region of interest (ROI) to chromatin. The measured value was subtracted by the mean value of three ROIs applied to the cytoplasm of the same cell.

Values from 300 – 1000 were assigned as low expression, from > 1000 – 3000 as medium expression, and from > 3000 to 6000 as high expression. Cells with EYFP values below 300 and above 6000 were excluded, since weak expression meant that lagging chromosomes could not be identified reliably and very high expression caused the HP1α tethering constructs to localise to non-centromeric regions on chromosomes.

2.10 Live cell imaging with labelled Fab fragments

For live cell imaging experiments with labelled Fab fragments, cells were grown in 35 mm glass bottom dishes (ibidi), which were covered with DIC lids (ibidi). Bead loading of the Fab fragments (Table 10) was performed as following:

Culture medium was aspirated and 2 µl of the Fab fragment solution were pipetted in the centre of the glass part. A single layer of glass beads (106 µm, Sigma-Aldrich) was sprinkled onto the cells. Next, the dish was firmly struck ten times against the hood table top and immediately 2 ml of pre-warmed antibiotic-free medium were added. Cells were repeatedly washed with medium to remove the glass beads and left in Leibovitz's L-15 medium (phenol red free) with 10 % FBS at 37°C and 5% CO2 in air for 2 to 4 hours prior to imaging. Imaging was performed using the earlier described Eclipse Ti widefield microscope (Nikon) with either a Plan Apo 100× NA 1.40 or Plan Apo 60× NA 1.4 objective. Movies were deconvolved using AutoQuant X3 (version X3.1.2) and maximum intensity projected.

Table 10 – Fab fragments

Fab Fragment	Source	Reference
H3S10ph (Fab313)	Hiroshi Kimura	(Hayashi-Takanaka *et al.*, 2009)
H3T3ph (Fab16B2)	Hiroshi Kimura	(Kelly *et al.*, 2010)

2.11 Automated quantification of histone H3S10ph-positive G_1 cells

Fixed cells were captured using the Eclipse Ti wide-field microscope (Nikon) with a Plan Fluor 40× NA 1.3 objective and optical sections were collected with a spacing of 0.7 µm using the CMOS camera ORCA-Flash 4.0 C11440-22CU (Hamamatsu). The software CellProfiler (Kamentsky *et al.*, 2011) was used to determine the number of histone H3S10ph-positive nuclei in transfected G_1 cells. Image stacks were maximum intensity projected and saved as TIFF files using the CellProfiler modules "MakeProjection" and "SaveImages". The quantification was performed as following:

In an initial step, the modules "IdentifyPrimaryObjects", "MeasureObjectIntensity", "ClassifyObjects", and "FilterObjects" were used to identify interphase nuclei and to distinguish them from mitotic cells based on the Hoechst 33342 staining. Next, "MeasureObjectIntensity", "ClassifyObjects", and "FilterObjects" were used to identify transfected cells based on the EYFP signal. The modules "MeasureObjectIntensity", "ClassifyObjects", and "FilterObjects" were also used to identify G_1 cells based on cyclin A2-negative nuclei (Alexa 647 fluorescence signal). Finally, "MeasureObjectIntensity" and "ClassifyObjects" were used to identify cells positive for histone H3S10ph (Alexa 594 fluorescence signal).

2.12 Automated quantification of Dsn1ph signal

The DeltaVision widefield micro scope (details described above) were used to capture fixed cells that were transfected. Images were deconvolved and sum intensity projected using the SoftWoRx software (Applied Precision). Image analysis was performed using a modified standard CellProfiler pipeline. Chromosomes were identified using the "IdentifyPrimaryObjects" module based on the Hoechst 33342 staining. Next, the Hec1 signal (Alexa 594) was identified using the "IdentifyPrimaryObjects", "EnhanceOrSuppressFeatures", and "MaskImage" modules. The Hec1 segmentation was expanded by 1 pixel using the "ExpandOrShrinkObjects" module, because the Hec1 signal did not completely

overlap with that of Dsn1ph. The quantification of the Dsn1ph signal (Alexa 647) was performed using the "MeasureObjectIntensity" module.

Some of the analysed cells exhibited Dsn1ph intensity values with up to 600 times the intensity of the median. To ensure that the results of the analysis were not distorted by these extreme values, I applied a general cut-off value of 10 in the same way in all experiments and repeats and cells were excluded if they exhibited values above this cut-off. This resulted in the exclusion of following cell numbers: CB-EY-HP1α: four cells; CB-EY-HP1α ^{W174A}: none; untransfected cells: three cells.

2.13 Microtubule quantification after cold treatment

The overall microtubule intensity after cold treatment was determined manually using the Fiji software (Schindelin *et al.*, 2012). Image stacks were sum intensity projected and an ROI was applied to the mitotic spindle. The measured RawIntDen value was subtracted by a RawIntDen ROI value measuring the background.

2.14 Flow cytometry

Hela cells grown in 6-well plates were transfected with the appropriate constructs or left untransfected. 24 hours after transfection, the cells were treated 3 µM ZM447439 or an equivalent amount of DMSO for 5 h, harvested and resuspended in ice-cold 70% ethanol for fixation. Ethanol-fixed cells were washed in 0.05% Tween20/PBS containing 1% BSA. Indirect immunofluorescence staining was performed using the MPM2 antibody (see Table 9) and subsequently incubated in PBS containing 5 µg/ml Hoechst 33342 over-night. Detection was performed using an LSRII flow cytometer (BD Biosciences). The FlowJo 8.7 software was used to set appropriate gates and the percentage of cells positive for the MPM2 staining was determined within the whole population of transfected cells.

As a side note, the mitotic index upon CB-EY-HP1α expression in this flow cytometry experiment (Fig. 17C) varied from the mitotic index shown in Figure 5B. This is most likely because of the different detection methods used, which were fluorescence microscopy for Fig. 5B and flow cytometry for Fig. 17C. Based on the flow cytometry results, the transfection efficiency was over 99%. However, analysis by eye, using a fluorescence microscope, suggested a transfection efficiency of ~ 70%. The difference might be due to the ability of the flow cytometer to detect cells with very low levels of expression. This assumption is supported by the fact that an adjustment of the gates in the flow cytometry experiment to ~ 70% CB-EY-HP1α transfection efficiency increased the mitotic index to 10.3% for CB-EY-HP1α expressing cells treated with DMSO and was, therefore, more similar to the mitotic index shown in Figure 5B. At the same time, the mitotic index of CB-EY-HP1α expressing cells treated with ZM447439 increased only from 3.9% to 4.2% after I altered the gating.

2.15 Fluorescence Recovery After Photobleaching (FRAP)

FRAP experiments were performed using a Leica SP5 confocal microscope with a 63×, 1.4 NA objective and an argon laser (laser line 488 nm). HeLa cells were grown on 25 mm round polylysine-coated coverslips and transfected with the appropriate constructs 24 h prior to the FRAP measurements. The medium was exchanged to FluoroBrite DMEM (phenol red free; Thermo Fisher Scientific) with 10 % FBS and cells were kept at 37 °C and 5% CO2 in air in an environmental chamber (Life Imaging Services) during imaging. For the FRAP experiment, first five pre-bleach images were captured followed by bleaching a ROI of 1.6 µm diameter for 1 s at full laser power, choosing a region where the individual HP1α-fusion constructs clustered in interphase cells. The subsequent images were captured in three different phases. The initial phase consisted of 20 frames every 0.65 seconds to capture a rapid recovery. The subsequent phase consisted of 30 frames every 2 seconds to capture slower

stages of recovery. The final phase consisted of 45 frames every 5 s to capture the complete recovery of all constructs.

Image processing was performed using the Image-Pro Premier software (Media Cybernetics). The intensity measurements were corrected for photobleaching and the values were normalised according to (Phair and Misteli, 2001), by applying an ROI to the bleach spot, to the background and to a non-bleached area of an adjacent cell. Normalisation was performed based on the five pre-bleach images. The halftime of recovery was calculated from the normalised values of ten cells.

3 Results chapter 1: Tethering HP1α to centromeres results in a mitotic delay and increased segregation errors

3.1 Tethering HP1α to the centromere via fusion to a CENP-B DNA-binding domain results in a mitotic delay

To investigate the effect of tethering HP1α at mitotic centromeres in HeLa cells, I used a fusion construct linking HP1α to the DNA-binding domain of CENP-B (CB) (Pluta *et al.*, 1992) and enhanced yellow fluorescent protein (EYFP / EY). I will refer to this construct as CB-EY-HP1α and also apply this nomenclature to the control constructs consisting of only yellow fluorescent protein (EY) or untethered HP1α (EY-HP1α) (Fig. 5A). The transient expression of CB-EY-HP1α resulted in a clear increase in the number of mitotic cells (Fig. 5B). Importantly, cells expressing the untethered HP1α (EY-HP1α) lacking the CENP-B DNA-binding domain, did not show an altered mitotic index compared to control cells expressing only yellow fluorescent protein (EY).

In a more detailed analysis, I determined the distribution of the individual mitotic stages in cells expressing the CB-EY-HP1α construct (Fig. 5C). This tethering of HP1α to centromeres led to an altered mitotic distribution with a clear accumulation of metaphase cells and a concomitant decrease in the number of cells in anaphase and telophase. Cells expressing the untethered HP1α construct EY-HP1α also showed no altered behaviour compared to control cells expressing only EYFP in this experiment. Both exhibited a similar mitotic progression profile with no statistically significant difference between the various mitotic phases.

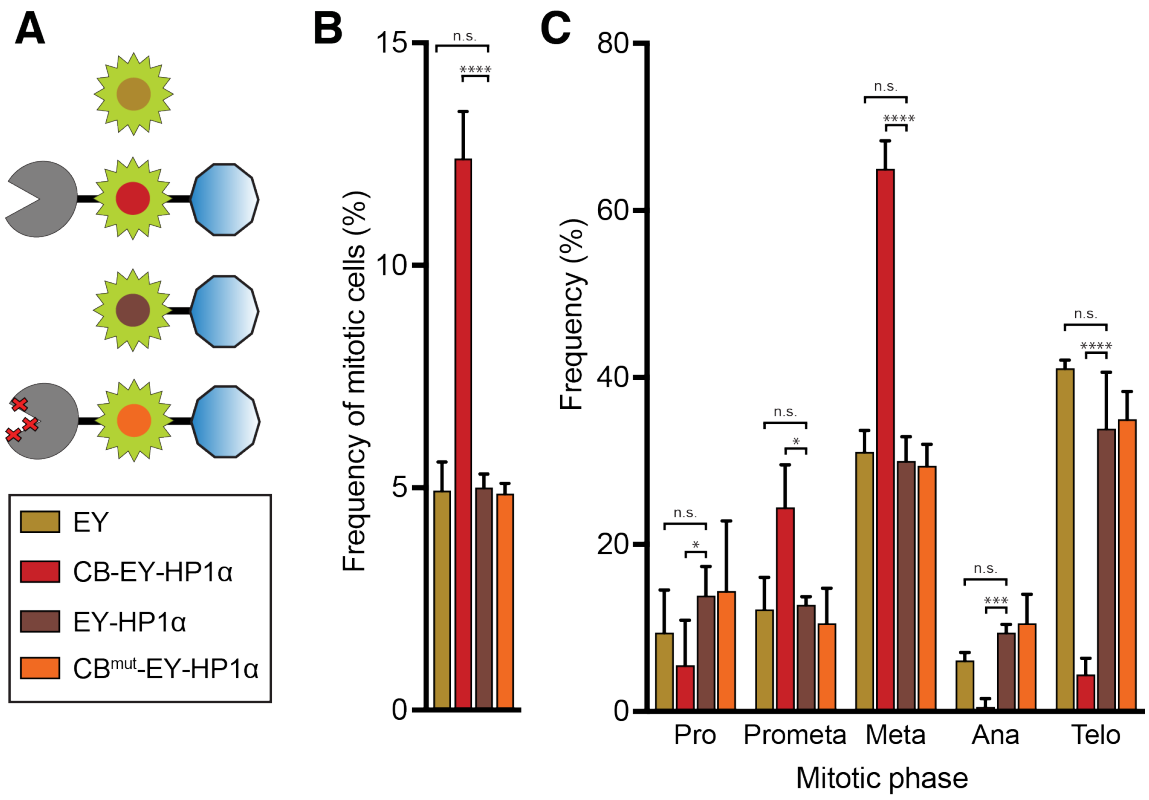

Figure 5: Tethering HP1α to the centromere via fusion to a CENP-B DNA-binding domain results in a mitotic delay.

(A) Schematic representation of the HP1α tethering constructs and different controls. HP1α (blue) is fused to EYFP (EY - green) and the DNA-binding domain of CENP-B (CB - grey), resulting in CB-EY-HP1α.

(B) Frequency of mitotic HeLa cells 24 h after transfection with the indicated constructs. Graphs represent the mean and standard deviation of three independent experiments, with n=500 cells per experiment. Statistical analysis: Fisher's exact test followed by the Benjamini–Hochberg multiple comparison test. ****, $P < 0.0001$; n.s., not significant.

(C) Frequency of the different mitotic phases in HeLa cells 24 h after transfection with the indicated constructs. Graphs represent the mean and standard deviation of three independent experiments, with n=60 mitotic cells per experiment. Statistical analysis: Fisher's exact test followed by the Benjamini–Hochberg multiple comparison test. *, $P < 0.05$; ***, $P < 0.001$; ****, $P < 0.0001$; n.s., not significant.

To analyse whether the chimeric CB-EY-HP1α specifically localises to centromeres, I transiently expressed this construct in HeLa cells and performed immunofluorescence staining for the centromere protein CENP-C (Fig. 6). Additionally, I stained for tubulin which facilitates the identification of the individual mitotic stages. The fluorescence microscopy analysis revealed that CB-EY-HP1α localises throughout the centromeric region beneath the kinetochore in mitotic cells, which is consistent with the normal localization of the CENP-B protein in HeLa cells (Cooke et al., 1990). These results confirm that specific tethering of HP1α to the centromere is possible using the CB-EY-HP1α construct.

3.2 Modulating the binding dynamics of the CENP-B tethering construct rescues the mitotic delay

To test whether the strength of HP1α tethering affects the metaphase delay phenotype, I mutated the CENP-B DNA-binding domain to perturb its DNA binding properties. I substituted the amino acid residues S40, N120 and R125 with alanine, resulting in the construct CB^{mut}-EY-HP1α. These residues were selected in consultation with A. Jeyaprakash Arulanandam based on their specific contacts with the DNA of the CENP-B boxes in the crystal structure of Tanaka and colleagues (Tanaka *et al.*, 2001) and their high degree of conservation among the following species: *Homo sapiens*, *Mus musculus*, *Cricetulus griseus*, *Rattus norvegicus*, *Schizosaccharomyces pombe* (CENP-B homolog protein1 and 2), *Ornithorhynchus anatinus*, *Bos taurus*, *Cavia porcellus*, *Macaca mulatta*, and *Pediculus humanus*. The sequence alignment and the diagram of the crystal structure (PDB: 1HLV) highlighting the mutated residues in "stick" were made by A. Jeyaprakash Arulanandam (Fig. 7).

Importantly, the mutant construct CB^{mut}-EY-HP1α did not cause cells to accumulate in mitosis compared to EYFP or EY-HP1α expressing cells and also did not show an altered mitotic phase distribution profile (Fig. 5).

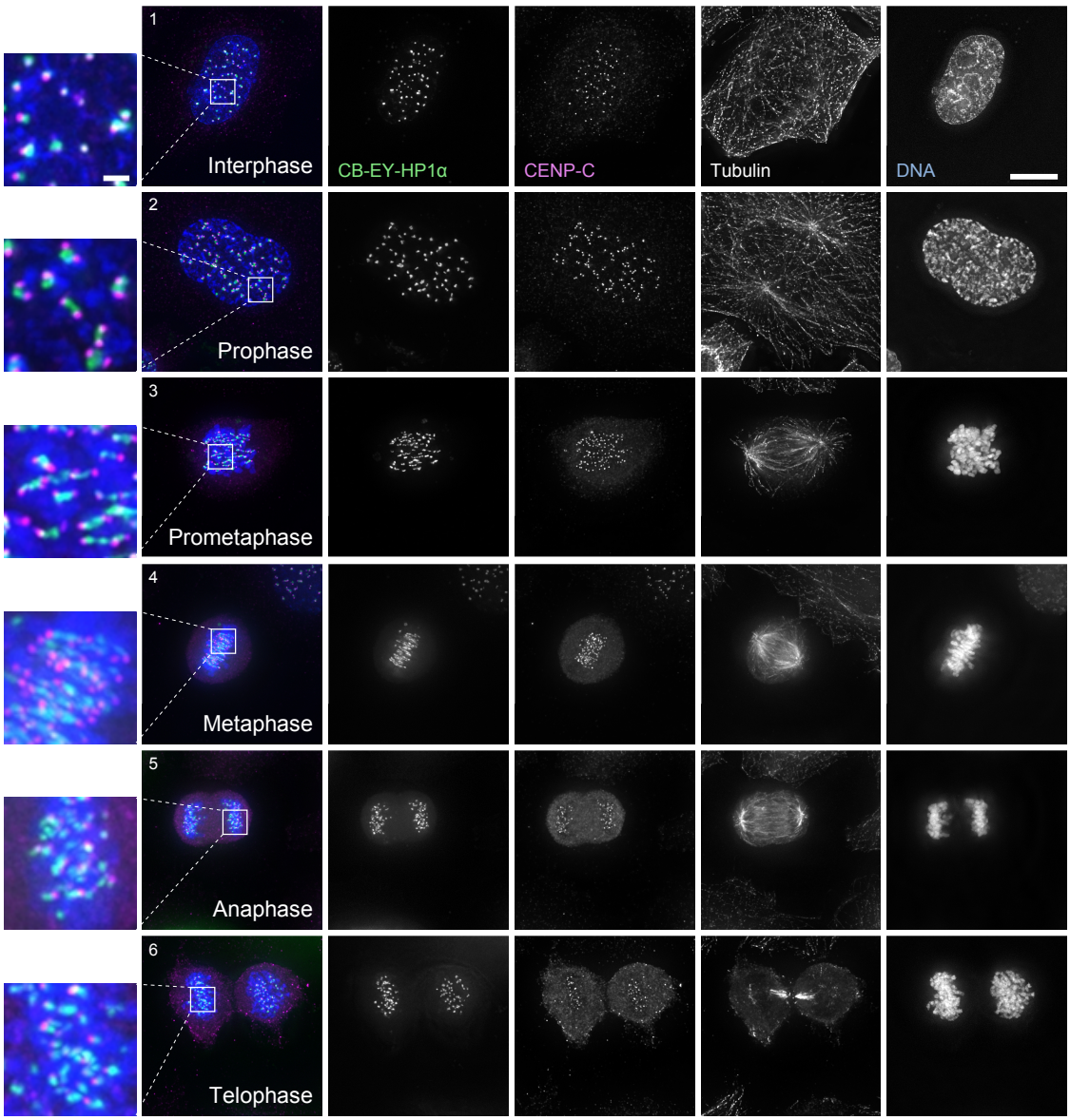

Figure 6: CB-EY-HP1α localises specifically to centromeres throughout the cell cycle.
Immunofluorescence analysis of Hela cells 24 h after transfection with a construct expressing CB-EY-HP1α (shown in green). Cells were stained with Hoechst 33342 (blue) and immunostained with antibodies recognising kinetochore marker CENP-C (magenta) and α-tubulin. Scale bar, 5 µm; in zoom, 1µm.

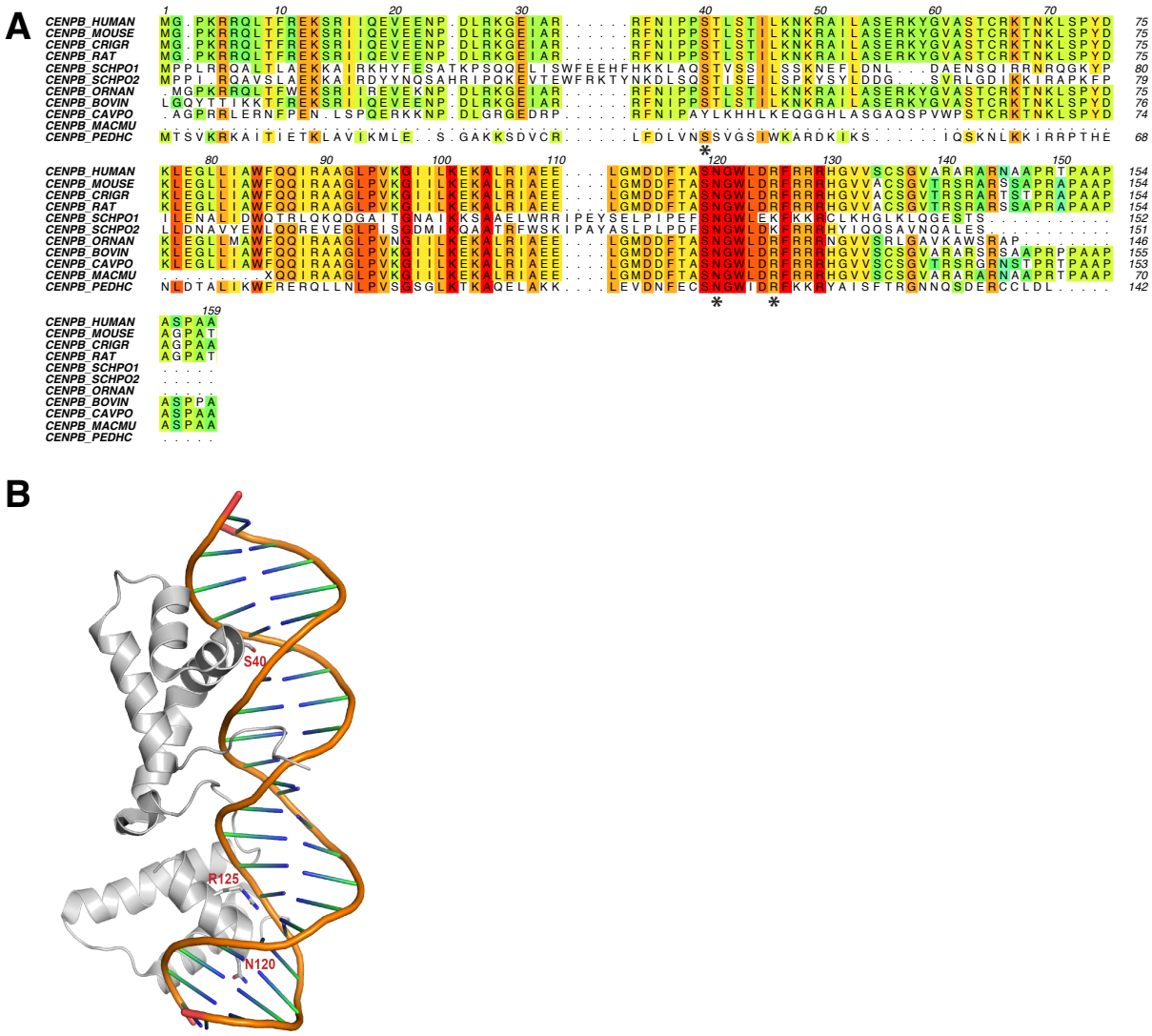

Figure 7: Selected amino acid residues of the CENP-B DNA-binding domain were mutated to perturb its DNA binding properties.

(A) Protein sequence alignment of the CENP-B DNA-binding from different species. Multiple sequence alignment was performed by A. Jeyaprakash Arulanandam using Clustal Omega and was edited with Aline for display. Asterisks indicate the residues selected for mutation. The protein sequence from following species were used for the alignment: *Homo sapiens*, *Mus musculus*, *Cricetulus griseus*, *Rattus norvegicus*, *Schizosaccharomyces pombe* (CENP-B homolog protein1 and 2), *Ornithorhynchus anatinus*, *Bos taurus*, *Cavia porcellus*, *Macaca mulatta*, and *Pediculus humanus*.

(B) Structure of the DNA-binding domain of CENP-B (grey) is shown as a ribbon diagram interacting with DNA (coloured) (PDB code 1HLV) and was made by A. Jeyaprakash Arulanandam. Residues selected for mutation are shown in stick.

Next, I sought to determine the exact centromeric localisation of the various HP1α constructs by use of line scan profiles at different stages of mitosis. HP1α tethered via the wildtype, or mutated CENP-B DBD showed the same localisation as untethered EY-HP1α at the inner centromere of prometaphase cells, judged by the staining for CENP-C (Fig. 8A). At this stage of mitosis, centromeres are not yet under tension. However, in metaphase cells, when chromosomes biorientate and centromeres are stretched, both HP1α tethering constructs divided into two peaks that moved together with the separating CENP-C staining, whereas the untethered EY-HP1α remained concentrated as one slightly broader peak at the inner centromere (Fig. 8B). Importantly, the tethered CB-EY-HP1α remained ~ 0.2 µm internal to the CENP-C signal, indicating that it occupies the kinetochore-proximal region of the inner centromere, as previously shown for tethering experiments using the CENP-B DNA-binding domain fused to the CPC subunit INCENP (Liu *et al.*, 2009; Wang *et al.*, 2011a; Hengeveld *et al.*, 2017).

Comparing the three HP1α constructs by Western blot analysis demonstrated that they are all expressed correctly, judged by the bands running at the expected size (Fig. 8C). Furthermore, the EYFP tagged HP1α was expressed at a level comparable to endogenous HP1α in the entire culture, and both CENP-B DBD tagged HP1α constructs were expressed at levels slightly less than endogenous HP1α.

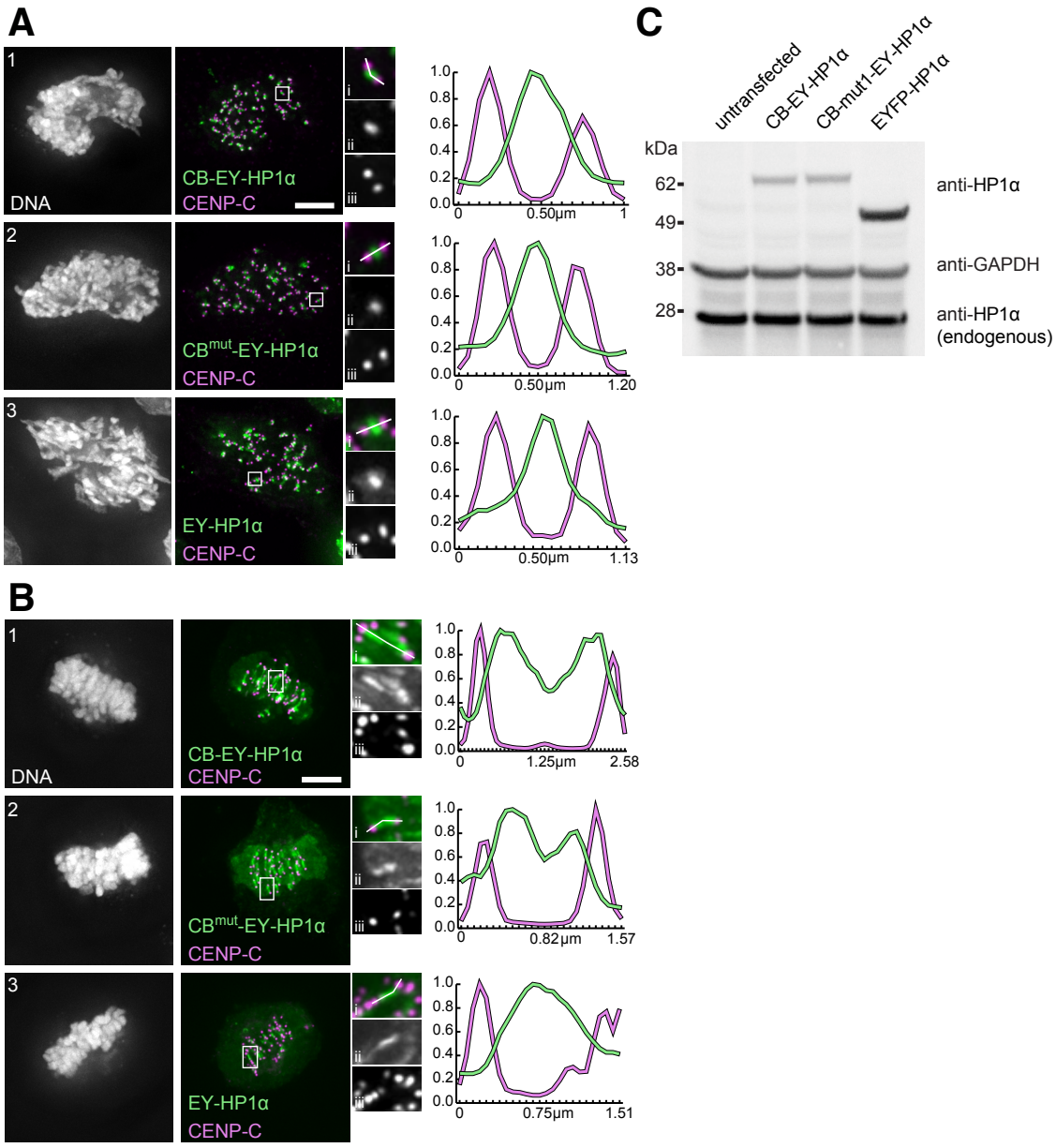

Figure 8: Localisation and expression level of chimeric HP1α tethering constructs compared to untethered HP1α.

(A, B) Immunofluorescence analysis of early prometaphase (A) or metaphase (B) Hela cells 24 h after transfection with constructs expressing CB-EY-HP1α (1), the tethering mutant CB^{mut}-EY-HP1α (2), or untethered EY-HP1α (3) (shown in green). Cells were stained with Hoechst 33342 and immunostained with an antibody recognising CENP-C (magenta) after pre-extraction with 0.1% Triton X-100/PHEM buffer for 1 min. Line scans are showing the HP1α construct and CENP-C (i); the HP1α construct alone (ii); or CENP-C alone (iii). Scale bar, 5 µm.

(C) Western blot analysis of Hela whole cell lysates 24 h after transfection with the indicated HP1α fusion constructs. Endogenous HP1α and HP1α fusion constructs were detected using an anti-HP1α antibody. GAPDH served as a loading control.

To analyse the effect of the introduced point mutations on the DNA-binding properties of the CENP-B DBD, I determined the dynamics of the different EYFP-tagged HP1α constructs using the Fluorescence Recovery After Photobleaching (FRAP) method (Fig. 9). I selected an area where HP1α was clustered in transiently transfected interphase cells, bleached a spot of 1.6 µm diameter, and measured the EYFP fluorescence recovery in three different phases (20 frames every 0.648 s, 30 frames every 2 s and 45 frames every 5 s) to capture both the dynamic recovery range and the complete steady-state recovery of the various HP1α fusion proteins.

In line with previous published observations, untethered EY-HP1α had a mean halftime of recovery ($t_{1/2}$) of 3.1 s (Schmiedeberg *et al.*, 2004). In contrast, tethering HP1α to the centromere via the DNA-binding domain of CENP-B had a substantial influence on its dynamics. The recovery halftime of CB-EY-HP1α was ~ 49 s, an increase by more than 15-fold compared to EY-HP1α. Introducing the three above-mentioned point mutations into the DNA-binding domain of the HP1α tethering construct resulted in nearly three-fold faster dynamics with a $t_{1/2}$ for CB^{mut}-EY-HP1α of 18 s. Together, these results suggest that decreasing HP1α dynamics at centromeres may be responsible for the accumulation of cells in mitosis.

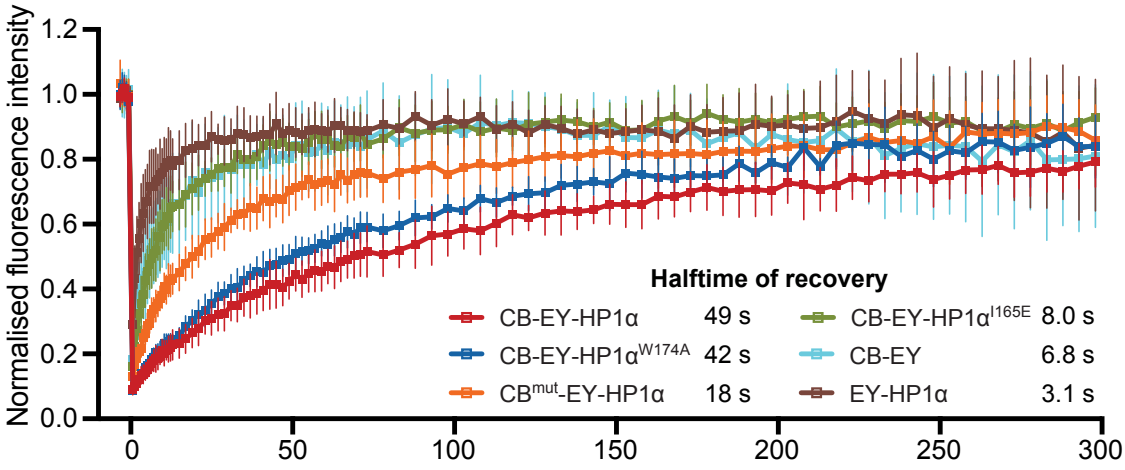

Figure 9: Binding dynamics of various HP1α tethering constructs determined by FRAP.
Quantitative fluorescence recovery after photobleaching (FRAP) analyses of the indicated EYFP containing constructs in interphase HeLa cells 24 h after transfection. Measurements were made in three different phases (20 frames every 0.648 s; 30 frames every 2 s; 45 frames every 5 s). Error bars represent standard deviation.

3.3 Preventing HP1 interaction with PxVxL/I motif-containing proteins eliminates the mitotic delay caused by centromeric HP1α tethering

HP1 interacts with a large number of client proteins as demonstrated by a previous mass spectrometry screen (Nozawa *et al.*, 2010). Therefore, I hypothesised that the mitotic delay caused by HP1α tethering to centromeres could be due to the centromeric retention of one or more of these mitotic regulators that interact with HP1α. In order to test my hypothesis, I introduced several point mutations into the HP1α domain of the CB-EY-HP1α construct that have been previously shown to perturb different HP1α functions (Fig. 10A). The V22M substitution in the chromo domain prevents HP1α binding to H3K9me2/3 (Bannister *et al.*, 2001; Lachner *et al.*, 2001; Nielsen *et al.*, 2001). The chromoshadow domain mutation I165E disrupts HP1 dimer formation, while W174A disrupts the formation of a hydrophobic pocket required to bind client proteins. Importantly, both mutations, I165E and W174A, perturb HP1 association with binding partners containing the PxVxL/I motif, but W174A does not interfere with the dimerization of HP1α (Brasher et al., 2000; Thiru et al., 2004; Nozawa et al., 2010).

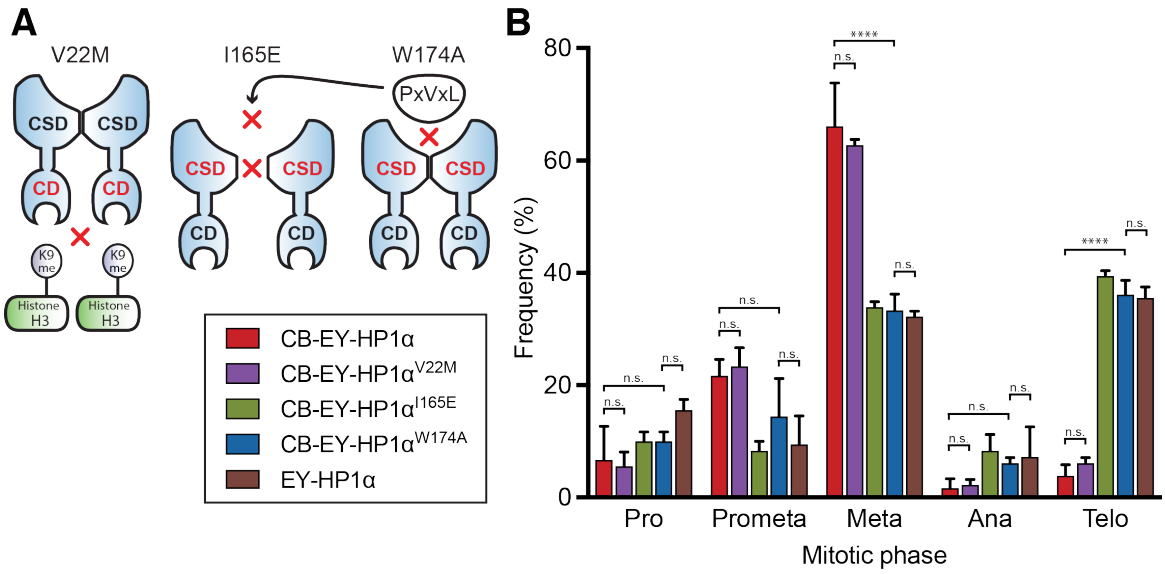

Figure 10: Preventing HP1 interaction with PxVxL/I motif-containing proteins eliminates the mitotic delay caused by centromeric HP1α tethering.

(A) Schematic representation of the tethered HP1α mutants, indicating their perturbed functions.

(B) Frequency of the different mitotic phases in HeLa cells 24 h after transfection with the indicated constructs. Graphs represent the mean and standard deviation of three independent experiments, with n=60 mitotic cells per experiment. Statistical analysis: Fisher's exact test followed by the Benjamini–Hochberg multiple comparison test. ****, $P < 0.0001$; n.s., not significant.

Western blot analysis confirmed that all HP1α mutants, when fused to the DBD of CENP-B, were expressed correctly and to a similar level (Fig. 11A). In this experiment, I used an antibody that detects the EYFP domain of the tethering constructs, in case the introduced point mutations perturb the epitope recognised by the anti-HP1α antibody used in the previous Western blot analysis (see Fig. 8C).

Fluorescence microscopy of transiently transfected cells showed that the localisation of the mutants was similar to that of CB-EY-HP1α containing wildtype HP1α, except for CB-EY-HP1α^{I165E}, which showed a higher diffuse background (Fig. 11B).

To investigate the reason for the more diffuse appearance of CB-EY-HP1α^{I165E}, I performed further FRAP experiments to determine the binding dynamics of the CB-EY-HP1α^{I165E} construct (Fig. 9). Interestingly, introducing the I165E mutation into CB-EY-HP1α, which prevents dimer formation in full-length HP1, resulted in a $t_{1/2}$ of ~ 8 s, which is more than 6-fold faster than the $t_{1/2}$ of the tethered wildtype HP1α. Moreover, for CB-EY, which consists of only the CENP-B DNA binding domain fused to EYFP without any further attached protein, I measured a similar halftime of recovery in FRAP experiments of 6.8 seconds. This suggests that CENP-B might require to dimerise for stable DNA binding. This suggestion is further supported by the FRAP result of the CSD mutant CB-EY-HP1α^{W174A}, which is able to dimerise, unlike CB-EY-HP1α^{I165E}. The halftime of recovery for CB-EY-HP1α^{W174A} was ~ 42 seconds, similar to the result of wildtype CB-EY-HP1α (~ 49 s) and a more than five-fold increase compared to the I165E CSD mutant construct. Together, these results reveal that the dimerisation mediated by HP1α results in stronger binding properties of the CENP-B DNA-binding domain.

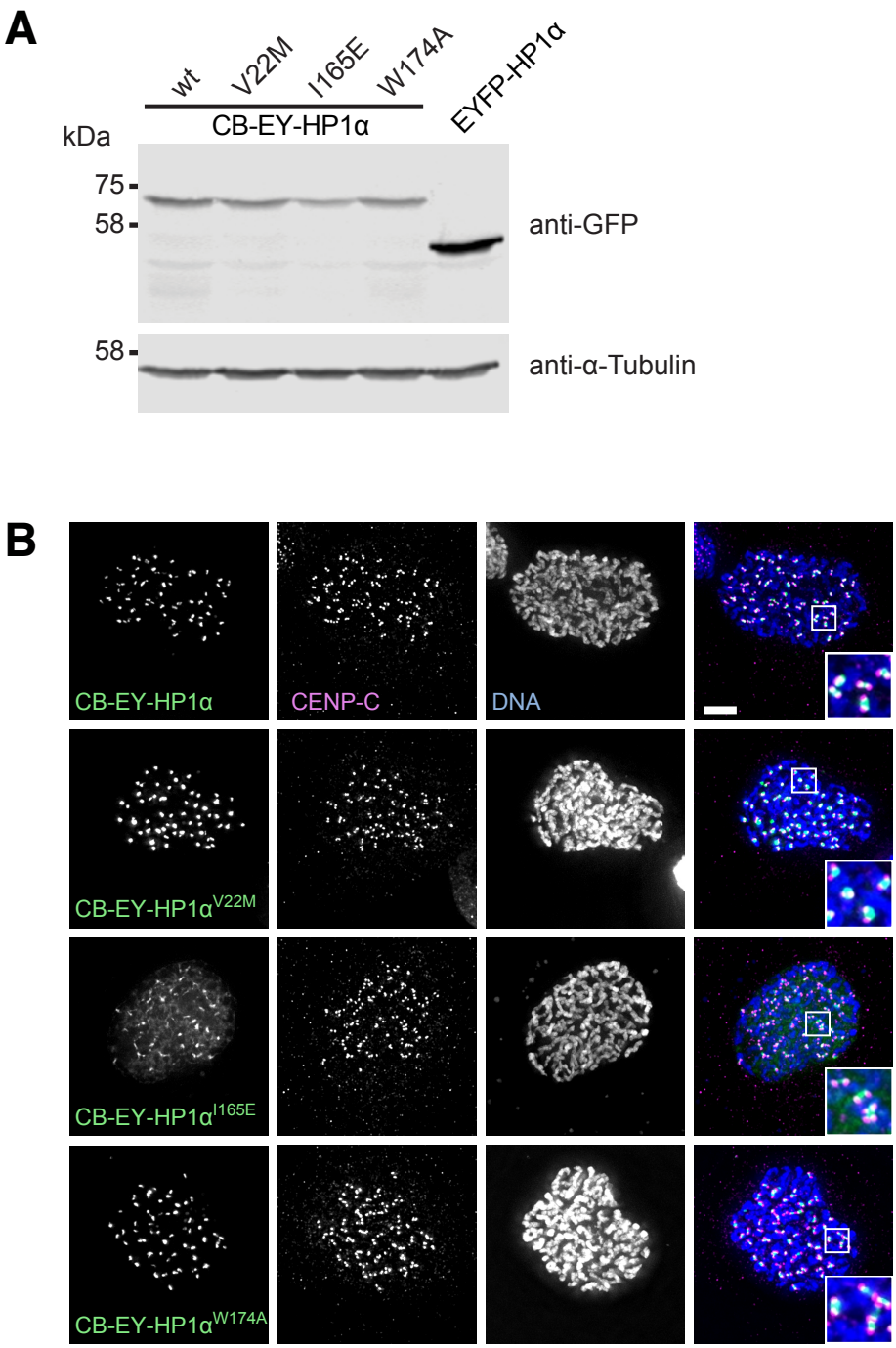

Figure 11: Expression level and localisation of different HP1α mutants fused to the CENP-B DBD.

(A) Western blot analysis of Hela whole cell lysates 24 h after transfection with the indicated HP1α fusion constructs. The HP1α constructs were detected using an anti-GFP antibody. α-tubulin served as a loading control.

(B) Immunofluorescence analysis of Hela cells 24 h after transfection with constructs expressing CB-EY-HP1α (1), or the tethered HP1 mutants CB-EY-HP1α^{V22M} (2), CB-EY-HP1α^{I165E} (3), and CB-EY-HP1α^{W174A} (4) (shown in green). Cells were stained with Hoechst 33342 (blue) and immunostained with an antibody recognising CENP-C (magenta). Scale bar, 5 µm.

Introducing the V22M mutation into CB-EY-HP1α had no effect on the metaphase delay phenotype, and its mitotic progression profile resembled that for wildtype CB-EY-HP1α (Fig. 10B). This was expected because the chimeric HP1α is tethered to centromeres via the DBD of CENP-B and therefore its localisation is unlikely to depend on the chromo domain binding to H3K9me3. Remarkably, both chromoshadow domain mutants I165E or W174A abolished the metaphase delay caused by centromeric tethering of HP1α: Cells expressing CB-EY-HP1α^{I165E} and CB-EY-HP1α^{W174A} exhibited mitotic progression profiles similar to cells expressing untethered EY-HP1α, which was shown to have no effect on mitotic progression (see Fig. 5).

These results suggest that the mitotic delay may be caused by proteins that bind to the chromoshadow domain of tethered HP1α at centromeres and most likely contain a PxVxL/I motif.

Due to the results described here, I used CB-EY-HP1α^{W174A} as a control construct for all following experiments. CB-EY-HP1α^{W174A} behaves very similarly to the wildtype CB-EY-HP1α construct regarding its expression level, specific localisation to the centromere region, and binding dynamics, however, it does not cause an altered mitotic progression, as observed upon CB-EY-HP1α expression.

3.4 Live cell imaging analysis of mitotic progression and chromosome segregation defects upon HP1α centromere tethering

I performed live cell imaging experiments to analyse the mitotic delay phenotype in greater detail and to determine the effect of HP1α centromere tethering on chromosome segregation errors.

3.4.1 The mitotic delay caused by centromeric tethering of HP1α is not a cell line specific effect

Imaging with Differential Interference Contrast (DIC) microscopy allowed me to determine precisely the times of nuclear envelope breakdown (NEB) (Fig. 12A – 0 min) and onset of anaphase (Fig. 12A – 84 min). Based on the identification of these two specific mitotic landmarks, I could accurately determine the timing of mitotic progression. Additionally, the live cell imaging indicated that cells with tethered HP1α at centromeres had no difficulties with chromosome congression. An example is shown in Figure 12A, where a well-organised metaphase plate forms within 12 minutes after NEB.

I grouped the imaged cells into categories of low (L), medium (M), and high (H) expression, depending on the level of the transiently transfected tethering construct (see the Materials and Methods chapter for a detailed explanation) (Fig. 12B). The live cell imaging experiments using HeLa cells confirmed the metaphase delay phenotype observed after wildtype HP1α tethering to centromeres in fixed cell samples (see Figs. 5C and 10B). The median ($\tilde{x}$) duration from NEB until anaphase onset in the three categories was 66 min (L), 120 min (M), and 111 (H) min, respectively. Remarkably, I could observe cells remaining over 38 hours in mitosis before anaphase onset. A robust mitotic delay was particularly present among cells expressing CB-EY-HP1α at a high level, shown by an upper quartile value of 1692 min. In contrast, cells expressing the control construct CB-EY-HP1α^{W174A} showed a progression through mitosis resembling that of untransfected cells, with a median of 36 min (L), 36 min (M), and 39 min (H), compared to 36 min of untransfected cells.

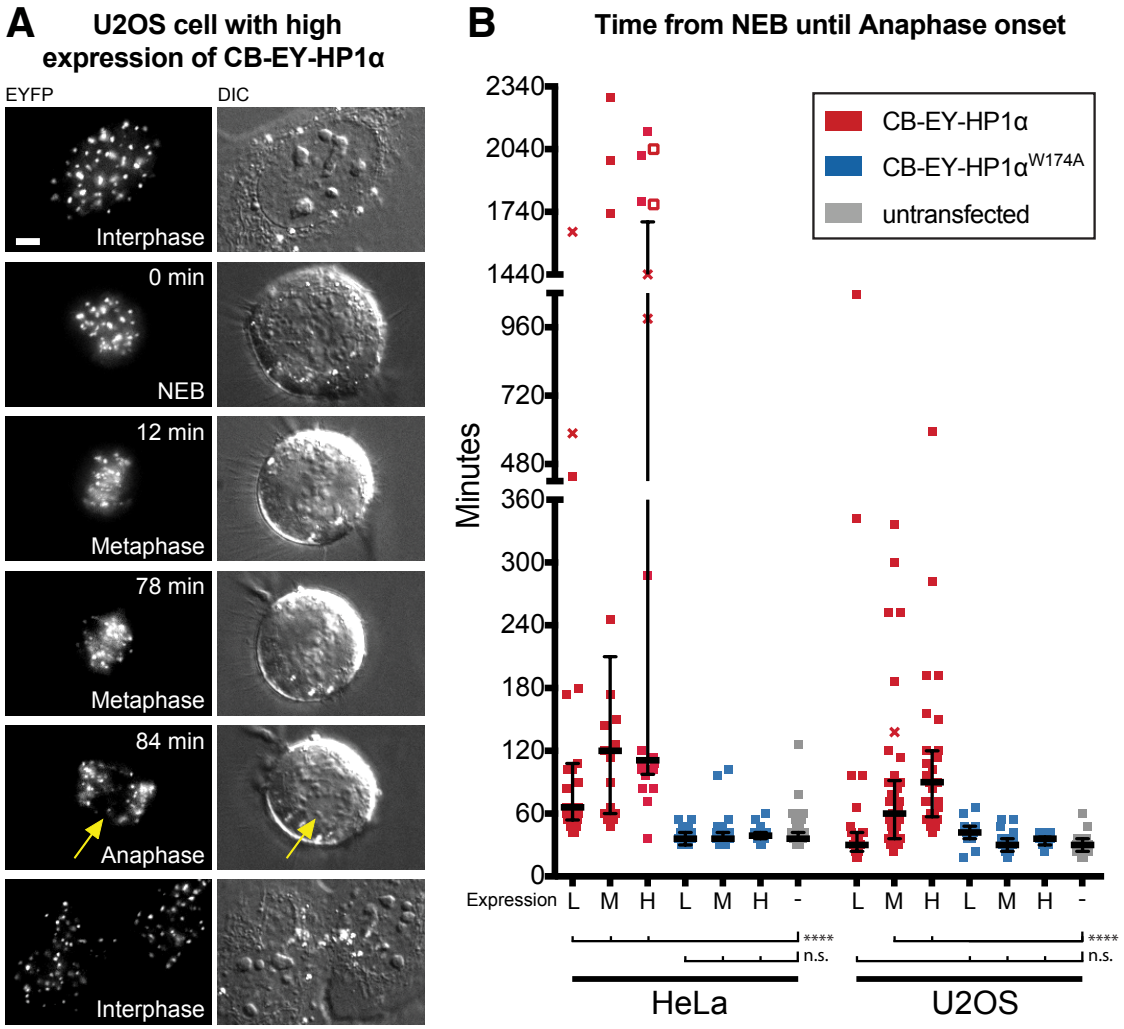

Figure 12: Live cell imaging experiments reveal the robustness of the mitotic delay caused by centromeric tethering of HP1α in different cell lines.

(A) Stills from a live cell imaging video using Differential Interference Contrast (DIC) microscopy. A U2OS cell from category "high level of CB-EY-HP1α expression" is shown. Arrow indicates lagging chromosome. Scale bar, 5 µm.

(B) Quantification of the timing from nuclear envelope breakdown (NEB) until anaphase onset analysed from live cell imaging movies of Hela or U2OS cell expressing either CB-EY-HP1α (red), CB-EY-HP1α^{W174A} (blue), or of untransfected cells (grey). Cells were grouped into categories of low (L), medium (M), or high (H) levels of protein expression (see Materials and Methods section for further details). Crosses represent cell death before the onset of anaphase, and empty squares represent the end of the movie before the onset of anaphase. Graphs indicate the median and interquartile range. Statistical analysis: Kolmogorov-Smirnov test followed by the Benjamini-Hochberg multiple comparison test. ****, $P < 0.0001$; n.s., not significant. The number of analysed cells per category are shown in Figure 13C.

Tethering HP1α to centromeres in U2OS osteosarcoma cells also produced a delayed mitotic progression in cells with a medium ($\tilde{x}$ = 60 min) or high ($\tilde{x}$ = 90 min) expression of CB-EY-HP1α compared to untransfected U2OS cells ($\tilde{x}$ = 30 min) (Fig. 12B). In contrast to Hela cells, a low expression of CB-EY-HP1α did not result in an overall delayed mitotic progression ($\tilde{x}$ = 30 min). U2OS cells expressing the mutated HP1α^{W174A} tethering construct also showed no significant difference compared to untransfected cells ($\tilde{x}$ = 42 min (L), 30 min (M), 36 min (H)).

Overall, the live cell imaging experiments confirmed the mitotic delay observed in fixed cell cultures upon tethering of wildtype HP1α to centromeres. Furthermore, the live cell imaging method indicates that it is not chromosome congression that is affected, but rather the mitotic progression after a metaphase plate is formed, revealing that CB-EY-HP1α can cause an extensive metaphase delay, whereas CB-EY-HP1α^{W174A} does not affect mitotic progression.

3.4.2 Centromere tethering of HP1α is accompanied by an increased number of cells with lagging chromosomes and micronuclei

The live cell imaging with the tethering constructs allowed me not only to define the exact duration of individual cells in mitosis but also to quantitate the frequency of chromosome segregation defects by monitoring the behaviour of fluorescently labelled centromeres. This analysis revealed that the tethering of HP1α to centromeres using the CENP-B DBD resulted in a substantial increase of lagging chromosomes: While HeLa cells expressing the control construct CB-EY-HP1α^{W174A} showed lagging chromosomes with a frequency up to 18 percent, the tethering of wildtype HP1α resulted in an increase to 42% (L), 66% (M), and 78% (H) (Fig. 13A).

In U2OS cells, I observed lagging chromosomes in 27% of cells expressing the control construct CB-EY-HP1α^{W174A} at low and medium levels Fig. 13A). This high frequency of lagging chromosomes appeared to reflect an elevated baseline value in U2OS cells and was also previously reported (Kabeche and Compton, 2013). U2OS

cells with a high expression of CB-EY-HP1α^{W174A} showed a slightly increased frequency of lagging chromosomes (41%), however this frequency was still lower than in cells with wildtype HP1α tethered to centromeres: In CB-EY-HP1α expressing U2OS cells I observed a frequency of lagging chromosomes from 44% (L), 86% (M), up to 100% (H).

Lagging chromosomes often result in the formation of micronuclei after mitosis. Therefore, I next analysed the frequency of micronuclei formation in cells expressing the HP1α tethering constructs. This analysis confirmed that a high rate of lagging chromosomes resulted indeed in an increased frequency of micronuclei in both cell lines (Fig. 13B).

Thus, tethering HP1α to centromeres by use of the CENP-B DBD causes an increase in the frequency of chromosome segregation errors rather than having a positive effect on chromosome mis-segregation as might have been predicted based on one published study (Abe *et al.*, 2016).

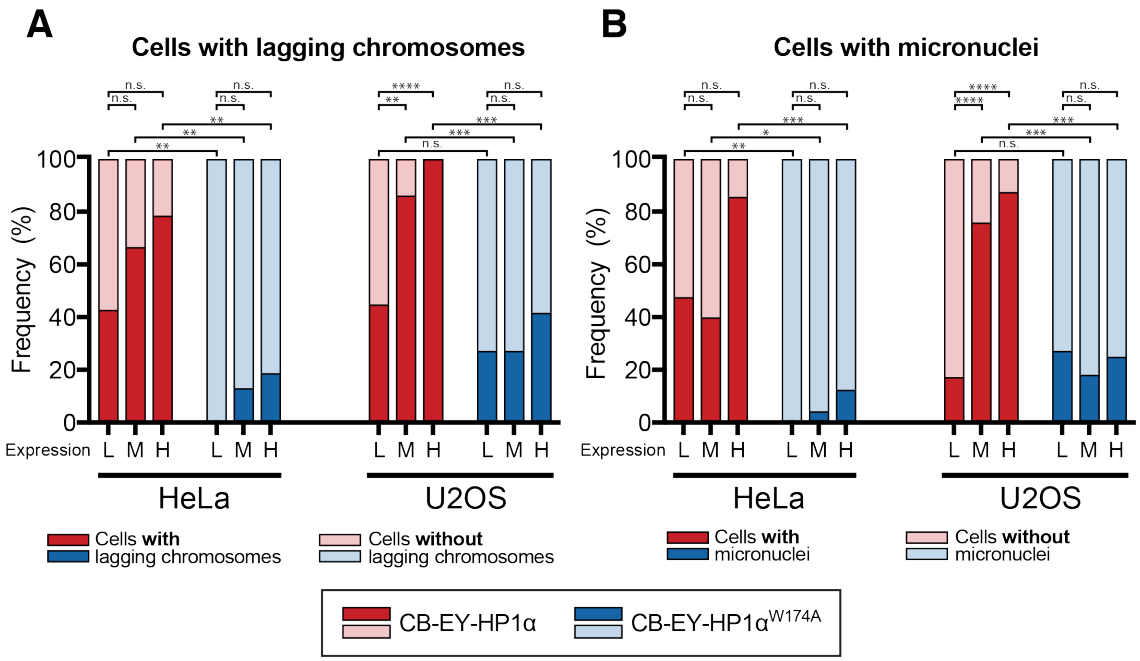

C

Cell type	Construct	Expression	n cells: Timing	n cells: Defects
HeLa	CB-EY-HP1α	low	23	21
HeLa	CB-EY-HP1α	medium	17	15
HeLa	CB-EY-HP1α	high	20	14
HeLa	CB-EY-HP1α^{W174A}	low	20	18
HeLa	CB-EY-HP1α^{W174A}	medium	23	23
HeLa	CB-EY-HP1α^{W174A}	high	16	16
HeLa	untransfected	-	50	-
U2OS	CB-EY-HP1α	low	34	29
U2OS	CB-EY-HP1α	medium	38	29
U2OS	CB-EY-HP1α	high	29	24
U2OS	CB-EY-HP1α^{W174A}	low	11	11
U2OS	CB-EY-HP1α^{W174A}	medium	23	22
U2OS	CB-EY-HP1α^{W174A}	high	14	12
U2OS	untransfected	-	24	-

Figure 13: Centromere tethering of HP1α is accompanied by an increased number of cells with lagging chromosomes and micronuclei.

(A, B) Graphs represent the frequency of lagging chromosomes (A) or micronuclei (B) observed in live cell imaging movies of Hela or U2OS cell expressing either CB-EY-HP1α (red) or CB-EY-HP1α^{W174A} (blue). Dark-coloured sections indicate frequencies of cells with lagging chromosomes (A) or with micronuclei (B). Pale-coloured sections indicate frequencies of cells without lagging chromosomes (A) or micronuclei (B). Statistical analysis: Fisher's exact test followed by the Benjamini-Hochberg multiple comparison test. *, $P < 0.05$; **, $P < 0.01$; ***, $P < 0.001$; ****, $P < 0.0001$; n.s., not significant.

(C) The number of cells used to quantify the mitotic timing (Fig. 12B) and defects (Figure 13A, B) from live cell imaging videos. Each cell line is shown either untransfected or expressing CB-EY-HP1α or CB-EY-HP1α^{W174A}, grouped by the expression level.

4 Results chapter 2: Centromere tethering of HP1 affects the CPC

4.1 The delay mechanism caused by centromeric HP1α tethering suggests an involvement of the CPC

To understand why CB-EY-HP1α expression leads to a mitotic delay instead of improving the rate of chromosome mis-segregation, I further investigated the molecular consequences of HP1 centromere tethering.

4.1.1 The mitotic delay caused by centromere tethering of HP1α is due to spindle assembly checkpoint activity

The live cell imaging experiments revealed that the cells expressing CB-EY-HP1α form a metaphase plate in a timely manner, but the onset of anaphase is delayed. Therefore, I hypothesised that the mitotic accumulation of cells expressing CB-EY-HP1α might be caused by an active spindle assembly checkpoint (SAC). To test this hypothesis, I used published siRNA oligonucleotides (Gorbsky *et al.*, 1998; Nitta *et al.*, 2004) to deplete the essential SAC component Mad2 in cells expressing either CB-EY-HP1α or, as a control, CB-EY-HP1α^{W174A}.

Immunoblot analysis confirmed that extracts from cells transfected with this specific siRNA showed reduced levels of Mad2 protein compared to the levels observed in cells transfected with a control siRNA, which exhibited similar protein levels of Mad2 as untransfected cells (Fig. 14A).

Cells expressing CB-EY-HP1α and treated with control siRNA showed a metaphase delay similar to that seen in Figures 5C and 10B (Fig. 14B). On the other hand, depletion of Mad2 in those cells resulted in a decreased frequency of metaphase cells and an increase of cells in anaphase and telophase to levels similar of CB-EY-HP1α^{W174A} expressing control cells (Fig. 14B). As observed in the live cell

imaging experiments (see Fig. 12B), cell expressing CB-EY-HP1α^{W174A} did not show a mitotic delay. However, as expected, cells progressed more quickly through metaphase upon Mad2 depletion, demonstrated by the decreased frequency of metaphase cells (Fig. 14B).

Overall, this experiment confirms that the mitotic delay induced by tethering HP1α to centromeres is dependent upon SAC activity.

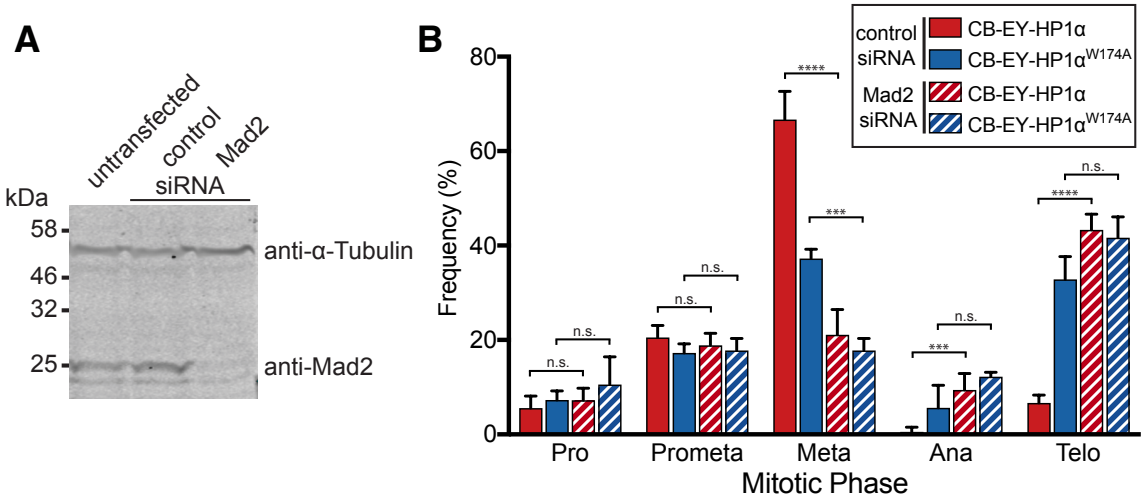

Figure 14: The mitotic delay caused by centromere tethering of HP1α is due to spindle assembly checkpoint activity.

(A) Western blot analysis of Hela whole cell lysates transfected with the indicated siRNA. Mad2 was detected using an anti-Mad2 antibody and demonstrates depletion of the Mad2 protein in the culture transfected with siRNA that targets Mad2 mRNA. α-tubulin served as a loading control.

(B) Frequency of the different mitotic phases in HeLa cells 24 h after transfection with the indicated HP1 tethering constructs and co-transfection with control siRNA (solid bars) or with Mad2 targeting siRNA (striped bars). Graphs represent the mean and standard deviation of three independent experiments, with n=60 mitotic cells per experiment. Statistical analysis: Fisher's exact test followed by the Benjamini–Hochberg multiple comparison test. ***, $P < 0.001$; ****, $P < 0.0001$; n.s., not significant.

4.1.2 Centromere tethering of HP1α results in impaired microtubule attachments to kinetochores

The SAC is active when kinetochores lack proper microtubule attachments. To test whether HP1α tethering leads to impaired microtubule attachment to kinetochores, I performed a cold-stable microtubule assay. This assay is based on the observation that microtubules that are end-on attached to kinetochores (so-called K-fibres), are more stable at low temperatures than unattached microtubules (Rieder, 1981). Therefore, the cold-stable microtubule assay can be used as a readout for the kinetochore-microtubule attachment status.

Immunofluorescence microscopy detecting microtubules and the inner kinetochore protein CENP-C revealed that CB-EY-HP1α expressing cells showed either a reduced microtubule density (Fig. 15A-2i) or even no microtubules (Fig. 15A-2ii) close to the CENP-C signal in metaphase cells after cold treatment. In contrast, untransfected cells or cells expressing the control construct CB-EY-HP1α^{W174A} showed robust microtubules close to the CENP-C signal in metaphase cells, indicating stable microtubule attachments even after cold treatment (Fig. 15A-1 and 15A-3).

To quantify this observation, I measured the overall microtubule intensity in metaphase cells after cold treatment (Fig. 15B). While CB-EY-HP1α^{W174A} expressing cells showed a microtubule intensity similar to untransfected cells, an apparent decrease of the overall microtubule intensity was detectable in CB-EY-HP1α expressing cells after cold treatment.

In summary, this cold-stable microtubule experiment indicates that microtubule attachments to kinetochores are impaired upon CB-EY-HP1α tethering to centromeres.

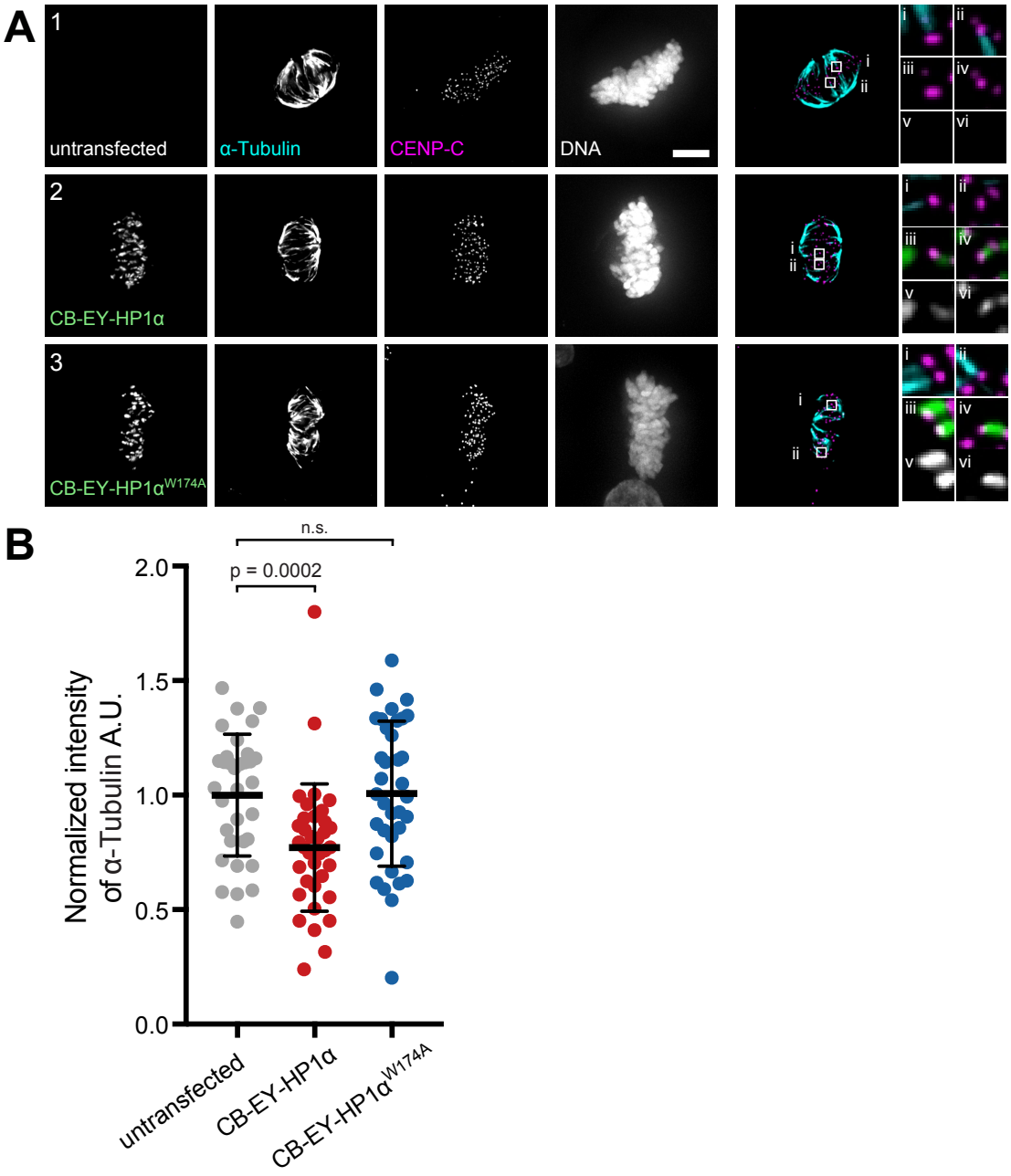

Figure 15: Centromere tethering of HP1α results in impaired microtubule attachments to kinetochores.

(A) Immunofluorescence analysis of untransfected Hela cells (1) or of HeLa cells 24 h after transfection with constructs expressing CB-EY-HP1α (2), or CB-EY-HP1α^{W174A} (3) (shown in green) and subjected to cold treatment. Cells were stained with Hoechst 33342 and immunostained with antibodies recognising α-tubulin (cyan) and CENP-C (magenta). The merge is a maximum intensity projection of 5 z-planes. Zooms are showing α-tubulin and CENP-C (i, ii), the HP1α tethering construct and CENP-C (iii and iv), or the HP1α tethering construct alone (v, vi). Scale bar, 5 µm.

(B) Quantification of the overall microtubule intensity after cold treatment of untransfected HeLa cells (grey) or cells transfected with constructs expressing CB-EY-HP1α (red), or CB-EY-HP1α^{W174A} (blue). Graphs indicate the mean and standard deviation of normalised values from three independent experiments with the following numbers of cells analysed: n=33 for untransfected cells, n=36 for cells transfected with the tethering constructs. Statistical analysis: Kolmogorov-Smirnov test.

4.1.3 Centromere tethering of HP1α leads to altered Aurora B distribution and results in increased levels of phosphorylated Dsn1

Because HP1 localisation to centromeres during mitosis depends on its interaction with the CPC core subunit INCENP (Kang *et al.*, 2011), I hypothesised that HP1α tethering by use of the CENP-B DBD might result in ectopic recruitment of the CPC, thereby causing the metaphase delay phenotype. This idea of a CPC contribution was supported by my previous experiments, demonstrating in Figure 15 that wildtype HP1α tethering to centromeres impaired kinetochore-microtubule attachments, but tethering the CSD mutant HP1α^{W174A} did not have an effect: The CPC is well-known to regulate microtubule attachments to the kinetochore and interacts with HP1 via its CSD.

In order to investigate the role of the CPC in the mitotic delay observed after HP1α tethering to centromeres, I first used indirect immunofluorescence to localise endogenous Aurora B, the kinase component of the CPC, in cells expressing CB-EY-HP1α. In control experiments, I also identified the localisation of Aurora B in cells expressing the HP1α CSD mutant construct (CB-EY-HP1α^{W174A}) and in untransfected cells (Fig. 16A).

Aurora B co-localised almost perfectly with the CB-EY-HP1α construct at centromeres in prometaphase cells (Fig. 16A2). In contrast, in cells expressing CB-EY-HP1α^{W174A}, Aurora B showed a localisation similar to that observed in untransfected cells, consisting of a centromeric pool plus diffuse staining along the chromosome arms (Fig. 16A1, A3). Remarkably, this Aurora B localisation to chromosome arms was seen to a much lesser extent in cells expressing CB-EY-HP1α (Figure 16A2).

To examine whether this altered Aurora B distribution had functional consequences, I analysed the phosphorylation level of the known Aurora B substrate Dsn1 (Yang *et al.*, 2008; Welburn *et al.*, 2010). Indeed, immunofluorescence experiments for phosphorylated Dsn1 (Dsn1ph), showed an increased signal in cells

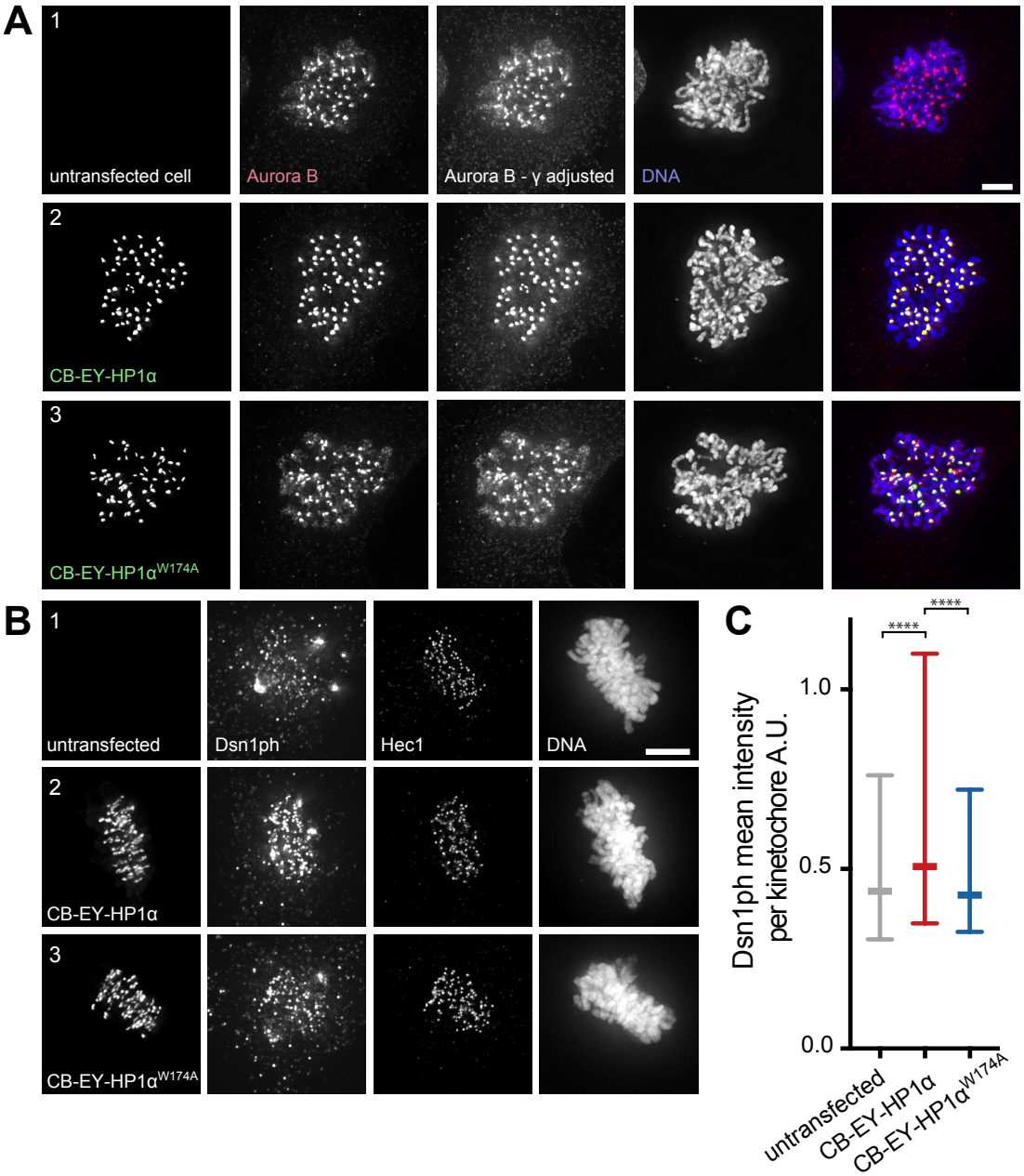

Figure 16: Centromere tethering of HP1α leads to altered Aurora B distribution and results in increased levels of phosphorylated Dsn1.

(A) Immunofluorescence analysis of untransfected Hela cells (1) or of HeLa cells 24 h after transfection with constructs expressing CB-EY-HP1α (2), or CB-EY-HP1α^{W174A} (3) (shown in green). Cells were stained with Hoechst 33342 (blue) and immunostained with an antibody recognising Aurora B (red). The gamma value was reduced by the same ratio for all images showing Aurora B staining (Aurora B - γ adjusted) to highlight the chromosome arm distribution of Aurora B. Scale bar, 5 µm.

(B) Immunofluorescence analysis of untransfected Hela cells (1) or of HeLa cells 24 h after transfection with constructs expressing CB-EY-HP1α (2), or CB-EY-HP1α^{W174A} (3). Cells were stained with Hoechst 33342 and immunostained with antibodies recognising phosphorylated Dsn1 (Dsn1ph) and Hec1 after pre-extraction.

(C) Quantification of the mean Dsn1ph value per individual kinetochore in metaphase cells. Graphs indicate the median and interquartile range of three independent experiments. Kinetochores were individually analysed and compared, with n=60 cells for CB-EY-HP1α expressing and untransfected cells or n=58 cells for CB-EY-HP1α^{W174W} expressing cells. Statistical analysis: Kolmogorov-Smirnov test.

expressing CB-EY-HP1α compared to the two control conditions, untransfected and CB-EY-HP1α^{W174A} expressing cells (Fig. 16B).

Quantification of the Dsn1ph signal by measuring the signal of individual kinetochores confirmed a minor but statistically significant increase in Dsn1 phosphorylation when wildtype HP1α was tethered to centromeres compared to the two control conditions, HP1α^{W174A} tethering or untransfected cells (Fig. 16C). This result is in line with a previous study that reported an increased level of Dsn1 phosphorylation when the CPC subunit INCENP is tethered to centromeres via the CENP-B DBD (Wang *et al.*, 2011a).

Together, these observations further support the hypothesis of a CPC contribution to the metaphase delay phenotype upon centromere tethering of HP1α.

4.1.4 The mitotic delay caused by centromere tethering of HP1α is sensitive to the Aurora B inhibitor ZM447439

To further determine whether Aurora B activity could be responsible for the observed metaphase delay following the tethering of HP1α to centromeres, I made use of the Aurora B inhibitor ZM447439.

In an initial experiment, I treated cells expressing CB-EY-HP1α with ZM447439 for 30 min before fixation and performed immunofluorescence microscopy to analyse these samples (Fig. 17A,B). The mitotic phase distribution of control cells expressing CB-EY-HP1α and treated with DMSO resembled the result of earlier experiments in which cells expressed CB-EY-HP1α without drug treatment (see Figs. 5C and 10B). However, after Aurora B inhibition, the proportion of cells in metaphase decreased substantially, and that of cells in anaphase and telophase increased (Fig. 17A). This shift in the mitotic phase distribution presumably represents the mitotic progression of cells that had previously accumulated in metaphase but now proceeded towards the mitotic exit. Interestingly, this change in cell cycle dynamics occurred even though Aurora B still co-localised with CB-EY-HP1α at chromatin. (Fig. 17B).

Next, I assessed the effect of ZM447439 on cells expressing the control construct CB-EY-HP1α^{W174A} and on untransfected cells (Fig. 17C). Flow cytometry analysis demonstrated that ZM447439 treatment led to a minor increase in the mitotic indices of control cells. Importantly, the mitotic index of cells expressing CB-EY-HP1α decreased when cultures were treated with ZM447439, resulting in a similar mitotic index for all three experimental conditions after treatment with ZM447439 (Fig. 17C).

Together, these results indicate that the mitotic delay caused by tethering HP1α to centromeres is sensitive to the Aurora B inhibitor ZM447439, suggesting that recruitment of the CPC might be responsible for the mitotic delay phenotype.

In summary, my results suggest that HP1α tethering using the DNA-binding domain of CENP-B phenocopies the effects observed following CENP-B tethering of the core CPC subunit INCENP, including a metaphase delay, activity of the SAC, impaired kinetochore-microtubule attachments, increased Aurora B activity at kinetochores, and ZM447439 sensitivity (Liu *et al.*, 2009).

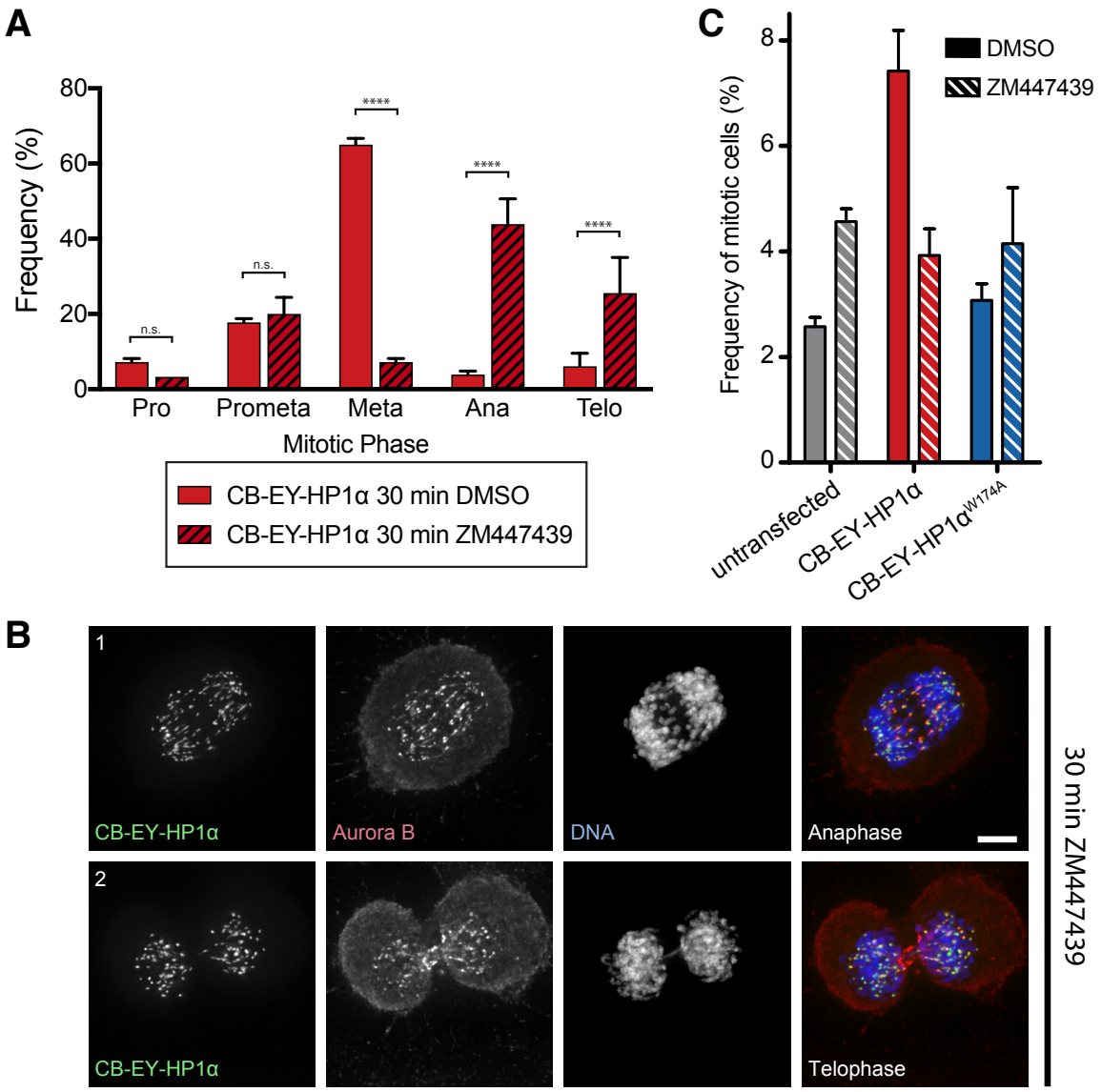

Figure 17: The mitotic delay caused by centromere tethering of HP1α is sensitive to the Aurora B inhibitor ZM447439.

(A) Frequency of the different mitotic phases in HeLa cells 24 h after transfection with a construct expressing CB-EY-HP1α and treatment with either DMSO (filled bars) or the Aurora B inhibitor ZM447439 (striped bars) for 30 min before fixing the cells. Graphs represent the mean and standard deviation of three independent experiments, with n=60 mitotic cells per experiment. Statistical analysis: Fisher's exact test followed by the Benjamini–Hochberg multiple comparison test. ****, $P < 0.0001$; n.s., not significant.

(B) Immunofluorescence analysis of Hela cells 24 h after transfection with a construct expressing CB-EY-HP1α (shown in green) and treated with the Aurora B inhibitor ZM447439 for 30 min before fixing the cells. Cells were stained with Hoechst 33342 (blue) and immunostained with an antibody recognising Aurora B (red). Scale bar, 5 µm.

(C) Flow cytometry analysis of HeLa cells that were treated with DMSO or 3 µM ZM447439 24 h after transfection with the indicated constructs. Mitotic indices were determined by use of a flow cytometer after cells were stained with Hoechst 33342 and immunostained with an antibody recognising MPM2. A minimum of 40,000 singlets were analysed per condition and individual experiment. Graphs represent the mean and standard deviation of three independent experiments.

4.2 Tethering HP1α highlights a strong interaction between the CPC and HP1 *in vivo*

When analysing the mitotic phase distribution following ZM447439 treatment, I detected a robust co-localisation of Aurora B with CB-EY-HP1α at centromeres in anaphase and telophase cells (see Figure 17B). This was unexpected as the CPC does not normally localise to the centromere at these stages of the cell cycle but instead shifts to the spindle midzone and midbody region (Earnshaw and Cooke, 1991). This observation suggests the existence of a strong interaction between the CPC and tethered HP1α.

4.2.1 Centromere tethering of HP1α leads to abnormal centromeric retention of Aurora B

I next tested whether the chromatin retention of Aurora B described in Figure 17B was an effect of the Aurora B inhibition, which is known to perturb CPC transfer to the spindle midzone (Xu *et al.*, 2009), or whether CB-EY-HP1α is also able to retain Aurora B at centromeres under physiological conditions. Therefore, I repeated the immunofluorescence experiment without drug treatment. Remarkably, even without perturbing Aurora B activity, a substantial amount of Aurora B continued to co-localise with CB-EY-HP1α at centromeres in telophase cells and only a fraction of the kinase localised to the midbody (Fig. 18-1). Importantly, I did not observe this abnormal retention of Aurora B at centromeres in telophase cells expressing the mutated CB-EY-HP1α^{W174A} construct, but rather detected the entire pool of Aurora B localised at the midbody, which is its physiological localisation at this stage of mitosis (Fig. 18-2).

The CB^{mut}-EY-HP1α construct, which shows faster binding dynamics than CB-EY-HP1α and does not cause a mitotic delay, also failed to retain Aurora B at centromeres in telophase (Fig. 18-3). Instead, I observed an EYFP signal at the midbody region in CB^{mut}-EY-HP1α expressing cells. Therefore, it appears that the CPC was dominant over CB^{mut}-EY-HP1α and instead determined the localisation of this HP1α tethering construct, resulting in its recruitment to the midbody region. I

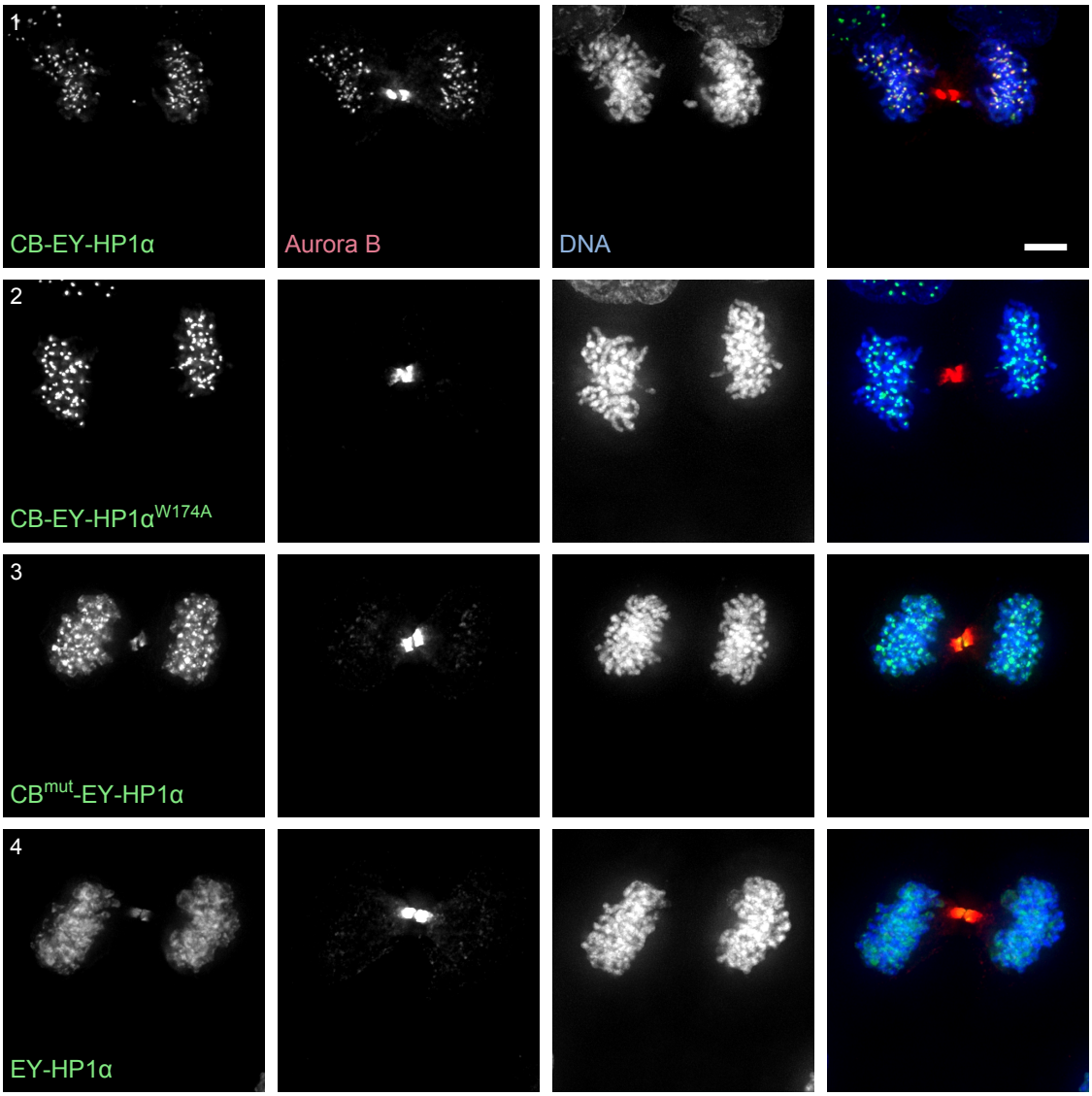

Figure 18: Centromere tethering of HP1α leads to abnormal centromeric retention of Aurora B in telophase.

Immunofluorescence analysis of Hela cells 24 h after transfection with constructs expressing CB-EY-HP1α (1), CB-EY-HP1α^{W174A} (2), CB^{mut}-EY-HP1α (3), or EY-HP1α (4) (shown in green). Cells were stained with Hoechst 33342 (blue) and immunostained with an antibody recognising Aurora B (red). Scale bar, 5 µm.

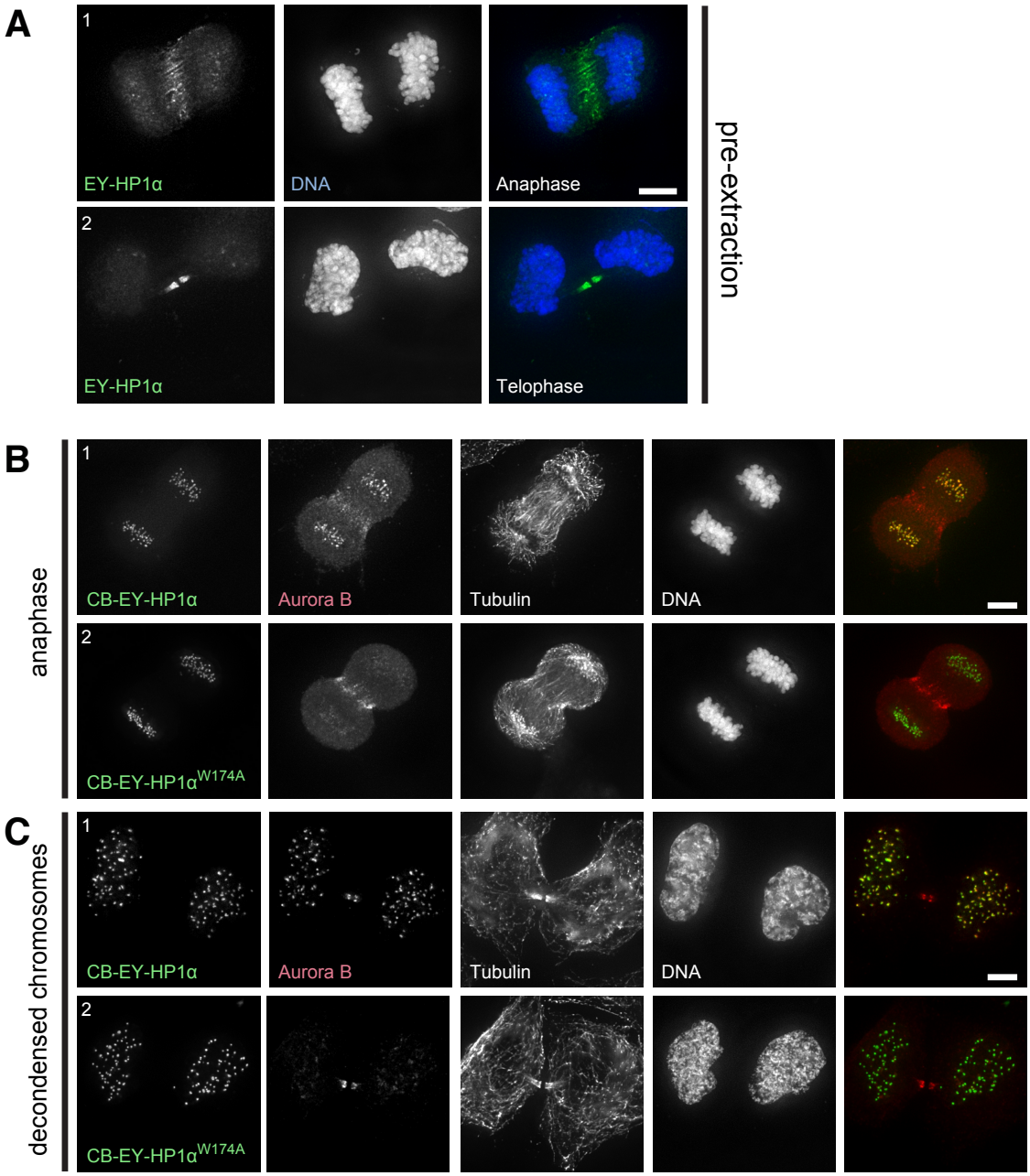

Figure 19: Tethering of HP1α to centromeres leads to abnormal centromeric retention of Aurora B in anaphase and after chromosome decondensation.

(A) Fluorescence microscopy analysis of Hela cells 24 h after transfection with a construct expressing EY-HP1α (shown in green). Cells were stained with Hoechst 33342 (blue) after pre-extraction with 0.1% Triton X-100/PHEM buffer for 1 min. Scale bar, 5 µm.

(B, C) Immunofluorescence analysis of Hela cells 24 h after transfection with constructs expressing CB-EY-HP1α (1) or CB-EY-HP1α^{W174A} (2) (shown in green). Cells were stained with Hoechst 33342 and immunostained with an antibody recognising Aurora B (red) and α-tubulin. The brightness of the channel showing the EYFP signal was scaled individually to optimise the clarity of the tethering, however, in both examples, CB-EY-HP1α^{W174A} was expressed at a higher level. Scale bar, 5 µm.

observed a similar EYFP signal at the midbody region in cells expressing the untethered EY-HP1α (Fig. 18-4), which has been previously reported to localise to the midbody in telophase (Hayakawa *et al.*, 2003). The recruitment of EY-HP1α to sites of CPC localisation in anaphase and telophase became even clearer when I performed pre-extraction before fixing the cells with PFA (Fig. 19A).

Additionally, the retention of Aurora B at centromeres was also visible in CB-EY-HP1α expressing cells at anaphase and even at much later stages when chromosomes began to decondense (Fig. 19B,C). By contrast, cells expressing the CB-EY-HP1α^{W174A} construct did not exhibit this clear Aurora B retention at any of these stages (Fig. 19B,C).

4.2.2 Retention of HP1-bound CPC leads to H3S10 phosphorylation in G_1 cells

When investigating the consequences of retaining Aurora B at centromeres during mitotic exit, I discovered a robust H3S10ph signal in interphase cells expressing CB-EY-HP1α (Fig. 20A-1). Importantly, co-staining with an anti-cyclin A2 antibody allowed me to identify cells in G_1 phase, indicated by the absence of a cyclin A2 signal. Thus, this histone H3S10 phosphorylation was independent of the physiological H3S10ph that occurs during G_2 phase (Hendzel *et al.*, 1997; Crosio *et al.*, 2002; Monier *et al.*, 2007; Hayashi-Takanaka *et al.*, 2009). The H3S10ph observed in G_1 phase was not detectable in cells expressing the construct CB-EY-HP1α^{W174A} (Fig. 20A-2), which did not retain Aurora B at telophase centromeres (see Fig. 18-2).

To quantify this observation, I used the automated image analysis software CellProfiler, which automatically quantified the number of histone H3S10ph-positive G_1 cells (Fig. 20B). In HeLa cells, the specific H3S10ph signal was detectable 24 h after transfection in 54% of CB-EY-HP1α expressing G_1 cells. However, when using the same detection parameters, I detected few, if any, G_1 cells positive for H3S10ph in cultures expressing CB-EY-HP1α^{W174A}, CB^{mut}-EY-HP1α, EY-HP1α, or in untransfected cells, which all did not retain Aurora B at centromeres in telophase. Analysing U2OS cells, I obtained a comparable result: CB-EY-HP1α expression led to H3S10ph-positive nuclei in 71% of G_1 cells 24 h after transfection (Fig. 20B). However, no H3S10ph

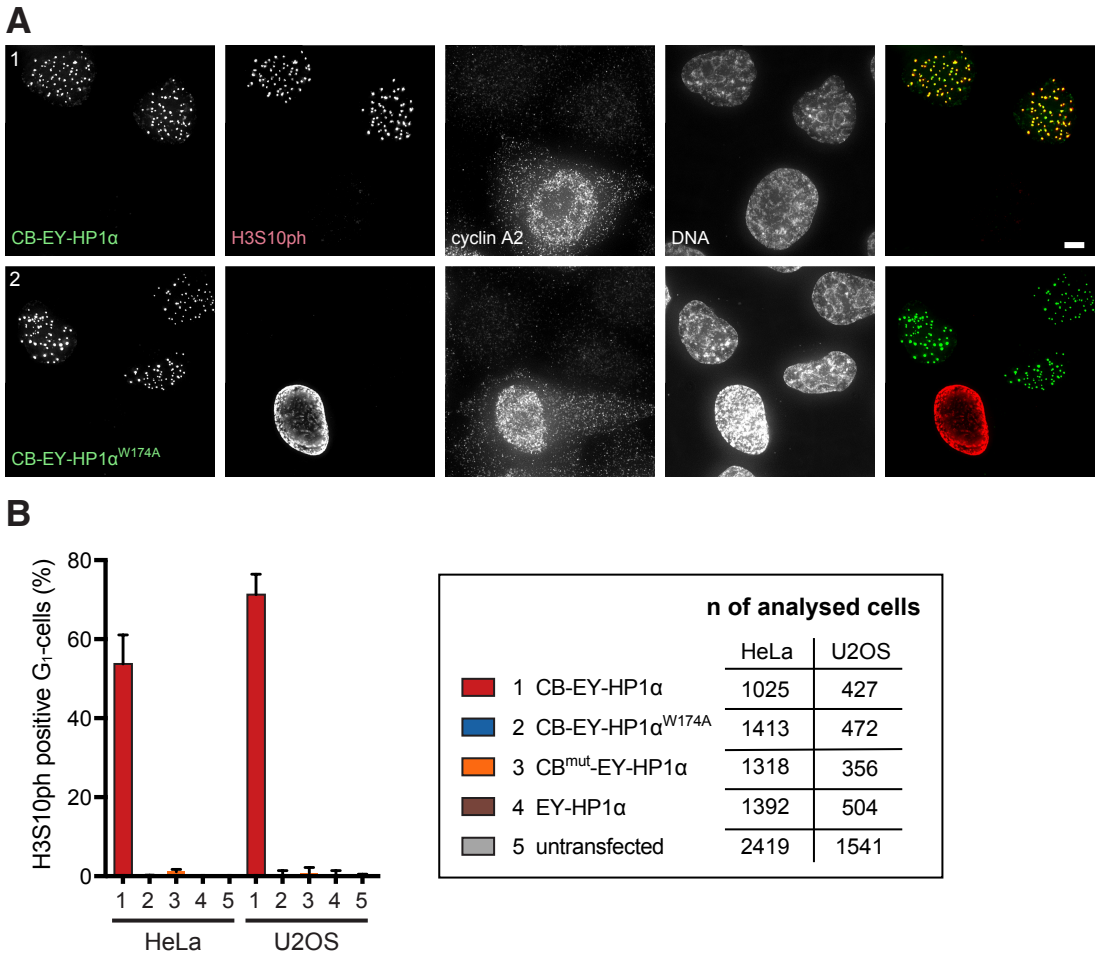

Figure 20: Retention of HP1-bound CPC leads to H3S10 phosphorylation in G_1 cells.

(A) Immunofluorescence analysis of Hela cells 24 h after transfection with constructs expressing CB-EY-HP1α (1) or CB-EY-HP1α^{W174A} (2) (shown in green). Cells were stained with Hoechst 33342 and immunostained with antibodies recognising histone H3S10 phosphorylation (red) and cyclin A2. The latter was used to identify cells at the G_1 stage of the cell cycle (indicated by the absence of cyclin A2). Scale bar, 5 µm.

(B) Quantification of G_1 cells positive for histone H3S10 phosphorylation 24 h after transfection with the indicated HP1α fusion constructs or in untransfected cells using the automated image analysis software CellProfiler. Graphs represent the mean and standard deviation of three independent experiments. The overall numbers of analysed cells which met the criteria of being transfected and negative for the cyclin A2 staining are shown in the table.

signal was observed with the automated image analysis (frequencies below 1%) following the expression of the above-mentioned controls.

The automated image analysis allowed me to quantify a large number of cells, emphasising the utility of an automated approach when analysing a distinct subpopulation, such as transfected cells that are in the G_1 phase, and detecting a specific phenotype, which in my experimental setup was H3S10ph-positive nuclei.

Together, these results reveal that Aurora B retained at centromeres in cells expressing CB-EY-HP1α remains active following mitotic exit, indicating that stably tethered HP1α can localise a functional CPC in G_1 cells, a cell cycle stage at which the CPC is typically inactive.

4.2.2.1 Live cell imaging highlights the robustness of the induced H3S10 phosphorylation throughout interphase

To determine the robustness of the induced H3S10ph interphase signal, I made use of a specific imaging technique, with which chromatin marks are traceable in live cell experiments. The imaging approach is based on fluorescently labelled antigen-binding fragments (Fabs), which I loaded into living transfected cells using glass beads (McNeil and Warder, 1987; Hayashi-Takanaka *et al.*, 2011). To ensure that the Fab recognises the H3S10ph mark at tethered HP1α clusters during interphase, I used Fab313, which can also react with H3S10ph next to a H3K9me3 mark, as demonstrated in a previous study (Hayashi-Takanaka *et al.*, 2009).

Using this experimental setup, I could track the specific H3S10ph signal localised at sites of the tethered CB-EY-HP1α foci for more than 8 h hours after mitotic exit (Fig. 21A; Movie 1). In control cells expressing CB-EY-HP1α^{W174A}, no such H3S10ph signal was detectable after cells left mitosis (Fig. 21B), which is in line with the fixed cell experiment (see Fig. 20A-2).

Reducing the frequency of image acquisition to every 30 min allowed me to track cells across an entire cell cycle. This experiment revealed that the H3S10ph signal was detectable continuously between two consecutive mitoses and therefore throughout the whole of interphase (Fig. 21C; Movie 2).

Together, the live cell imaging experiments using fluorescently labelled Fabs revealed that the H3S10 phosphorylation induced by tethering of wildtype HP1α is stable throughout interphase.

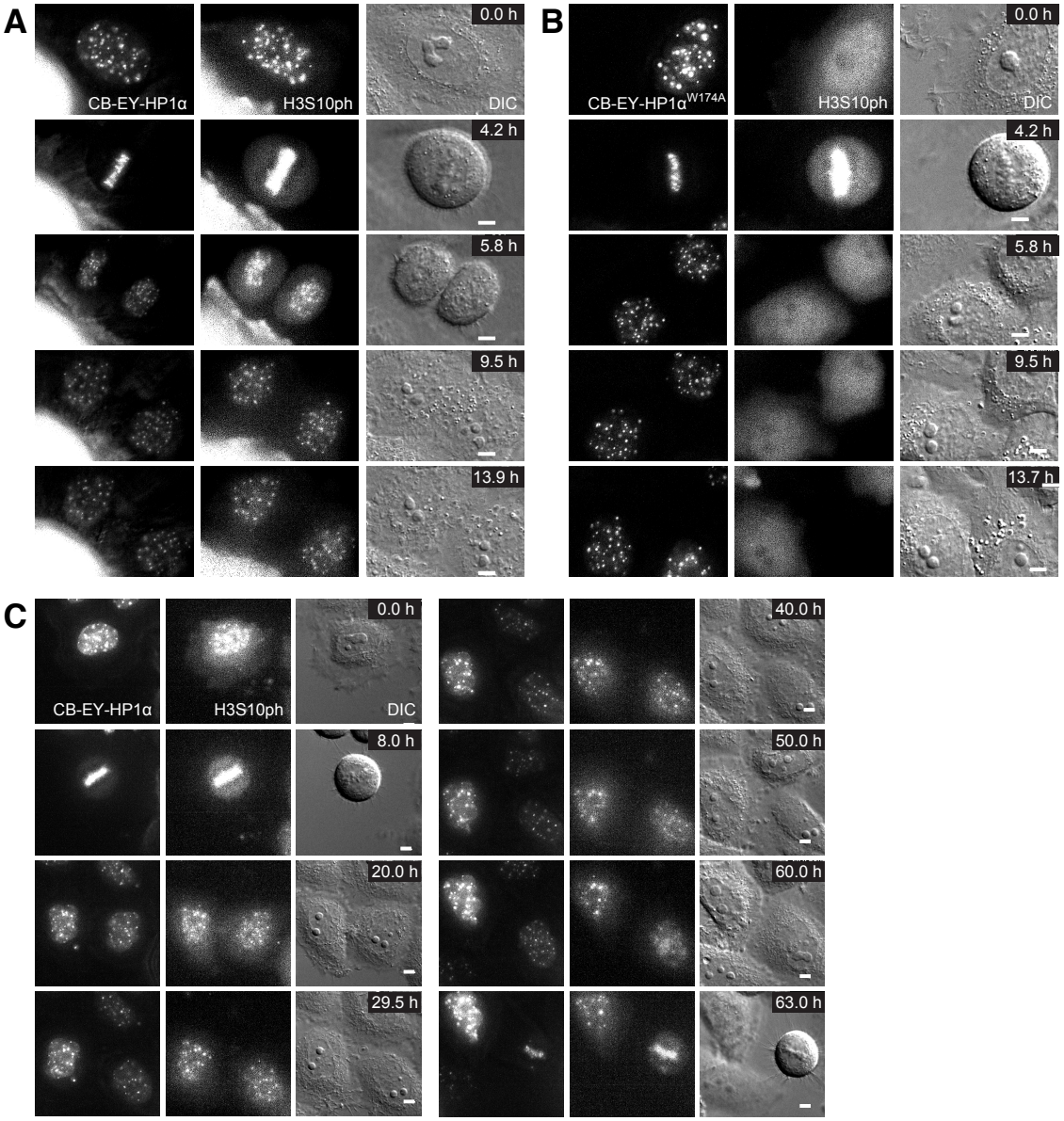

Figure 21: Live cell imaging highlights the robustness of the induced H3S10 phosphorylation throughout interphase.

(A, B) Stills of live cell imaging movies analysing HeLa cells expressing CB-EY-HP1α (A) or CB-EY-HP1α^{W174A} (B). Live cell imaging was performed using CF640R-labelled Fab fragments that recognise H3S10 phosphorylation, together with differential interference contrast (DIC) microscopy. Movies were acquired with a 100× objective every 10 min and five z-sections every 2 µm. Scale bar, 5 µm.

(C) Stills of a live cell imaging movie analysing HeLa cells expressing CB-EY-HP1α. Live cell imaging was performed using CF640R-labelled Fabs that recognise H3S10 phosphorylation, together with differential interference contrast (DIC) microscopy. Movies were acquired with a 60× objective every 30 min and five z-sections every 2 µm. Scale bar, 5 µm.

4.2.2.2 The induced interphase H3S10 phosphorylation is sensitive to a low dosage of the Aurora B inhibitor ZM447439

Use of the Aurora B inhibitor ZM447439 allowed me to test whether the persistence of the H3S10ph signal co-localising with the CB-EY-HP1α construct in interphase required continuous Aurora B activity (Fig. 22A). Interestingly, the H3S10ph signal in interphase cells vanished after treatment with a low dosage (0.5μM) of ZM447439, a concentration that has no apparent effect on H3S10ph in mitotic cells (Fig. 22A2).

The disappearance of the H3S10ph signal occurred even though Aurora B remained localised at the CB-EY-HP1α foci (Fig. 22B2). Therefore, the addition of ZM447439 did not disrupt the CPC-HP1α interaction, but this experiment instead indicates that Aurora B activity might be more sensitive to inhibition during interphase than it is during mitosis.

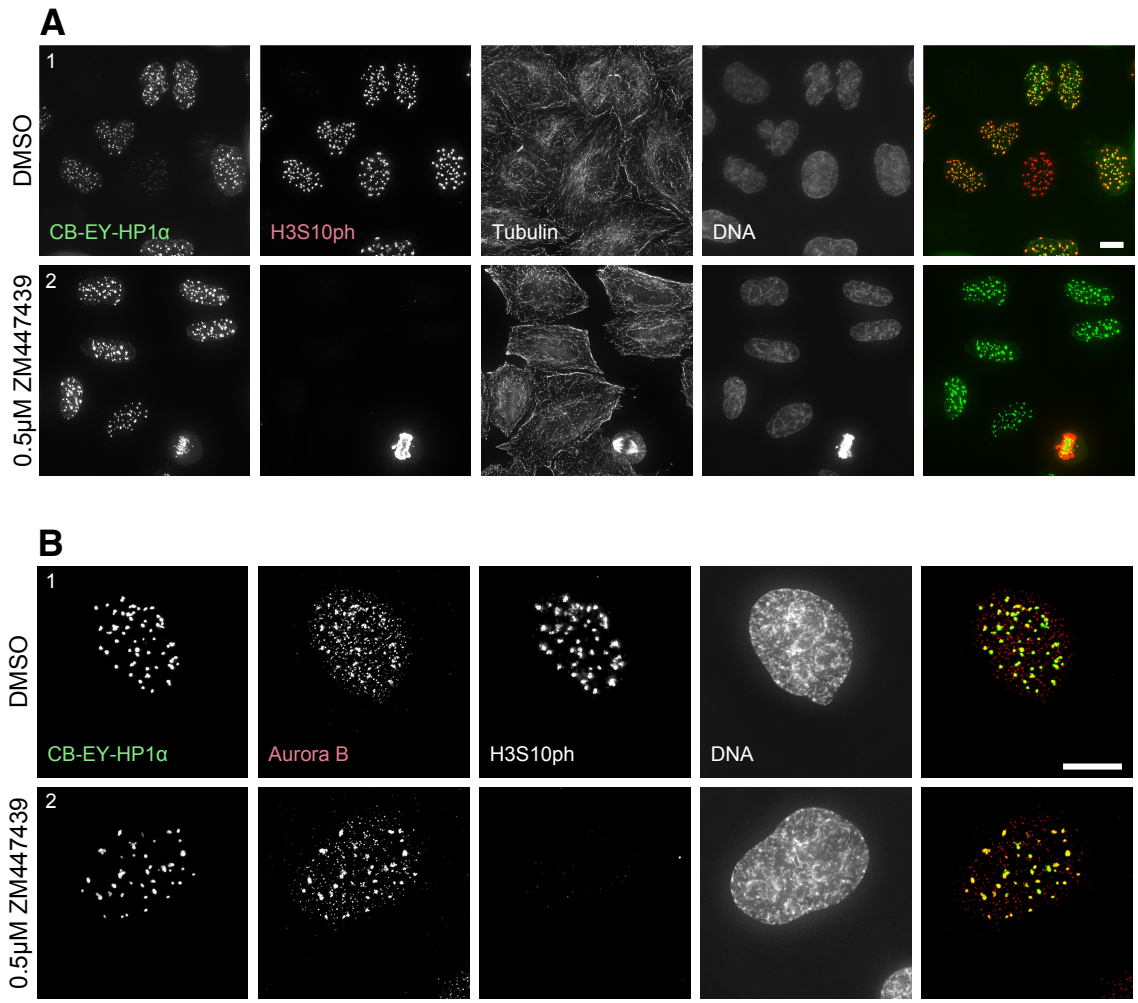

Figure 22: The induced interphase H3S10 phosphorylation is sensitive to a low dose of the Aurora B inhibitor ZM447439.

(A) Immunofluorescence analysis of Hela cells 24 h after transfection with a construct expressing CB-EY-HP1α (shown in green) treated with either DMSO (1) or with 0.5 μM ZM447439 (2) for 60 minutes before fixing the cells. Cells were stained with Hoechst 33342 and immunostained with antibodies recognising histone H3S10 phosphorylation (red) and α-tubulin. Scale bar, 10 μm.

(B) Immunofluorescence analysis of Hela cells 24 h after transfection with a construct expressing CB-EY-HP1α (shown in green) treated with either DMSO (1) or with 0.5 μM ZM447439 (2) for 60 minutes before fixing the cells. Cells were stained with Hoechst 33342 and immunostained with antibodies recognising Aurora B (red) and histone H3S10 phosphorylation. Scale bar, 10 μm.

5 Results chapter 3: Investigating the molecular mechanism of endogenous H3S10ph foci in G_2 cells

5.1 Analysing endogenous H3S10ph foci in G_2 cells

The results I described so far have revealed a strong interaction between HP1α and the CPC *in vivo*. Furthermore, tethered HP1α is able to concentrate Aurora B resulting in H3S10ph foci at CB-EY-HP1α clusters in interphase. Therefore, I decided to examine the possible contribution of HP1α to the CPC-dependent emergence of endogenous H3S10ph in interphase cells during G_2.

5.1.1 H3S10ph foci co-localise with untethered EY-HP1α in G_2 cells

As shown earlier in Figures 20, 21, and 22, clear H3S10ph foci co-localised with CB-EY-HP1α in interphase cells (Fig. 23-1). Furthermore, I also detected distinct H3S10ph foci in untransfected cells in the G_2 stage of the cell cycle, indicated by positive staining for cyclin B (Fig. 23-2, see asterisk). Various studies previously described this observed emergence of H3S10ph foci in G_2 cells (Hendzel *et al.*, 1997; Crosio *et al.*, 2002; Monier *et al.*, 2007; Hayashi-Takanaka *et al.*, 2009). Interestingly, the H3S10ph signal in G_2 cells co-localised with foci of untethered EY-HP1α (Fig. 23-2). This H3S10ph signal was most likely not artificially induced by the expression of EY-HP1α, as a similar signal was detectable in the untransfected G_2 cells of the same culture (Fig. 23-2, see asterisk). Moreover, EY-HP1α was not, in contrast to CB-EY-HP1α, able to induce H3S10ph in G_1 cells, as described earlier (see Fig. 20B).

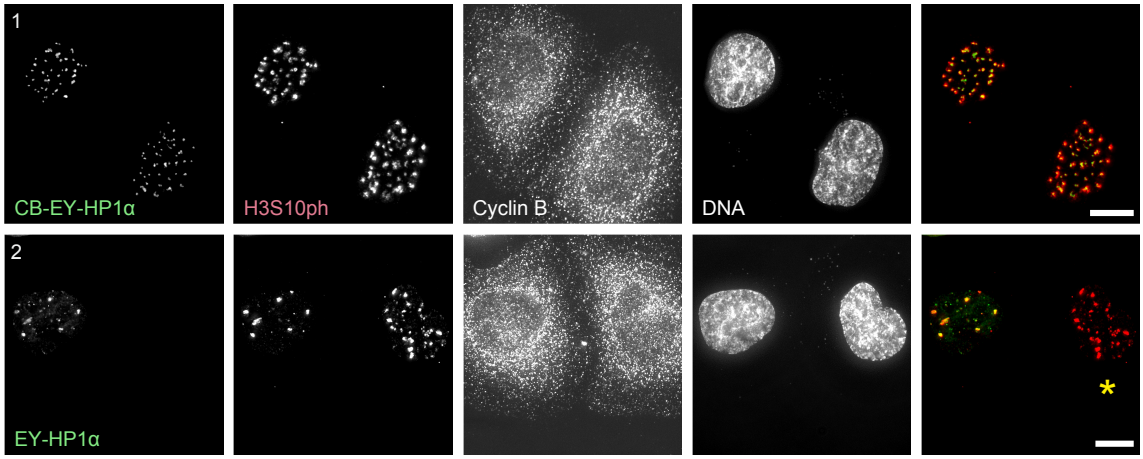

Figure 23: H3S10ph foci co-localise with untethered EY-HP1α in G_2 cells.

Immunofluorescence analysis of Hela cells 24 h after transfection with constructs expressing CB-EY-HP1α (1) or EY-HP1α (2) (shown in green). Cells were stained with Hoechst 33342 and immunostained with antibodies recognising histone H3S10 phosphorylation (red) and cyclin B. The latter was used to identify cells at the G_2 stage of the cell cycle. Scale bar, 10 μm.

5.1.2 Characteristic endogenous H3S10ph foci at the CDK1 arrest point in G_2

The H3S10ph chromatin mark typically emerges in G_2 cells at heterochromatin foci and spreads across the entire nucleus with progression towards the G_2/M transition. Therefore, I detected a broad spectrum of different H3S10ph staining patterns in unsynchronised cultures (Fig. 24A). These included cells with a few isolated H3S10ph foci in the nucleus (1), cells with larger and more abundant H3S10ph foci (2), and nuclei that showed a more general H3S10ph staining that started to spread through the nucleus (3), eventually leading to a H3S10ph labelling of the entire chromatin in mitosis (4).

The rapid progression of the H3S10ph chromatin labelling in the G_2 phase, resulting in those various H3S10ph staining patterns, made it challenging to precisely analyse the emergence of the H3S10ph foci. Therefore, I used Hela cells whose cell cycle progression is driven by a CDK1-analogue sensitive (-as) kinase (Fig. 24B). The ATP-binding pocket of *Xenopus laevis* CDK1 was modified using chemical genetics, allowing a reversible inhibition with the bulky ATP analogue 1NM-PP1 (Hochegger *et al.*, 2007). Incubation with 1NM-PP1 synchronised cells at the CDK1 arrest point in the G_2 phase and cells entered mitosis in less than 60 minutes after 1NM-PP1 removal. This allowed me to analyse the H3S10ph foci in a highly synchronous culture of G_2 cells and therefore with high temporal accuracy.

Analysing the pattern of H3S10ph foci in cells after incubation with 1NM-PP1 for 20 h revealed a striking consistency throughout the culture, as nearly all cells exhibited 3 to 6 distinct H3S10ph foci (Fig. 24C). Therefore, the CDK1-as approach allowed me to study precisely the formation of H3S10ph foci in G_2 cells and further revealed that this H3S10 phosphorylation is independent of CDK1 activity.

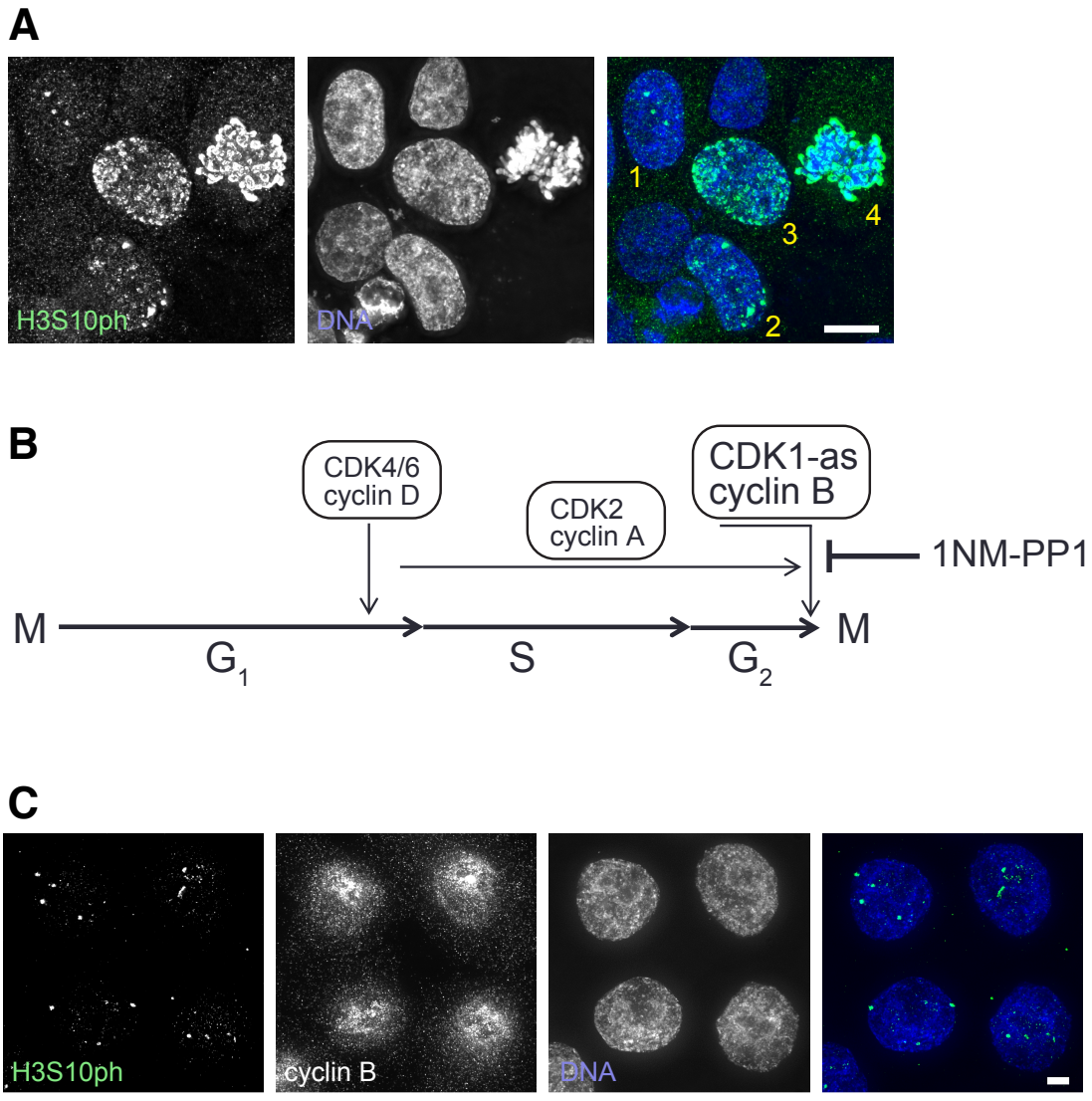

Figure 24: Characteristic endogenous H3S10ph foci at the CDK1 arrest point in G_2.
(A) Immunofluorescence analysis of unsynchronised Hela CDK1-as (analogue sensitive) cells stained with Hoechst 33342 (blue) and immunostained with an antibody recognising histone H3S10 phosphorylation (green). Numbers indicate different levels of H3S10 phosphorylation (see main text for detailed description). Scale bar, 10 µm.
(B) Schematic representation of the cell cycle and the effect of 1NM-PP1 treatment on cell cycle progression in HeLa CDK1-as cells.
(C) Immunofluorescence analysis of Hela CDK1-as cells synchronised with 10 µM 1NM-PP1 for 20 h. Cells were stained with Hoechst 33342 (blue) and immunostained with antibodies recognising histone H3S10 phosphorylation (green) and cyclin B. Scale bar, 5 µm.

5.1.2.1 Live cell imaging highlights the robustness of the H3S10ph foci at the CDK1 arrest point

To characterise the dynamics of the H3S10ph foci at the CDK1 arrest point in more detail, I used the fluorescently labelled Fab fragments recognising H3S10ph, that I described in section 4.2.2.1. The H3S10ph foci appeared to be very stable and hardly changed over a recorded period of 12 h when monitored with Fab fragments in living CDK1-as cells synchronised with 1NM-PP1 (Fig. 25; Movie 3). The decreasing intensity of the H3S10ph foci over the duration of the movie was most likely due to photobleaching, as images were acquired every 6 min, the overall fluorescent signal decreased, and in contrast to fluorescent proteins like GFP, which are continuously expressed, the amount of fluorescent probe within the cell is not renewed when using labelled Fab fragments.

Together, the live cell imaging revealed that the H3S10ph foci remain at a distinct chromatin localisation when cells are kept at the CDK1 arrest point. Additionally, CDK1 inhibition appeared to not only prevent cell cycle progression but also spreading of the H3S10ph signal throughout the nucleus.

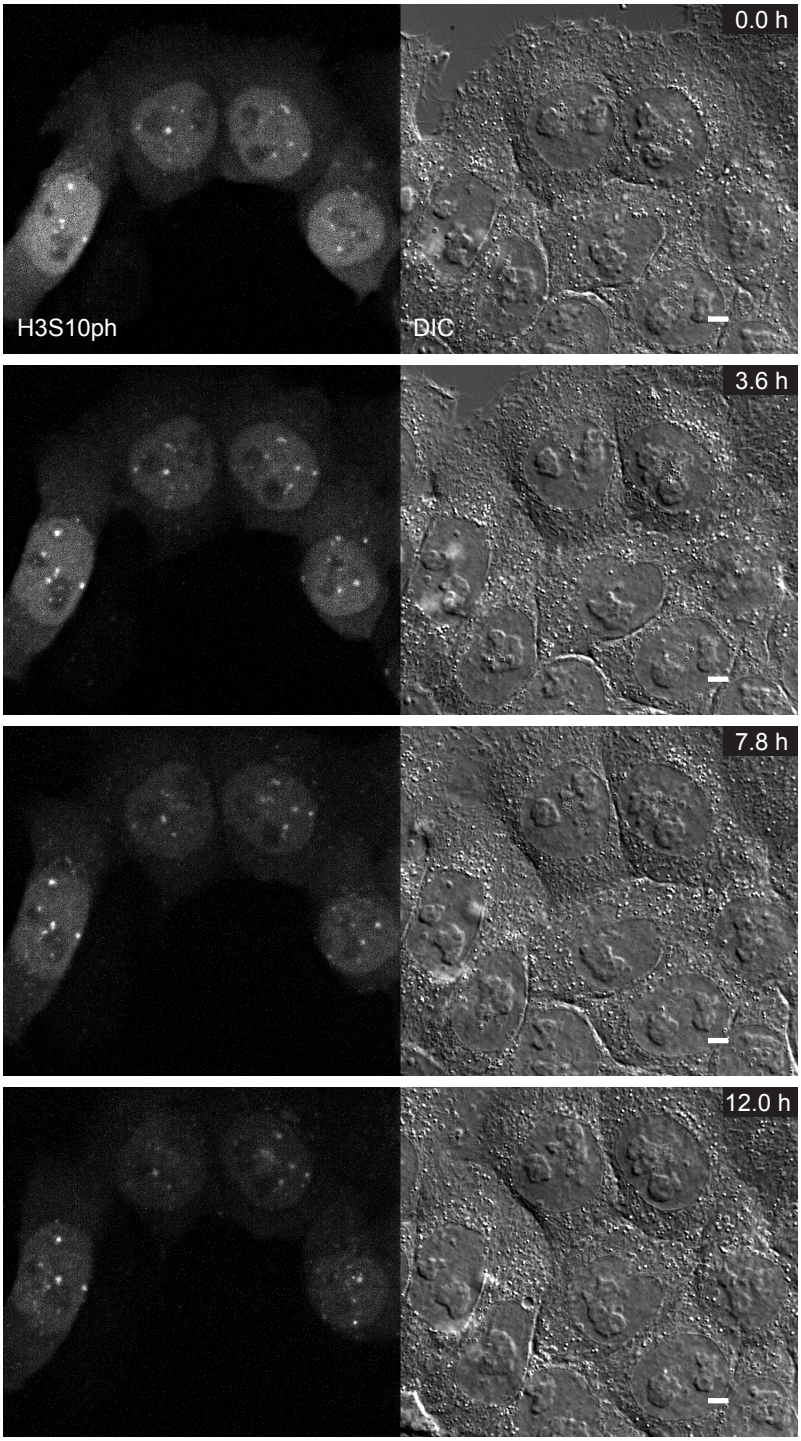

Figure 25: Live cell imaging highlights the robustness of the H3S10ph foci at the CDK1 arrest point.

Stills of a live cell imaging movie analysing HeLa CDK1-as cells that were synchronised with 10 µM 1NM-PP1. Live cell imaging was performed using Cy5-labelled Fab fragments that recognise H3S10 phosphorylation, together with differential interference contrast (DIC) microscopy. Movies were acquired with a 100× objective every 6 min and five z-sections every 1 µm. Scale bar, 5 µm.

5.1.2.2 Endogenous interphase H3S10ph foci are sensitive to a low dosage of the Aurora B inhibitor ZM447439

I next tested the sensitivity of the endogenous G_2 H3S10ph foci to inhibition with a low concentration of the Aurora B inhibitor ZM447439 (Fig. 26). Similar to the induced H3S10ph signal in CB-EY-HP1α-expressing interphase cells, 0.5 µM of ZM447439 entirely abolished the H3S10ph signal in 1NM-PP1 synchronised CDK1-as cells. The H3S10ph signal was not detectable upon ZM447439 treatment, although Aurora B kinase continued to co-localise with EY-HP1α foci (Fig. 26-1).

I also observed this co-localisation between EY-HP1α and Aurora B in cultures that were not synchronised with 1NM-PP1 (-1NM-PP1) (Fig. 26-2). Similar to the synchronised cells, 0.5 µM ZM447439 abolished H3S10ph in interphase of the unsynchronised culture. However, a clear signal of H3S10ph remained detectable in mitotic cells, overall confirming the results obtained from experiments analysing interphase H3S10ph foci induced by CB-EY-HP1α (see Fig. 22). Together, these results indicate that endogenous interphase H3S10ph requires continuous Aurora B activity and is more sensitive to low dosage Aurora B inhibition than H3S10ph in mitosis.

The results presented in this section suggest that endogenous H3S10ph foci that emerge at the G_2 stage of the cell cycle co-localise with EY-HP1α clusters, occur before CDK1 activation, and require continuous Aurora B activation.

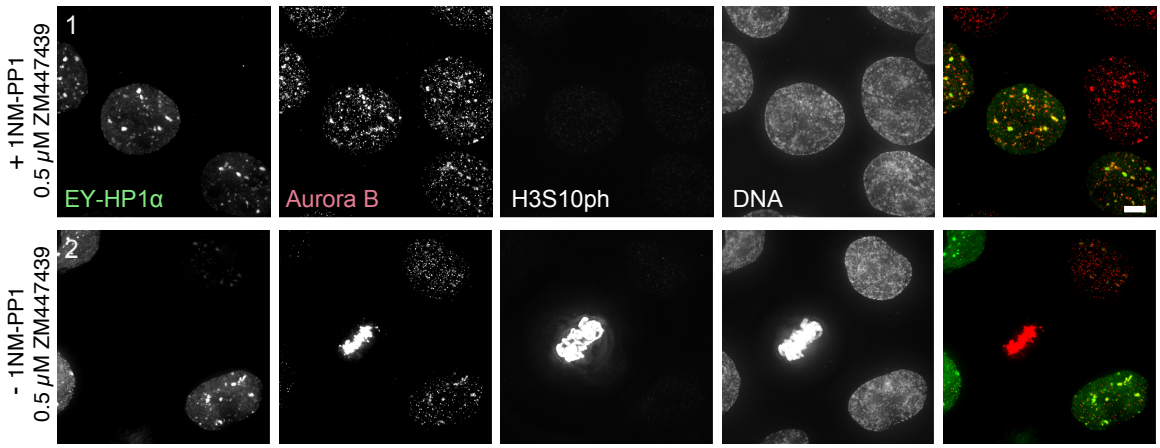

Figure 26: Endogenous interphase H3S10ph foci are sensitive to a low dose of the Aurora B inhibitor ZM447439.

Immunofluorescence analysis of Hela CDK1-as cells 24 h after transfection with a construct expressing EY-HP1α (shown in green) and treated with 0.5 µM ZM447439 for 60 minutes before fixing cells. Cells were synchronised for 20h with 10 µM 1NM-PP1 (+1NM-PP1) (1) or left unsynchronised by addition of only DMSO (-1NM-PP1) (2). Cells were stained with Hoechst 33342 and immunostained with antibodies recognising Aurora B (red) and histone H3S10 phosphorylation. Scale bar, 5 µm.

5.2 H3S10ph foci in G_2 precede histone modifications that cause CPC clustering in mitosis

The centromere localisation of the CPC during mitosis is reported to be determined by two histone tail post-translational modification, H3T3ph and H2AT120ph. Thus, targeting of the CPC to centromeres is achieved through direct binding of survivin to H3T3ph and via Shugoshin, which binds H2AT120ph and interacts with borealin (Kelly *et al.*, 2010; Wang *et al.*, 2010; Yamagishi *et al.*, 2010). I therefore next investigated whether these mechanisms of CPC clustering also apply in the G_2 phase and lead to the observed H3S10ph foci.

5.2.1 H3S10ph foci precede emergence of H3T3 phosphorylation

To determine a potential connection between H3T3ph and the occurrence of H3S10ph foci in G_2 cells, I performed immunofluorescence experiments and co-stained for these two histone marks. The entire culture of CDK1-as cells synchronised

with 1NM-PP1 was negative for the H3T3ph staining. However, the above described H3S10ph foci that occur at the CDK1 arrest point were detectable in almost every cell (Fig. 27A1).

To take into account the possibility that the inhibition of the CDK1 kinase had an effect on Haspin activity in these 1NM-PP1 synchronised G_2 cells, I also analysed cells that were not synchronised (-1NM-PP1) (Fig. 27A2). The unsynchronised culture showed the same trend: H3S10ph foci emerged in nuclei before I could detect any H3T3ph signal (Fig. 27A2). Increasing the image intensities highlights the state in which the H3S10ph foci started to emerge while the H3T3ph signal was still not present (Fig. 27A3 - outlined cells). The H3T3ph mark only appeared when nuclei already showed a general H3S10ph signal all over chromatin (Fig. 27A2).

In an additional control, I stained for the two histone marks H3S10ph and H3T3ph in wildtype HeLa cells to exclude the possibility of a specific effect in Hela CDK1-as cells due to the modified CDK1 kinase. Staining of the wildtype HeLa cells led to the same result (Fig. 27B): I observed clear H3S10ph foci in cells that were negative for H3T3ph staining. Moreover, chromatin labelling with H3T3ph occurred only in cells that exhibited strong H3S10ph staining throughout the nucleus.

I further resolved the temporal relationship between the H3T3ph and H3S10ph marks in cells normally passing through the cell cycle by using fluorescently labelled Fab fragments and live cell imaging. To allow a simultaneous detection of two histone marks, I used CF640R-labelled Fab fragments detecting H3T3ph and Alexa488-labelled Fab fragments detecting H3S10ph. This experimental setup allowed me to study the formation of these two histone marks in living cells with a very accurate temporal resolution (Fig. 28; Movie 4).

The live cell analysis revealed that the typical H3S10ph foci seen in the G_2 phase are present in interphase cells long before the H3T3ph mark emerges (Fig. 28 - 6.0 h/8.7 h). It was only with the breakdown of the nuclear envelope that a simultaneous signal for both chromatin marks was detectable and appeared all over chromatin (Fig. 28 - 9.5 h).

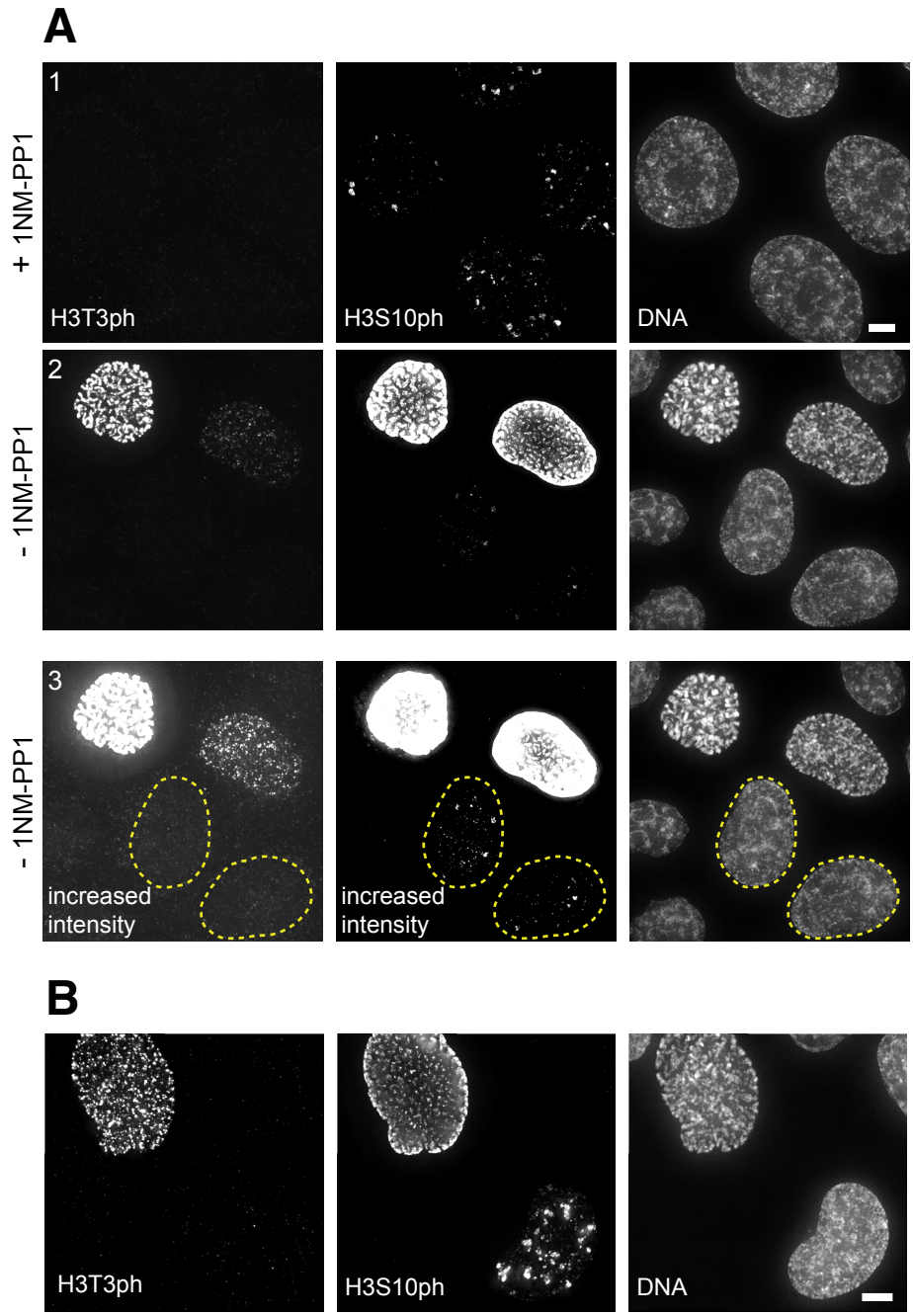

Figure 27: H3S10ph foci precede emergence of H3T3 phosphorylation.
(A) Immunofluorescence analysis of Hela CDK1-as cells synchronised with 10 µM 1NM-PP1 for 20 h (+1NM-PP1) (1) or left unsynchronised (-1NM-PP1) (2). Cells were stained with Hoechst 33342 and immunostained with antibodies recognising histone H3T3 phosphorylation and histone H3S10 phosphorylation. Scale bar, 5 µm.
Panel 3 shows the same cells as those in panel 2, but with increased image intensities of the channels representing the H3T3ph and H3S10ph staining. The outlined nuclei show the stage at which H3S10ph foci are already present while a H3T3ph signal is not yet detectable.
(B) Immunofluorescence analysis of Hela cells with a wildtype CDK1 kinase. Cells were stained with Hoechst 33342 and immunostained with antibodies recognising histone H3T3 phosphorylation and histone H3S10 phosphorylation. Scale bar, 5 µm.

Besides the emergence of H3T3ph and H3S10ph, the live cell imaging also provided insight into the removal of those marks. Remarkably, H3T3ph disappeared quickly after the onset of anaphase, whereas the chromatin remained positive for the H3S10ph mark for a longer time (Fig. 28 - 10.8 h).

Together, the formation of the H3S10ph foci in G_2 cells appears to be independent of H3T3ph, as the H3T3ph mark only emerges after foci of H3S10ph had already been present.

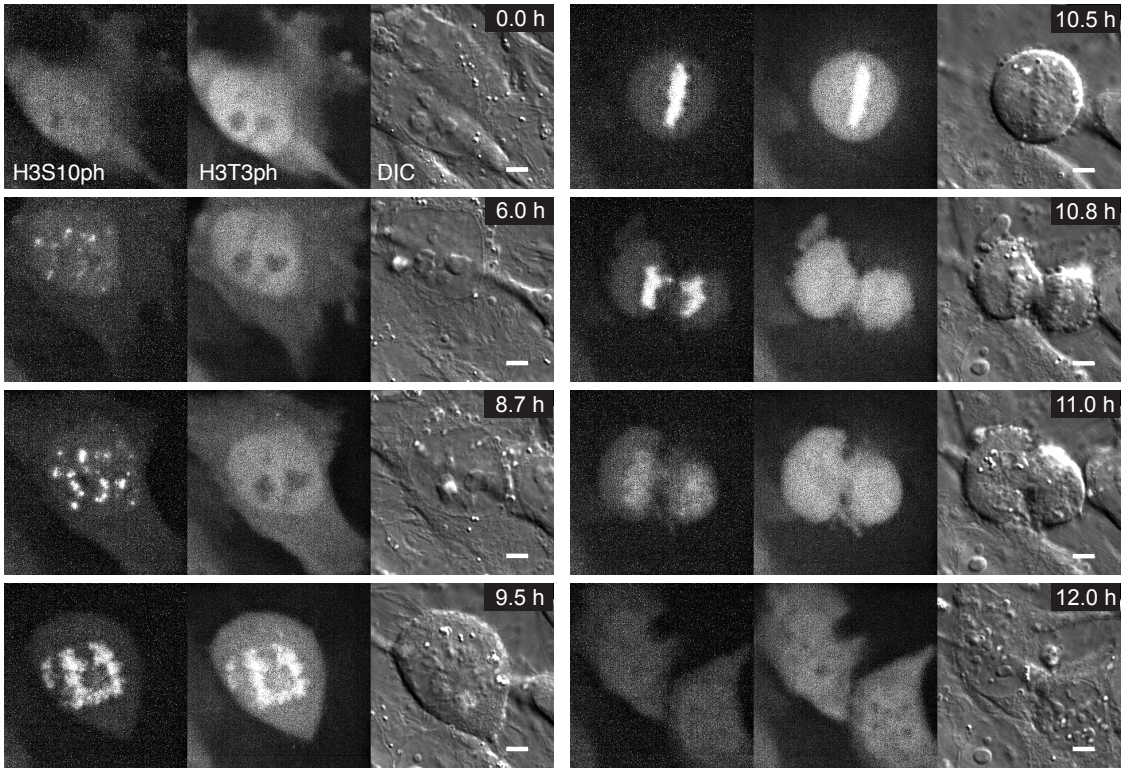

Figure 28: Live cell imaging reveals the relative timing of the H3S10ph and H3T3ph marks.

Stills of a live cell imaging movie analysing HeLa cells with two different fluorescently labelled Fab fragments. Alexa488-labelled Fab fragments recognise histone H3S10 phosphorylation and CF640R-labelled Fabs recognise H3T3 phosphorylation. Movies were acquired with a 100× objective every 10 min, with five z-sections every 1.2 µm and using Differential Interference Contrast (DIC) microscopy. Scale bar, 5 µm.

5.2.2 H3S10ph foci precede clustering of the H2AT120 phosphorylation mark

Besides the H3T3ph mark, H2AT120ph also contributes to CPC clustering at the centromere region of mitotic chromosomes (Yamagishi *et al.*, 2010). Therefore, I next examined a possible role of H2AT120ph in H3S10ph focus formation in G_2 cells.

Similar to the experiments investigating a contribution of H3T3ph in H3S10ph focus formation in G_2, I performed immunofluorescence experiments and co-stained for H3S10ph and H2AT120ph in 1NM-PP1 synchronised HeLa CDK1-as cells (Fig. 29-1). In contrast to the H3T3ph signal, which was absent at the CDK1 arrest point, I observed a diffuse labelling of the entire nucleoplasm in the channel detecting the H2AT120ph staining. Because the whole culture was synchronised and exhibited the same staining pattern, I could not determine whether the staining represented the correct H2AT120ph detection or was an unspecific background labelling.

Therefore, I next analysed cells that were not synchronised (-1NM-PP1) (Fig. 29-2). In the unsynchronised culture, I also observed nuclei with a staining pattern similar to that present in the synchronised culture, with individual H3S10ph foci and a diffuse H2AT120ph labelling. However, in cells that were in early mitosis, judged by the condensed chromatin and strong H3S10ph signal throughout the nucleus, clear foci of H2AT120ph were visible, representing the typical H2AT120ph staining at mitotic centromeres.

These observations suggest that the anti-H2AT120ph antibody recognises the correct epitope and that H3S10ph foci appear at centromeres at a time when the H2AT120ph mark still localises diffusely throughout the nucleus.

Next, I planned to investigate the temporal relationship between H2AT120ph and H3S10ph in more detail, but I did not have access to Fab fragments that recognise H2AT120ph. However, my knowledge about H3S10ph progression from previous live cell imaging experiments using Fab fragments allowed me to arrange imaged cells from a fixed culture in a progressive sequence from G_2 toward mitosis (Fig. 30).

The diffuse labelling of H2AT120ph throughout nuclei was present in cells that were negative for the H3S10ph staining (Fig.30-1). Note that the smaller cell, presumably representing the G_1 stage, was negative for the H2AT120ph staining, indicating that diffuse staining of the H2AT120ph mark through nuclei emerges after the G_1 phase and before H3S10ph foci are established in G_2. When the H3S10ph foci emerged, the H2AT120ph labelling did not change (Fig. 30-2). Even as the H3S10ph became more prominent and more abundant, I did not observe a change in the H2AT120ph staining pattern (Fig. 30-3). Only when the H3S10ph signal started to spread through the nucleus did the H2AT120ph signal begin to concentrate in small foci (Fig. 30-4). Once the entire chromatin was positive for the H3S10ph mark, the H2AT120ph foci became clearer, increasing in size and brightness (Fig. 30-5). After the H3S10ph labelling became abundant, the increasing chromosome condensation allowed me to determine the stage of individual cells in mitotic progression further. At the stage in which condensed chromosomes became apparent, strong H2AT120ph foci were present (Fig. 30-6).

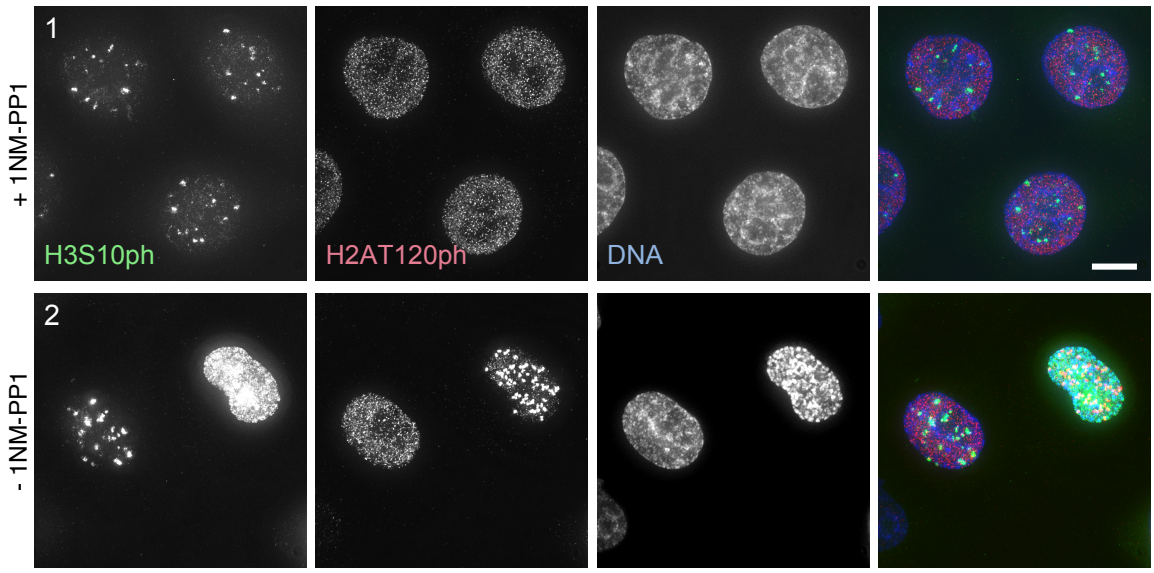

Figure 29: Diffuse nuclear labelling of H2AT120 phosphorylation at the CDK1 arrest point.
Immunofluorescence analysis of Hela CDK1-as cells synchronised with 10 µM 1NM-PP1 for 20 h (+1NM-PP1) (1) or left unsynchronised (-1NM-PP1) (2). Cells were stained with Hoechst 33342 (blue) and immunostained with antibodies recognising histone H3S10 phosphorylation (green) and histone H2AT120 phosphorylation (red). Scale bar, 10 µm.

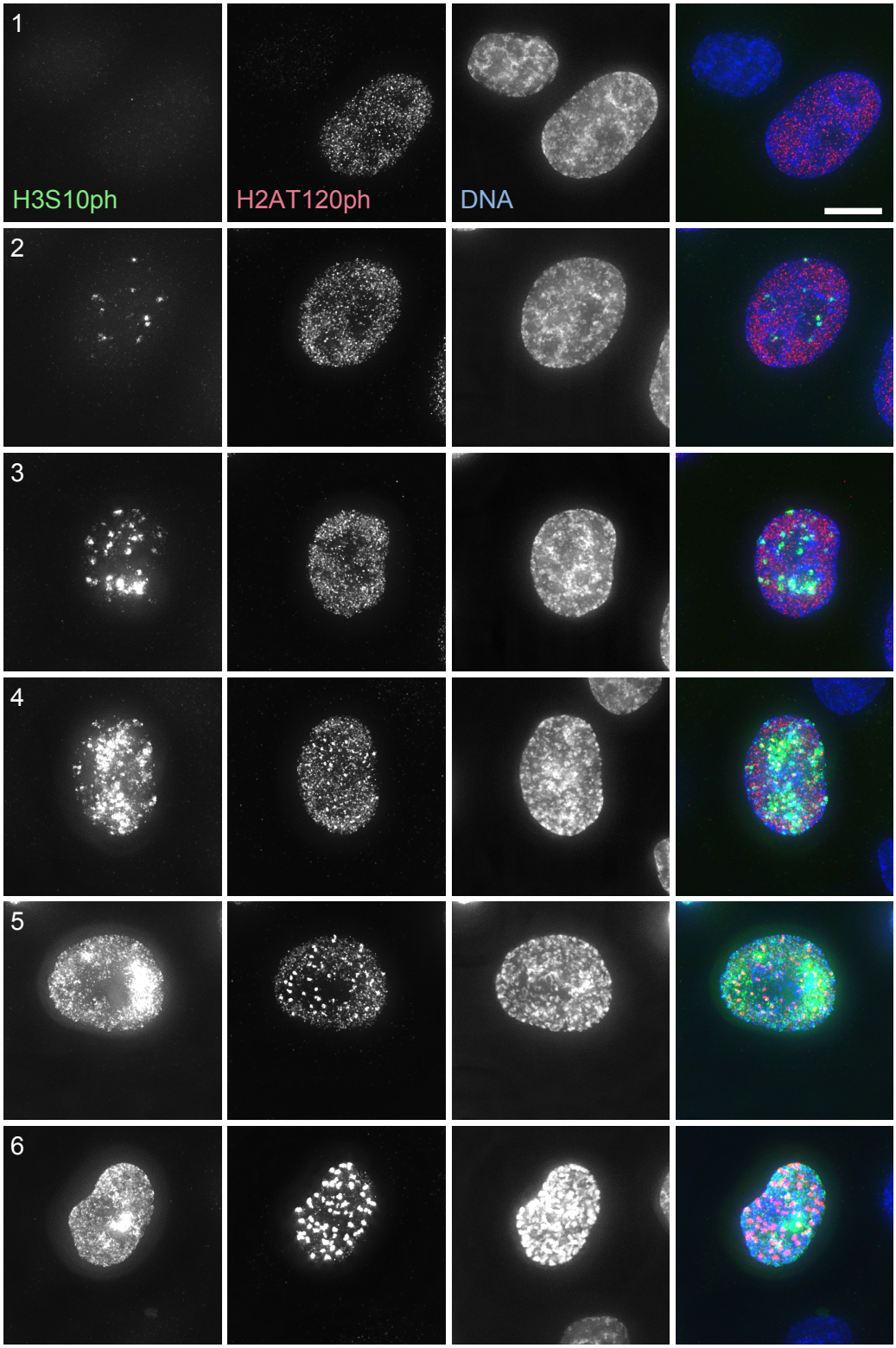

Figure 30: H3S10ph foci precede clustering of the H2AT120 phosphorylation mark.
Immunofluorescence analysis of unsynchronised Hela CDK1-as cells that are arranged in a sequence from the early G_2 stage (1) towards prophase (6) based on the H3S10 phosphorylation staining and the chromosome condensation state. Cells were stained with Hoechst 33342 (blue) and immunostained with antibodies recognising histone H3S10 phosphorylation (green) and histone H2AT120 phosphorylation (red). Scale bar, 10 µm.

Together, these results indicate that H3S10ph foci form independently of H2AT120ph clustering, which begins only once the H3S10ph mark starts to spread through the nucleus.

Overall, the investigation of the histone marks H3T3ph and H2AT120ph, which are reported to be responsible for CPC localisation at centromeres in mitosis, revealed that they only begin to concentrate at centromeres at the G_2/M transition. Therefore, this suggests that these marks do not contribute to H3S10ph focus formation during G_2, and instead other molecular mechanisms are responsible for CPC clustering and activation in the G_2 phase of the cell cycle.

5.3 H3S10ph foci in G_2 depend on HP1

In light of my previous results, including the independence of H3S10ph focus formation in G_2 cells from H3T3ph and H2AT120ph (see Figs. 27 - 30), the strong interaction between the CPC and CB-EY-HP1α in mitosis (see Figs. 18 and 19), and the clear co-localisation between H3S10ph foci and clusters of EY-HP1α (see Fig. 23), I hypothesized that HP1α might contribute to Aurora B clustering and activation in G_2 cells.

5.3.1 H3S10ph foci appear at clusters of endogenous HP1α

To determine whether HP1α is responsible for H3S10ph focus formation in G_2 cells, I first performed immunofluorescence experiments and stained for H3S10ph and endogenous HP1α in 1NM-PP1 synchronised CDK1-as cells. As was the case for clusters of expressed EY-HP1α (see Fig. 23), the H3S10ph foci co-localised precisely with clusters of endogenous HP1α (Fig. 31A). Furthermore, endogenous HP1α clusters showed a clear co-localisation with Aurora B in the entire synchronised culture (Fig. 31B). These results indicate that Aurora B clustering and the formation of H3S10ph foci occur at sites of endogenous HP1α clusters in G_2 cells.

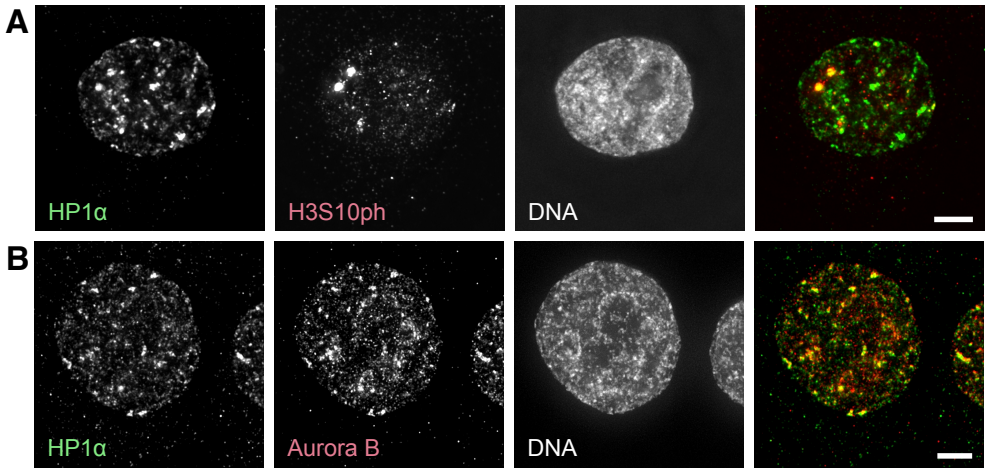

Figure 31: Aurora B concentration and H3S10ph foci appear at clusters of endogenous HP1α.

(A) Immunofluorescence analysis of Hela CDK1-as cells synchronised with 10 µM 1NM-PP1 for 20 h. Cells were stained with Hoechst 33342 and immunostained with antibodies recognising HP1α (green) and histone H3S10 phosphorylation (red). Scale bar, 5 µm.

(B) Immunofluorescence analysis of Hela CDK1-as cells synchronised with 10 µM 1NM-PP1 for 20 h. Cells were stained with Hoechst 33342 and immunostained with antibodies recognising HP1α (green) and Aurora B (red). Scale bar, 5 µm.

5.3.2 Loss of HP1α + HP1γ eliminates H3S10ph foci at the G_2 stage

To analyse the role of the three HP1 isoforms in H3S10ph focus formation in G_2 cells, I used various single and double knockouts of HP1α, HP1β, and HP1γ in HeLa cells. The individual knockout cells were generated using the CRISPR/Cas9 system in the laboratory of Shinya Ohta at Kochi University, Japan and a Western blot analysis provided by him demonstrates the successful depletion of the indicated HP1 isoforms (Fig. 32A). The HP1 knockout cell lines were generated based on cells with a wildtype CDK1 kinase. Therefore, I used RO-3306, a CDK1 inhibitor, to synchronise cells at the CDK1 arrest point in G_2. However, RO-3306 does not work as reliably as the CDK1-as/1NM-PP1 system in terms of synchronisation, and hence, I stained for cyclin B to evaluate the cell cycle stage of the analysed cells more precisely.

In line with previous experiments, I detected evident H3S10ph foci in wildtype G_2 cells, which expressed all three HP1 isoforms (Fig. 32B1). In HP1α KO cells, I still identified H3S10ph foci in cyclin B-positive G_2 cell, but with a reduced frequency (in 67% of HP1α KO cell versus in 93% of wildtype cells) and a somewhat decreased signal intensity (Fig. 32B2). A further analysis of various HP1 single and double knockout cell lines revealed that only the simultaneous knockout of HP1α and HP1γ led to the loss of H3S10ph foci in almost all G_2 cells (Fig. 32B3): Instead of H3S10ph foci, a diffuse H3S10ph staining evenly labelled the nuclei of HP1α + HP1γ double KO cells. In a few cases (< 5%), I observed cells with H3S10ph foci in the HP1α + HP1γ double knockout culture (Fig. 32B4). However, the staining for cyclin B was much stronger in these cells, suggesting that they were approaching the G_2/M transition.

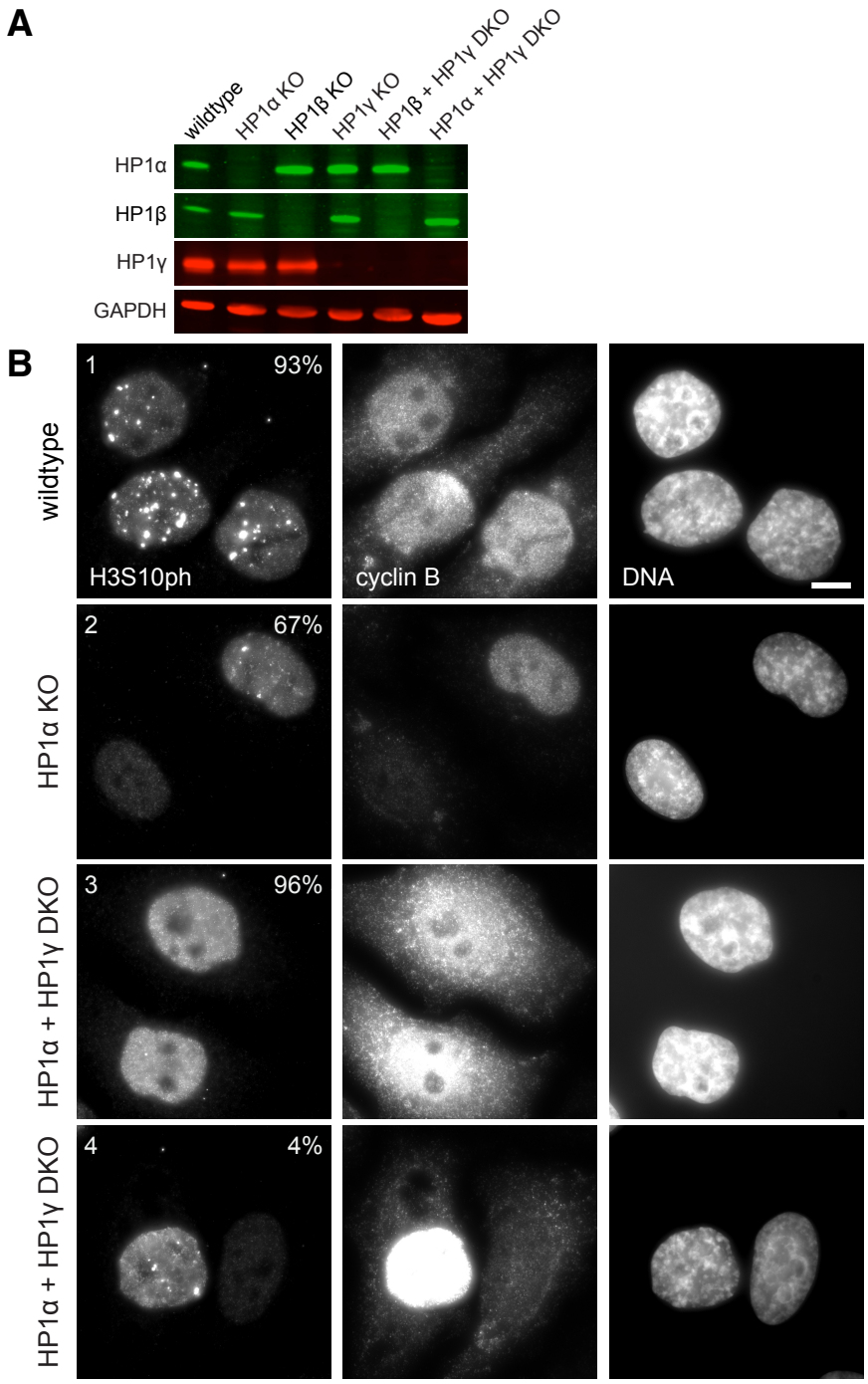

Figure 32: Loss of HP1α + HP1γ eliminates H3S10ph foci at the G_2 stage.

(A) Western blot analysis of Hela whole cell lysates using the indicated HP1 single or double knockout cell (KO) lines. The individual HP1 isoforms were detected using anti-HP1α, anti-HP1β or anti-HP1γ antibodies. GAPDH served as a loading control. Western blot figure was provided by Shinya Ohta who generated the various HP1 KO cell lines.

(B) Immunofluorescence analysis of Hela wildtype (1), HP1α knockout (2), or HP1α + HP1γ double knockout (DKO) cells (3,4). Cells were synchronised for 18 h with 9 µM of RO-3306 and stained with Hoechst 33342 and immunostained with antibodies recognising histone H3S10 phosphorylation and cyclin B. Image processing was performed without deconvolution to preserve the actual appearance of the cyclin B staining. The numbers indicate the frequency of cells with the phenotype shown (n = 100 per cell line). Scale bar,10 µm.

Indeed, I could confirm this assumption by use of live cell imaging with Fab fragments (Fig. 33; Movie 5). Detecting H3S10ph in cycling cells revealed that the H3S10ph foci were present long before the onset of mitosis in wildtype cells, whereas weak H3S10ph foci typically appeared just four frames (which equals 24 min) before NEB in the HP1α + HP1γ double knockout cells (Fig. 33 1.6h). Similar to wildtype cells, the entry into mitosis was accompanied by a H3S10ph signal all over chromatin also in the HP1α + HP1γ double knockout cells (Fig. 33 2.0h).

Together, these results indicate that HP1α and HP1γ contribute to the initial formation of H3S10ph foci in the G_2 phase of the cell cycle.

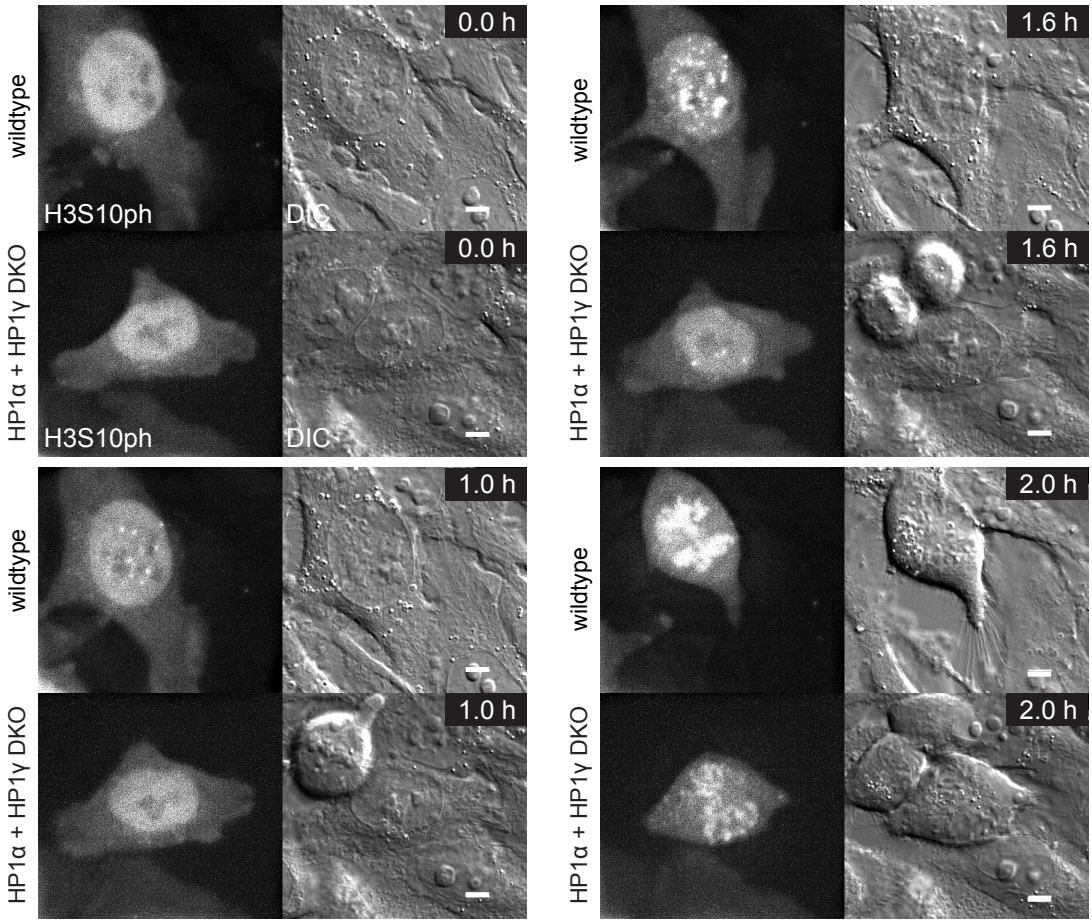

Figure 33: Live cell imaging reveals the delayed appearance of H3S10ph foci in HP1α + HP1γ double KO cells.

Stills of live cell imaging movies analysing wildtype HeLa cells and HP1α + HP1γ double knockout (DKO) HeLa cells. Live cell imaging was performed using Cy5-labelled Fab fragments that recognise H3S10 phosphorylation, together with differential interference contrast (DIC) microscopy. The brightness of the channels representing the Cy5 signal was adjusted individually between the movies of wildtype cells and HP1α + HP1γ DKO cells (0.65% difference), to compensate for the slightly larger amount of loaded Fabs in the wildtype HeLa cell. Movies were acquired with a 100x objective every 6 min, five z-sections every 1.2 µm. Scale bar, 5 µm.

5.3.3 Loss of HP1α + HP1γ abolishes Aurora B clusters in G_2 cells.

Given the diffuse H3S10ph staining in HP1α + HP1γ double KO G_2 cells (Fig. 32B3), I also investigated the localisation of Aurora B, the kinase catalysing the H3S10ph signal. Similar to the diffuse H3S10ph, Aurora B showed a diffuse distribution in synchronised HP1α + HP1γ double KO G_2 cells (Fig. 34-2). By contrast, Aurora B formed clusters that co-localised with endogenous HP1α foci in wildtype cells (Fig. 34-1), as earlier shown in CDK1-as cells synchronised with 1NM-PP1 (see Fig. 31B). Therefore, a double knockout of HP1α + HP1γ eliminates the clustering of Aurora B kinase in G_2 cells.

Together, these results indicate that HP1α and HP1γ contribute to the clustering of Aurora B in G_2 cells.

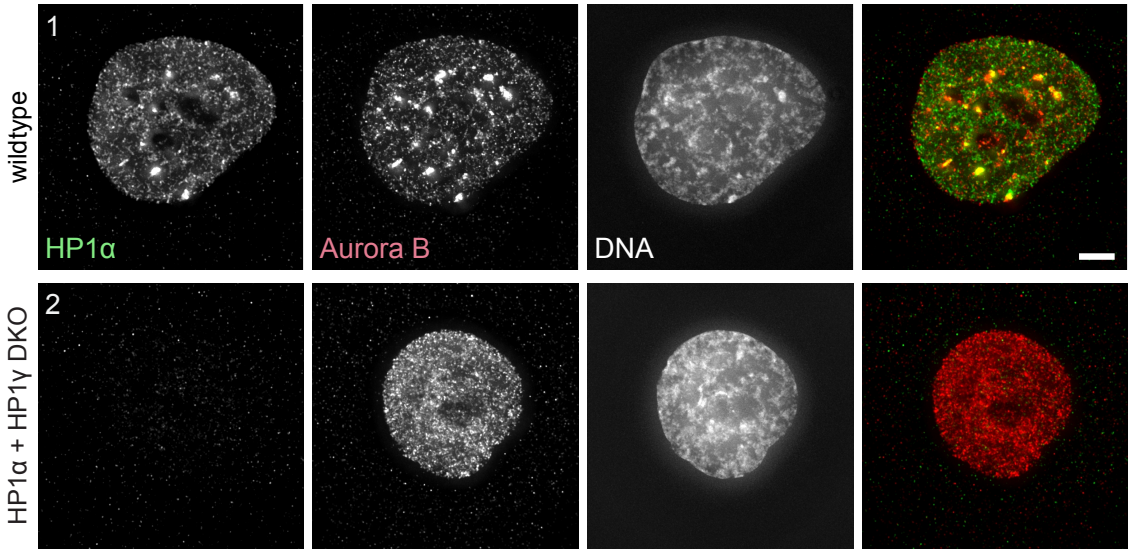

Figure 34: Loss of HP1α + HP1γ abolishes Aurora B clusters in G_2 cells.
Immunofluorescence analysis of Hela wildtype (1) or HP1α + HP1γ double knockout (DKO) cells (2). Cells were synchronised for 18 h with 9 µM of RO-3306 and stained with Hoechst 33342 and immunostained with antibodies recognising HP1α (green) and Aurora B (red). Scale bar, 5 µm.

5.3.4 Time difference between the emergence of H3S10ph foci and histone marks that cluster the CPC in mitosis appears smaller in HP1α + HP1γ double KO cell

Next, I investigated whether the H3S10ph foci that appear in HP1α + HP1γ double KO cells close to the G_2/M transition, could be mediated by CPC clustering through histone marks that are responsible for CPC localisation during early mitosis.

Co-staining for H3S10ph and H3T3ph in fixed HP1α + HP1γ double KO cells suggested that H3S10ph foci appear in cells with emerging H3T3ph (Fig. 35A2). By contrast, the H3S10ph mark labelled the whole nucleus when the H3T3ph signal started to emerge in wildtype cells (Fig. 35A1), as I previously described in earlier experiments (see Fig. 27). However, in some cases of the HP1α + HP1γ double KO culture, I observed cells that did not exhibit any H3T3ph signal but showed individual H3S10ph foci (Fig. 35A2).

I observed a similar trend when co-staining for H3S10ph and H2AT120ph in fixed cells: H3S10ph foci appeared when the H2AT120ph signal became somewhat more granular, but no specific clusters of H2AT120ph were yet detectable in those HP1α + HP1γ double KO cells (Fig. 35B2). Evident H2AT120ph foci started to emerge only in cells with a strong H3S10ph labelling of the nucleus. Similar to previous results (see Figs. 29 and 30), H3S10ph foci were present in wildtype cells when the nuclei still showed diffuse H2AT120ph labelling (Fig. 35B1).

Together, these results indicate that the time difference between the formation of H3S10ph foci and the appearance of chromatin marks that cluster the CPC in mitosis is much smaller in HP1α + HP1γ double KO cells compared to wildtype cells.

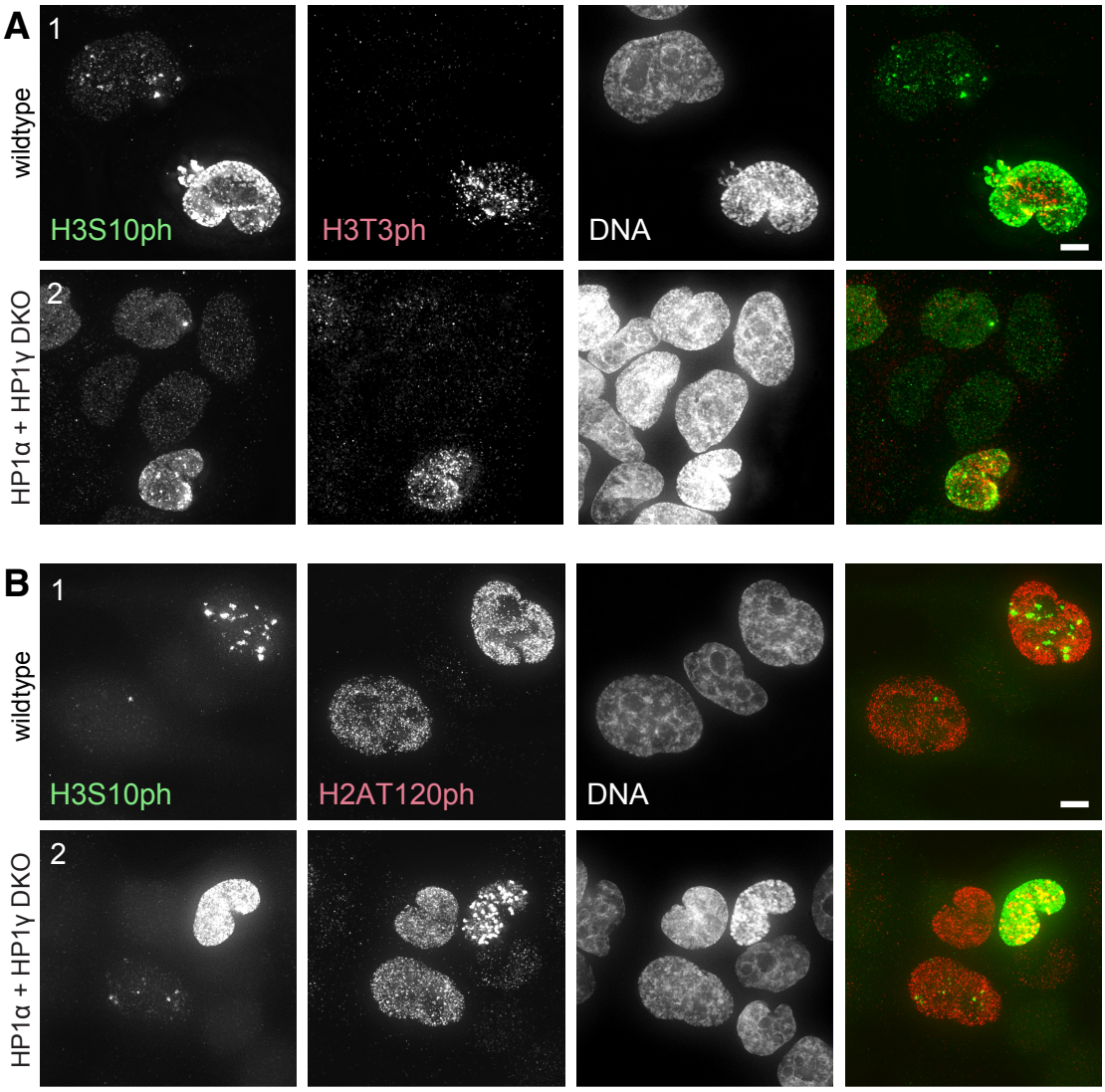

Figure 35: Time difference between the emergence of H3S10ph foci and histone marks that cluster the CPC in mitosis appears smaller in HP1α + HP1γ double KO cells.

(A) Immunofluorescence analysis of Hela wildtype (1) and HP1α + HP1γ double knockout (DKO) cells (2). Cells were stained with Hoechst 33342 and immunostained with antibodies recognising histone H3S10 phosphorylation (green) and histone H3T3 phosphorylation (red). Scale bar, 5 µm.

(B) Immunofluorescence analysis of Hela wildtype (1) and HP1α + HP1γ double knockout (DKO) cells (2). Cells were stained with Hoechst 33342 and immunostained with antibodies recognising histone H3S10 phosphorylation (green) and histone H2AT120 phosphorylation (red). Scale bar, 5 µm.

5.3.4.1 Live cell imaging reveals the timing of H3S10ph focus formation and H3T3ph emergence in HP1α + HP1γ double KO cell

I wanted to investigate the emergence of the H3S10ph foci and the H3T3ph mark in HP1α + HP1γ double KO cells with a more precise temporal resolution. Therefore, I made use of the dual labelling approach with two fluorescent Fab fragments, recognising H3S10ph and H3T3ph simultaneously in live cell imaging (Fig. 36; Movie 6).

These experiments confirmed that the time difference between the emergence of H3S10ph foci and the appearance of the H3T3ph mark was indeed very short in HP1α + HP1γ double KO cells. However, H3S10ph foci still seemed to appear shortly before the H3T3ph labelling became visible (Fig. 36 1.5h). Again, this contrasts with the results obtained in wildtype cells, in which I observed clear H3S10ph foci a long time before the H3T3ph mark could be detected.

5.3.5 Expression of EYFP-HP1α in HP1α + HP1γ double KO cells restores H3S10ph focus formation in G_2 cells

To confirm that HP1 contributes to CPC clustering, which in turn leads to H3S10ph focus formation in G_2 cells, I expressed EY-HP1α in the HP1α + HP1γ double KO cells (Fig. 37). Indeed, the presence of EY-HP1α in these double KO cells resulted in the appearance of H3S10ph foci, co-localising with EY-HP1α clusters in cyclin B-positive cells. Importantly, cells that did not express EY-HP1α showed a diffuse H3S10ph labelling even when their cell cycle stage was closer to the G_2/M transition, as indicated by a stronger cyclin B signal (Fig. 37).

Overall, these results suggest that HP1α and HP1γ contribute to the clustering and activation of the CPC in the G_2 phase of the cell cycle. This is a novel mode of CPC recruitment that occurs before the CPC concentration takes place via histone marks at mitotic centromeres.

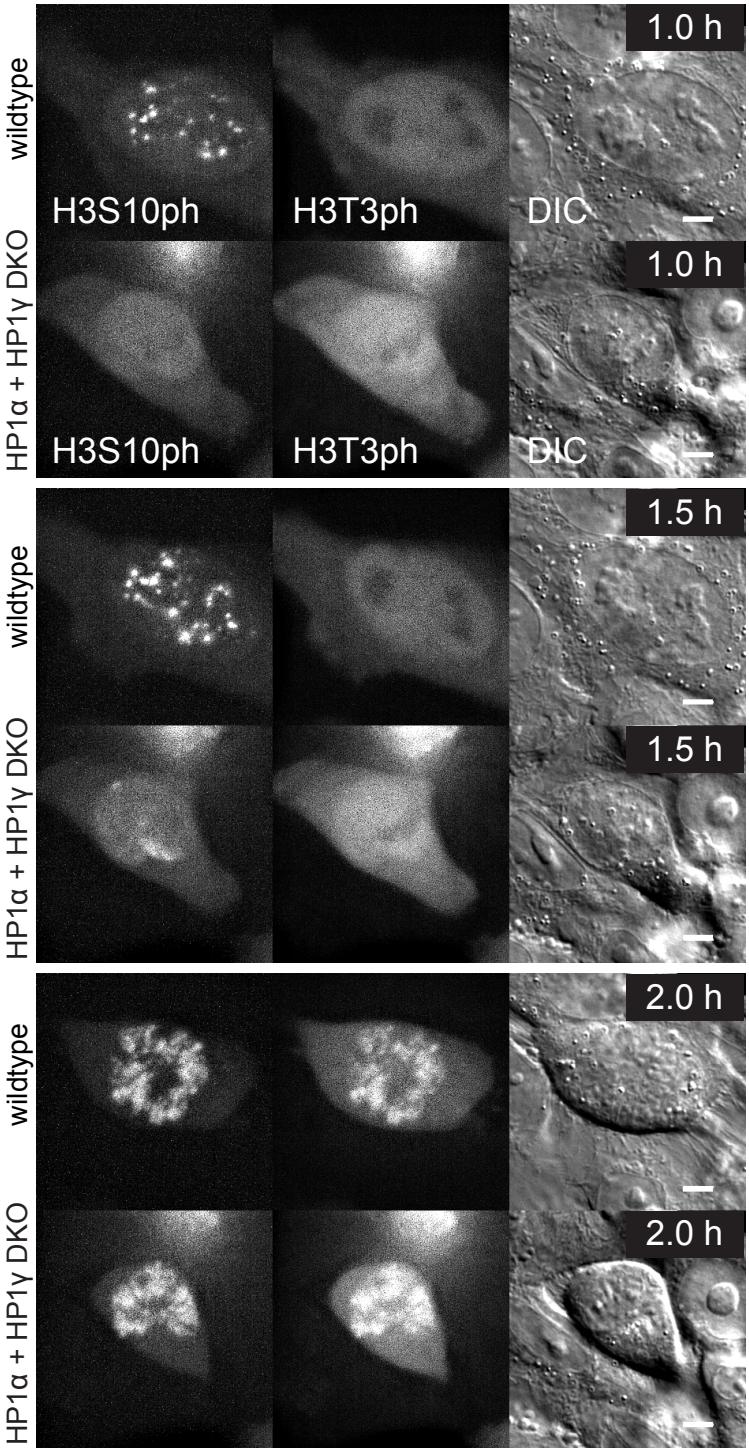

Figure 36: Live cell imaging reveals the delayed appearance of H3S10ph foci in HP1α + HP1γ double KO cells.

Stills of live cell imaging movies analysing wildtype HeLa cells and HP1α + HP1γ double knockout (DKO) HeLa cells. Live cell imaging was performed using Cy5-labelled Fab fragments that recognise H3S10 phosphorylation, together with differential interference contrast (DIC) microscopy. The brightness of the channels representing the Cy5 signal was adjusted individually between the movies of wildtype cells and HP1α + HP1γ DKO cells (0.65% difference), to compensate for the slightly larger amount of loaded Fabs in the wildtype HeLa cell. Movies were acquired with a 100x objective every 6 min, five z-sections every 1.2 µm. Scale bar, 5 µm.

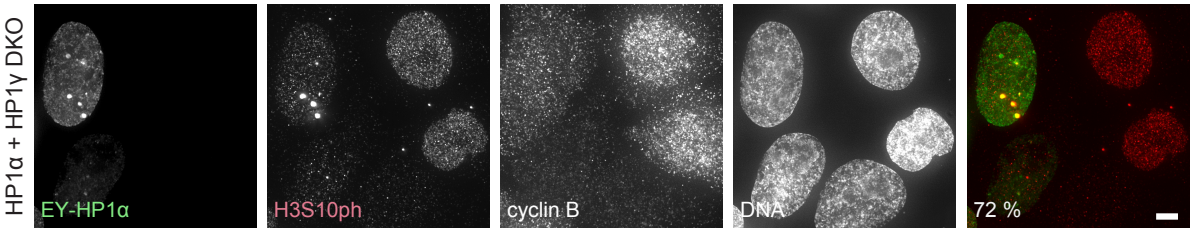

Figure 37: Expression of EYFP-HP1α in HP1α + HP1γ double KO cells restores H3S10ph focus formation in G_2 cells.

Immunofluorescence analysis of HP1α + HP1γ double knockout (DKO) HeLa cells 24 h after transfection with a construct expressing EY-HP1α (shown in green). Cells were synchronised for 12 h with 9 µM RO-3306 and stained with Hoechst 33342 and immunostained with antibodies recognising histone H3S10 phosphorylation (red) and cyclin B. The percentage of cyclin B positive EY-HP1α expressing cells that showed H3S10ph foci is indicated (n = 100). Scale bar, 5 µm.

6 Results chapter 4: HeLa CDK1-as characterisation

Chemical genetics can be used to modify the ATP-binding site in kinases so that they become sensitive to selective inhibitors. 1NM-PP1 is an ATP analogue that contains a large hydrophobic group and therefore fits only in an engineered ATP-binding site removing the bulky "gatekeeper" residue (Shokat and Velleca, 2002), allowing a specific inhibition of the modified kinase. This approach was previously made mainly in yeast cells, but also in vertebrate cells (Weiss *et al.*, 2000; Grzegorz *et al.*, 2004; Hochegger *et al.*, 2007). Hochegger and colleagues described in their work that selective inhibition of the CDK1 kinase leads to an arrest in the G_2 stage of the cell cycle (Hochegger *et al.*, 2007). This arrest is reversible upon 1NM-PP1 washout and results in a rapid entry into mitosis of the entire synchronised culture. Therefore, the CDK1-as/1NM-PP1 system allows a specific synchronisation at the CDK1 arrest point and a strong enrichment of mitotic cells. Because of the various applications of the CDK1-as/1NM-PP1 system, our research group decided to generate a HeLa CDK1-as cell line. HeLa cells are one of the most widely used human cell lines in cell biology research and have good imaging properties because of being adherent and relatively non-motile.

6.1 Cloning of HeLa CDK1-as cells

The original transfection and cloning to generate the HeLa CDK1-as cells was done by Kumiko Samejima and Melpomeni Platani according to the following strategy. The cell line HeLa MKF1 was used to create the HeLa CDK1-as cells (Klebig *et al.*, 2009). First, cells were transfected with Xenopus CDK1as cDNA that was linked to a puromycin resistance gene via a sequence coding for the T2A peptide (see Appendix for the plasmid map). Puromycin-resistant clones were analysed by Western blot to determine the expression level of the CDK1-as protein. Clones with an adequate expression level of CDK1-as were subjected to inactivation of the endogenous CDK1 gene by the CRISPR/Cas9 system. Cells were transiently transfected with a construct expressing human codon-optimised Cas9 nuclease

(hCas9; Addgene ID41815) together with a construct containing the guide RNA (gRNA) (Addgene ID41824). Both constructs were previously described in (Mali *et al.*, 2013) and the insertion of the gRNA against the targeting sequence ATTTCCCGAATTGCAGTACTAGG within the CDK1 gene into the gRNA cloning vector was done in the laboratory of Masato Kanemaki at the National Institute of Genetics, Japan. After geneticin selection for six days, colonies were grown in standard DMEM growth medium for two weeks. In total, 96 colonies were picked and treated with 1NM-PP1 for two days. Colonies that showed mitotic cells were discarded and the remaining clones were subjected to a 1NM-PP1 washout. Cells were examined for the presence of mitotic cells 1 hour after the washout, and 18 clones were picked for further characterisation. This was the point at which my contribution to the project started.

6.2 Characterising synchronisation and release of HeLa CDK1-as cells to identify a suitable clone

To identify a suitable HeLa CDK1-as clone, I characterised in an initial step seven different clones regarding their synchronisation ability at the CDK1 arrest point by use of 1NM-PP1 and their behaviour upon 1NM-PP1 washout (Fig. 38). All clones, except clone 10 and 14, showed a uniform synchronisation in interphase 24 h after 1NM-PP1 addition with no mitotic cells detectable (Fig. 38A). However, a strong variability between the individual clones was detectable at 90 min after 1NM-PP1 washout, with the mitotic indices ranging from ~ 50% up to over 90% (Fig. 38A).

Clones number 1 and 3 showed the highest mitotic index among those analysed and were therefore used for a more detailed examination. This included fixing cells 60, 90, and 120 min after 1NM-PP1 washout (Fig. 38B) and an analysis of the mitotic phases (Fig. 38C). More than 80% of cells in both clones entered mitosis 60 min after 1NM-PP1 washout. However, even at 120 min after 1NM-PP1 washout, some cells remained in interphase. I did not detect a difference in the mitotic index between 90 and 120 min after 1NM-PP1 washout, suggesting that this small population of interphase cells is not progressing into mitosis opposed to the rest of the culture.

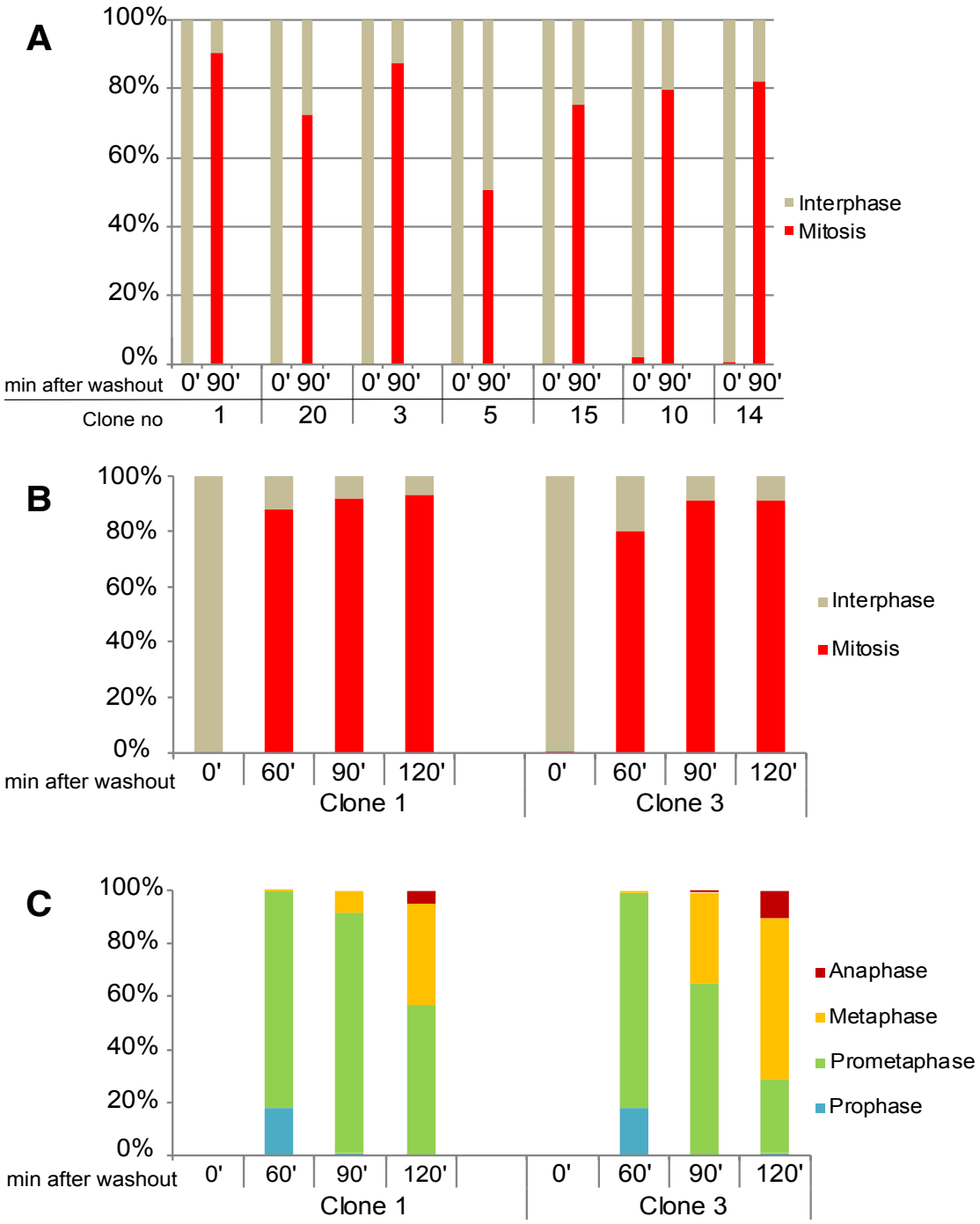

Figure 38: Characterising synchronisation and release of the first set of HeLa CDK1-as cells to identify a suitable clone.

Frequency of mitotic cells **(A, B)** or of the different mitotic phases **(C)** in a culture of HeLa CDK1-as cells treated with 1NM-PP1for 24 h. Cells were fixed after the 1NM-PP1 washout at the indicated time points (in minutes), with n=300 cells analysed per clone and time point.

Next, I determined the progress of the released cultures through mitosis (Fig. 38C). A majority of cells had already entered prometaphase 60 min after 1NM-PP1 washout, but hardly any cells had reached the metaphase stage yet. The analysis of cells fixed 90 min after 1NM-PP1 washout suggested that cells of clone 3 progressed faster through mitosis than cells of clone 1, indicated by a higher ratio of cells being in metaphase (37% clone 3 versus. 9% clone 1). Analysis of cells fixed 120 min after 1NM-PP1 washout showed a similar trend with more cells being at later mitotic stages in the culture of clone 3 than of clone 1.

To identify a HeLa CDK1-as clone which shows a more synchronous release, I characterised ten additional clones and compared them to clones number 1 and 3 (Fig. 39A). Clone number 11, 16, and 17 did not show a complete cell cycle arrest after 24 h of 1NM-PP1 treatment. Upon release from the 1NM-PP1 block, only clone 21 showed a mitotic index comparable to clone 1 and 3. Therefore, I chose clone 1, 3, and 21 for a more detailed characterisation.

First, I blocked with 1NM-PP1 for 24 h and characterised the mitotic stages 90 min after 1NM-PP1 washout (Fig. 39B). At this time point, 77% of cells of clone 21 appeared to be in prometaphase and 22% of cells in metaphase. In contrast to this, clone 3 appeared to progress faster through mitosis with only 26% of cells in prometaphase but 72.7% in metaphase. The values for clone 1 were between of the two other clones, with 54.7% of cells in prometaphase and 45.3% in metaphase.

During this analysis, I noticed a large number of cells with multipolar spindles, with frequencies between 2.67% and 4.67%, judged by the α-tubulin staining (Fig. 39C)

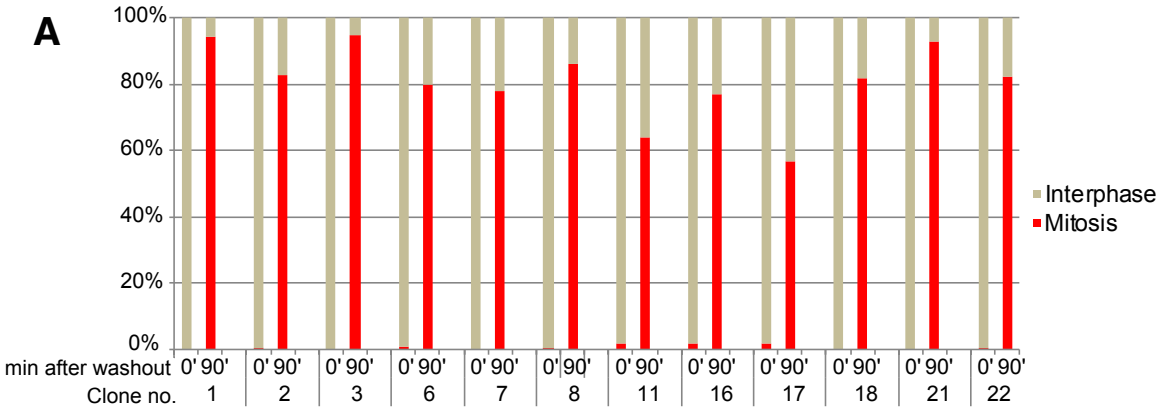

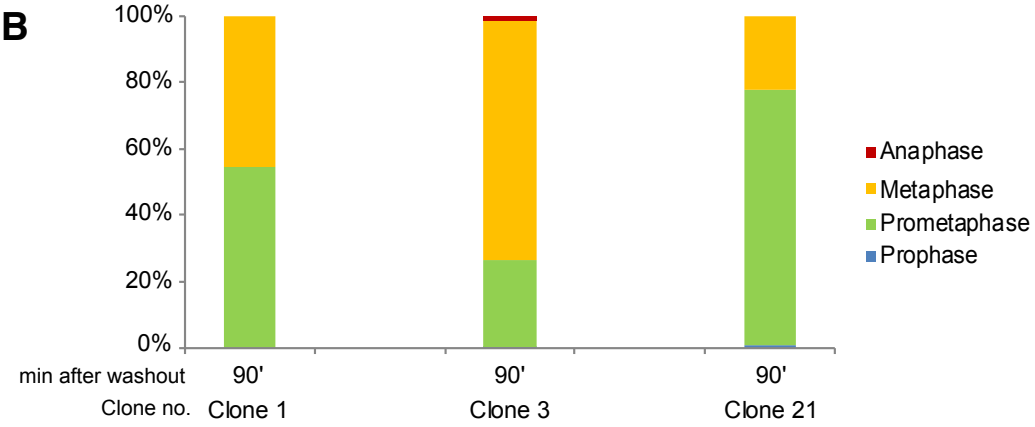

C

Clone number	Frequency of multipolar spindles
Clone 1	2.7 %
Clone 3	4.3 %
Clone 21	4.7 %

Figure 39: Characterising synchronisation and release of the second set of HeLa CDK1-as cells to identify a suitable clone.

(A, B) Frequency of mitotic cells (A) or of the different mitotic phases (B) in the culture of HeLa CDK1-as cells treated with 1NM-PP1for 24 h. Cells were fixed after the 1NM-PP1 washout at the indicated time points (in minutes), with n=300 cells analysed per clone and time point.

(C) Frequency of mitotic cells with multipolar spindles judged by the immunostaining with an antibody recognising α-tubulin, with n=300 mitotic cells analysed.

6.3 Determining the doubling time of CDK1-as clones

Because of the unusually large number of cells with multipolar spindles, I determined the doubling time of the different CDK1-as clones and compared it to the cells with a wildtype CDK1 kinase. This served as a further characterisation of the individual clones but also helped me to judge whether it is possible to reduce the duration of the 1NM-PP1 treatment and at the same time keep the high synchrony of the cell population released from a 1NM-PP1 block.

First, I determined the growth rate of these clones compared to the wildtype cells containing an unmodified CDK1 kinase (Fig. 40A). I counted the number of cells every 24 h over a period of 5 days. All CDK1-as clones showed a similar growth rate like the wildtype cells. Based on the growth rate it was possible to calculate the doubling time using following formula:

$$\text{Doubling time} = \frac{\text{Duration of culture} * \log(2)}{\log(\text{final concentration}) - \log(\text{initial concentration})}$$

Calculating the doubling time revealed a similar timing for all clones of ~ 20 h (Fig. 40B). Therefore, I reduced the duration of the 1NM-PP1 treatment to 20 h, as an approach to minimise the number of cells with multipolar spindles.

A

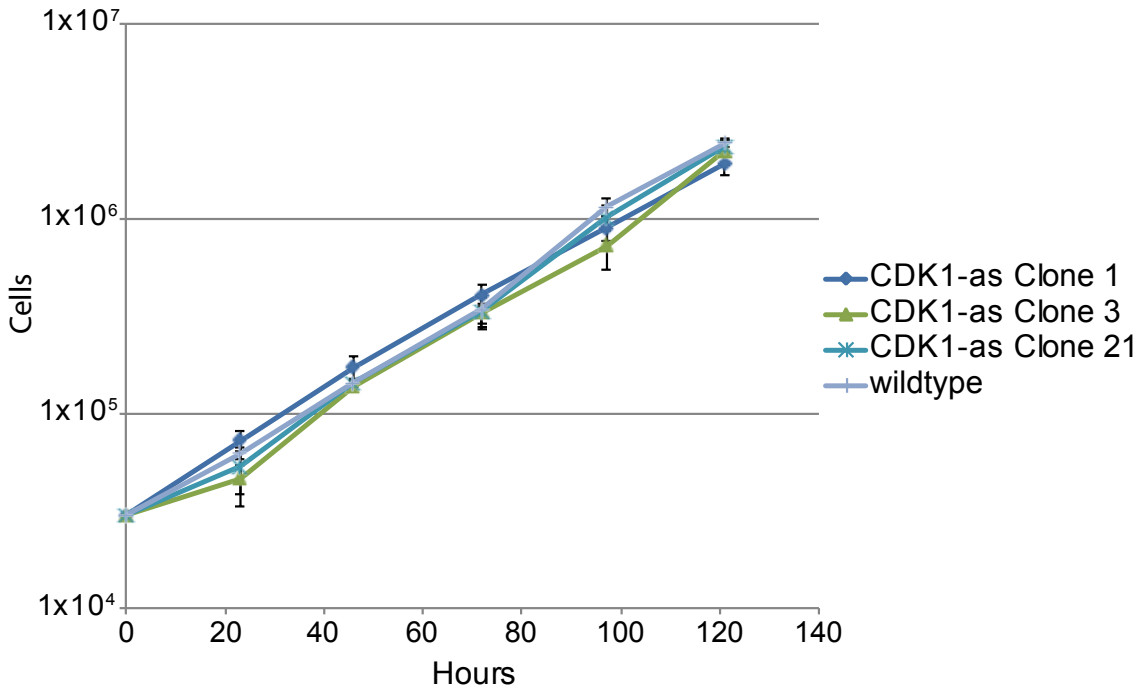

B

Cell type	Doubling time
Clone 1	20.18 h
Clone 3	19.46 h
Clone 21	19.22 h
wildtype	19.08 h

Figure 40: Growth curve and doubling time of selected HeLa CDK1-as clones compared to wildtype cells.

(A) 30,000 cells were seeded per well of a 6-well plate and the cell number was determined every 24 h in triplicate. Graphs represent the mean and standard deviation using a logarithmic scale.

(B) The doubling time of the indicated clones was calculated based on the initial cell number and the cell number at the last timepoint.

6.4 Sequencing of the CDK1 gene

In parallel to the examination of the doubling time, I sequenced the genomic region of the CRISPR/Cas9 cut site to determine the exact sequence of the inactivated CDK1 gene (Fig. 41). Each of the clones showed only two variants of the repaired Cas9 cut site, suggesting that two CDK1 alleles are present in this HeLa cell line. The analysis revealed that clone 1 and 21 contain frameshift mutations in both alleles, which led to the inactivation of the endogenous CDK1 kinase. Interestingly, Clone 3 contained deletions which were in frame, with 21 and 24 base pairs deleted, respectively. The affected sequence codes for the CDK signature motif PSTAIRE (Jeffrey *et al.*, 1995) and the 21 and 24 base pair deletions result in a removal of either the amino acid residues 47-53 (TAIREIS) or 45-52 (PSTAIREI). These deletions most likely destroy the endogenous CDK1 activity of clone 3, because although this clone has no frameshift mutation, it showed similar properties (1NM-PP1 block/release, cell growth etc.) to the other two sequenced clones, which have frameshift mutations in the CDK1 gene.

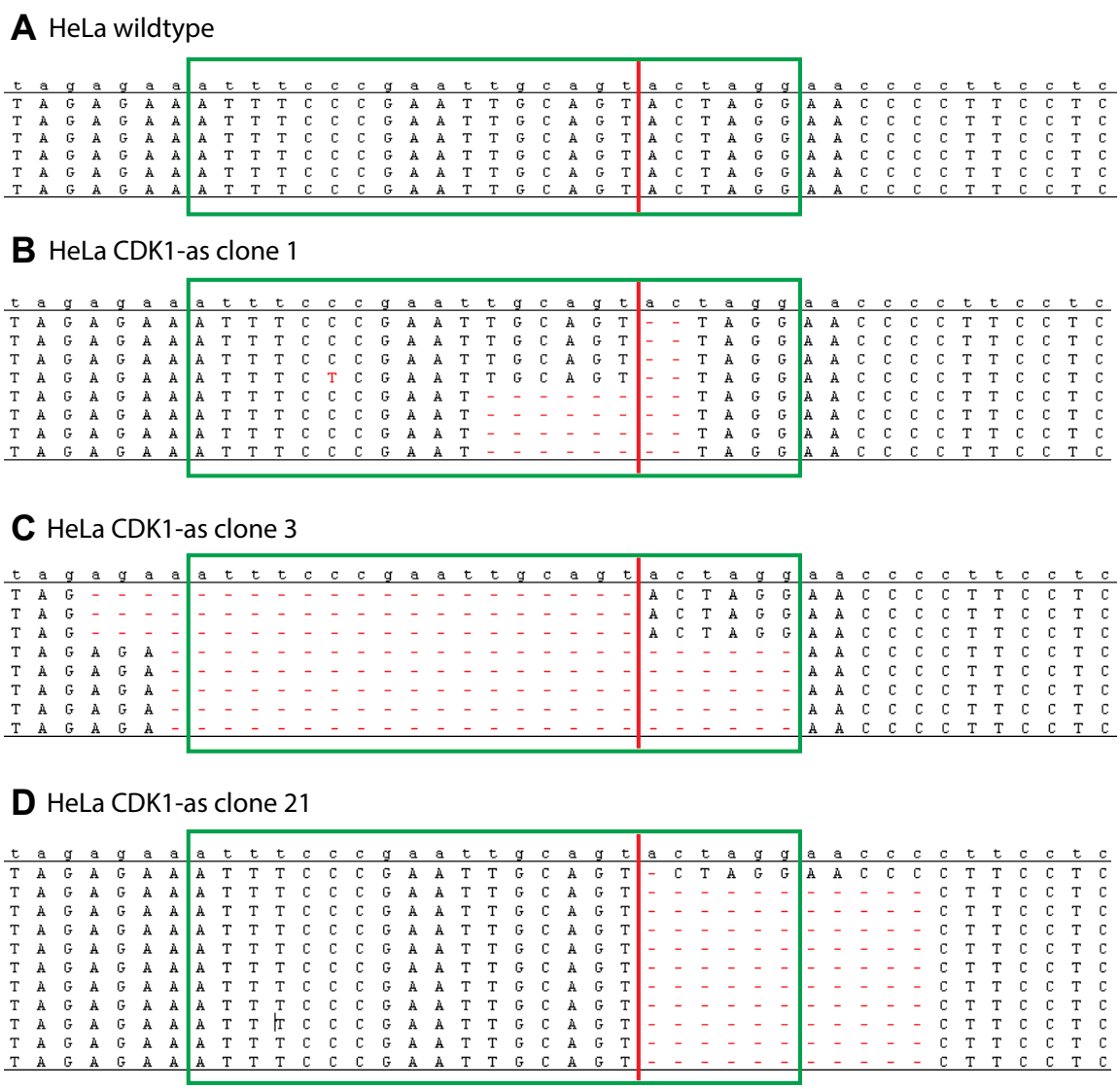

Figure 41: Sequencing of the CDK1 gene.

The genomic region within the CDK1 gene that was recognised by the guide RNA is shown in green, with the Cas9 cut site in red. (A) displays the sequence of the wildtype cells. (B) Hela CDK1-as clone 1 shows deletions of two and eight base pairs, respectively. (C) Hela CDK1-as clone 3 shows deletions of 21 and 24 base pairs, respectively. (D) Hela CDK1-as clone 21 shows deletions of one and 11 base pairs, respectively.

6.5 Reducing the duration of the 1NM-PP1 synchronisation

To reduce the number of cells with multipolar spindles after the release from 1NM-PP1 synchronisation, I shortened the duration of the block from 24 h to 20 h based on the determined doubling time of ~20 h. No mitotic cells were detectable after 20 h of 1NM-PP1 block (Fig. 42A). However, the decreased duration of the 1NM-PP1 block resulted in a reduced number of mitotic cells 90 min after 1NM-PP1 washout, from > 90% to ~ 80% for all three clones.

Additionally, I determined the mitotic phase distribution 60 min after washout of the 20 h 1NM-PP1 treatment (Fig. 42B). Clone 1 and 3 showed a similar distribution with ~ 43% of cells in prometaphase and ~ 56% in metaphase. Clone 21 exhibited a slower progression through mitosis compared to clone 1 and 3 with > 60% of cells scored as prometaphase cells. The high number of prometaphase cells in the clone 21 culture could be due to a high frequency of cells with multipolar spindles, which may have a negative impact on proper chromosome congression and therefore mitotic progression.

For the analysis of multipolar spindles, I stained cells with an anti-Pericentrin antibody. Pericentrin was identified as a core component of the centrosome and is therefore used as a centrosome marker (Doxsey *et al.*, 1994). This staining allowed a much more precise analysis whether a cell had a multipolar spindle and revealed that Clone 1 and 3 both showed multipolar spindles with a frequency of 8.3% in mitotic cells (Fig. 42C). Remarkably, the rate of mitotic cells with multipolar spindles was 27% for clone 21.

Because of the persistent high number of cells with multipolar spindles, I examined the effect of reducing the duration of the 1NM-PP1 block to 4 h (Fig. 43A). This reduced duration was sufficient to eliminate mitotic cells from the entire culture (Fig. 43A). For clone 1 and 3, ~ 17% of cells entered mitosis 60 min after 1NM-PP1 washout, and none of them showed multipolar spindles, judged by staining for Pericentrin (Fig. 43B). However, clone 21 showed cells with multipolar spindles even after only 4 h of 1NM-PP1 block and was therefore excluded from the further characterisation.

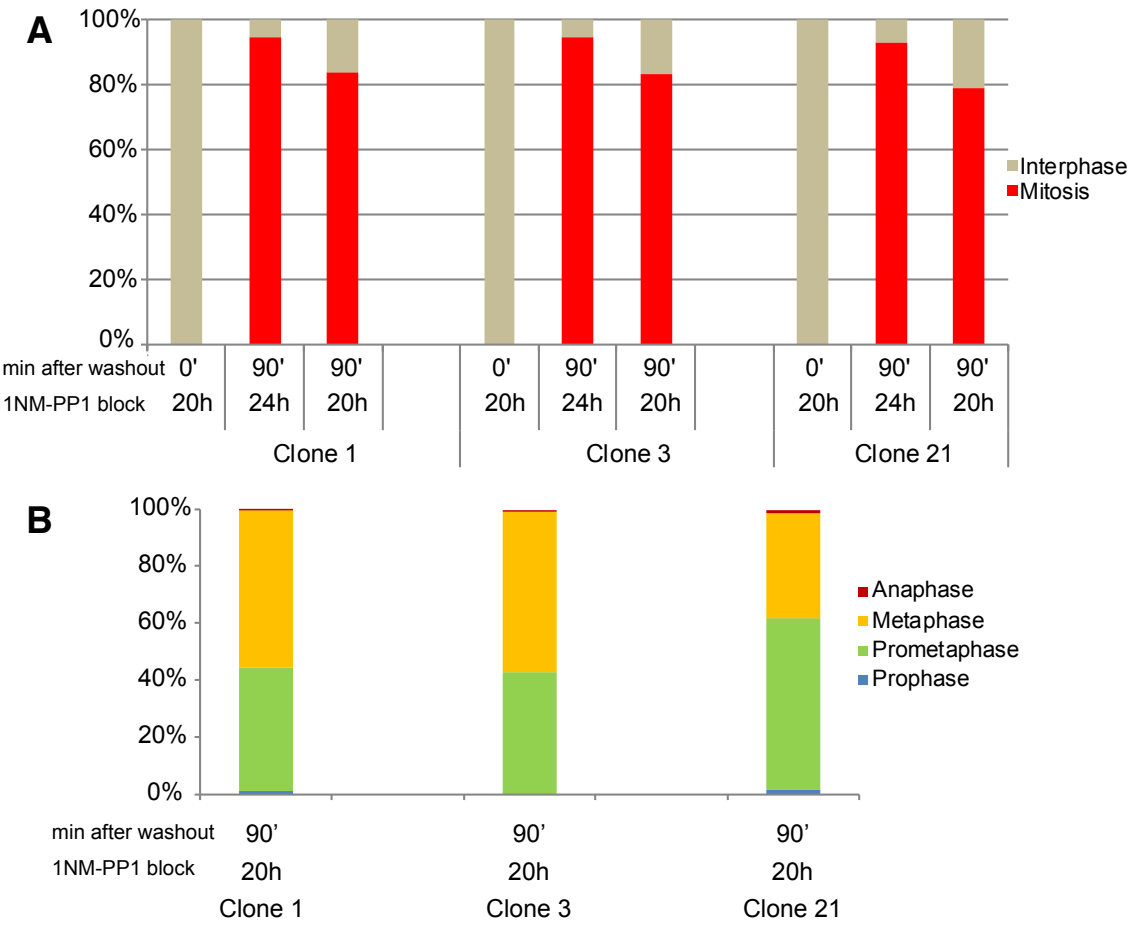

C

Clone number	Frequency of multipolar spindles
Clone 1	8.3 %
Clone 3	8.3 %
Clone 21	27 %

Figure 42: Reducing the duration of the 1NM-PP1 synchronisation to 20 h.

(A, B) Frequency of mitotic cells (A) or of the different mitotic phases (B) in the culture of HeLa CDK1-as cells treated with 1NM-PP1 for 20 h. Data of HeLa CDK1-as cells treated for 24 h with 1NM-PP1 were reproduced from Figure 35A for comparison. Cells were fixed after the 1NM-PP1 washout at the indicated time points (in minutes), with n=300 cells analysed per clone and time point.

(C) Frequency of mitotic cells with multipolar spindles judged by the immunostaining with an antibody recognising Pericentrin, with n=300 mitotic cells analysed.

A

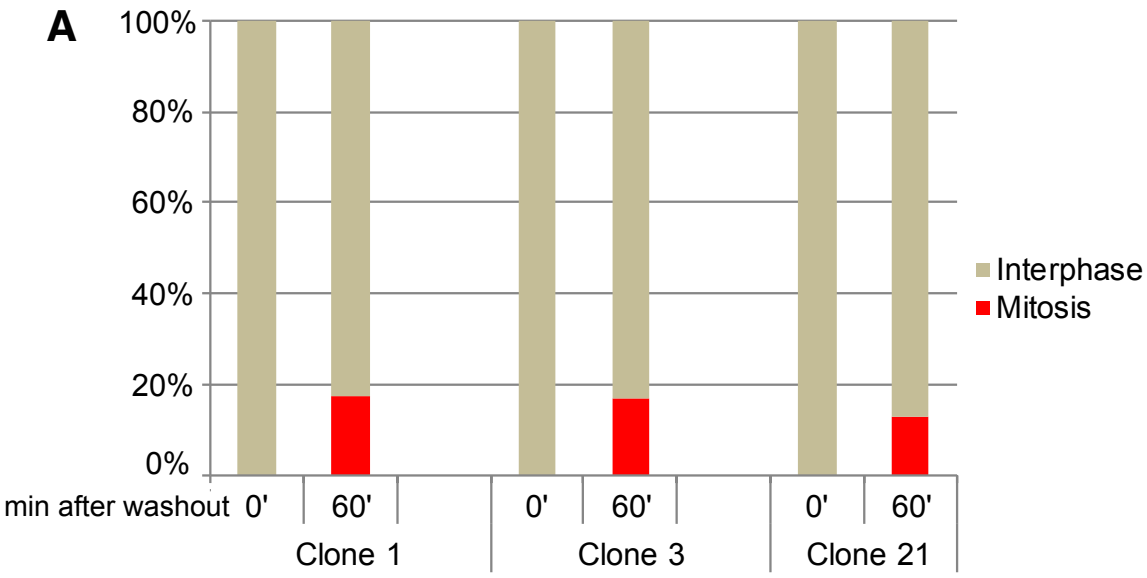

B

Clone number	Number of cells with multipolar spindles
Clone 1	0
Clone 3	0
Clone 21	2

Figure 43: Reducing the duration of the 1NM-PP1 synchronisation to 4 h.

(A) Frequency of mitotic cells in the culture of HeLa CDK1-as cells treated with 1NM-PP1 for 4 h. Cells were fixed 60 minutes after the 1NM-PP1 washout, with n=300 cells analysed per clone and time point.

(B) Total number of mitotic cells with multipolar spindles judged by the immunostaining with an antibody recognising Pericentrin, with n=300 mitotic cells analysed.

6.6 Comparing the CDK1-as clones to wildtype cells

To complete the characterisation of clone 1 and 3, I examined their properties compared to the parental cell line which contains a wildtype CDK1 kinase (Fig. 44). First, I determined the mitotic index in a population which was not treated with 1NM-PP1 (Fig. 44A). Both CDK1-as clones showed a mitotic index of ~ 4%, which was similar to the wildtype cells.

Next, I investigated the occurrence of mitotic abnormalities, such as uncongressed chromosomes or multipolar spindles, and consequences thereof, which are anaphase bridges, micronuclei and multinucleate cells (Fig. 44B). None of these abnormalities was increased in the two CDK1-as clones compared to the wildtype cells. Indeed, clone 3 showed a decreased frequency of anaphase bridges and micronuclei compared to the wildtype cells.

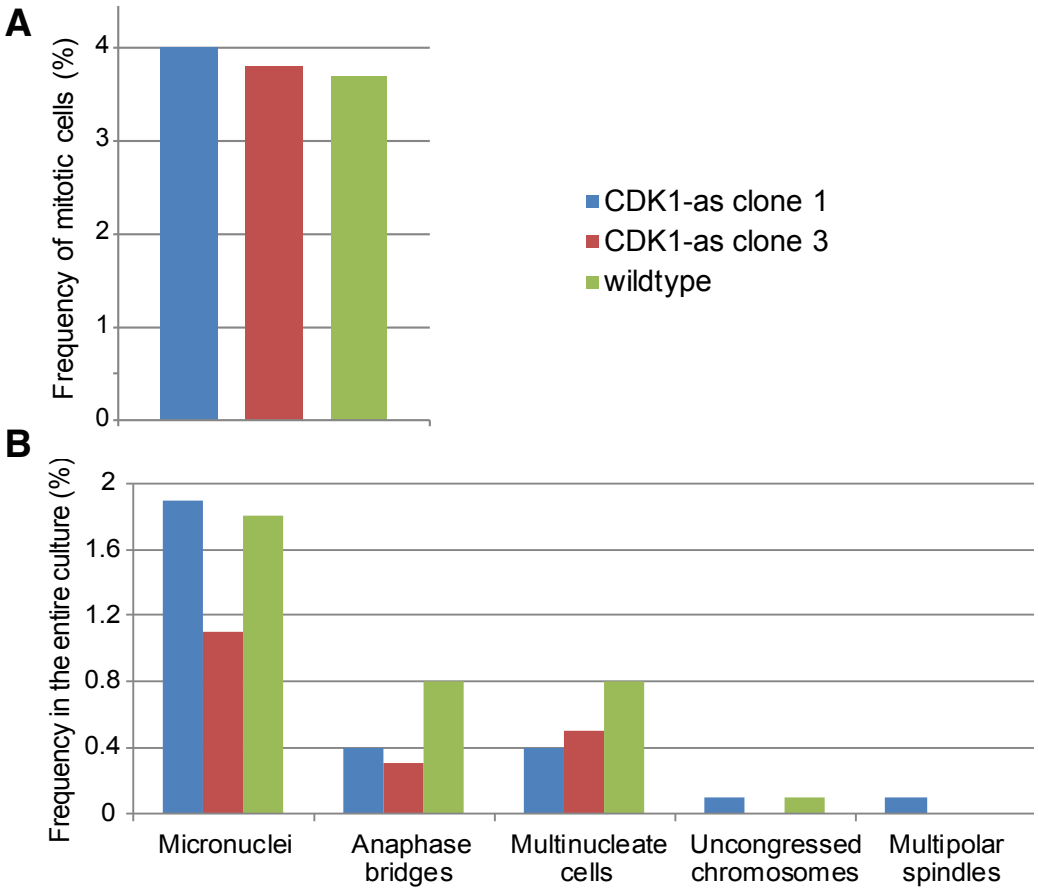

Figure 44: Comparison of the CDK1-as clones to wildtype cells.
(A) Frequency of mitotic cells in the culture of HeLa CDK1-as cells and of HeLa wildtype cells without 1NM-PP1 treatment, with n=1000 cells analysed.
(B) Frequency of the indicated abnormalities in the entire culture of HeLa CDK1-as cells and of HeLa wildtype cells without 1NM-PP1 treatment, with n=1000 cells analysed.

6.7 Western blot analysis of the endogenous CDK1 and the CDK1-as protein

In the final characterisation experiment, I determined the protein level of the exogenous CDK1-as compared to the level of the endogenous CDK1 kinase by Western blot analysis (Fig. 45). Both clones showed a CDK1-as expression which was similar to the level of endogenous CDK1 in the wildtype cells. Interestingly, no band for the endogenous CDK1 was detectable in the lane of clone 3, although this clone has no frameshift mutations and no more than eight amino acid residues were depleted. A possible explanation could be that the protein is not stable after the signature motif PSTAIRE is deleted. Another possibility might be that the antibody cannot recognise the altered CDK1 protein. However, this is rather unlikely because a recombinant fragment corresponding to amino acid residue 50 to the C-terminus of *Xenopus laevis* CDK1 was used as an immunogen and the epitope is considered to be amino acid residue 220-227 (LGTPNNEV) of mouse CDK1, according to the product information of the used anti-CDK1 antibody.

Altogether, this characterisation demonstrated that CDK1-as clones 1 and 3 can be effectively synchronised at the CDK1 arrest point, a mitotic index of > 90% can be achieved after the release from 1NM-PP1 and no altered properties are apparent compared to the parental CDK1 wildtype cell line. However, further optimisation may be necessary to reduce the number of cells with multipolar spindles that occur after extended treatment with 1NM-PP1.

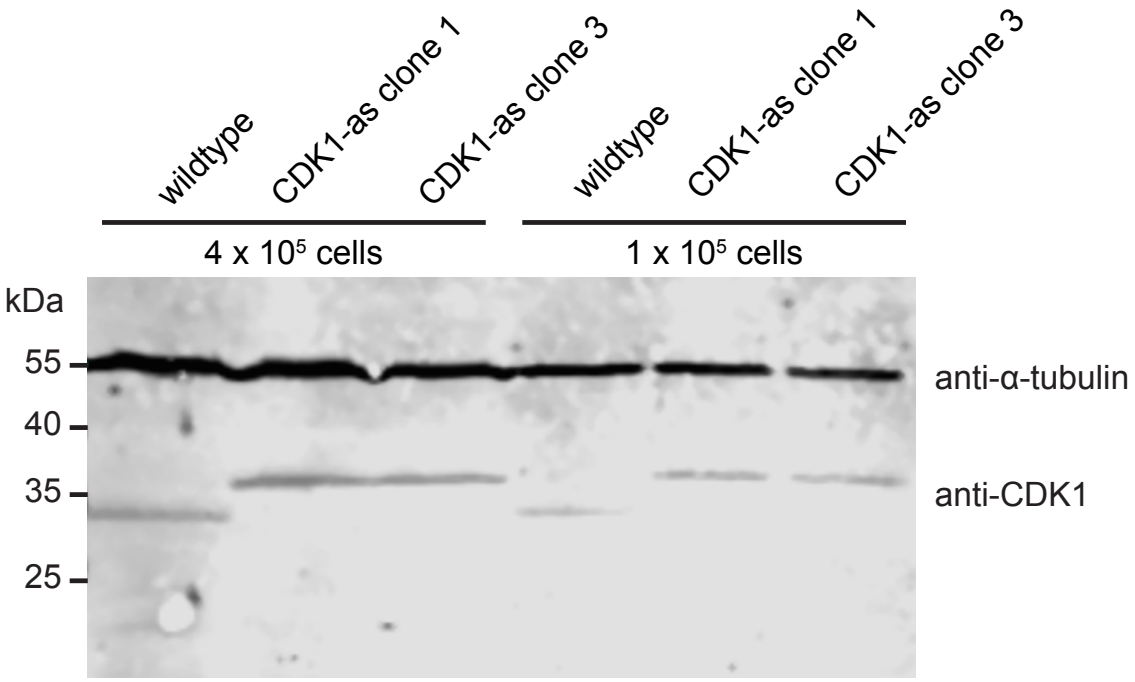

Figure 45: Western blot analysis of the endogenous CDK1 and the CDK1-as protein.
Western blot analysis of the indicated HeLa CDK1-as clones or of HeLa wildtype cells. Whole cell lysates of either 4 x 10^5 or 1 x 10^5 cells were loaded per lane. The endogenous CDK1 and the CDK1-as protein were detected using an anti-CDK1 antibody. α-tubulin served as a loading control.

7 Discussion

7.1 Robust interaction between tethered HP1α and the CPC

The CPC is a critical component of the centromere machinery that ensures faithful chromosome segregation during mitosis. In my work, I analysed the impact of tethered HP1α on the mitotic signalling network at centromeres and its potential effect on chromosome segregation. While tethering HP1α via the CENP-B DBD did not have a beneficial influence on the rate of chromosome mis-segregation in these cancer cell lines, these experiments highlight the tight association of the CPC with the chimeric HP1α protein. Thus, CB-EY-HP1α can determine the localisation of the CPC throughout mitosis, resulting in a strong localisation of Aurora B at centromeres, even in telophase. Thus, tethered HP1α can circumvent the complex epigenetic signalling network that normally determines the centromeric CPC localisation.

However, this strong interaction goes in both directions and is robust enough so that not only can tethered HP1α dictate the localisation of the CPC, but the CPC can also affect the localisation of HP1α: When the CENP-B DNA-binding domain is mutated, the CPC determines the localisation of CB^{mut}-EY-HP1α and carries it to the midbody in telophase. This is similar to the localisation of untethered EY-HP1α and is most likely due to the perturbed DNA binding properties of the mutated CENP-B DNA-binding domain compared to the wildtype DNA-binding domain in the chimeric protein.

In my experiments, all constructs containing a wildtype HP1α show a colocalisation with the CPC in telophase cells, either at centromeres or the midbody region. These interactions are all most likely due to conventional HP1α CSD interaction with client proteins, as the single point mutation W174A in the CSD eliminates this interaction and all phenotypes resulting from the HP1α tethering. Thus, when HP1α binding becomes independent of chromatin marks and HP1α is instead tethered through the DBD of CENP-B, the CPC partially loses its passenger abilities.

7.2 CB-EY-HP1α causes effects similar to those produced by directly tethering the core CPC subunit INCENP to centromeres via CENP-B tethering

I present in this study that specific tethering of HP1α to centromeric CENP-B boxes by use of the DBD of CENP-B produces a mitotic delay. In controls, EYFP-HP1α expression did not result in an altered mitotic progression, indicating that the specific tethering of HP1α to the centromere region causes the metaphase delay phenotype. In line with the above-described robust interaction between the CPC and HP1α, tethering the CPC core subunit INCENP via the CENP-B DBD produces phenotypes similar to those described in my study using CB-EY-HP1α. The effects of INCENP tethering include an increase of the mitotic index due to SAC activity and caused by perturbed kinetochore-microtubule interactions (Liu *et al.*, 2009). Additionally, INCENP tethering to centromeres results in increased phosphorylation of Aurora B substrates such as Dsn1 phosphorylation (Wang *et al.*, 2011a), which I also observed in cells expressing CB-EY-HP1α.

Liu and colleagues describe that the Aurora B is spatially separated from its kinetochore substrates once chromosomes bi-orientate and kinetochores stretch (Liu *et al.*, 2009). They conclude from their experiments that placing Aurora B artificially closer to the kinetochore by using CENP-B DBD tethering of INCENP results in increased phosphorylation of kinetochore substrates and leads to destabilisation of kinetochore-microtubule attachments. This idea is in agreement with the “dog leash” model, which assumes that the SAH of INCENP can extend and allow Aurora B to phosphorylate outer kinetochore substrates despite the binding of the CPC localisation module to the inner centromere (Krenn and Musacchio, 2015; Samejima *et al.*, 2015). However, at the same time, the range of Aurora B activity might be precisely regulated through this “leash”. Therefore, the tethering approach, which brings Aurora B closer to the kinetochore, could enable phosphorylation of kinetochore substrates that can normally not be reached and phosphorylated once bi-orientation is established and the kinetochore stretched.

In addition to the model that the precise localisation of Aurora B is critical, my results suggest that the binding dynamics could also be important for correct Aurora B activity at mitotic centromeres. The CB^{mut}-EY-HP1α construct shows a similar shift as CB-EY-HP1α towards the kinetochore proximal centromere when chromosomes bi-orientate in metaphase, whereas untethered HP1α remains closer to the inner centromere. However, the mutated tethering construct does not cause an accumulation of mitotic cells, demonstrating that it does not induce an activation of the SAC that leads to the metaphase delay phenotype. My FRAP analysis indicates that CB^{mut}-EY-HP1α has nearly three times faster binding dynamics than the HP1α tethering construct containing a wildtype CENP-B DBD. Additionally, it was previously shown that the CPC component survivin exhibits much faster binding dynamics at prometa- and metaphase compared to interphase centromeres or at the ana- or telophase stage (Beardmore *et al.*, 2004). Based on these observations and my results, I speculate that the complex regulation of centromeric CPC might be necessary to ensure precise CPC dynamics at mitotic centromeres. In summary, I conclude that CENP-B DBD driven HP1α tethering to centromeres causes a mitotic delay due to altered Aurora B distribution and/or dynamics.

7.3 HP1α tethering produces H3S10ph foci that are persistent throughout interphase

The strong interaction between tethered HP1α and the CPC described above results not only in the retention of the CPC at centromeres in telophase cells, but the CPC also remains trapped at CB-EY-HP1α clusters even in G_1. Remarkably, a clear H3S10ph signal persists around the clusters of tethered HP1α, indicating that the Aurora B retains its catalytic activity when trapped by CB-EY-HP1α. These H3S10ph foci vanished when cells were treated with 0.5 µM of the Aurora B inhibitor ZM447439, a dosage that had no apparent impact on the H3S10ph levels in mitosis. Aurora B inhibition most likely has no effect on its interaction with HP1α, as a clear

colocalisation was visible even in the presence of ZM447439. It was previously described that the general Aurora B localisation in interphase is independent of its own activity (Hayashi-Takanaka *et al.*, 2009). Together, these results indicate that the H3S10ph signal in interphase requires continuous Aurora B activity.

Aurora B activity is usually down-regulated at the end of mitosis by Cdh1 mediated proteasomal degradation (Nguyen *et al.*, 2005; Stewart and Fang, 2005) and an increase in counteracting phosphatases (Murnion *et al.*, 2001; Vagnarelli *et al.*, 2011; Wurzenberger and Gerlich, 2011; Lee *et al.*, 2016). Therefore, it is surprising that the activity of tethered Aurora B appears sufficient to counteract any conflicting phosphatase activity. This might be achieved through continuous intermolecular self-activation, possibly through CB-EY-HP1α facilitated concentration. It is indeed well demonstrated that clustering of the CPC leads to its activation, possibly through the phosphorylation of the INCENP C-terminus by Aurora B, which stimulates Aurora B kinase activity (Sessa *et al.*, 2005; Kelly *et al.*, 2007; Tseng *et al.*, 2010; Wang *et al.*, 2011a).

Overall, my results indicate that Aurora B activity itself does not seem to be subject to an intrinsic cell cycle control. When the CPC is retained in CB-EY-HP1α clusters at centromeres, it remains active throughout interphase. Therefore, I suggest that Aurora B degradation during mitotic exit may require a relocation of the CPC from centromeres. This suggestion is supported by the observation that depletion of the ubiquitination machinery components Cul3, KLHL9, or KLHL13 causes a failure in inactivating and displacing Aurora B from chromatin in ana- and telophase, resulting in an abnormal H3S10ph chromatin signal in late mitosis (Sumara *et al.*, 2007).

The H3S10ph mark induced by HP1α tethering in the G_1 cells is found only in close proximity to the CB-EY-HP1α clusters and does not spread all over chromatin as is the case in early mitosis. I speculate that the firm tethering of HP1α may prevent the spreading of active Aurora B along chromosomes because the H3S10ph signal does not result in a weaker HP1α interaction with chromatin as would normally be the case for methyl/phos switching during mitotic entry.

Alternatively, a lack of sufficient Aurora B activity could be the reason why the H3S10ph signal does not spread within the nucleus in G_1 cells. Potential reasons for low Aurora B activity during early interphase could be that the general protein level of the kinase is not sufficient to phosphorylate the entire chromatin. Additionally, activating phosphorylations, such as phosphorylated threonine 232, might not be present and Aurora B therefore not fully activated.

I hypothesise that CDK1 activity perhaps contributes to fully activate Aurora B, as I did not observe spreading of the H3S10ph mark in synchronised CDK1-as cells, in which CDK1 is inhibited. Instead, the H3S10ph foci remain highly stable without showing any dynamic behaviour in live cell imaging experiments.

Taken together, the retention of Aurora B and the consequential H3S10ph in G_1 cells is an event that does not occur in wildtype cells. This suggests that the CB-EY-HP1α-driven clustering results in Aurora B activity that can counteract the level of phosphatases in G_1, possibly through continuous intermolecular self-activation at the CB-EY-HP1α clusters.

7.4 A novel HP1-driven mode of CPC clustering occurs prior to the chromatin marks that determine CPC localisation during mitosis

CPC accumulation at mitotic centromeres is widely believed to depend on two epigenetic marks: Haspin kinase binds to cohesin and phosphorylates histone H3T3, creating an interaction site for the BIR domain of the CPC component survivin (Dai *et al.*, 2005; Kelly *et al.*, 2010; Wang *et al.*, 2010; Yamagishi *et al.*, 2010). Additionally, H2AT120 phosphorylated by the Bub1 kinase in the vicinity of the kinetochore creates a binding site for Shugoshin, which recruits CPC via interaction with borealin (Kawashima *et al.*, 2010; Yamagishi *et al.*, 2010).

In my experiments, I made use of synchronised fixed cells and live cell imaging with Fab fragments in cycling cells to analyse the dynamic behaviour of these

chromatin marks at the G_2 stage. I used this experimental setup to examine the potential contribution of these marks in CPC clustering and activation at the G_2 phase of the cell cycle. Simultaneous detection of H3T3ph and H3S10ph by live cell imaging revealed the precise sequential timing of these marks and demonstrates that H3S10ph foci appear long before H3T3ph mark becomes detectable, as previously suggested by fixed cell experiments (Polioudaki *et al.*, 2004). The H2AT120ph mark is detectable before H3S10ph foci form, however, H2AT120ph appears as a diffuse labelling of the entire nucleus instead of concentrated clusters. This diffuse labelling of H2AT120ph persists even after H3S10ph foci emerge, and H2AT120ph clusters only form when cells enter prophase. Together these results demonstrate that CPC clustering and activation occurs in G_2 cells independent of the chromatin marks that define CPC localisation at mitotic centromeres and suggest a new mode responsible for CPC localisation.

In line with the above-described clusters of active CPC at sites of CB-EY-HP1α tethering, my further results indicate that the concentration and initial activation of the CPC during the G_2 phase is induced by the interactions with endogenous HP1. For a precise temporal resolution, I used CDK1-as cells synchronised by CDK1 inhibition through the ATP analogue 1NM-PP1. At the CDK1 arrest point, cells show a remarkably reproducible pattern of H3S10ph foci, that co-localise with endogenous HP1α. HP1 KO experiments revealed that HP1α and HP1γ seem to redundantly mediate this CPC clustering and activation, as the individual knockouts of either did not result in a loss of H3S10ph focus formation during G_2, whereas focus formation was lost in the double knockout.

An important observation for the mode of CPC recruitment in G_2 cells was reported by Perera and Taylor (Perera and Taylor, 2010). They described that the clustering of shugoshin is driven by the Suv39h / HP1 pathway in G_2 cells. Therefore, it could be possible that shugoshin, which probably binds directly to HP1 in G_2 cells, mediates the recruitment of the CPC through its interaction with the borealin subunit. Furthermore, it is conceivable that the isoforms HP1α and HP1γ might bind shugoshin whereas HP1β might not, resulting in the loss of CPC clustering at the G_2

stage specifically in HP1α + HP1γ double KO cells. However, the interaction between borealin and shugoshin is promoted by CDK1 phosphorylation of borealin (Tsukahara *et al.*, 2010), which should not occur in 1NM-PP1 synchronised CDK1as cells. Therefore, an indirect CPC recruitment to HP1 clusters via shugoshin in G_2 cells appears less likely than a direct HP1-CPC binding.

Interestingly, HP1-driven clustering of the CPC appears to facilitate CPC activity even when counteracting phosphatases are present. Indeed, H3S10ph is limited by PP1 activity in interphase cells, as it was earlier described that selective inhibition of PP1 promotes formation of interphase H3S10ph (Hayashi-Takanaka *et al.*, 2009). Therefore, it is tempting to speculate that HP1 provides a microenvironment which protects either activating CPC phosphorylation or the H3S10ph itself against counteracting phosphatases. The recently described phase separation properties of HP1 could allow the formation of this specific microenvironment and are discussed in more detail below (Larson *et al.*, 2017; Strom *et al.*, 2017)

7.5 Functional implication of the H3S10ph foci in G_2 cells

The functional significance of the clustered CPC activity at sites of HP1 foci is not known. An earlier study reported that the timing of Aurora B activation in late interphase, which was determined by H3S10ph appearance, correlates with the frequency of chromosome mis-segregation events (Hayashi-Takanaka *et al.*, 2009). The H3S10ph signal emerges much later, i.e. closer to the G_2/M transition, in cells that have a high frequency of chromosome segregation errors compared to cells with a low chromosome mis-segregation rate. Additionally, recent work described that a HP1α KO in mouse embryonic fibroblasts leads to an increased frequency of merotelic chromosome attachments (Bosch-Presegué *et al.*, 2017), which is reported to also be a result of impaired CPC function (Gassmann *et al.*, 2004; Cimini *et al.*, 2006).

When analysing a general HP1 KO, it is difficult to distinguish between the effect of perturbing the early CPC clustering in G_2 phase and interfering with CPC function in mitosis, as HP1 also affects the level of Aurora B activity during mitosis (Abe *et al.*, 2016). In general, the regulation of CPC function is highly complex, involving numerous factors and extensive crosstalk. This makes it challenging to draw conclusions from experiments that perturb individual processes of the functional CPC network.

A previous study elegantly circumvented this problem by only transiently inhibiting Aurora B function by use of ZM447439 in interphase cells showing H3S10ph foci (Hayashi-Takanaka *et al.*, 2009). This temporary Aurora B inhibition during interphase resulted in an increased frequency of chromosome segregation errors in the subsequent mitosis. This observation indicates that Aurora B activity during late interphase has a functional implication and the exact molecular mechanism should be investigated in future studies.

7.6 The dual mode of CPC concentration is possibly controlled by methyl/phos switching

The general H3T3ph labelling of nuclei and the concentration of the H2AT120ph mark appear only as the H3S10ph signal spreads all over chromatin. Therefore, I speculate that a change in the mode of CPC clustering may take place once the H3S10ph mark generally labels chromatin and as a consequence, methyl/phos switching prevents the HP1 interaction with nucleosomes. With the entry into mitosis, the two histone marks H3T3ph and H2AT120ph start to determine the CPC localisation and thus concentrate the CPC at mitotic centromeres, most likely after the methyl/phos switch inactivates the HP1-driven mode of CPC clustering.

The reason for this dual mode of CPC concentration at centromeres is not known. However, it is tempting to speculate that it allows the transitional localisation of the CPC to chromosome arms. This idea may explain why the mitotic H3S10ph

signal is so widely conserved: The methyl/phos switch disrupts HP1-chromatin binding and thus possibly ensures CPC mobility during mitosis, a key feature of the CPC that is even included in the name of the complex (chromosome passenger complex). Therefore, H3S10ph might be considered a further histone mark that determines CPC localisation during mitosis, but instead of serving as an additional binding site, it rather disrupts HP1 binding to methylated H3K9 and thus prevents the pathway that defines CPC localisation in interphase. Indeed, it was previously shown that ZM447439 treatment, resulting in reduced levels of the chromatin marks H3S10ph and H3T3ph, leads to decreased localisation of HP1 and INCENP at centromeres and a concomitant HP1-dependent increase of INCENP on chromosome arms (Nozawa *et al.*, 2010).

Taken together, I propose that the methyl/phos switch possibly ensures CPC mobility during mitosis and promotes the shift from HP1-driven interphase CPC localisation to the mitotic localisation directed by H3T3ph and H2AT120ph.

7.7 How is H3S10ph focus formation induced in the absence of HP1α and HP1γ?

In HP1α + HP1γ double KO cells, the H3S10ph mark shows a weak diffuse labelling all over chromatin at the CDK1 arrest point in G_2. Interestingly, foci of H3S10ph still appear, but just prior to the G_2/M transition, which is close to the appearance of H3T3ph and the beginning of H2AT120ph clustering. This suggests that the late clustering of Aurora B activity in the absence of HP1α and HP1γ could depend on these histone marks that are well-known to concentrate the CPC at mitotic centromeres.

An alternative hypothesis is that HP1β, the only remaining HP1 isoform, could mediate the late CPC clustering in those cells. I speculate that HP1β may have a lower binding affinity for the CPC compared to HP1α and HP1γ, as was previously shown for other proteins interacting with the HP1 CSD (Bosch-Presegué *et al.*, 2017; Yi *et al.*, 2018). It is possible that the CPC components within the nucleus must be present at

a higher concentration before stable HP1β-CPC clusters form, whereas the tighter binding HP1α and HP1γ isoforms can cluster the CPC at lower concentrations. Perhaps the level of CPC components is high enough at the end of the G_2 phase that even HP1β can contribute to CPC clustering and activation if it is the only HP1 isoform present.

7.8 Persistent H3S10ph may facilitate the shift of the CPC from chromatin to the central spindle

The live cell imaging approach with fluorescently labelled Fab fragments detecting H3S10ph and H3T3ph allowed me to compare precisely the timing of these two marks in the same cell. The analysis showed not only a different timing in the appearance of these marks, as discussed above, but also revealed that H3T3ph vanishes after the onset of anaphase as previously reported (Dai *et al.*, 2005; Kelly *et al.*, 2010; Qian *et al.*, 2011), whereas the H3S10ph labelling of chromatin remains present for somewhat longer. I speculate that the different timing presumably facilitates the correct transition of the CPC from chromatin to the central spindle. With the rapid disappearance of H3T3ph, survivin is no longer recruited to centromeres, and the persistent H3S10ph labelling continues to inhibit HP1 binding to chromatin. This hypothesis is supported by my tethering experiments, which indicate that HP1α's binding to chromatin is regulated rather than its interaction with the CPC, probably contributing to proper CPC complex formation and functionality, as suggested by Abe and colleagues (Abe *et al.*, 2016).

Together, the prolonged persistence of the H3S10ph signal compared to H3T3ph serves as a further example of how H3S10 phosphorylation might contribute to CPC mobility, in this case supporting the shift away from chromatin.

In general, my results suggest that the dynamics of chromatin reader proteins have a direct influence on the mobility and activity of factors that attach to them. In line with this, it is conceivable that components that bind to chromatin readers could

actively regulate the dynamics of these readers and as a consequence, their own dynamics. In the case of HP1, this can be by either enhancing (e.g. H3K9me2/3 by Suv39h1) or weakening (e.g. H3S10ph by Aurora B) its chromatin association.

7.9 The phase separation properties of HP1α may facilitate H3S10ph focus formation in interphase

Two recent studies report that HP1α forms liquid-like droplets *in vitro* and suggest that heterochromatin domain formation is mediated by HP1α-driven phase separation (Larson *et al.*, 2017; Strom *et al.*, 2017). These described phase separation properties of HP1α might explain how H3S10ph foci can form at HP1 clusters even in the presence of counteracting phosphatases in interphase. I speculate that HP1α forms liquid-like domains at heterochromatin clusters that allow CPC components to be incorporated but might exclude phosphatases from entering. This possibly forms a microenvironment, in which H3S10ph is stable despite low kinase activity, as Aurora B is not yet fully activated, and despite an interphase level of counteracting phosphatases. This hypothesis is supported through the results presented by Larson and colleagues (Larson *et al.*, 2017), which demonstrate that Aurora B can localise inside of phase-separated HP1α droplets *in vitro*, whereas other proteins such as Hsp90 are excluded, which may also apply to phosphatases or ubiquitin ligases that target Aurora B for degradation.

7.10 Why is HP1 not released from chromatin at H3S10ph foci in G_2 cells?

A crucial question remains about the H3S10ph foci at endogenous HP1 clusters: why is HP1 not released from chromatin when H3S10ph foci form at the same location during the G_2 phase? A possible explanation might be the low density of the H3S10ph mark in the G_2 phase foci compared to later stages in which H3S10ph labels

the entire nucleus. The idea of a low H3S10ph density is based on the assumption that the H3S10ph mark is only present on one of the histone H3 tails within a nucleosome and no H3S10ph exists next to the H3K9me2/3 mark on the histone tail to which HP1 is bound. It is possible that an equilibrium state prevails in those H3S10ph foci before Aurora B is fully activated and the H3S10ph signal spreads all over chromatin: If the H3S10ph signal within the foci becomes too strong, it leads to HP1 displacement due to the methyl/phos switch. As a result, the CPC cluster could be perturbed and the H3S10ph density may decrease, which would allow HP1 to rebind to heterochromatin and re-establish a stable CPC cluster and H3S10ph foci. However, once Aurora B is fully activated, its activity possibly is no longer dependent on HP1 mediated clustering, and the H3S10ph signal spreads all over chromatin.

An alternative explanation for why HP1 is not released from H3S10ph foci in G_2 cells may be provided by Mateescu and colleagues (Mateescu *et al.*, 2004). Their work describes that H3S10ph surprisingly promotes HP1 binding to chromatin rather than perturbing it. Instead, a further histone modification, namely acetylation of histone H3 residue lysine 14, is necessary in combination with H3S10ph to release HP1 from H3K9me2/3 and occurs only with the entry into prophase. Therefore, it would be important to study the exact contribution of acetylated histone H3K14 in terms of HP1 displacement from chromatin and CPC mobility in future experiments. A potential approach could be the use of fluorescently labelled Fabs, which would enable the detection of this mark in live cell imaging experiments and would allow a precise temporal resolution.

7.11 CENP-B dimerisation may promote stable binding to DNA

The CENP-B DNA-binding domain is commonly used to target proteins to centromeres. However, my FRAP analysis provided essential information in choosing the right control in the CB-EY-HP1α tethering experiments. Analysing the binding dynamics showed that CB-EY, which consists of the DNA-binding domain and EYFP but is lacking HP1α, has a $t_{1/2}$ of only 6.8 s. This is ~ 7 times faster than the binding dynamics of the chimeric CB-EY-HP1α construct, revealing that CB-EY is not a suitable control. In contrast, CB-EY-HP1α^{W174A} has a $t_{1/2}$ of recovery of 42 s, similar to that of CB-EY-HP1α, but does not cause an altered mitotic progression or other phenotypes when compared to untransfected cells. Therefore, I used CB-EY-HP1α^{W174A} (which can dimerise via the HP1α CSD) rather than CB-EY as a control construct for all my experiments. The slightly faster dynamics of CB-EY-HP1α^{W174A} compared to CB-EY-HP1α might be explained by the observation that protein binding to the CSD, which is prevented in CB-EY-HP1α^{W174A}, strengthens HP1α's dimerisation (Mendez *et al.*, 2011; Kilic *et al.*, 2015).

Indeed, introducing the I165E mutation into CB-EY-HP1α, which prevents dimer formation in full-length HP1α, results in a $t_{1/2}$ of 8 s, a value similar to that of CB-EY. These findings suggest that the dimerisation ability of HP1α may compensate for the missing CENP-B dimerisation domain when fused to only the DNA-binding domain of CENP-B. Together, these results argue that although CENP-B can apparently bind to α-satellite DNA as a monomer, it probably requires dimer formation for stable binding. This observation could have implications for other studies in which the DNA-binding domain of CENP-B has been used to target proteins to the centromere.

7.12 Increased p31^{comet} level may alter the SAC sensitivity in U2OS cells

I observed in the live cell imaging experiments that U2OS cells do not show an overall delayed progression through mitosis when expressing CB-EY-HP1α at low levels. This contrasts HeLa cells, which show a distinct mitotic delay upon low-level expression of CB-EY-HP1α.

Low levels of CB-EY-HP1α presumably cause only a low-level activity of the SAC, which apparently can be bypassed in U2OS but not in HeLa cells. A possible explanation for the different response to low levels of CB-EY-HP1α might be the increased amount of the protein p31^{comet} in U2OS cells compared to HeLa cells (Habu and Matsumoto, 2013). It was previously described that p31^{comet} contributes to SAC inactivation through binding to active Mad2 (C-Mad), thus competing with O-Mad2 activation (Habu *et al.*, 2002; Xia *et al.*, 2004; Yang *et al.*, 2007) and by destabilisation of the mitotic checkpoint complex (MCC) (Teichner *et al.*, 2011; Varetti *et al.*, 2011; Westhorpe *et al.*, 2011).

Therefore, the increased p31^{comet} level in U2OS cells could result in a slippage through the SAC in cells expressing a low level of CB-EY-HP1α. Furthermore, a p31^{comet}-induced SAC impairment and premature progression into anaphase may also be considered as a potential explanation why U2OS cells show a relatively high baseline rate of chromosome mis-segregation (Kabeche and Compton, 2013).

7.13 DNMT1 depletion may affect HP1 clustering

Contrary to my findings that HP1α and HP1γ induce Aurora B clustering and H3S10ph focus formation in G_2 cells, Monier and colleagues describe in their work that DNMT1 depletion causes Aurora B mis-localisation and a decrease of pericentromeric H3S10ph in the G_2 phase (Monier *et al.*, 2007). Depletion of DNMT1 did not inhibit the formation of HP1α clusters. Instead, they reported that the frequency of cells with HP1α clusters increases upon DNMT1 depletion, which was presumably caused by reduced levels of H3S10ph. Based on this observation, Monier

and colleagues conclude that HP1α is not a dominant factor that determines Aurora B recruitment to pericentromeres. However, they did not analyse these HP1α clusters in detail but only distinguish between cells that either show HP1α clusters or do not show HP1α clusters at all. It would have been useful to determine various factors that may influence the ability of HP1α clusters to concentrate Aurora B after DNMT1 depletion. Possible factors include: The size of the HP1α foci, the level of H3K9 methylation and, most importantly, the dynamics of the clustered HP1α. These factors are important because previous work demonstrated that the density of H3K9me2/3 determines the residence time of HP1α on chromatin (Kilic *et al.*, 2015). HP1α dynamics, in turn, may affect the efficacy of CPC clustering and therefore H3S10ph focus formation.

Furthermore, H3S10ph foci preferentially form at large heterochromatin regions (Monier *et al.*, 2007). This observation further supports the idea that HP1α dynamics could be important to establish H3S10ph foci in the G_2 phase, as large heterochromatin regions may favour the formation of particularly stable HP1α clusters. Additionally, my tethering experiments also indicate that HP1α dynamics have a critical influence on CPC localisation and activity in interphase cells.

Moreover, Monier and colleagues reported that cells with more than 10 H3S10ph foci did not show any clusters of HP1α. This highlights the difficulties to interpret data about the emergence of H3S10ph in a non-synchronous culture. This described loss of HP1α clusters is most likely due to the methyl/phos switch, which displaces HP1 from chromatin. Therefore, it is crucial to analyse cells that are at the same stage of the cell cycle when determining factors that influence H3S10ph focus formation, as I did by synchronising cells at the CDK1 arrest point in this study.

7.14 Use of HeLa CDK1-as cells to study mitotic entry

The characterisation of the HeLa CDK1-as cells revealed that remarkable synchrony of the entire culture can be achieved using the CDK1-as/1NM-PP1 system. I further confirmed this in my studies by staining for H3S10ph in fixed cells and live cell imaging experiments, revealing that the entire culture shows a uniform H3S10ph staining pattern that is highly stable at the CDK1 arrest point.

However, if the scientific question does not focus on cell synchrony at the CDK1 arrest point but instead requires a uniform entry of the entire culture into mitosis, further optimisation of the 1NM-PP1 block will be necessary. At the moment, a high number of cells entering mitosis is achieved only with a concomitant increase in the frequency of cells with multipolar spindles. It is known that a lengthy arrest in the G_2 phase, for example caused by DNA damage, results in centrosome amplification (Dodson *et al.*, 2004). Therefore, it is crucial to reduce the duration of the 1NM-PP1 block in G_2 if the occurrence of multipolar spindles interferes with the experimental setup. However, if a high number of mitotic cells is desired, a preceding synchronisation could be useful, such as thymidine induced-arrest in S phase or synchronisation in G_1 through CDK4/6 inhibition.

A further challenge will be to achieve a synchronous progression of cells through mitosis. In my initial 1NM-PP1 washout experiments, roughly half of the mitotic cells were already in metaphase, while the remaining cells were still at the prometaphase stage. The presence of multipolar spindles could be a reason why some cells show a delayed mitotic progression and reducing the number of cells with multipolar spindles may improve the synchrony in mitosis. However, a certain non-uniformity in mitotic progression will most likely be always present, as the correct microtubule attachments to kinetochores occur in a stochastic manner with the transient existence of erroneous attachment that needs to be resolved. One approach could be to use cell lines with a smaller number of chromosomes, such as haploid cell lines which have only one copy of every chromosome.

Taken together, I identified two suitable HeLa CDK1-as clones which show an accurate synchronisation at the CDK1 arrest point and release into mitosis upon

1NM-PP1 washout. In general, the CDK1-as/1NM-PP1 system can allow the studying of cells with remarkable synchrony and temporal precision. The CDK1-as cells that I characterised can be useful for a variety of scientific questions that focus on the G_2 stage or require a precise mitotic entry of almost the entire culture.

7.15 Model of HP1-driven CPC clustering in the G_2 phase

Based on my observations and the relevant literature, I suggest the following model for how H3S10ph foci emerge in G_2 cells. Initially, HP1 forms clusters at H3K9me2/3 rich regions, such as pericentromeric heterochromatin (Bannister *et al.*, 2001; Lachner *et al.*, 2001) (Fig. 46A). As cells progress from S phase into G_2, the levels of CPC components increase (Stewart and Fang, 2005). HP1 binds through its CSD the PxVxL/I motif of the CPC members INCENP and possibly borealin (Ainsztein *et al.*, 1998; Nozawa *et al.*, 2010; Kang *et al.*, 2011; Liu *et al.*, 2014). This further increases the association of HP1 with chromatin, potentially resulting in a more robust clustering (Kilic *et al.*, 2015). The stable HP1 clustering may initiate the formation of CPC complexes, perhaps supported through the phase separation properties of HP1α, as a concentration of Aurora B within HP1α-formed compartments was previously shown (Larson *et al.*, 2017) (Fig. 46B). The CPC clustering presumably promotes the reciprocal trans-activation of CPC complexes, resulting in activated Aurora B (Kelly *et al.*, 2007; Tseng *et al.*, 2010; Wang *et al.*, 2011a) and leading to the initial H3S10ph focus formation at the pericentromeric heterochromatin in G_2 cells (Hendzel *et al.*, 1997; Crosio *et al.*, 2002; Monier *et al.*, 2007) (Fig. 46C). Once Aurora B is fully activated, the methyl/phos switch triggers the displacement of HP1 from chromatin (Fischle *et al.*, 2005; Hirota *et al.*, 2005) (Fig. 46D). This HP1 displacement may allow the spreading of H3S10ph throughout the entire nucleus, and CPC concentration is then determined by the histone marks H3T3ph and H2AT120ph at mitotic centromeres.

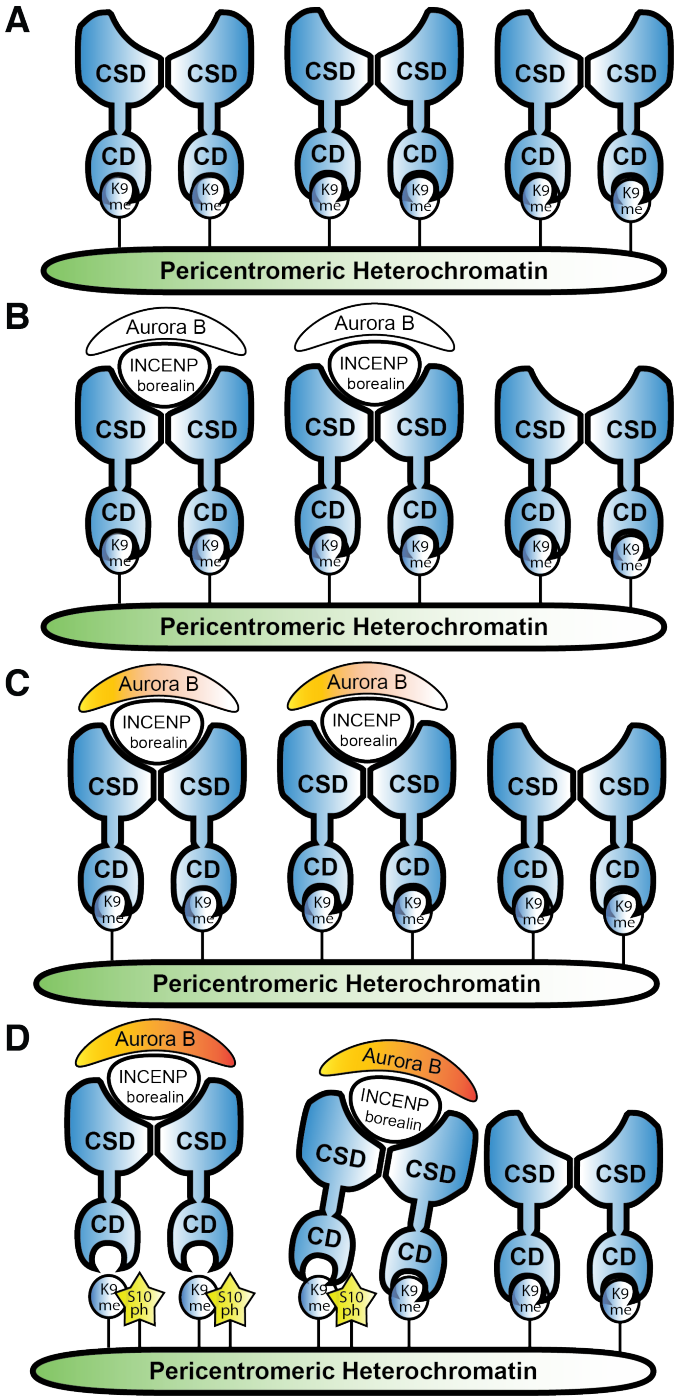

Figure 46: Model of HP1-driven CPC clustering in the G_2 phase.

(A) HP1 binds via its chromo domain (CD) to histone H3 methylated at residue lysine 9 (K9me). HP1 clusters form at regions with a high density of H3K9me, such as the pericentromeric heterochromatin.

(B) The CPC components INCENP and borealin interact though a PxVxL/I motif with the chromoshadow domain (CSD) of HP1. The phase separation properties of HP1 may facilitate a concentration of Aurora B, which interacts with the C-terminus of INCENP.

(C) Local enrichment of the CPC may promote an initial transactivation of Aurora B (light orange).

(D) Fully activated Aurora B (dark orange) phosphorylates histone H3 at residue serine 10 (S10ph), which displaces HP1 from chromatin by the methyl/phos switch and allows the shift to the mitotic mode of CPC localisation.

Overall, recent work indicates that the role of HP1 goes far beyond its contribution to heterochromatin integrity. The newly revealed HP1 functions include CPC clustering and activation in interphase, shown by my work (Ruppert *et al.*, 2018); contribution to full Aurora B activity in mitosis (Abe *et al.*, 2016); and further centromere related processes like cohesion protection (Yi *et al.*, 2018). Therefore, it will be crucial to determine in future studies the exact molecular contribution of HP1 in faithful chromosome segregation and include these findings in models of the complex centromere signalling network.

8 References

Aasland, R., and Stewart, A. F. (1995). The chromo shadow domain, a second chromo domain in heterochromatin-binding protein 1, HP1. Nucleic Acids Res. *23*, 3168–3173.

Abe, Y., Sako, K., Takagaki, K., Hirayama, Y., Uchida, K. S. K., Herman, J. A., DeLuca, J. G., and Hirota, T. (2016). HP1-Assisted Aurora B Kinase Activity Prevents Chromosome Segregation Errors. Dev. Cell *36*, 487–497.

Adams, R. R., Maiato, H., Earnshaw, W. C., and Carmena, M. (2001). Essential roles of Drosophila inner centromere protein (INCENP) and aurora B in histone H3 phosphorylation, metaphase chromosome alignment, kinetochore disjunction, and chromosome segregation. J. Cell Biol. *153*, 865–879.

Adams, R. R., Wheatleya, S. P., Gouldsworthy, A. M., Kandels-Lewis, S. E., Carmena, M., Smythe, C., Gerloff, D. L., and Earnshaw, W. C. (2000). INCENP binds the Aurora-related kinase AIRK2 and is required to target it to chromosomes, the central spindle and cleavege furrow. Curr. Biol. *10*, 1075–1078.

Ainsztein, A. M., Kandels-Lewis, S. E., Mackay, A. M., and Earnshaw, W. C. (1998). INCENP centromere and spindle targeting: Identification of essential conserved motifs and involvement of heterochromatin protein HP1. J. Cell Biol. *143*, 1763–1774.

Akiyoshi, B., and Gull, K. (2014). Discovery of unconventional kinetochores in kinetoplastids. Cell *156*, 1247–1258.

Allan, C. *et al.* (2012). OME Remote Objects (OMERO): a flexible, model-driven data management system for experimental biology. Nat. Methods *9*, 245–253.

Aloia, L., Di Stefano, B., and Di Croce, L. (2013). Polycomb complexes in stem cells and embryonic development. Development *140*, 2525–2534.

Alushin, G. M., Ramey, V. H., Pasqualato, S., Ball, D. A., Grigorieff, N., Musacchio, A., and Nogales, E. (2010). The Ndc80 kinetochore complex forms oligomeric arrays along microtubules. Nature *467*, 805–810.

Ambrosini, G., Adida, C., and Altieri, D. C. (1997). A novel anti-apoptosis gene, survivin, expressed in cancer and lymphoma. Nat. Med. *3*, 917–921.

Amor, D. J., Kalitsis, P., Sumer, H., and Choo, K. H. A. (2004). Building the centromere: from foundation proteins to 3D organization. Trends Cell Biol. *14*, 359–368.

Ando, S., Yang, H., Nozaki, N., Okazaki, T., and Yoda, K. (2002). CENP-A, -B, and -C chromatin complex that contains the I-type alpha-satellite array constitutes the prekinetochore in HeLa cells. Mol. Cell. Biol. *22*, 2229–2241.

Anest, V., Hanson, J. L., Cogswell, P. C., Steinbrecher, K. A., Strahl, B. D., and Baldwin, A. S. (2003). A nucleosomal function for IkappaB kinase-alpha in NF-kappaB-dependent gene expression. Nature *423*, 659–663.

De Antoni, A. *et al.* (2005). The Mad1/Mad2 complex as a template for Mad2 activation in the spindle assembly checkpoint. Curr. Biol. *15*, 214–225.

Baek, S. H. (2011). When Signaling Kinases Meet Histones and Histone Modifiers in the Nucleus. Mol. Cell *42*, 274–284.

Bannister, A. J., Zegerman, P., Partridge, J. F., Miska, E. A., Thomas, J. O., Allshire, R. C., and Kouzarides, T. (2001). Selective recognition of methylated lysine 9 on histone H3 by the HP1 chromo domain. Nature *410*, 120–124.

Barisic, M., Silva E Sousa, R., Tripathy, S. K., Magiera, M. M., Zaytsev, A. V., Pereira, A. L., Janke, C., Grishchuk, E. L., and Maiato, H. (2015). Microtubule detyrosination guides chromosomes during mitosis. Science *348*, 799–803.

Barnhart, M. C., Kuich, P. H. J. L., Stellfox, M. E., Ward, J. A., Bassett, E. A., Black, B. E., and Foltz, D. R. (2011). HJURP is a CENP-A chromatin assembly factor sufficient to form a functional de novo kinetochore. J. Cell Biol. *194*, 229–243.

Bassett, E. A., Wood, S., Salimian, K. J., Ajith, S., Foltz, D. R., and Black, B. E. (2010). Epigenetic centromere specification directs aurora B accumulation but is insufficient to efficiently correct mitotic errors. *190*, 177–185.

Beardmore, V. A., Ahonen, L. J., Gorbsky, G. J., and Kallio, M. J. (2004). Survivin dynamics increases at centromeres during G2 / M phase transition and is regulated by microtubule-attachment and Aurora B kinase activity. J. Cell Sci., *117*(18), 4033–4042.

Beaudouin, J., Gerlich, D., Daigle, N., Eils, R., and Ellenberg, J. (2002). Nuclear envelope breakdown proceeds by microtubule-induced tearing of the lamina. Cell *108*, 83–96.

Becker, J. S., Nicetto, D., and Zaret, K. S. (2016). H3K9me3-Dependent Heterochromatin: Barrier to Cell Fate Changes. Trends Genet. *32*, 29–41.

Bishop, J. D., and Schumacher, J. M. (2002). Phosphorylation of the carboxyl terminus of inner centromere protein (INCENP) by the Aurora B kinase stimulates Aurora B kinase activity. J. Biol. Chem. *277*, 27577–27580.

Bodor, D. L., Mata, J. F., Sergeev, M., David, A. F., Salimian, K. J., Panchenko, T., Cleveland, D. W., Black, B. E., Shah, J. V., and Jansen, L. E. T. (2014). The quantitative architecture of centromeric chromatin. Elife *2014*, 1–26.

Booher, R. N., Alfa, C. E., Hyams, J. S., and Beach, D. H. (1989). The fission yeast cdc2/cdc13/suc1 protein kinase: Regulation of catalytic activity and nuclear localization. Cell *58*, 485–497.

Bosch-Presegué, L. *et al.* (2017). Mammalian HP1 Isoforms Have Specific Roles in Heterochromatin Structure and Organization. Cell Rep. *21*, 2048–2057.

Bourhis, E., Hymowitz, S. G., and Cochran, A. G. (2007). The mitotic regulator survivin binds as a monomer to its functional interactor borealin. J. Biol. Chem. *282*, 35018–35023.

Brasher, S. V, Smith, B. O., Fogh, R. H., Nietlispach, D., Thiru, a, Nielsen, P. R., Broadhurst, R. W., Ball, L. J., Murzina, N. V, and Laue, E. D. (2000). The structure of mouse HP1 suggests a unique mode of single peptide recognition by the shadow chromo domain dimer. EMBO J. *19*, 1587–1597.

Caldas, G. V., and DeLuca, J. G. (2014). KNL1: Bringing order to the kinetochore. Chromosoma *123*, 169–181.

Canzio, D., Larson, A., and Narlikar, G. J. (2014). Mechanisms of functional promiscuity by HP1 proteins. Trends Cell Biol. *24*, 377–386.

Carmena, M., Wheelock, M., Funabiki, H., and Earnshaw, W. C. (2012). The chromosomal passenger complex (CPC): from easy rider to the godfather of mitosis. Nat. Rev. Mol. Cell Biol. *13*, 789–803.

Chan, Y. W., Jeyaprakash, A. A., Nigg, E. A., and Santamaria, A. (2012). Aurora B controls kinetochore-microtubule attachments by inhibiting Ska complex-KMN network interaction. J. Cell Biol. *196*, 563–571.

Chang, L., and Barford, D. (2014). Insights into the anaphase-promoting complex: A molecular machine that regulates mitosis. Curr. Opin. Struct. Biol. *29*, 1–9.

Cheeseman, I. M. (2014). The kinetochore. Cold Spring Harb Perspect Biol *94*, 77–105.

Cheeseman, I. M., Chappie, J. S., Wilson-Kubalek, E. M., and Desai, A. (2006). The Conserved KMN Network Constitutes the Core Microtubule-Binding Site of the Kinetochore. Cell *127*, 983–997.

Cheeseman, I. M., and Desai, A. (2008). Molecular architecture of the kinetochore-microtubule interface. Nat. Rev. Mol. Cell Biol. *9*, 33–46.

Cheeseman, I. M., Hori, T., Fukagawa, T., and Desai, A. (2008). KNL1 and the CENP-H/I/K complex coordinately direct kinetochore assembly in vertebrates. Mol Biol Cell *19*, 587–594.

Ciferri, C. *et al.* (2008). Implications for Kinetochore-Microtubule Attachment from the Structure of an Engineered Ndc80 Complex. Cell *133*, 427–439.

Cimini, D., Wan, X., Hirel, C. B., and Salmon, E. D. (2006). Aurora Kinase Promotes Turnover of Kinetochore Microtubules to Reduce Chromosome Segregation Errors. Curr. Biol. *16*, 1711–1718.

Ciosk, R., Zachariae, W., Michaelis, C., Shevchenko, A., Mann, M., and Nasmyth, K. (1998). An ESP1/PDS1 complex regulates loss of sister chromatid cohesion at the metaphase to anaphase transition in yeast. Cell *93*, 1067–1076.

Cooke, C. a., Bernat, R. L., and Earnshaw, W. C. (1990). CENP-B: A major human centromere protein located beneath the kinetochore. J. Cell Biol. *110*, 1475–1488.

Cooke, C. A., Heck, M. M. S., and Earnshaw, W. C. (1987). The inner centromere protein (INCENP) antigens: Movement from inner centromere to midbody during mitosis. J. Cell Biol. *105*, 2053–2067.

Crosio, C. *et al.* (2002). Mitotic Phosphorylation of Histone H3 : Spatio-Temporal Regulation by Mammalian Aurora Kinases Mitotic Phosphorylation of Histone H3 : Spatio-Temporal Regulation by Mammalian Aurora Kinases. Mol. Cell. Biol. *22*, 874–885.

Dai, J., Sultan, S., Taylor, S. S., and Higgins, J. M. G. (2005). The kinase haspin is required for mitotic histone H3 Thr 3 phosphorylation and normal metaphase chromosome alignment. Genes and Development, *19*(4), 472–488.

Daujat, S., Zeissler, U., Waldmann, T., Happel, N., and Schneider, R. (2005). HP1 binds specifically to Lys26-methylated histone H1.4, whereas simultaneous Ser27 phosphorylation blocks HP1 binding. J. Biol. Chem. *280*, 38090–38095.

DeLuca, J. G., Gall, W. E., Ciferri, C., Cimini, D., Musacchio, A., and Salmon, E. D. (2006). Kinetochore Microtubule Dynamics and Attachment Stability Are Regulated by Hec1. Cell *127*, 969–982.

DeLuca, K. F., Lens, S. M. A., and DeLuca, J. G. (2011). Temporal changes in Hec1 phosphorylation control kinetochore-microtubule attachment stability during mitosis. J. Cell Sci. *124*, 622–634.

Dialynas, G. K., Terjung, S., Brown, J. P., Aucott, R. L., Baron-Luhr, B., Singh, P. B., and Georgatos, S. D. (2007). Plasticity of HP1 proteins in mammalian cells. J. Cell Sci. *120*, 3415–3424.

Dieterich, K. *et al.* (2007). Homozygous mutation of AURKC yields large-headed polyploid spermatozoa and causes male infertility. Nat. Genet. *39*, 661–665.

Ditchfield, C., Johnson, V. L., Tighe, A., Ellston, R., Haworth, C., Johnson, T., Mortlock, A., Keen, N., and Taylor, S. S. (2003). Aurora B couples chromosome alignment with anaphase by targeting BubR1, Mad2, and Cenp-E to kinetochores. J. Cell Biol. *161*, 267–280.

Dodson, H., Bourke, E., Jeffers, L. J., Vagnarelli, P., Sonoda, E., Takeda, S., Earnshaw, W. C., Merdes, A., and Morrison, C. (2004). Centrosome amplification induced by DNA damage occurs during a prolonged G2 phase and involves ATM. EMBO J. *23*, 3864–3873.

Doxsey, S. J., Stein, P., Evans, L., Calarco, P. D., and Kirschner, M. (1994). Pericentrin, a highly conserved centrosome protein involved in microtubule organization. Cell *76*, 639–650.

Du, J., Kelly, A. E., Funabiki, H., and Patel, D. J. (2012). Structural basis for recognition of H3T3ph and Smac/DIABLO N-terminal peptides by human survivin. Structure *20*, 185–195.

Earnshaw, W. C., Bernat, R. L., Cooke, C. A., and Rothfield, N. F. (1991). Role of the centromere/kinetochore in cell cycle control. Cold Spring Harb. Symp. Quant. Biol. *56*, 675–685.

Earnshaw, W. C., and Cooke, C. a (1991). Analysis of the distribution of the INCENPs throughout mitosis reveals the existence of a pathway of structural changes in the chromosomes during metaphase and early events in cleavage furrow formation. J. Cell Sci. *98 (Pt 4)*, 443–461.

Earnshaw, W. C., and Migeon, B. R. (1985). Three related centromere proteins are absent from the inactive centromere of a stable isodicentric chromosome. Chromosoma *92*, 290–296.

Earnshaw, W. C., Ratrie, H., and Stetten, G. (1989). Visualization of centromere proteins CENP-B and CENP-C on a stable dicentric chromosome in cytological spreads. Chromosoma *98*, 1–12.

Earnshaw, W. C., and Rothfield, N. (1985). Identification of a family of human centromere proteins using autoimmune sera from patients with scleroderma. Chromosoma *91*, 313–321.

Elbashir, S. M., Harborth, J., Lendeckel, W., Yalcin, A., Weber, K., and Tuschl, T. (2001). Duplexes of 21 ± nucleotide RNAs mediate RNA interference in cultured mammalian cells. Nature *411*, 494–498.

Evans, T., Rosenthal, E. T., Youngblom, J., Distel, D., and Hunt, T. (1983). Cyclin: A protein specified by maternal mRNA in sea urchin eggs that is destroyed at each cleavage division. Cell *33*, 389–396.

Fachinetti, D., Han, J. S., McMahon, M. A., Ly, P., Abdullah, A., Wong, A. J., and Cleveland, D. W. (2015). DNA Sequence-Specific Binding of CENP-B Enhances the Fidelity of Human Centromere Function. Dev. Cell *33*, 314–327.

Fischle, W., Tseng, B. S., Dormann, H. L., Ueberheide, B. M., Garcia, B. a, Shabanowitz, J., Hunt, D. F., Funabiki, H., and Allis, C. D. (2005). Regulation of HP1-chromatin binding by histone H3 methylation and phosphorylation. Nature *438*, 1116–1122.

Flemming, W. (1882). Zellsubstanz, kern und zelltheilung. F.C.W. Vogel, Leipzig, 419.

Fukagawa, T., and Earnshaw, W. C. (2014). The Centromere: Chromatin Foundation for the Kinetochore Machinery. Dev. Cell *30*, 496–508.

Fuks, F., Hurd, P. J., Deplus, R., and Kouzarides, T. (2003). The DNA methyltransferases associate with HP1 and the SUV39H1 histone methyltransferase. Nucleic Acids Res. *31*, 2305–2312.

Gartenberg, M. (2009). Heterochromatin and the cohesion of sister chromatids. Chromosome Res. *17*, 229–238.

Gascoigne, K. E., and Cheeseman, I. M. (2013). CDK-dependent phosphorylation and nuclear exclusion coordinately control kinetochore assembly state. J. Cell Biol. *201*, 23–32.

Gassmann, R., Carvalho, A., Henzing, A. J., Ruchaud, S., Hudson, D. F., Honda, R., Nigg, E. A., Gerloff, D. L., and Earnshaw, W. C. (2004). Borealin: A novel chromosomal passenger required for stability of the bipolar mitotic spindle. J. Cell Biol. *166*, 179–191.

Gautier, J., Solomon, M. J., Booher, R. N., Bazan, J. F., and Kirschner, M. W. (1991). Cdc25 Is a Specific Tyrosine Phosphatase That Directly Activates P34Cdc2. Cell *67*, 197–211.

Ghenoiu, C., Wheelock, M. S., and Funabiki, H. (2013). Autoinhibition and polo-dependent multisite phosphorylation restrict activity of the histone H3 kinase haspin to mitosis. Mol. Cell *52*, 734–745.

Glotzer, M., Murray, A. W., and Kirschner, M. W. (1991). Cyclin is degraded by the ubiquitin pathway. Nature *349*, 132–138.

Gorbsky, G. J., Chen, R. H., and Murray, A. W. (1998). Microinjection of antibody to Mad2 protein into mammalian cells in mitosis induces premature anaphase. J. Cell Biol. *141*, 1193–1205.

Goodpasture, C., and Bloom, S. E. (1975). Visualization of nucleolar organizer regions im mammalian chromosomes using silver staining. Chromosoma, *53*(1), 37–50.

Gregan, J., Polakova, S., Zhang, L., Tolić-Nørrelykke, I. M., and Cimini, D. (2011). Merotelic kinetochore attachment: Causes and effects. Trends Cell Biol 21, 374–381.

Grzegorz, I. *et al.* (2004). DNA end resection, homologous recombination and DNA damage checkpoint activation require CDK1. Nature *431*, 1011–1017.

Guimaraes, G. J., Dong, Y., McEwen, B. F., and DeLuca, J. G. (2008). Kinetochore-Microtubule Attachment Relies on the Disordered N-Terminal Tail Domain of Hec1. Curr. Biol. *18*, 1778–1784.

Gurley, L. R., D'Anna, J. A., Barham, S. S., Deaven, L. L., and Tobey, R. A. (1978). Histone Phosphorylation and Chromatin Structure during Mitosis in Chinese Hamster Cells. Eur. J. Biochem. *84*, 1–15.

Gurley, L. R., Walters, R. A., and Tobey, R. A. (1974). Cell cycle-specific changes in histone phosphorylation associated with cell proliferation and chromosome condensation. J. Cell Biol. *60*, 356–864.

Haarhuis, J. H. I., Elbatsh, A. M. O., Van Den Broek, B., Camps, D., Erkan, H., Jalink, K., Medema, R. H., and Rowland, B. D. (2013). WAPL-mediated removal of cohesin protects against segregation errors and aneuploidy. Curr. Biol. *23*, 2071–2077.

Haarhuis, J. H. I., Elbatsh, A. M. O., and Rowland, B. D. (2014). Cohesin and its regulation: On the logic of X-shaped chromosomes. Dev. Cell *31*, 7–18.

Haase, J., Bonner, M. K., Halas, H., and Kelly, A. E. (2017). Distinct Roles of the Chromosomal Passenger Complex in the Detection of and Response to Errors in Kinetochore-Microtubule Attachment. Dev. Cell *42*, 640–654.e5.

Habu, T., Kim, S. H., Weinstein, J., and Matsumoto, T. (2002). Identification of a MAD2-binding protein, CMT2, and its role in mitosis. EMBO J. *21*, 6419–6428.

Habu, T., and Matsumoto, T. (2013). p31comet inactivates the chemically induced Mad2-dependent spindle assembly checkpoint and leads to resistance to anti-mitotic drugs. Springerplus *2*, 1–15.

Hahn, M. *et al.* (2013). Suv4-20h2 mediates chromatin compaction and is important for cohesion recruitment to heterochromatin. Genes Dev. *27*, 859–872.

Hannak, E., Kirkham, M., Hyman, A. A., and Oegema, K. (2001). Aurora-A kinase is required for centrosome maturation in Caenorhabditis elegans. J. Cell Biol. *155*, 1109–1115.

Harvey, S. L., Charlet, A., Haas, W., Gygi, S. P., and Kellogg, D. R. (2005). Cdk1-dependent regulation of the mitotic inhibitor Wee1. Cell *122*, 407–420.

Hauf, S., Cole, R. W., LaTerra, S., Zimmer, C., Schnapp, G., Walter, R., Heckel, A., Van Meel, J., Rieder, C. L., and Peters, J. M. (2003). The small molecule Hesperadin reveals a role for Aurora B in correcting kinetochore-microtubule attachment and in maintaining the spindle assembly checkpoint. J. Cell Biol. *161*, 281–294.

Hayakawa, T., Haraguchi, T., Masumoto, H., and Hiraoka, Y. (2003). Cell cycle behavior of human HP1 subtypes: distinct molecular domains of HP1 are required for their centromeric localization during interphase and metaphase. J. Cell Sci. *116*, 3327–3338.

Hayashi-Takanaka, Y. *et al.* (2011). Tracking epigenetic histone modifications in single cells using Fab-based live endogenous modification labeling. Nucleic Acids Res. *39*, 6475–6488.

Hayashi-Takanaka, Y., Yamagata, K., Nozaki, N., and Kimura, H. (2009). Visualizing histone modifications in living cells: Spatiotemporal dynamics of H3 phosphorylation during interphase. J. Cell Biol. *187*, 781–790.

Hebbes, T. R., Thorne, A. W., and Crane-Robinson, C. (1988). A direct link between core histone acetylation and transcriptionally active chromatin. EMBO J. *7*, 1395–1402.

Heitz, E. (1929). Heterochromatin, Chromocentren, Chromomeren. (Vorlaufige Mitteilung.). BER DEUTSCH BOT GES *47*, 274–284.

Henderson, A. S., Warburton, D., and Atwood, K. C. (1972). Location of Ribosomal DNA in the Human Chromosome Complement. Proc. Natl. Acad. Sci. *69*(11), 3394–3398.

Hendzel, M. J., Wei, Y., Mancini, M. A., Van Hooser, A., Ranalli, T., Brinkley, B. R., Bazett-Jones, D. P., and Allis, C. D. (1997). Mitosis-specific phosphorylation of histone H3 initiates primarily within pericentromeric heterochromatin during G2 and spreads in an ordered fashion coincident with mitotic chromosome condensation. Chromosoma *106*, 348–360.

Hengeveld, R. C. C., Vromans, M. J. M., Vleugel, M., Hadders, M. A., and Lens, S. M. A. (2017). Inner centromere localization of the CPC maintains centromere cohesion and allows mitotic checkpoint silencing. Nat. Commun. *8*, 15542.

Hergeth, S. P., Dundr, M., Tropberger, P., Zee, B. M., Garcia, B. A., Daujat, S., and Schneider, R. (2011). Isoform-specific phosphorylation of human linker histone H1.4 in mitosis by the kinase Aurora B. J. Cell Sci. *124*, 1623–1628.

van den Heuvel, S., and Harlow, E. (1993). Distinct roles for cyclin-dependent kinases in cell cycle control. Science *262*, 2050–2054.

Hindriksen, S., Lens, S. M. A., and Hadders, M. A. (2017). The Ins and Outs of Aurora B Inner Centromere Localization. Front. Cell Dev. Biol. *5*.

Hinshaw, S. M., and Harrison, S. C. (2018). Kinetochore Function from the Bottom Up. Trends Cell Biol. *28*, 22–33.

Hirota, T., Lipp, J. J., Toh, B.-H., and Peters, J.-M. (2005). Histone H3 serine 10 phosphorylation by Aurora B causes HP1 dissociation from heterochromatin. Nature *438*, 1176–1180.

Hochegger, H., Dejsuphong, D., Sonoda, E., Saberi, A., Rajendra, E., Kirk, J., Hunt, T., and Takeda, S. (2007). An essential role for Cdk1 in S phase control is revealed via chemical genetics in vertebrate cells. J. Cell Biol. *178*, 257–268.

Hochegger, H., Takeda, S., and Hunt, T. (2008). Cyclin-dependent kinases and cell-cycle transitions: Does one fit all? Nat. Rev. Mol. Cell Biol. *9*, 910–916.

Hoffmann, I., Clarke, P. R., Marcote, M. J., Karsenti, E., and Draetta, G. (1993). Phosphorylation and activation of human cdc25-C by cdc2-cyclin B and its involvement in the self-amplification of MPF at mitosis. EMBO J. *12*, 53–63.

Honda, R., Koerner, R., and Nigg, E. A. (2003). Exploring the Functional Interactions between Aurora B, INCENP, and Survivin in Mitosis. Mol. Biol. Cell *14*, 2372–2384.

Hori, T., Kagawa, N., Toyoda, A., Fujiyama, A., Misu, S., Monma, N., Makino, F., Ikeo, K., and Fukagawa, T. (2017). Constitutive centromere-associated network controls centromere drift in vertebrate cells. J. Cell Biol. *216*, 101–113.

Van Hooser, A. A., Ouspenski, I. I., Gregson, H. C., Starr, D. A., Yen, T. J., Goldberg, M. L., Yokomori, K., Earnshaw, W. C., Sullivan, K. F., and Brinkley, B. R. (2001). Specification of kinetochore-forming chromatin by the histone H3 variant CENP-A. J. Cell Sci. *114*, 3529–3542.

Howell, B. J., McEwen, B. F., Canman, J. C., Hoffman, D. B., Farrar, E. M., Rieder, C. L., and Salmon, E. D. (2001). Cytoplasmic dynein/dynactin drives kinetochore protein transport to the spindle poles and has a role in mitotic spindle checkpoint inactivation. J. Cell Biol. *155*, 1159–1172.

Hsu, J.-Y. *et al.* (2000). Mitotic Phosphorylation of Histone H3 Is Governed by Ipl1/aurora Kinase and Glc7/PP1 Phosphatase in Budding Yeast and Nematodes. Cell *102*, 279–291.

Hudson, D. F. *et al.* (1998). Centromere protein B null mice are mitotically and meiotically normal but have lower body and testis weights. J. Cell Biol. *141*, 309–319.

Hümmer, S., and Mayer, T. U. (2009). Cdk1 Negatively Regulates Midzone Localization of the Mitotic Kinesin Mklp2 and the Chromosomal Passenger Complex. Curr. Biol. *19*, 607–612.

Izawa, D., and Pines, J. (2015). The mitotic checkpoint complex binds a second CDC20 to inhibit active APC/C. Nature *517*, 631–634.

Jeffrey, P. D., Russo, A. A., Polyak, K., Gibbs, E., Hurwitz, J., Massagué, J., and Pavletich, N. P. (1995). Mechanism of CDK activation revealed by the structure of a cyclinA-CDK2 complex. Nature *376*, 313–320.

Jeyaprakash, A. A., Klein, U. R., Lindner, D., Ebert, J., Nigg, E. A., and Conti, E. (2007). Structure of a Survivin-Borealin-INCENP Core Complex Reveals How Chromosomal Passengers Travel Together. Cell *131*, 271–285.

Jost, K. L., Bertulat, B., and Cardoso, M. C. (2012). Heterochromatin and gene positioning: Inside, outside, any side? Chromosoma *121*, 555–563.

Kabeche, L., and Compton, D. A. (2013). Cyclin A regulates kinetochore microtubules to promote faithful chromosome segregation. Nature *502*, 110–113.

Kalantzaki, M., Kitamura, E., Zhang, T., Mino, A., Novák, B., and Tanaka, T. U. (2015). Kinetochore-microtubule error correction is driven by differentially regulated interaction modes. Nat. Cell Biol. *17*, 421–433.

Kamentsky, L., Jones, T. R., Fraser, A., Bray, M. A., Logan, D. J., Madden, K. L., Ljosa, V., Rueden, C., Eliceiri, K. W., and Carpenter, A. E. (2011). Improved structure, function and compatibility for cellprofiler: Modular high-throughput image analysis software. Bioinformatics *27*, 1179–1180.

Kang, J., Chaudhary, J., Dong, H., Kim, S., Brautigam, C. a, and Yu, H. (2011). Mitotic centromeric targeting of HP1 and its binding to Sgo1 are dispensable for sister-chromatid cohesion in human cells. Mol. Biol. Cell *22*, 1181–1190.

Kapoor, M., Montes De Oca Luna, R., Liu, G., Lozano, G., Cummings, C., Mancini, M., Ouspenski, I., Brinkley, B. R., and May, G. S. (1998). The cenpB gene is not essential in mice. Chromosoma *107*, 570–576.

Kasuboski, J. M. *et al.* (2011). Zwint-1 is a novel Aurora B substrate required for the assembly of a dynein-binding platform on kinetochores. Mol. Biol. Cell *22*, 3318–3330.

Kawashima, S. A., Yamagishi, Y., Honda, T., Lshiguro, K. I., and Watanabe, Y. (2010). Phosphorylation of H2A by Bub1 prevents chromosomal instability through localizing shugoshin. Science *327*, 172–177.

Kelly, A. E., Ghenoiu, C., Xue, J. Z., Zierhut, C., Kimura, H., and Funabiki, H. (2010). Survivin Reads Phosphorylated Histone H3 Threonine 3 to Activate the Mitotic Kinase Aurora B. Science *330*, 235–239.

Kelly, A. E., Sampath, S. C., Maniar, T. A., Woo, E. M., Chait, B. T., and Funabiki, H. (2007). Chromosomal Enrichment and Activation of the Aurora B Pathway Are Coupled to Spatially Regulate Spindle Assembly. Dev. Cell *12*, 31–43.

Kilic, S., Bachmann, A. L., Bryan, L. C., and Fierz, B. (2015). Multivalency governs HP1α association dynamics with the silent chromatin state. Nat. Commun. *6*, 7313.

Kim, S., Sun, H., Tomchick, D. R., Yu, H., and Luo, X. (2012). Structure of human Mad1 C-terminal domain reveals its involvement in kinetochore targeting. Proc. Natl. Acad. Sci. *109*, 6549–6554.

Kim, S. Y., and Ferrell, J. E. (2007). Substrate Competition as a Source of Ultrasensitivity in the Inactivation of Wee1. Cell *128*, 1133–1145.

Kim, S., and Yu, H. (2015). Multiple assembly mechanisms anchor the KMN spindle checkpoint platform at human mitotic kinetochores. J. Cell Biol. *208*, 181–196.

Kim, Y., Holland, A. J., Lan, W., and Cleveland, D. W. (2010). Aurora kinases and protein phosphatase 1 mediate chromosome congression through regulation of CENP-E. Cell *142*, 444–455.

Kimmins, S., Crosio, C., Kotaja, N., Hirayama, J., Monaco, L., Höög, C., van Duin, M., Gossen, J. A., and Sassone-Corsi, P. (2007). Differential Functions of the Aurora-B and Aurora-C Kinases in Mammalian Spermatogenesis. Mol. Endocrinol. *21*, 726–739.

Kimura, M., Matsuda, Y., Yoshioka, T., and Okano, Y. (1999). Cell cycle-dependent expression and centrosome localization of a third human Aurora/Ip11-related protein kinase, AIK3. J Biol Chem *274*, 7334–7340.

Klebig, C., Korinth, D., and Meraldi, P. (2009). Bub1 regulates chromosome segregation in a kinetochore-independent manner. J. Cell Biol. *185*, 841–858.

Koch, B., Kueng, S., Ruckenbauer, C., Wendt, K. S., and Peters, J. M. (2008). The Suv39h-HP1 histone methylation pathway is dispensable for enrichment and protection of cohesin at centromeres in mammalian cells. Chromosoma *117*, 199–210.

Krenn, V., and Musacchio, A. (2015). The Aurora B Kinase in Chromosome Bi-Orientation and Spindle Checkpoint Signaling. Front. Oncol. *5*.

Kumagai, A., and Dunphy, W. G. (1991). The cdc25 protein controls tyrosine dephosphorylation of the cdc2 protein in a cell-free system. Cell *64*, 903–914.

Kumagai, A., and Dunphy, W. G. (1992). Regulation of the cdc25 protein during the cell cycle in Xenopus extracts. Cell *70*, 139–151.

De La Barre, A. E., Angelov, D., Molla, A., and Dimitrov, S. (2001). The N-terminus of histone H2B, but not that of histone H3 or its phosphorylation, is essential for chromosome condensation. EMBO J. *20*, 6383–6393.

Lachner, M., O'Carroll, D., Rea, S., Mechtler, K., and Jenuwein, T. (2001). Methylation of histone H3 lysine 9 creates a binding site for HP1 proteins. Nature *410*, 116–120.

Lampson, M. A, Renduchitala, K., Khodjakov, A., and Kapoor, T. M. (2004). Correcting improper chromosome-spindle attachments during cell division. Nat. Cell Biol. *6*, 232–237.

Larson, A. G., Elnatan, D., Keenen, M. M., Trnka, M. J., Johnston, J. B., Burlingame, A. L., Agard, D. A., Redding, S., and Narlikar, G. J. (2017). Liquid droplet formation by HP1α suggests a role for phase separation in heterochromatin. Nature *547*, 236–240.

Laurell, E., Beck, K., Krupina, K., Theerthagiri, G., Bodenmiller, B., Horvath, P., Aebersold, R., Antonin, W., and Kutay, U. (2011). Phosphorylation of Nup98 by multiple kinases is crucial for NPC disassembly during mitotic entry. Cell *144*, 539–550.

Lee, S. *et al.* (2016). IK-guided PP2A suppresses Aurora B activity in the interphase of tumor cells. Cell. Mol. Life Sci. *73*, 3375–3386.

Liu, D., Vader, G., Vromans, M. J. M., Lampson, M. a, and Lens, M. a (2009). Sensing Chromosome Bi-Orientation Kinase from Kinetochore Substrates. Science *323*, 1350–1353.

Liu, D., Vleugel, M., Backer, C. B., Hori, T., Fukagawa, T., Cheeseman, I. M., and Lampson, M. A. (2010). Regulated targeting of protein phosphatase 1 to the outer kinetochore by KNL1 opposes Aurora B kinase. J. Cell Biol. *188*, 809–820.

Liu, X. *et al.* (2014). Chromatin protein HP1α interacts with the mitotic regulator borealin protein and specifies the centromere localization of the chromosomal passenger complex. J. Biol. Chem. *289*, 20638–20649.

Lomberk, G., Bensi, D., Fernandez-Zapico, M. E., and Urrutia, R. (2006). Evidence for the existence of an HP1-mediated subcode within the histone code. Nat. Cell Biol. *8*, 407–415.

London, N., Ceto, S., Ranish, J. A., and Biggins, S. (2012). Phosphoregulation of Spc105 by Mps1 and PP1 regulates Bub1 localization to kinetochores. Curr. Biol. *22*, 900–906.

Luger, K., Mäder, A. W., Richmond, R. K., Sargent, D. F., and Richmond, T. J. (1997). Crystal structure of the nucleosome core particle at 2.8 Å resolution. Nature *389*, 251–260.

Machida, S., Takizawa, Y., Ishimaru, M., Sugita, Y., Sekine, S., Nakayama, J. ichi, Wolf, M., and Kurumizaka, H. (2018). Structural Basis of Heterochromatin Formation by Human HP1. Mol. Cell *69*, 385–397.e8.

Maiato, H., Gomes, A., Sousa, F., and Barisic, M. (2017). Mechanisms of Chromosome Congression during Mitosis. Biology (Basel). *6*, 13.

Mali, P., Yang, L., Esvelt, K. M., Aach, J., Guell, M., DiCarlo, J. E., Norville, J. E., and Church, G. M. (2013). RNA-guided human genome engineering via Cas9. Science *339*, 823–826.

Mapelli, M. *et al.* (2006). Determinants of conformational dimerization of Mad2 and its inhibition by p31comet. EMBO J. *25*, 1273–1284.

Mapelli, M., and Musacchio, A. (2007). MAD contortions: conformational dimerization boosts spindle checkpoint signaling. Curr. Opin. Struct. Biol. *17*, 716–725.

Marshall, O. J., Chueh, A. C., Wong, L. H., and Choo, K. H. A. (2008). Neocentromeres: New Insights into Centromere Structure, Disease Development, and Karyotype Evolution. Am. J. Hum. Genet. *82*, 261–282.

Masumoto, H., Masukata, H., Muro, Y., Nozaki, N., and Okazaki, T. (1989). A human centromere antigen (CENP-B) interacts with a short specific sequence in alphoid DNA, a human centromeric satellite. J. Cell Biol. *109*, 1963–1973.

Mateescu, B., England, P., Halgand, F., Yaniv, M., and Muchardt, C. (2004). Tethering of HP1 proteins to chromatin is relieved by phosphoacetylation of histone H3. EMBO Rep. *5*, 490–496.

McNeil, P. L., and Warder, E. (1987). Glass beads load macromolecules into living cells. J. Cell Sci. *88 (Pt 5)*, 669–678.

Mendez, D. L., Kim, D., Chruszcz, M., Stephens, G. E., Minor, W., Khorasanizadeh, S., and Elgin, S. C. R. (2011). The HP1a Disordered C Terminus and Chromo Shadow Domain Cooperate to Select Target Peptide Partners. ChemBioChem *12*, 1084–1096.

Mendiburo, M. J., Padeken, J., Fülöp, S., Schepers, A., and Heun, P. (2011). Drosophila CENH3 Is Sufficient for Centromere Formation. Science (80-.). *334*, 686–690.

Meppelink, A., Kabeche, L., Vromans, M. J. M., Compton, D. A., and Lens, S. M. A. (2015). Shugoshin-1 Balances Aurora B Kinase Activity via PP2A to Promote Chromosome Bi-orientation. Cell Rep. *11*, 508–515.

Meunier, S., and Vernos, I. (2012). Microtubule assembly during mitosis – from distinct origins to distinct functions? J. Cell Sci. *125*(12), 2805–2814

Miller, S. A., Johnson, M. L., and Stukenberg, P. T. (2008). Kinetochore Attachments Require an Interaction between Unstructured Tails on Microtubules and Ndc80Hec1. Curr. Biol. *18*, 1785–1791.

Minc, E., Courvalin, J. C., and Buendia, B. (2000). HP1gamma associates with euchromatin and heterochromatin in mammalian nuclei and chromosomes. Cytogenet. Cell Genet. *90*, 279–284.

Monier, K., Mouradian, S., and Sullivan, K. F. (2007). DNA methylation promotes Aurora-B-driven phosphorylation of histone H3 in chromosomal subdomains. J. Cell Sci. *120*, 101–114.

Mueller, P. R., Coleman, T. R., and Dunphy, W. G. (1995a). Cell cycle regulation of a Xenopus Wee1-like kinase. Mol. Biol. Cell *6*, 119–134.

Mueller, P. R., Coleman, T. R., Kumagai, A., and Dunphy, W. G. (1995b). Myt1: A membrane-associated inhibitory kinase that phosphorylates Cdc2 on both threonine-14 and tyrosine-15. Science *270*, 86–90.

Murnion, M. E., Adams, R. R., Callister, D. M., Allis, C. D., Earnshaw, W. C., and Swedlow, J. R. (2001). Chromatin-associated Protein Phosphatase I Regulates Aurora-B and Histone H3 Phosphorylation. J. Biol. Chem. *276*, 26656–26665.

Musacchio, A., and Desai, A. (2017). A Molecular View of Kinetochore Assembly and Function. Biology (Basel). *6*, 5.

Nakayama, J., Rice, J. C., Strahl, B. D., Allis, C. D., and Grewal, S. I. S. (2001). Role of Histone H3 Lysine 9 Methylation in Epigenetic Control of Heterochromatin Assembly. Science *292*, 110–113.

Nasa, I., Rusin, S. F., Kettenbach, A. N., and Moorhead, G. B. (2018). Aurora B opposes PP1 function in mitosis by phosphorylating the conserved PP1-binding RVxF motif in PP1 regulatory proteins. Science Signaling, *11* (530)

Neill, L. R. O., and Turner, B. M. (1995). Acetylation Distinguishes Coding Regions. *14*, 3946–3957.

Neurohr, G., Naegeli, A., Titos, I., Theler, D., Greber, B., Díez, J., Gabaldón, T., Mendoza, M., and Barral, Y. (2011). A Midzone-Based Ruler Adjusts Chromosome Compaction to Anaphase Spindle Length. *1037*, 465–468.

Nguyen, H. G., Chinnappan, D., Urano, T., and Ravid, K. (2005). Mechanism of Aurora-B degradation and its dependency on intact KEN and A-boxes: identification of an aneuploidy-promoting property. Mol. Cell. Biol. *25*, 4977–4992.

Nielsen, A. L., Oulad-Abdelghani, M., Ortiz, J. A., Remboutsika, E., Chambon, P., and Losson, R. (2001). Heterochromatin formation in mammalian cells: interaction between histones and HP1 proteins. Mol. Cell *7*, 729–739.

Nijenhuis, W., Von Castelmur, E., Littler, D., De Marco, V., Tromer, E., Vleugel, M., Van Osch, M. H. J., Snel, B., Perrakis, A., and Kops, G. J. P. L. (2013). A TPR domain-containing N-terminal module of MPS1 is required for its kinetochore localization by Aurora B. J. Cell Biol. *201*, 217–231.

Nijenhuis, W., Vallardi, G., Teixeira, A., Kops, G. J. P. L., and Saurin, A. T. (2014). Negative feedback at kinetochores underlies a responsive spindle checkpoint signal. Nat. Cell Biol. *16*, 1257–1264.

Nitta, M., Kobayashi, O., Honda, S., Hirota, T., Kuninaka, S., Marumoto, T., Ushio, Y., and Saya, H. (2004). Spindle checkpoint function is required for mitotic catastrophe induced by DNA-damaging agents. Oncogene *23*, 6548–6558.

Nozawa, R.-S., Nagao, K., Masuda, H.-T., Iwasaki, O., Hirota, T., Nozaki, N., Kimura, H., and Obuse, C. (2010). Human POGZ modulates dissociation of HP1alpha from mitotic chromosome arms through Aurora B activation. Nat. Cell Biol. *12*, 719–727.

Olszak, A. M., Van Essen, D., Pereira, A. J., Diehl, S., Manke, T., Maiato, H., Saccani, S., and Heun, P. (2011). Heterochromatin boundaries are hotspots for de novo kinetochore formation. Nat. Cell Biol. *13*, 799–808.

Parker, L. L., and Piwnica-Worms, H. (1992). Inactivation of the p34cdc2-Cyclin B Complex by the Human WEEl Tyrosine Kinase. Science *257*, 1955–1957.

Perera, D., and Taylor, S. S. (2010). Sgo1 establishes the centromeric cohesion protection mechanism in G2 before subsequent Bub1-dependent recruitment in mitosis. J. Cell Sci. *123*, 653–659.

Perez-Castro, A. V., Shamanski, F. L., Meneses, J. J., Lovato, T. L., Vogel, K. G., Moyzis, R. K., and Pedersen, R. (1998). Centromeric protein B null mice are viable with no apparent abnormalities. Dev. Biol. *201*, 135–143.

Peter, M., Nakagawa, J., Dorée, M., Labbé, J. C., and Nigg, E. A. (1990). In vitro disassembly of the nuclear lamina and M phase-specific phosphorylation of lamins by cdc2 kinase. Cell *61*, 591–602.

Petrovic, A. *et al.* (2010). The MIS12 complex is a protein interaction hub for outer kinetochore assembly. J. Cell Biol. *190*, 835–852.

Petrovic, A. *et al.* (2016). Structure of the MIS12 Complex and Molecular Basis of Its Interaction with CENP-C at Human Kinetochores. Cell *167*, 1028–1040.e15.

Phair, R. D., and Misteli, T. (2001). Kinetic modelling approaches to in vivo imaging. Nat. Rev. Mol. Cell Biol. *2*, 898–907.

Pinsky, B. A., Kung, C., Shokat, K. M., and Biggins, S. (2006). The Ipl1-Aurora protein kinase activates the spindle checkpoint by creating unattached kinetochores. Nat. Cell Biol. *8*, 78–83.

Pluta, A. F., Saitoh, N., Goldberg, I., and Earnshaw, W. C. (1992). Identification of a subdomain of CENP-B that is necessary and sufficient for localization to the human centromere. J. Cell Biol. *116*, 1081–1093.

Polioudaki, H., Markaki, Y., Kourmouli, N., Dialynas, G., Theodoropoulos, P. A., Singh, P. B., and Georgatos, S. D. (2004). Mitotic phosphorylation of histone H3 at threonine 3. FEBS Lett. *560*, 39–44.

Pradhan, K., and Gadgil, M. (2012). Effect of addition of “carrier” DNA during transient protein expression in suspension CHO culture. Cytotechnology *64*, 613–622.

Qian, J., Beullens, M., Huang, J., De Munter, S., Lesage, B., and Bollen, M. (2015). Cdk1 orders mitotic events through coordination of a chromosome-associated phosphatase switch. Nat. Commun. *6*, 1–13.

Qian, J., Beullens, M., Lesage, B., and Bollen, M. (2013). Aurora B defines its own chromosomal targeting by opposing the recruitment of the phosphatase scaffold Repo-Man. Curr. Biol. *23*, 1136–1143.

Qian, J., Lesage, B., Beullens, M., Van Eynde, A., and Bollen, M. (2011). PP1/repo-man dephosphorylates mitotic histone H3 at T3 and regulates chromosomal aurora B targeting. Curr. Biol. *21*, 766–773.

Rieder, C. L. (1981). The structure of the cold-stable kinetochore fiber in metaphase PtK1 cells. Chromosoma *84*, 145–158.

Rieder, C. L., Schultz, A., Cole, R., and Sluder, G. (1994). Anaphase onset in vertebrate somatic cells is controlled by a checkpoint that monitors sister kinetochore attachment to the spindle. J. Cell Biol. *127*, 1301–1310.

Ruchaud, S., Carmena, M., and Earnshaw, W. C. (2007). Chromosomal passengers: conducting cell division. Nat. Rev. Mol. Cell Biol. *8*, 798–812.

Ruppert, J. G., Samejima, K., Platani, M., Molina, O., Kimura, H., Jeyaprakash, A. A., Ohta, S., and Earnshaw, W. C. (2018). HP1α targets the chromosomal passenger complex for activation at heterochromatin before mitotic entry. EMBO J. *37*, e97677.

Saitoh, H., Tomkiel, J., Cooke, C. A., Ratrie, H., Maurer, M., Rothfield, N. F., and Earnshaw, W. C. (1992). CENP-C, an autoantigen in scleroderma, is a component of the human inner kinetochore plate. Cell *70*, 115–125.

Samejima, K., Platani, M., Wolny, M., Ogawa, H., Vargiu, G., Knight, P. J., Peckham, M., and Earnshaw, W. C. (2015). The inner centromere protein (INCENP) coil is a single α-helix (SAH) domain that binds directly to microtubules and is important for chromosome passenger complex (CPC) localization and function in mitosis. J. Biol. Chem. *290*, 21460–21472.

Sampath, S. C., Ohi, R., Leismann, O., Salic, A., Pozniakovski, A., and Funabiki, H. (2004). The chromosomal passenger complex is required for chromatin-induced microtubule stabilization and spindle assembly. Cell *118*, 187–202.

du Sart, D., Cancilla, M. R., Earle, E., Mao, J. I., Saffery, R., Tainton, K. M., Kalitsis, P., Martyn, J., Barry, A. E., and Andy Choo, K. H. (1997). A functional neo-centromere formed through activation of a latent human centromere and consisting of non-alpha-satellite DNA. Nat. Genet. *16*, 144–153.

Saunders, W. S., Chue, C., Goebl, M., Craig, C., Clark, R. F., Powers, J. A., Eissenberg, J. C., Elgin, S. C., Rothfield, N. F., and Earnshaw, W. C. (1993). Molecular cloning of a human homologue of Drosophila heterochromatin protein HP1 using anti-centromere autoantibodies with anti-chromo specificity. J. Cell Sci. *104 (Pt 2*, 573–582.

Saurin, A. T., Van Der Waal, M. S., Medema, R. H., Lens, S. M. A., and Kops, G. J. P. L. (2011). Aurora B potentiates Mps1 activation to ensure rapid checkpoint establishment at the onset of mitosis. Nat. Commun. *2*.

Schindelin, J. *et al.* (2012). Fiji: an open-source platform for biological-image analysis. Nat. Methods *9*, 676–682.

Schmiedeberg, L., Weisshart, K., Diekmann, S., Meyer, G., Hemmerich, P., Biotechnology, M., Gmbh, C. J., and Imaging, A. (2004). High- and Low-mobility Populations of HP1 in Heterochromatin of Mammalian Cells. Mol. Biol. Cell *15*, 2819–2833.

Schueler, M. G., Higgins, A. W., Rudd, M. K., Gustashaw, K., and Willard, H. F. (2001). Genomic and Genetic Definition of a Functional Human Centromere. Science *294*, 109–115.

Screpanti, E., De Antoni, A., Alushin, G. M., Petrovic, A., Melis, T., Nogales, E., and Musacchio, A. (2011). Direct binding of Cenp-C to the Mis12 complex joins the inner and outer kinetochore. Curr. Biol. *21*, 391–398.

Seeler, J. S., Marchio, a, Sitterlin, D., Transy, C., and Dejean, A (1998). Interaction of SP100 with HP1 proteins: a link between the promyelocytic leukemia-associated nuclear bodies and the chromatin compartment. Proc. Natl. Acad. Sci. U. S. A. *95*, 7316–7321.

Serrano, Á., Rodríguez-Corsino, M., and Losada, A. (2009). Heterochromatin protein 1 (HP1) proteins do not drive pericentromeric cohesin enrichment in human cells. PLoS One *4*.

Sessa, F., Mapelli, M., Ciferri, C., Tarricone, C., Areces, L. B., Schneider, T. R., Stukenberg, P. T., and Musacchio, A. (2005). Mechanism of Aurora B activation by INCENP and inhibition by hesperadin. Mol. Cell *18*, 379–391.

Sherr, C. J. (1993). Mammalian G1 cyclins. Cell *73*, 1059–1065.

Shogren-Knaak, M., Ishii, H., Sun, J. M., Pazin, M. J., Davie, J. R., and Peterson, C. L. (2006). Histone H4-K16 acetylation controls chromatin structure and protein interactions. Science *311*, 844–847.

Shokat, K., and Velleca, M. (2002). Novel chemical genetic approaches to the discovery of signal transduction inhibitors. Drug Discov. Today *7*, 872–879.

Shrestha, R. L., and Draviam, V. M. (2013). Lateral to end-on conversion of chromosome-microtubule attachment requires kinesins cenp-e and MCAK. Curr. Biol. *23*, 1514–1526.

Simon, J. A., and Kingston, R. E. (2009). Mechanisms of Polycomb gene silencing: Knowns and unknowns. Nat. Rev. Mol. Cell Biol. *10*, 697–708.

Singh, P. B., Miller, J. R., Pearce, J., Kothary, R., Burton, R. D., Paro, R., and James, T. C. (1991). A sequence motif found in a Drosophila heterochromatin protein is conserved in animals and plants. Nucleic Acids Research *19*, 789.

Smothers, J. F., and Henikoff, S. (2000). The HP1 chromo shadow domain binds a consensus peptide pentamer. Curr. Biol. *10*, 27–30.

Soloaga, A., Thomson, S., Wiggin, G. R., Rampersaud, N., Dyson, M. H., Hazzalin, C. A., Mahadevan, L. C., and Arthur, J. S. C. (2003). MSK2 and MSK1 mediate the mitogen- and stress-induced phosphorylation of histone H3 and HMG-14. EMBO J. *22*, 2788–2797.

Starr, D. A., Williams, B. C., Hays, T. S., and Goldberg, M. L. (1998). ZW10 helps recruit dynactin and dynein to the kinetochore. J. Cell Biol. *142*, 763–774.

Stewart, S., and Fang, G. (2005). Destruction Box – Dependent Degradation of Aurora B Is Mediated by the Anaphase-Promoting Complex / Cyclosome and Cdh1. Cancer Research*, 65(19), 8730–8735*.

Strom, A. R., Emelyanov, A. V., Mir, M., Fyodorov, D. V., Darzacq, X., and Karpen, G. H. (2017). Phase separation drives heterochromatin domain formation. Nature *547*, 241–245.

Sullivan, K. F., Hechenberger, M., and Masri, K. (1994). Human CENP-A contains a histone H3 related histone fold domain that is required for targeting to the centromere. Cancer Discov. *3*, 581–592.

Sumara, I., Quadroni, M., Frei, C., Olma, M. H., Sumara, G., Ricci, R., and Peter, M. (2007). A Cul3-Based E3 Ligase Removes Aurora B from Mitotic Chromosomes, Regulating Mitotic Progression and Completion of Cytokinesis in Human Cells. Dev. Cell *12*, 887–900.

Taddei, A., Maison, C., Roche, D., and Almouzni, G. (2001). Reversible disruption of pericentric heterochromatin and centromere function by inhibiting deacetylases. Nat. Cell Biol. *3*, 114–120.

Tanaka, T. U. (2010). Kinetochore-microtubule interactions: Steps towards bi-orientation. EMBO J. *29*, 4070–4082.

Tanaka, T. U., Rachidi, N., Janke, C., Pereira, G., Galova, M., Schiebel, E., Stark, M. J. R., and Nasmyth, K. (2002). Evidence that the Ipl1-Sli15 (Aurora Kinase-INCENP) complex promotes chromosome bi-orientation by altering kinetochore-spindle pole connections. Cell *108*, 317–329.

Tanaka, Y., Nureki, O., Kurumizaka, H., Fukai, S., Kawaguchi, S., Ikuta, M., Iwahara, J., Okazaki, T., and Yokoyama, S. (2001). Crystal structure of the CENP-B protein-DNA complex: The DNA-binding domains of CENP-B induce kinks in the CENP-B box DNA. EMBO J. *20*, 6612–6618.

Tawaramoto, M. S., Park, S. Y., Tanaka, Y., Nureki, O., Kurumizaka, H., and Yokoyama, S. (2003). Crystal Structure of the Human Centromere Protein B (CENP-B) Dimerization Domain at 1.65-Å Resolution. J. Biol. Chem. *278*, 51454–51461.

Taylor, S. S., Ha, E., and McKeon, F. (1998). The human homologue of Bub3 is required for kinetochore localization of Bub1 and a Mad3/Bub1-related protein kinase. J. Cell Biol. *142*, 1–11.

Teichner, A., Eytan, E., Sitry-Shevah, D., Miniowitz-Shemtov, S., Dumin, E., Gromis, J., and Hershko, A. (2011). p31comet promotes disassembly of the mitotic checkpoint complex in an ATP-dependent process. Proc. Natl. Acad. Sci. *108*, 3187–3192.

Thiru, A., Nietlispach, D., Mott, H. R., Okuwaki, M., Lyon, D., Nielsen, P. R., Hirshberg, M., Verreault, A., Murzina, N. V, and Laue, E. D. (2004). Structural basis of HP1/PXVXL motif peptide interactions and HP1 localisation to heterochromatin. EMBO J. *23*, 489–499.

Thomson, S., Clayton, A. L., Hazzalin, C. A., Rose, S., Barratt, M. J., and Mahadevan, L. C. (1999). The nucleosomal response associated with immediate-early gene induction is mediated via alternative MAP kinase cascades: MSK1 as a potential histone H3/HMG-14 kinase. EMBO J. *18*, 4779–4793.

Toth, K. F., Knoch, T. A., Wachsmuth, M., Frank-Stohr, M., Stohr, M., Bacher, C. P., Muller, G., and Rippe, K. (2004). Trichostatin A-induced histone acetylation causes decondensation of interphase chromatin. J. Cell Sci. *117*, 4277–4287.

Trivedi, P., and Stukenberg, P. T. (2016). Review A Centromere-Signaling Network Underlies the Coordination among Mitotic Events. Trends Biochem. Sci. *41*, 160–174.

Tseng, B. S., Tan, L., Kapoor, T. M., and Funabiki, H. (2010). Dual detection of chromosomes and microtubules by the chromosomal passenger complex drives spindle assembly. Dev. Cell *18*, 903–912.

Tsukahara, T., Tanno, Y., and Watanabe, Y. (2010). Phosphorylation of the CPC by Cdk1 promotes chromosome bi-orientation. Nature *467*, 719–723.

Vader, G., Kauw, J. J. W., Medema, R. H., and Lens, S. M. A. (2006). Survivin mediates targeting of the chromosomal passenger complex to the centromere and midbody. EMBO Rep. *7*, 85–92.

Vagnarelli, P., Ribeiro, S., Sennels, L., Sanchez-Pulido, L., de Lima Alves, F., Verheyen, T., Kelly, D. A., Ponting, C. P., Rappsilber, J., and Earnshaw, W. C. (2011). Repo-Man Coordinates Chromosomal Reorganization with Nuclear Envelope Reassembly during Mitotic Exit. Dev. Cell *21*, 328–342.

Varetti, G., Guida, C., Santaguida, S., Chiroli, E., and Musacchio, A. (2011). Homeostatic control of mitotic arrest. Mol. Cell *44*, 710–720.

Vleugel, M., Hoogendoorn, E., Snel, B., and Kops, G. J. P. L. (2012). Evolution and Function of the Mitotic Checkpoint. Dev. Cell *23*, 239–250.

van der Waal, M. S., Hengeveld, R. C. C., van der Horst, A., and Lens, S. M. a (2012). Cell division control by the Chromosomal Passenger Complex. Exp. Cell Res. *318*, 1407–1420.

Wang, E., Ballister, E. R., and Lampson, M. A. (2011a). Aurora B dynamics at centromeres create a diffusion-based phosphorylation gradient. J. Cell Biol. *194*, 539–549.

Wang, F., Dai, J., Daum, J. R., Niedzialkowska, E., Banerjee, B., Stukenberg, P. T., Gorbsky, G. J., and Higgins, J. M. G. (2010). Histone H3 Thr-3 phosphorylation by Haspin positions Aurora B at centromeres in mitosis. Science *330*, 231–235.

Wang, F., Ulyanova, N. P., Van Der Waal, M. S., Patnaik, D., Lens, S. M. a, and Higgins, J. M. G. (2011b). A positive feedback loop involving haspin and aurora B promotes CPC accumulation at centromeres in mitosis. Curr. Biol. *21*, 1061–1069.

Wang, J., Jia, S. T., and Jia, S. (2016). New Insights into the Regulation of Heterochromatin. Trends Genet. *32*, 284–294.

Watson, N. A., and Higgins, J. M. G. (2016). Histone Kinases and Phosphatases. Chromatin Signal. Dis., 75–94.

Wei, R. R., Al-Bassam, J., and Harrison, S. C. (2007). The Ndc80/HEC1 complex is a contact point for kinetochore-microtubule attachment. Nat. Struct. Mol. Biol. *14*, 54–59.

Wei, Y., Yu, L., Bowen, J., Gorovsky, M. a, and Allis, C. D. (1999). Phosphorylation of histone H3 is required for proper chromosome condensation and segregation. Cell *97*, 99–109.

Weiss, E. L., Bishop, A. C., Shokat, K. M., and Drubin, D. G. (2000). Chemical genetic analysis of the budding-yeast p21-activated kinase Cla4p. Nat. Cell Biol. *2*, 677–685.

Welburn, J. P. I., Vleugel, M., Liu, D., Iii, J. R. Y., Lampson, M. A., and Fukagawa, T. (2010). Aurora B Phosphorylates Spatially Distinct Targets to Differentially Regulate the Kinetochore-Microtubule Interface. Mol. Cell *38*, 383–392.

Westhorpe, F. G., Tighe, A., Lara-Gonzalez, P., and Taylor, S. S. (2011). p31comet-mediated extraction of Mad2 from the MCC promotes efficient mitotic exit. J. Cell Sci. *124*, 3905–3916.

Wurzenberger, C., and Gerlich, D. W. (2011). Phosphatases: Providing safe passage through mitotic exit. Nat. Rev. Mol. Cell Biol. *12*, 469–482.

Xia, G., Luo, X., Habu, T., Rizo, J., Matsumoto, T., and Yu, H. (2004). Conformation-specific binding of p31comet antagonizes the function of Mad2 in the spindle checkpoint. EMBO J. *23*, 3133–3143.

Xu, Z., Ogawa, H., Vagnarelli, P., Bergmann, J. H., Hudson, D. F., Ruchaud, S., Fukagawa, T., Earnshaw, W. C., and Samejima, K. (2009). INCENP–aurora B interactions modulate kinase activity and chromosome passenger complex localization. J. Cell Biol. *187*, 637-653.

Yamagishi, Y., Honda, T., Tanno, Y., and Watanabe, Y. (2010). Two histone marks establish the inner centromere and chromosome bi-orientation. Science *330*, 239–243.

Yamagishi, Y., Yang, C. H., Tanno, Y., and Watanabe, Y. (2012). MPS1/Mph1 phosphorylates the kinetochore protein KNL1/Spc7 to recruit SAC components. Nat. Cell Biol. *14*, 746–752.

Yamamoto, K., and Sonoda, M. (2003). Self-interaction of heterochromatin protein 1 is required for direct binding to histone methyltransferase, SUV39H1. Biochem. Biophys. Res. Commun. *301*, 287–292.

Yamamoto, Y., Verma, U. N., Prajapati, S., Kwak, Y.-T., and Gaynor, R. B. (2003). Histone H3 phosphorylation by IKK-alpha is critical for cytokine-induced gene expression. Nature *423*, 655–659.

Yang, M., Li, B., Tomchick, D. R., Machius, M., Rizo, J., Yu, H., and Luo, X. (2007). p31cometBlocks Mad2 Activation through Structural Mimicry. Cell *131*, 744–755.

Yang, Y. *et al.* (2008). Phosphorylation of HsMis13 by Aurora B kinase is essential for assembly of functional kinetochore. J. Biol. Chem. *283*, 26726–26736.

Yasui, Y., Urano, T., Kawajiri, A., Nagata, K. I., Tatsuka, M., Saya, H., Furukawa, K., Takahashi, T., Izawa, I., and Inagaki, M. (2004). Autophosphorylation of a Newly Identified Site of Aurora-B Is Indispensable for Cytokinesis. J. Biol. Chem. *279*, 12997–13003.

Yi, Q., Chen, Q., Liang, C., Yan, H., Zhang, Z., Xiang, X., Zhang, M., Qi, F., Zhou, L., and Wang, F. (2018). HP1 links centromeric heterochromatin to centromere cohesion in mammals. EMBO Rep. 19, e45484.

Yun, M., Wu, J., Workman, J. L., and Li, B. (2011). Readers of histone modifications. Cell Res. *21*, 564–578.

Zeitlin, S. G., Shelby, R. D., and Sullivan, K. F. (2001). CENP-A is phosphorylated by Aurora B kinase and plays an unexpected role in completion of cytokinesis. J. Cell Biol. *155*, 1147–1157.

Zhou, L. *et al.* (2017). The N-Terminal Non-Kinase-Domain-Mediated Binding of Haspin to Pds5B Protects Centromeric Cohesion in Mitosis. Curr. Biol. *27*, 992–1004.

Zhou, L., Tian, X., Zhu, C., Wang, F., and Higgins, J. M. (2014). Polo-like kinase-1 triggers Histone phosphorylation by Haspin in mitosis. EMBO Rep. *15*, 273–281.

Zippo, A., De Robertis, A., Serafini, R., and Oliviero, S. (2007). PIM1-dependent phosphorylation of histone H3 at serine 10 is required for MYC-dependent transcriptional activation and oncogenic transformation. Nat. Cell Biol. *9*, 932–944.

Zou, H., McGarry, T. J., Bernal, T., and Kirschner, M. W. (1999). Identification of a vertebrate sister-chromatid separation inhibitor involved in transformation and tumorigenesis. Science *285*, 418–421.

9 Appendix

Map of a plasmid that contains Xenopus CDK1as cDNA that was linked to a puromycin resistance gene via a sequence coding for the T2A peptide (see section 6.1).